

Statistical methods for accounting and understanding ozone trends derived from observations.

Présentée le 28 février 2020

à la Faculté de l'environnement naturel, architectural et construit
Laboratoire de recherche sur les particules atmosphériques
Programme doctoral en génie civil et environnement

pour l'obtention du grade de Docteur ès Sciences

par

Eirini BOLETI

Acceptée sur proposition du jury

Prof. U. von Gunten, président du jury
Prof. S. Takahama, Dr C. Hueglin, directeurs de thèse
Dr F. Dentener, rapporteur
Dr C. Ordonez, rapporteur
Dr D. Brunner, rapporteur

The real journey begins only after completion of another journey.

Dedicated to Antoni

Στον Αντωνάκη μου

Acknowledgements

First, I would like to express my appreciation to my supervisor Christoph Hueglin, who supported me at all stages of my PhD. With his supervision, I had the freedom to explore research possibilities according to my interests, while at the same time he offered valuable guidance which shaped my project and led to the successful completion of my PhD thesis. I am also very grateful to my advisor Satoshi Takahama, who has been providing his valuable insights and innovative ideas both in technical and conceptual points whenever needed.

I am particularly thankful to our Laboratory in Empa - Air Pollution/Environmental Technology - for giving me the opportunity to pursue my research. Within this friendly and supportive environment, I could always count on my colleagues' encouragement.

It was a pleasure to work alongside Dominik Brunner and Stephan Henne, who actively contributed to my project through constructive discussions and offered their experience and expertise on the subject. During our regular meetings I had the chance to discuss my results with them and their group and receive useful feedback.

I am grateful to the members of the committee Frank Dentener and Carlos Ordóñez for their feedback and constructive comments, which made my project more concise and complete. Also, I would like to thank the Swiss Federal Office of Environment (BAFU) for financing this project.

My deepest gratitude belongs to the most important person in my life, my partner Antonio. He has been by my side all the way through this new start in my life, that I have been longing for for a long time. His love, patience and advise helped me carry through the most difficult times and enjoy the most happy and successful ones.

Utrecht, 09.03.2019

E. B.

Abstract

Emissions of ozone precursors have been regulated in Europe since around 1990 with air quality control measures, which resulted in reductions of nitrogen oxides and volatile organic compounds concentrations. In order to understand how these measures have affected tropospheric ozone, it is important to investigate its long-term temporal evolution in different types of environments and various geographic regions. Uncertainties in ozone long-term trends are associated to variations originating from meteorological influence on ozone. Also, ozone temporal evolution can vary significantly among different regions and types of environment. In this PhD thesis we used sophisticated statistical tools, and developed robust statistical approaches to study long-term trends of tropospheric ozone that reflect emissions reductions. First, we focus on a meteorological adjustment of ozone observations in order to derive long-term trends with lower uncertainties compared to common practices. In addition, a classification scheme for stations in Europe is needed to understand ozone trends based on site groups with similar spatio-temporal characteristics.

A detailed long-term trend analysis was performed based on decomposition of the mean ozone observations in the time domain. The different time-dependent variations of ozone were extracted, namely the long-term trend, seasonal and short-term variability. This allows subtraction of the meteorologically driven seasonal variation from the observations and estimation of long-term trends on de-seasonalized concentrations. In addition, ozone peak concentrations were investigated using a regression approach based on temporally localized events, which corrects for meteorological influence. The meteorological adjustment of the mean and peak ozone allows estimation of long-term trends with lower uncertainty. A site grouping in Europe was developed using the long-term and seasonal variations of ozone. The implemented clustering approach based on the long-term variation resulted in a site type classification while a geographical classification was achieved on the seasonal variation.

We observed that, despite the implementation of regulations, mean ozone has been increasing in most of the sites until mid-2000s, although, afterwards, a decline or a leveling off was detected. The time when the trend changes from increasing to decreasing depends on the site type; the closer a site locates to emission sources the later the change occurred. Also, it was concluded that urban and rural environments become with time more similar in terms of ozone concentrations. On the other hand, peak ozone has been reducing in most stations, while in sites close to emissions it increased until mid-2000s when it started to level off. The influence of air pollutants hemispheric transport is depicted in remote sites, where ozone increased until beginning of 2000s and decreased afterwards. A two-dimensional classification

scheme, reflecting site type and region, has showed that mainly the site type influences ozone long-term trends, while the location is more important for temporal changes in ozone inter-annual cycle and relationship to temperature.

Zusammenfassung

Emissionen von Ozonvorläufern wurden in den 1990-er Jahren in Europa durch Massnahmen geregelt. Diese führten zur Reduktion der Stickstoffoxid-Konzentrationen, sowie Konzentrationen von flüchtigen organischen Verbindungen. Um die Auswirkungen der Kontrollmassnahmen auf das troposphärische Ozon besser zu verstehen, ist es wichtig, die langfristige zeitliche Entwicklung von Ozon in verschiedenen Umgebungen und geographischen Regionen zu untersuchen. Unsicherheiten im langfristigen Trend der Ozonkonzentration sind mit dem Einfluss von meteorologischen Variationen auf Ozonkonzentrationen verbunden. Ausserdem ist der Unterschied in der zeitlichen Entwicklung des Ozons zwischen verschiedenen Regionen und Stationstypen oft gross. In dieser PhD Dissertation wurden fortschrittliche statistische Methoden eingesetzt, um langfristige Ozontrends zu untersuchen.

Um die Unsicherheiten im langfristigen Ozontrend verglichen mit anderen verbreiteten Methoden zu minimieren, werden die Ozonmessdaten hinsichtlich der meteorologischen Einflüsse angepasst. Ausserdem wurde ein Klassifikationsschema für zahlreiche Stationen in Europa entwickelt, damit die Einflussfaktoren auf die zeitliche Entwicklung von Ozon untersucht werden können. Eine detaillierte Analyse des langfristigen Ozontrends wurde durch Frequenzerlegung der Ozonzeitreihen durchgeführt. d.h. die Messreihen wurden in den langfristigen Trend, sowie die saisonale und kurzzeitige Ozonvariabilität zerlegt. Dadurch wurde die durch die Meteorologie entstandene saisonale Variabilität von Ozonmessdaten extrahiert und schlussendlich wurde der langfristige Trend von den de-seasonalized Ozonkonzentrationen ermittelt. Der Einfluss der Meteorologie auf die maximalen Ozonkonzentrationen wurden mit einem Regressionsansatz geschätzt und die Messwerte wurden bezüglich des Einflusses der Meteorologie korrigiert. Die Variabilität in diesen korrigierten Werten ist gegenüber den Beobachtungen deutlich reduziert, was ein früheres Erkennen von signifikanten Trends ermöglicht. Ein Klassifikationsschema für europäische Stationen wurde basierend auf der langfristigen und saisonalen Variabilität von Ozon erstellt. Der basierend auf der langfristigen Variabilität implementierte Clusteringansatz ergab eine Stationstypklassifizierung, wobei der Ansatz basierend auf der saisonalen Variabilität eine Stationsklassifizierung mit Klimaeinfluss ermöglichte. Trotz der Implementierung von Kontrollmassnahmen hat die Ozonkonzentration in fast allen Stationen bis Mitte der 2000er Jahre zugenommen, und danach hat sie abgenommen oder ist bis 2015 stabil geblieben. Der Zeitpunkt, an dem sich der Trend von positiv zu negativ ändert, hängt vom Stationstyp ab: je stärker die Station durch Emissionen von Ozonvorläufern beeinflusst ist, desto später ist die Veränderung aufgetreten. Ausserdem, wurde festgestellt, dass städtische und ländliche Umgebungen mit der Zeit in Hinsicht auf Ozon-

konzentrationen ähnlicher werden. Die Ozonspitzenkonzentrationen haben an den meisten Stationen abgenommen. An Standorten im unmittelbaren Einflussbereich von Emissionen von Ozonvorläufern haben die Ozonspitzenwerte noch bis Mitte der 2000er Jahre zugenommen haben und sind seither nahezu konstant. Der Einfluss des hemisphärischen Transports von Luftschadstoffen kann von Ozonmessungen an Hintergrundstationen abgeleitet werden, an denen Ozon bis Anfangs der 2000er Jahre zugenommen und danach abgenommen hat. Eine geographische Klassifikation wurde mittels Clusteranalyse des saisonalen Variabilität erhalten. Ein zwei-dimensionales Klassifikationsschema, welche eine Unterscheidung der Stationen nach Typ und geographischer Lage der Station ermöglichte, hat gezeigt, dass der langzeitigen Ozontrend am stärksten vom Statiostyp abhängt. Der saisonale Verlauf von Ozon hängt dagegen stark von der geographischen Lage ab.



Keywords

Ozone; ozone peak concentrations; trend analysis; long-term trends; seasonal variability; time scale decomposition; meteorological adjustment; variable selection; clustering; site classification

Contents

Acknowledgements	v
Abstract (English/Deutsch)	vii
Keywords	xi
Contents	xv
List of figures	xxiii
List of tables	xxvi
1 Introduction	1
1.1 Tropospheric O ₃ chemistry	4
1.2 O ₃ variability and meteorological influence	8
1.3 Motivation	9
1.4 Scientific questions and approach	12
2 Ozone time scale decomposition and trend assessment from surface observations in Switzerland.	15
2.1 Introduction	16
2.2 Data	17
2.3 Methods	18
2.3.1 De-seasonalized trends	18
2.3.2 Meteo-adjusted trends	23
2.4 Results	24
2.4.1 Comparison of long-term trends based on EEMD and the parametric approach	24
2.4.2 Meteorological adjustment	28
2.4.3 Trends of mean O ₃ in Switzerland	29
2.5 Conclusions	36
3 Trends of surface maximum ozone concentrations in Switzerland based on meteorological adjustment for the period 1990-2014.	39
3.1 Introduction	40

Contents

3.2	Data	41
3.3	Methodology	42
3.3.1	Trend estimation of peak O ₃	42
3.3.2	Generalized additive models (GAMs)	44
3.3.3	Selection of meteorological variables	44
3.3.4	Meteorological adjustment	45
3.4	Results	46
3.4.1	Meteorological influence on maximum O ₃ concentrations	46
3.4.2	Trends of peak O ₃ concentrations	48
3.5	Conclusions	57
4	Temporal and spatial analysis of ozone concentrations in Europe based on time scale decomposition and a multi-clustering approach.	59
4.1	Introduction	60
4.2	Data	62
4.3	Methods	63
4.3.1	Time scale decomposition of daily mean and MDA8 O ₃	63
4.3.2	Cluster analysis of O ₃ variations	64
4.3.3	Daily mean and MDA8 O ₃ long-term trend analysis	65
4.3.4	Peak O ₃ concentrations long-term trend analysis	65
4.3.5	O ₃ seasonal cycle trend analysis	66
4.3.6	Relationship between O ₃ and temperature	66
4.4	Results	67
4.4.1	Cluster analysis	67
4.4.2	Trends of daily mean O ₃ concentrations	71
4.4.3	Trends of peak O ₃ concentrations	72
4.4.4	O ₃ seasonal cycle trends	74
4.4.5	O ₃ and temperature relationship	76
4.5	Conclusions	78
5	Conclusions	81
5.1	Time scale decomposition	81
5.2	Meteorological adjustment practices	82
5.2.1	Mean O ₃ meteorological adjustment	82
5.2.2	Peak O ₃ meteorological adjustment	83
5.3	Clustering based on different time scale variations	84
5.4	Long-term O ₃ trends	84
5.4.1	Mean O ₃ trends	84
5.4.2	Peak O ₃ trends	85
5.5	Outlook	86

A Appendix A	87
A.1 Convergence tests for ensemble empirical mode decomposition	87
A.2 Frequency analysis	88
A.3 Generalized additive models	88
A.4 Trends based on NO categorization	93
B Appendix B	97
B.1 Trends of 90th percentile, A-MDA8, AOT40 and MTDM-cold season	97
B.2 Daily maximum O ₃ and temperature	102
B.3 Daily maximum O ₃ and day of week	103
B.4 Comparison to different time periods	104
B.5 Variables selected in the GAMs	107
B.6 Generalized additive models	110
B.7 O ₃ and temperature sensitivity in the GAMs	115
B.8 Comparison of Theil-Sen trends and Linear Regression	115
C Appendix C	119
C.1 Choice of number of clusters	119
C.2 Assessment of clusters	120
C.3 Additional information on clusters	127
C.4 MDA8 and 4-MDA8 trends	131
C.5 Sites with negative Sihlouette width	131
Bibliography	151
Curriculum Vitae	153

List of Figures

1.1	Global distribution of annual mean RF of tropospheric O ₃ between 1850–2000 (scale in mW/m ² , from the multi-model mean of the ACCMIP models, using the Edwards–Slingo radiation scheme (Stevenson et al., 2013). Figure from Monks et al. (2015).	2
1.2	Source attribution of the O ₃ measured at a rural location in southern England during January 2006 (Derwent, 2008, averaged over the 12-month study period). Results are obtained by a global model coupled to a regional model (from Derwent (2008)).	3
1.3	Sources and sinks of tropospheric O ₃ . Numbers refer to annual global fluxes estimated by a global chemistry-transport model, i.e. stratospheric-tropospheric exchange, chemical production and loss, and deposition to terrestrial and marine surfaces. Source: IPCC Fourth Assessment Report Working Group I Report "The Physical Science Basis" (Denman et al., 2007).	5
1.4	EKMA diagram with O ₃ isopleths. Adapted from Finlayson-Pitts and Pitts (1986).	7
1.5	Emissions trends in the EMEP area (including stations in most parts of Europe with scarce network in the southern and eastern countries) based on data reported by countries and gap-filled with expert estimates (shipping emission are not included, figure from EMEP (2017)).	10
1.6	Composite of annual mean O ₃ (black) and 4th highest MDA8 (red) O ₃ recorded at 55 EMEP rural monitoring sites between 1990 and 2012. The thick line is the network-wide annual median and lower/higher bounds of the shaded areas are for the 25th and 75th percentiles. Thin straight lines show the linear trend over the 1990-2001 and 2002-2012 periods and dashed lines indicate the WHO air quality guideline (50 ppb) and the EU long term objective (60 ppb). Source: EMEP, Co-operative Programme for Monitoring and Evaluation of the Long-Range Transmission of Air Pollutants in Europe (2016).	11
2.1	Example of the procedure for calculating an IMF for daily mean O ₃ concentrations (data set from Dübendorf). Red dots show the local extrema of the signal and red lines the fitted envelopes based on these extrema. The green dashed line is the mean of the upper and lower envelope.	20

List of Figures

2.2	EEMD results for daily mean O ₃ concentrations in Dübendorf, a suburban background site. Shown is the daily mean observations (gray line), the long-term variation (red line) yielded from the residue of the EEMD, the seasonal variation (purple line) by adding together the IMFs 7-11 and the short term variation (light blue line) from the IMFs 1-6. For illustration reasons, the long-term signal was added to the seasonal and short-term signals.	21
2.3	Seasonal variation signals for daily mean O ₃ concentrations in Dübendorf, obtained from the EEMD and from the parametric approach.	22
2.4	Map of Switzerland and location of the sites that were considered for this study. The site types are distinguished by color.	26
2.5	Bar-plots for the trends of the daily mean O ₃ concentrations during the identified first and second period for the five categories (indicated as Cat.). The bars show the magnitude of the Theil-Sen slopes (in ppb/year) for the studied sites (Table 2.1). The lines represent the 95% CI of the estimated trend. The blue colors show the trends estimated from de-seasonalized data, with the subtraction of the seasonal variation obtained either from the parametric approach (light blue bar) or the EEMD (dark blue bar). The pink colors show the meteo-adjusted trends based on the parametric approach (light pink bar) and EEMD (dark pink bar), respectively. The right panel indicates the time when the trend changes from positive to negative, i.e. the breakpoints as calculated from EEMD. Note that no breakpoint was found in LIE, ZUE and HAE. In LAU and BER the breakpoint occurred late, the trends in all these sites were therefore calculated for only one period. Also, the meteo-adjustment has not been applied for the sites GRE, FRA and LIE.	27
2.6	As for Fig. 2.5 but for MDA8 O ₃	28
2.7	As for Fig. 2.5 but for daily mean O _x	29
2.8	Theil-Sen trends of daily mean O ₃ concentrations estimated from monthly de-seasonalized values separated for stations in categories A-E. The categories have been defined based on the prevailing NO _x mixing ratio. The averages (red dashed lines) are based on the averaged de-seasonalized time series in each category and breakpoints on the averaged <i>LT(t)</i>	30
2.9	Theil-Sen trends of MDA8 O ₃ estimated from monthly de-seasonalized values separated for stations in categories A-E. The categories have been defined based on the prevailing NO _x mixing ratio. The averages (red dashed lines) are based on the averaged de-seasonalized time series in each category and breakpoints on the averaged <i>LT(t)</i>	31
2.10	Theil-Sen trends of daily mean O _x mixing ratios estimated from monthly de-seasonalized values separated for stations in categories A-E. The categories have been defined based on the prevailing NO _x mixing ratio. The averages (red dashed lines) are based on the averaged de-seasonalized time series in each category and breakpoints on the averaged <i>LT(t)</i>	32

2.11 Trends of O_3 and O_x (in ppb/year) for the site categories A to E (indicated as Cat.). Shown are the Theil-Sen trends of the averaged de-seasonalized data for each category. The two identified time periods and the breakpoint are based on the averaged $LT(t)$ at each category. The hatched bars indicate non-significant trends, i.e. with a p-value larger than 0.05.	35
2.12 Bar plots with the Theil-Sen trends of daily mean NO and NO_2 mixing ratios annually averaged for the whole studied period in ppb/year. Trends are also shown in two successive periods that correspond to the periods that were detected for the daily mean O_3 mixing ratios. Stations are grouped according to mean NO_x mixing ratio levels over the studied period in categories A-E (indicated as Cat.).	37
2.13 Differences between the categories A-E of the averaged $LT(t)$. A-B is the $LT(t)$ difference between categories A and B, B-C between B and C etc.	38
3.1 Example of relationship between daily maximum O_3 and some of selected meteorological variables for the suburban site Dübendorf.	48
3.2 Daily maximum O_3 for different daily maximum temperature ranges and time periods averaged for all studied sites. Box encompasses 25th to 75th percentile with a line at the median; whiskers extend to 1.5 times the interquartile range. Values for each site category are shown in the supplementary material.	49
3.3 Measured and meteo-adjusted daily maximum O_3 (left) and MDA8 O_3 (right) time series for the suburban site in Dübendorf.	50
3.4 Box-whisker plot for the MTDM and 4-MDA8 mixing ratios as calculated from measured and meteo-adjusted data separated for the different site categories.	50
3.5 Theil-Sen trends of MTDM for the studied sites across Switzerland. Error bars show the 95% CI. Note that, for the stations FRA, GRE and LIE, no complete meteorological information was available; therefore, meteo-adjustment was not applied.	51
3.6 Same as in Fig. 3.5 for 4-MDA8.	52
3.7 Trends of measured and meteo-adjusted MTDM (left) and 4-MDA8 (right) for the suburban site in Dübendorf.	53
3.8 Theil-Sen trends of daily mean NO and NO_2 during 1990-2014 (in ppb/year) for the studied sites in Switzerland based on yearly averages. Error bars show the 95% CIs obtained by the Theil-Sen trend estimator.	54
3.9 Theil-Sen trend lines are shown as means of all sites in each category for the meteo-adjusted MTDM. Points show the yearly average value for all sites in the category. Trend in Bern (BER) is shown additionally for the MTDM in two periods (1990-2004 and 2004-2014), due to exceptional behavior compared to the other studied sites. Sites in category D located south and north of the Alps are indicated with different color and shapes to point out their differences in O_3 mixing ratios trends.	55

List of Figures

3.10	Same as in Fig. 3.9 for SOMO35. Note that meteo-adjustment was not applied for SOMO35. A linear trend is not shown for categories A and B as there is an inflection point during the studied time period.	56
4.1	European map showing the location of the studied sites. Type of environment (symbols) and altitude (color bar) are indicated.	63
4.2	Schematic illustration for explaining the estimation of the ($S_{max}(t)$ and $S_{min}(t)$) and the annual day of maximum of the seasonal signal ($S_{DoM}(t)$) as calculated from the daily mean O ₃ time series.	67
4.3	Clusters based on daily mean O ₃ LT(t). Average LT(t) in each cluster with \pm the standard deviation (left) and histograms for the site type included in each cluster.	68
4.4	Map with the site clusters derived from daily O ₃ S(t), and average S(t) in each site cluster.	69
4.5	Annual cycle of daily mean O ₃ S(t) for the daily mean S(t) clusters.	70
4.6	Box-plots of de-seasonalized daily mean O ₃ trends for the LT(t)- and S(t)-clusters. LT(t)-clusters represent a site type classification while the S(t)-clusters a geographical one that is influenced by climatic conditions.	72
4.7	MDA8 LT(t) in Mace Head extracted with the EEMD (left) and the corresponding de-seasonalized Theil-Sen trend (right).	73
4.8	Box-plots of meteo-adjusted MTDM trends for the daily mean O ₃ LT(t)- and S(t)-clusters. LT(t)-clusters represent a site type classification while the S(t)-clusters a geographical one that is influenced by climatic conditions.	74
4.9	Temporal evolution of S_{max} and S_{min} for the daily mean O ₃ S(t) clusters together with the average S(t) (bands indicate the average <i>pm</i> the standard deviation). Lines show the linear trends of S_{max} and S_{min} and dashed lines the 90% confidence interval.	76
4.10	Linear trends of the S_{DoMax} for the daily mean S(t) clusters (dashed lines show the 90% confidence interval).	77
4.11	Linear trend of the slope between O ₃ -temperature daily maximum values for the warm season between May and September. The trends are calculated on the average values for each daily mean S(t) cluster and for the year groups 2000-2005, 2005-2010 and 2010-2015. Points show the mean value for the indicated temperature bin together with the corresponding standard deviation.	80
A.1	The convergence test results for the sufficient number of trials in the EEMD. Here we show the number of trials performed for each case study (10 tests for each case) against the corresponding magnitude of the Theil-Sen trend (data from Basel). In the inset we show the standard deviation for each of the cases.	88
A.2	The convergence test for the amplitude of the added white noise series. We show the noise amplitude against the calculated Theil-Sen trend for each noise amplitude and in the inset the corresponding standard deviation (data from Basel).	89
A.3	Periodogram based on Hilbert spectrum for the suburban site of Dübendorf.	90

A.4	Percentage of meteorologically driven variability of daily mean O ₃ , MDA8 O ₃ and daily mean O _x concentrations for the studied stations explained by the GAMs. Meteorological adjustment is not applied for the sites GRE, FRA and LIE.	91
A.5	Example of relationship between short-term variability of daily mean O ₃ concentration and daily means of meteorological variables for Dübendorf. Note that x- and y-axis refer to short-term variation of the parameters and not the actual daily mean values.	92
A.6	Bar-plots for the trends of the daily mean O ₃ concentrations during the identified first and second period for the five categories based on mean NO mixing ratio (indicated as Cat.). The bars show the magnitude of the Theil-Sen slopes (in ppb/year) for the studied sites. The lines represent the 95% CI of the estimated trend. The blue colors show the trends estimated from de-seasonalized data, with the subtraction of the seasonal variation obtained either from the parametric approach (light blue bar) or the EEMD (dark blue bar). The pink colors show the meteo-adjusted trends based on the parametric approach (light pink bar) and EEMD (dark pink bar), respectively. The right panel indicates the time when the trend changes from positive to negative, i.e. the breakpoints as calculated from EEMD. Note that due to late breakpoints in Lausanne (LAU) and Bern (BER) the trend in these sites was calculated in one period. Also, the meteo-adjustment has not been applied for the sites GRE, FRA and LIE.	93
A.7	As for Fig. A.6 but for MDA8 O ₃	94
A.8	As for Fig. A.6 but for daily mean O _x	95
B.1	Bar-plots with the Theil-Sen slopes for the annual maximum O ₃ (A-MDA8) and the 90th percentile of daily maximum O ₃ before and after meteo-adjustment.	98
B.2	Same as Fig. B.1 for the SOMO35 and AOT40 without meteo-adjustment. Note that SOMO35 trends are not shown due to an inflection point during the studied period (see discussion of results in the main text).	99
B.3	Same as Fig. B.1 for the MTDM between October and April.	100
B.4	Theil-Sen trend of MTDM for the season May to September for the site in Härkingen (HAE).	100
B.5	Theil-Sen trends of the number of days with MDA8 O ₃ >35 ppb during summer months (June, July and August). Red bars indicate the sites where positive SOMO35 trends were found, and * the significant trends (p-value<0.1).	101
B.6	Box-and-whisker plots for daily maximum O ₃ in different temperature ranges and time periods averaged for the sites categories.	102
B.7	Whisker-plot for the daily maximum O ₃ and the day of week for the sites in Chaumont (CHA) and Zürich (ZUE). Warm season refers to the months May to September and cold season to the months October to April.	103
B.8	Theil-Sen trends of the 90th percentile of daily maximum O ₃ during the warm season for the time period 1992-2002.	104

List of Figures

B.9	MTDM Theil-Sen trends during the warm season for the time period between 1995 and 2005.	105
B.10	SOMO35 Theil-Sen trends during the warm season for the time period between 2000 and 2014.	106
B.11	Bar charts for frequency of occurrence (%) and ranking (1st, 2nd, 3rd-6th, and 7th-10th position) of the meteorological variables in the GAMs for O ₃ daily maximum in the warm period (May-September) after the model selection. The percentage shows the frequency of occurrence of the parameter in the models and colors show the ranking of the parameter in the model, i.e. as a 1st parameter, as a 2nd, between 3rd and 6th position and 7th to 10th position.	107
B.12	Same as Fig. B.11 but for MDA8 O ₃	108
B.13	Same as Fig. B.11 but for the cold period.	108
B.14	Same as Fig. B.11 but for MDA8 O ₃ in cold period.	109
B.15	A test regarding the choice of AIC in the variable selection approach.	109
B.16	Bar-plots for the variation of O ₃ (R^2) explained by the most important meteorological variables and time. The value in the bars indicates the number of meteorological variables that were selected in the model selection procedure.	111
B.17	Example of relationship of O ₃ daily maximum and the selected meteorological variables for the suburban site Dübendorf. Above we show the results for the daily maximum values and below for the MDA8 values during the cold season October-April.	112
B.18	Example of relationship of O ₃ daily maximum and the Julian day parameter ($s_0(t)$).	113
B.19	Model assumptions check for GAMs O ₃ daily maximum (left) and MDA8 (right) in warm (up) and cold (down) season for the suburban site Dübendorf.	114
B.20	A comparison of the observations with the fitted values in the GAM. The percentage of the difference $(O_{3fitted} - O_{3observed}) / O_{3fitted} \%$ is shown in the y-axis for the intermediate values (<150 ppb, left) and the extreme values (>150 ppb, right).	114
B.21	Partial plots between O ₃ and temperature daily maximum values for the indicated time periods.	115
B.22	Scatter plot comparing the Theil-Sen and Linear Regression slopes for the MTDM between May and September and 4-MDA8. Straight line shows the 1-1 line.	116
B.23	Comparison of the Theil-Sen trends with and without the effect of the hot summers 2003 and 2006.	117
B.24	Theil-Sen trends of daily maximum temperature (yearly average).	118
C.1	Sum of squared distance error within a cluster against number of clusters for daily mean O ₃ LT(t), S(t) and W(t).	119
C.2	Same as Fig. C.1 but for MDA8 O ₃	119
C.3	Silhouette width plots for daily mean O ₃ LT(t).	121
C.4	Same as in Fig. C.3 but for S(t).	122
C.5	Same as in Fig. C.3 but for S(t).	123
C.6	Same as in Fig. C.3 but for MDA8 LT(t).	124

C.7 Same as in Fig. C.6 but for S(t).	125
C.8 Same as in Fig. C.6 but for W(t).	126
C.9 Clusters based on MDA8 O ₃ LT(t). Map indicating the sites that belong in each cluster and average LT(t) in each cluster with ± the standard deviation of the sites that have SW>0.	127
C.10 Clusters derived from MDA8 O ₃ S(t). Map indicating the sites that belong in each cluster and average S(t) (standard deviation) in each cluster of the sites that have SW>0.	128
C.11 Clusters derived from MDA8 O ₃ W(t). Map indicating the sites that belong in each cluster and average W(t) in each cluster of the sites that have SW>0.	129
C.12 Clusters derived from daily mean O ₃ W(t).(a) Map indicating the sites that belong in each cluster and average W(t) in each cluster of the sites that have SW>0.	130
C.13 De-seasonalized MDA8 O ₃ trends for the daily mean O ₃ LT(t)- and S(t)-clusters.	131
C.14 Trends of meteo-adjusted 4-MDA8 for the daily mean O ₃ LT(t)- and S(t)-clusters.	132
C.15 Sites with negative SW in the LT(t)-clustering, in comparison with the clusters average LT(t).	132
C.16 Example cases of sites with negative SW in the S(t)-clustering (black dashed line) in comparison with the clusters average S(t).	133

List of Tables

2.1	Studied stations in Switzerland, ranked by increasing mean NO_x concentration from top to the bottom. The duration of the data set is also shown. Stations are categorized according to mean NO_x value during the studied period, where A: $\text{NO}_x \leq 1$ ppb, B: $1 \leq \text{NO}_x \leq 10$ ppb, C: $10 \leq \text{NO}_x \leq 20$ ppb, D: $20 \leq \text{NO}_x \leq 40$ ppb, and E: $\text{NO}_x \geq 40$ ppb. (Cat. indicates the station's category.)	25
2.2	Average magnitudes of the Theil-Sen trends (ppb/year) for daily mean O_3 and MDA8 O_3 , and daily mean O_x for the two consecutive time periods in Swiss sites based on the EEMD de-seasonalization method and the time of breakpoint. P1 and P2 indicate the first and second period's average trend respectively and BP the average year of breakpoint in the trend. All numbers are based on the averaged de-seasonalized time series in each category and breakpoints on the averaged $LT(t)$. The numbers in italics are non-significant trends (p-value > 0.05).	36
3.1	Table with the studied stations in Switzerland, ranked by increasing mean NO_x concentration from top to bottom. Stations are categorized according to mean NO_x value during the studied period, where A: $\text{NO}_x \leq 1$ ppb, B: $1 < \text{NO}_x \leq 10$ ppb, C: $10 < \text{NO}_x \leq 20$ ppb, D: $20 < \text{NO}_x \leq 40$ ppb, and E: $\text{NO}_x \geq 40$ ppb. Category E2 indicates sites in urban environment with high traffic activity throughout the day. (Cat. indicates the station's category.)	43
3.2	Table with the most often selected meteorological variables and the number of sites in which they were selected for the GAMs for the warm period May–September (in total 18 sites, where the selection was applied).	47
3.3	Theil-Sen trends (mean value per group) of MTDM, 4-MDA8 and SOMO35. First and second values indicate the measured and meteo-adjusted trend respectively. In category D the mean trends are additionally shown for the sites north and south of the Alps separately. For SOMO35 meteo-adjustment was not applied and a linear trend is not meaningful for categories A and B due an inflection point during the studied time period. Cat. indicates the station's category.	53
4.1	Number of sites in each site group based on the $LT(t)$ and $S(t)$ clusters.	71

List of Tables

4.2 Linear trends of S_{max} , S_{min} and S_{DoMax} for the daily mean O_3 S(t) clusters during 2000-2015. ** indicate highly significant trend (p-value < 0.01), * significant (p-value < 0.05) and – indicate non-significant trend (p-value > 0.05). 77

4.3 Linear trends of the O_3 -temperature slope (based on daily maximum values) for the daily mean O_3 S(t)-clusters for the time period 2000-2015. ** indicate highly significant trend (p-value < 0.01), * significant (p-value < 0.05) and – indicate non-significant trend (p-value > 0.05). 78

4.4 Linear trends of the O_3 -temperature slope (based on daily maximum values) for the daily mean O_3 LT(t)-clusters for the time period 2000-2015. ** indicate highly significant trend (p-value < 0.01), * significant (p-value < 0.05) and – indicate non-significant trend (p-value > 0.05). 78

1 Introduction

Ozone (O₃) is one of the most important trace gases in the atmosphere, due to its role in photochemical processes taking place in the troposphere and the stratosphere. On the one hand, O₃ needs to be preserved in the stratosphere, because it protects living organisms at the surface by absorbing the harmful solar ultraviolet radiation. On the other hand, in the troposphere it is recognized as a threat for humans health and vegetation (WHO, 2013; LRTAP Convention, 2015; National Research Council, 1991). Together with particulate matter and nitrogen dioxide (NO₂), tropospheric O₃ is one of the most harmful air pollutants in Europe (Guerreiro et al., 2016). Short or long-term exposure of humans to high O₃ levels can induce inflammation of the entire respiratory system and premature death (Bell et al., 2006; Gryparis et al., 2004). O₃-related deaths are estimated to make up about 5–20% of all those related to air pollution (e.g. Silva et al., 2013). In addition, high levels of tropospheric O₃ are responsible for damaging ecosystems and agricultural production, forests and grasslands mainly by reducing the plants growth rate (Mills et al., 2000, 2018; Dentener et al., 2010). This occurs through the stomatal uptake of O₃, which then reacts with the internal plant tissues and produces highly reactive oxidants that disturb the physiological processes of the plant (Matyssek et al., 2008, 2010; Fowler et al., 2009).

O₃ absorbs both infrared and ultraviolet light, thus, fluctuations of its concentration in the atmosphere have an impact on climate (Seinfeld and Pandis, 2016). Tropospheric O₃ has a globally averaged radiative forcing (RF) of around $0.4 \pm 0.2 \text{ W/m}^2$, as estimated for the time period between 1750 and 2011 based on model simulations (Stevenson et al., 2013), making it the third most important greenhouse gas (IPCC, 2013). Spatial distribution of annual mean tropospheric O₃ RF varies greatly around the globe (Fig. 1.1). For instance, O₃ RF is largest over the southern margins of the northern mid-latitudes and subtropics over land. In these regions temperature differences between the surface and the tropopause are large, leading to the observed large long-wave RF over land in the tropics and subtropics. Reflective surfaces, such as the desert, increase short-wave RF. These interactions lead to the observed high net O₃ RF in northern Africa and the Middle East.

Baseline O₃ refers to concentrations that are not influenced by recent, locally emitted or

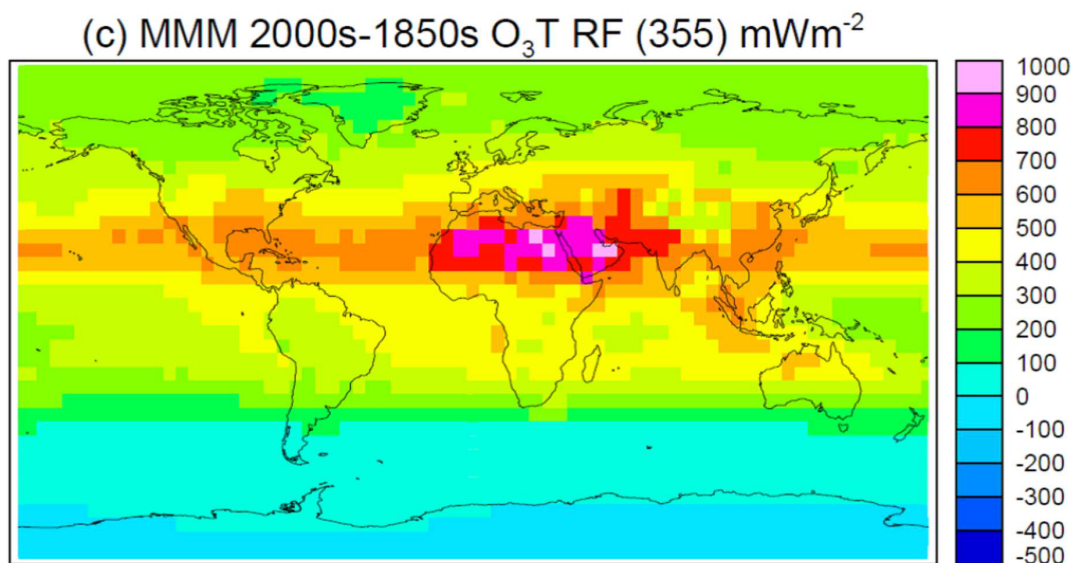


Figure 1.1 – Global distribution of annual mean RF of tropospheric O₃ between 1850–2000 (scale in mW/m², from the multi-model mean of the ACCMIP models, using the Edwards–Slingo radiation scheme (Stevenson et al., 2013). Figure from Monks et al. (2015).

produced anthropogenic pollution, and is transported from elsewhere (Dentener et al., 2010). The global or hemispheric background concentration of a pollutant refers to the atmospheric concentration of a pollutant due to natural sources only that is estimated by models applying various source apportionment techniques (Dentener et al., 2010). Transport of O₃ can occur between nearby regions, within a continent or even across continents (hemispheric) and is linked to the lifetime of O₃. O₃ lifetime varies depending on the environment and altitude; in environments with high concentrations of its precursors – nitrogen oxides (NO_x) and volatile organic compounds (VOCs) – O₃ has a short atmospheric lifetime of some hours; in the boundary layer it can live for 1-2 days, while in the free troposphere it can stay for several weeks (Stevenson et al., 2006; Young et al., 2013) making it possible to travel even across continents. Also, it can be produced from its precursors long after they have been emitted (Seinfeld and Pandis, 2016). Transport pathways follow the predominately westerly flows in the mid-latitudes, i.e. O₃ can travel from North America to Europe, from East Asia to North America, or even around the globe (Jacob et al., 1999; Jaffe et al., 1999; Lewis et al., 2007; Wild, 2007). Thus, besides its importance on a regional scale, it also influences air quality on a hemispheric scale (Akimoto, 2003; Dentener et al., 2010). Hemispheric transport of O₃ across continents is an important issue, because it can counteract efforts to reduce O₃ concentrations. For instance, increasing NO_x concentrations in East and South Asia have an influence on the air quality in western America (Cooper et al., 2010). In addition, flux of O₃ from the stratosphere to the troposphere, the so-called stratospheric-tropospheric exchange, affects O₃ variability, with a peak activity in May for northern mid-latitudes and a minimum in November (Hsu and Prather, 2009). This is especially noticeable at stations located at

higher altitudes (Cui et al., 2011; Ordóñez et al., 2007). Chemistry-climate models have been utilized to quantify baseline O₃ (Dentener et al., 2010), but due to different handling of several factors, such as lightning NO_x, biogenic emissions etc, differences amongst models are still large (Fiore et al., 2014). In Fig. 1.2 an example of a source attribution modeling study for O₃ concentrations at a rural site in southern England is shown. In the studied site two-thirds of the observed O₃ is attributed to large scale inter-continental transport, with North America being the main contributor, while the rest is of European regional origin (Derwent, 2008). A large portion of this polluted air that is produced outside of Europe will travel further into the European domain, contributing by a significant fraction to the local pollution concentrations. The contribution from transported O₃ is especially high during the cold period, when local O₃ formation is low. At the receptor site in Fig. 1.2 the contribution from background O₃ during summer is around 20 ppb, while during O₃ formation episodes O₃ concentrations in central and southern Europe reach and often exceed 60 ppb. Current legislation that could probably lead to reductions of NO_x and VOCs by between 50 to 75%, may reduce the regional scale O₃ contribution by almost 50% (Derwent, 2008).

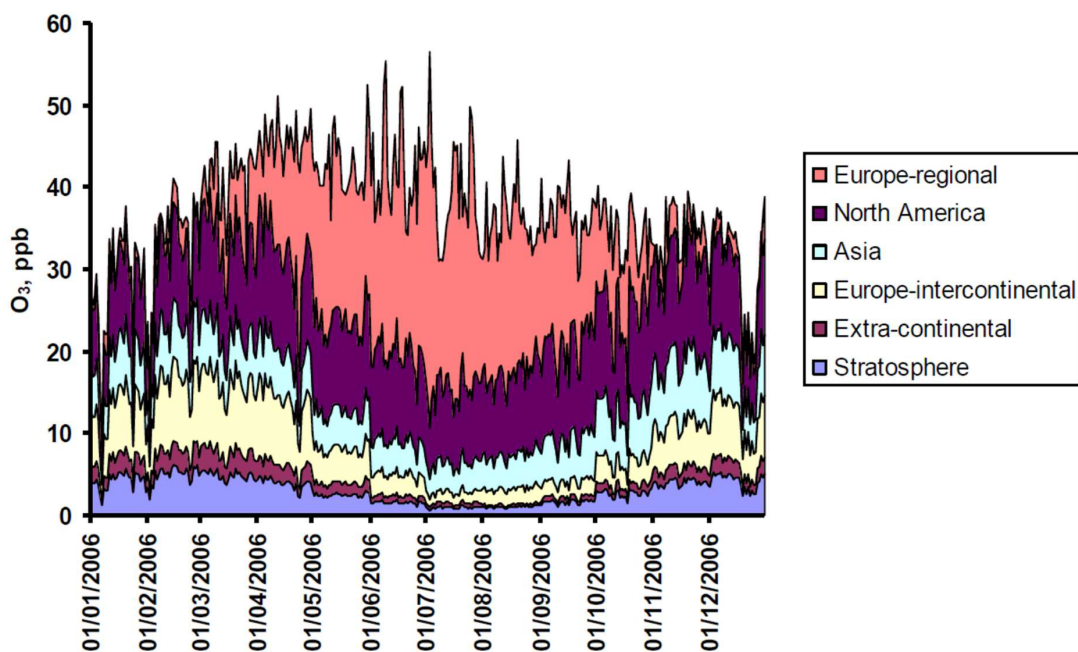


Figure 1.2 – Source attribution of the O₃ measured at a rural location in southern England during January 2006 (Derwent, 2008, averaged over the 12-month study period). Results are obtained by a global model coupled to a regional model (from Derwent (2008)).

Climate change can play a decisive role on O₃ levels, by modifying several factors. Higher temperatures affect O₃ concentrations through: (a) shorter lifetime of peroxyacetyl nitrate (PAN), (b) higher water vapor content in the atmosphere and (c) higher biogenic emissions of isoprene (Doherty et al., 2013; Jacob and Winner, 2009). More specifically, changes in temperature and water vapor modify the chemical environment and therefore affect the rates of chemical reactions that produce and deplete O₃ (Dentener et al., 2010). PAN is an

important reservoir species, that facilitates long-range transport of O₃ precursors. At higher temperatures, thermal decomposition of PAN occurs more often, decreasing the lifetime of PAN and eventually altering the long-range transport of O₃ (Schultz et al., 1998). Also, warmer temperatures are associated with increased water vapor content, that increases O₃ depletion, i.e. shortens lifetime of O₃ (Johnson et al., 1999). Finally, meteorological transport mechanisms (e.g. cyclonic activity, mid-latitude air-streams and stratosphere-troposphere exchange) can be altered through changes in climatic conditions (Doherty et al., 2013; Ordóñez et al., 2007), thus, the lifetime and concentrations of several air pollutants are influenced.

1.1 Tropospheric O₃ chemistry

O₃ that is produced in the troposphere accounts for approximately 4500 Tg/year, while influx from the stratosphere to the troposphere is estimated to around 540 Tg/year (The Royal Society, 2008). The O₃ budget, i.e. total amount of O₃ in the troposphere, is determined by two major processes: (a) production rate through chemical reaction with its precursors NO_x and VOCs and (b) chemical loss or destruction (around 4100 Tg/year) and dry deposition into the Earth's surface (around 1000 Tg/year) (Fig. 1.3) (Wild, 2007; Denman et al., 2007; Stevenson et al., 2006).

In general, O₃ is produced in the troposphere by photochemical reactions, that involve sunlight and anthropogenic and natural O₃ precursor gases, i.e. NO_x (= NO₂ + NO), non-methane hydrocarbons (NMHCs), methane (CH₄) and carbon monoxide (CO) (Maas and Grennfelt, 2016; Monks et al., 2015). A big part of O₃ in the troposphere is produced during the reactions 1.1 - 1.2). During these reactions, NO₂ is photolyzed by reacting with sunlight at wavelengths smaller than 424 nm (reaction 1.1), and the resulting ground-state oxygen atoms react with oxygen to produce O₃ (reaction 1.2).



where J_{NO_2} is the photolysis frequency of NO₂.



where M stands for any co-reactant, e.g. N₂.

The so called titration reaction, leads to depletion of O₃ and reproduction of NO₂ (reaction 1.3).



The photostationary state (reactions 1.1-1.3), which is reached within minutes, does not lead

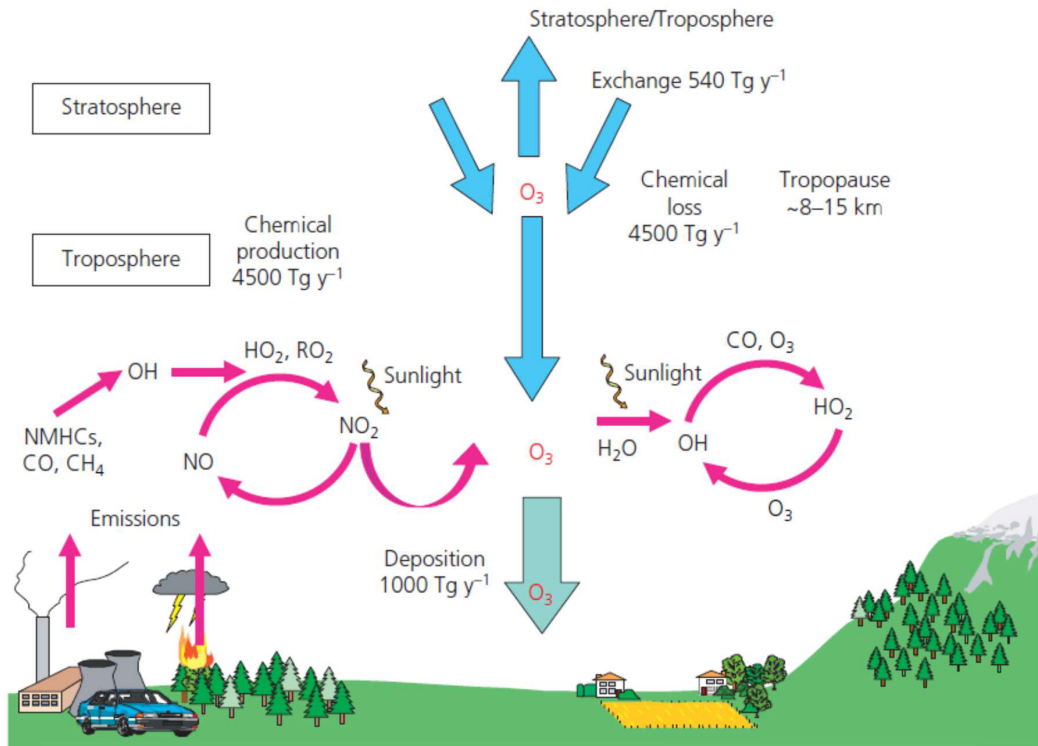


Figure 1.3 – Sources and sinks of tropospheric O₃. Numbers refer to annual global fluxes estimated by a global chemistry-transport model, i.e. stratospheric-tropospheric exchange, chemical production and loss, and deposition to terrestrial and marine surfaces. Source: IPCC Fourth Assessment Report Working Group I Report "The Physical Science Basis" (Denman et al., 2007).

to net O₃ production. O₃ concentration during the photostationary state is estimated as:

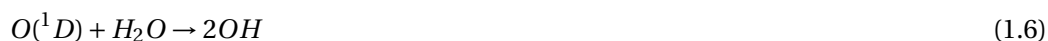
$$[O_3] = \frac{J_{NO_2} \cdot [NO_2]}{k \cdot [NO]} \quad (1.4)$$

where [O₃], [NO₂], [NO] are the concentrations of O₃, NO₂ and NO respectively.

In addition, O₃ photolysis is important in tropospheric chemistry, because it leads to production of the highly reactive OH, the so called "cleansing agent" of the troposphere. OH reacts with almost all trace gases in the atmosphere, making it the primary oxidizing species in the troposphere. More specifically, O₃ is photolyzed at wavelengths smaller than 320 nm to produce an electronically excited oxygen atom O(¹D) (reaction 1.5), which then reacts with water vapor to produce OH (reaction 1.6).



Chapter 1. Introduction



Net O₃ production occurs in the presence of VOCs, which are typically produced through industrial activities or emitted from biogenic sources. An example of the complex relationship between O₃, NO_x and VOCs is demonstrated in the following reactions 1.7-1.11, where R is an arbitrary hydrocarbon fragment. Note that OH plays a key role in O₃ formation in relation to VOC and NO_x concentrations. First, the hydrocarbon RH is oxidized by OH and forms an organic peroxy radical (RO₂) (reactions 1.7 and 1.8).



The RO₂ produced in reaction 1.8 reacts with NO, which results to NO₂ and an organic oxy radical (RO).



NO₂ photolyzes to produce O₃ (reaction 1.1 and 1.2), while RO oxidizes to produce HO₂ and carbonyl compounds (R'CHO) (reaction 1.10).



The resulting HO₂ reacts with NO producing NO₂ which again leads to O₃ formation, while the R'CHO may either photolyze to produce HO_x or react with OH to continue the chain propagation. The net reaction is the following:



Biogenic emissions of VOCs (e.g. isoprene) are an additional important factor for tropospheric O₃ levels, mainly through production of the hydroxyl radical (OH) (Simpson, 1995; Taraborrelli et al., 2012). Biomass burning especially leads to increased emissions of O₃ precursors such as CO, hydrocarbons (e.g. CH₄), PAN, as well as NO_x and ammonia (NH₃) (Seinfeld and Pandis, 2016). CO in particular plays a significant role in the production of O₃ through reaction with OH in the presence of NO, that leads to the net reaction 1.12.



The termination reaction (reaction 1.13) of the NO_x and HO_x radical chains oxidation cycle is important in environments with high NO_x concentrations, because it leads to reduced O₃

formation.



CH₄ is much less reactive toward OH and therefore less important compared to the other organic compounds for photooxidant pollution on regional scales. On the other hand as a hydrocarbon it is by far the most abundant, thus, CH₄ is also important on a global scale (West et al., 2006).

The VOC to NO_x ratio is an important factor to understand the interaction between O₃-VOC-NO_x. When VOC/NO_x is high, OH will mostly react with VOCs leading to peroxyradical formation. O₃ production is then reached through oxidation of NO to NO₂. If the ratio VOC/NO_x is low, OH reacts preferably with NO₂ forming HNO₃, which is a termination reaction suppressing O₃ formation. At a given initial VOC and NO_x concentrations OH reacts about 5.5 times more rapidly with NO₂ than with VOCs. In absence of NO_x emissions the VOC/NO_x increases with time, because of the fast reaction of NO₂ with OH. Eventually, VOC/NO_x will reach a point, where OH reacts preferably with VOCs to maintain the O₃ formation cycle.

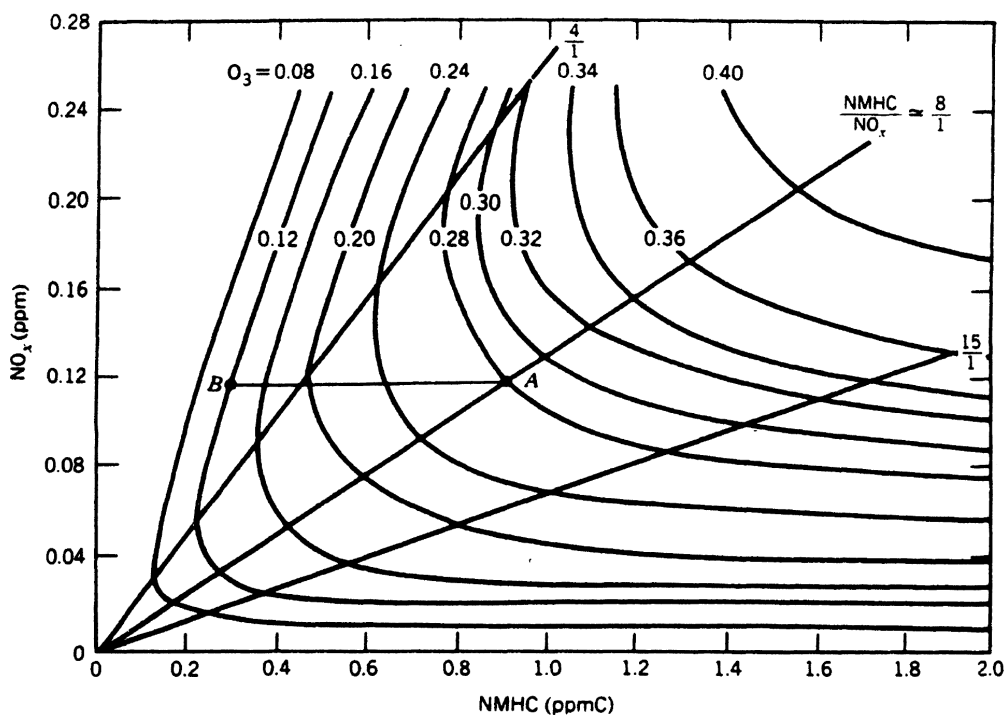


Figure 1.4 – EKMA diagram with O₃ isopleths. Adapted from Finlayson-Pitts and Pitts (1986).

In Fig. 1.4 isopleths of O₃ maximum mixing ratios that are reached for different combinations of initial VOC and NO_x concentrations are shown. The diagram is produced by box model simulations using the EKMA (Empirical Kinetic Modeling Approach) technique (Finlayson-Pitts and Pitts, 1986). The high NO_x limit (VOC-limited regime) is representative for urban

environments, where NO_x concentrations are high. According to the diagram, in this case O_3 formation rate increases with increasing VOC, but decreases with increasing NO_x . The latter happens because, with a further increase in NO_x , the termination reaction 1.13 becomes more important than the OH reaction, reducing this way O_3 formation. While moving from an urban to a suburban environment NO_2 concentration decreases by reacting with available OH. This way the ratio VOC/NO_x reaches a state where local O_3 production maximizes, which is called the transition regime. Further decrease of NO_x reduces O_3 production. In this low NO_x regime (NO_x -limited), which is representative for rural environments, O_3 formation rate increases with increasing NO_x .

1.2 O_3 variability and meteorological influence

O_3 concentrations are governed by various meteorological and atmospheric processes, such as reactions rates, dry and wet deposition, long-range and local transport mechanisms etc. (Camalier et al., 2007; Davis et al., 1998; Bloomfield et al., 1996; Flaum et al., 1996). Initially, solar radiation triggers photochemistry reactions that produce O_3 (see section 1.1, reactions 1.1, 1.5, 1.12), while increasing temperature increases O_3 concentrations. Temperature and solar radiation affect biogenic emissions of VOCs, which in turn enhance O_3 production. Concurrently, strong winds result in dilution of precursors and O_3 , reducing O_3 concentrations. Strong (reduced) vertical mixing leads to smaller (stronger) accumulation of precursors and O_3 at the surface. Finally, increased dry and wet deposition act to reduce O_3 , especially at shallow boundary layer conditions.

The above interactions result in O_3 variabilities at different time scales, such as diurnal due to temperature daily cycle or inter-annual which is driven by the annual cycle of solar radiation that leads to the observed pattern with high concentrations in summer and low in winter. In addition, O_3 formation is favored by specific short-term meteorological conditions, e.g. stagnant weather conditions. Large part of O_3 variability is influenced by seasonal meteorological variations, for instance the heat wave of 2003 in Europe led to persistently elevated values of O_3 (Yan et al., 2017; Schnell et al., 2014; Carro-Calvo et al., 2017).

The main influencing meteorological factor for O_3 is temperature, mainly through increasing rate of reactions that produce O_3 (Bloomfield et al., 1996). In addition, high temperature conditions lead to higher emissions of biogenic VOCs and enhance the thermal decomposition of PANs; both VOCs and PANs contribute to more O_3 production. (Dawson et al., 2007; Sillman and Samson, 1995; Vogel et al., 1999; Bärtsch-Ritter et al., 2004). However, there are indications that the sensitivity of O_3 to temperature has changed in the last 20 years due to strong NO_x emission reductions. Indeed, it has been found that O_3 climate penalty ($d\text{O}_3/dT$) reduced from 3.2 ppbv/ $^{\circ}\text{C}$ to 2.2 ppbv/ $^{\circ}\text{C}$ in the U.S. (Bloomer et al., 2009) .

Boundary layer height affects O_3 concentrations by vertical mixing in two ways. On the one hand, a shallow boundary layer (stable atmospheric conditions) reduces vertical mixing, which leads to accumulation of precursors and O_3 , thus, to higher O_3 concentrations at the surface.

On the other hand, O₃ is reduced by dry deposition in a shallow boundary layer, especially during night.

Wind velocity and direction strongly influence O₃ concentrations, because e.g. increased wind velocity usually dilutes O₃ and its precursors (Solberg, 2009; Ordóñez et al., 2005; Pearce et al., 2011). Nevertheless, the effect of wind is variable amongst different locations. For instance, depending on the wind direction and the station topography, increased transport of O₃ or its precursors downwind from nearby emission sources might lead to increased O₃ levels.

Another important factor influencing O₃ concentrations is air humidity. More precisely, increased water vapor content in the atmosphere enhances production of hydroxyl radicals (OH), which leads to higher O₃ production in environments with high NO_x emissions (Vogel et al., 1999; Seinfeld and Pandis, 2016). On the other hand, high water vapor is connected to more cloudiness, thus, might lead to lower O₃ concentrations.

Moreover, synoptic weather patterns affect O₃ levels. The more prominent synoptic patterns are high-pressure systems that are associated with increased incoming solar radiation, high temperatures, and stagnant air conditions (National Research Council (1991), Chapter 4), thus, less convective mixing, lower temperature inversion layer, and reduced wind velocities. The above weather conditions lead to accumulation of O₃ and its precursors in the atmospheric boundary layer (Thompson et al., 2001). Moreover, warm conditions with less cloudiness are favorable for increased photochemical production of O₃ (Thompson et al., 2001).

Finally, O₃ concentrations exhibit a weekly cycle driven by traffic emissions, which are higher during weekdays and lower in the weekend. Especially NO, which mainly originates from local emissions, is reduced on Sundays by around 30-60% in Switzerland (Brönnimann and Neu, 1997). In general, under favorable weather conditions for O₃ formation, O₃ peaks are lower on Sundays than weekdays, but, under unfavorable weather conditions weekend peak levels are higher than in the weekdays (Brönnimann and Neu, 1997). The observed decrease during the weekend is explained by reduced emissions of NO₂ and VOCs, thus, less O₃ production. The increase during the week is attributed to increased NO_x emissions and at the same time to O₃ accumulation. The inverted pattern, i.e. increase in weekend, can be attributed to reduced O₃ titration due to lower NO emissions.

1.3 Motivation

It has been reported that O₃ concentrations at remote, rural regions in Europe have almost doubled between the 1950s and 1990s due to increasing emissions of the O₃ precursors NO_x and VOCs (Staehelin et al., 1994; Cooper et al., 2014; Parrish et al., 2012). In the 1990s emission control legislation was enacted in Europe to regulate air pollution, mainly with measures applied to vehicles and industries. For instance, the Gothenburg Protocol, was enforced in 1999 (with a revision in 2012) to tackle acidification, eutrophication and ground-level O₃, by reducing emissions of NO_x, VOCs, sulfur dioxide (SO₂) and NH₃. As a result, NO_x

and VOC emissions decreased across most part of Europe (Fig. 1.5) (EMEP, 2017; Vestreng et al., 2009; Colette et al., 2011; Guerreiro et al., 2014; Henschel et al., 2015; Granier et al., 2011); Downward trends of NO₂ concentrations were also observed, especially in urban areas except in southeastern France and northern Italy (Colette et al., 2011). On the other hand, O₃ concentrations moderately increased especially in urban areas (Colette et al., 2011). As shown in Fig. 1.6 for rural sites across Europe, annual mean O₃ has increased since 1990 and started to stabilize with signs of a decrease after the mid-2000s (EMEP, 2017).

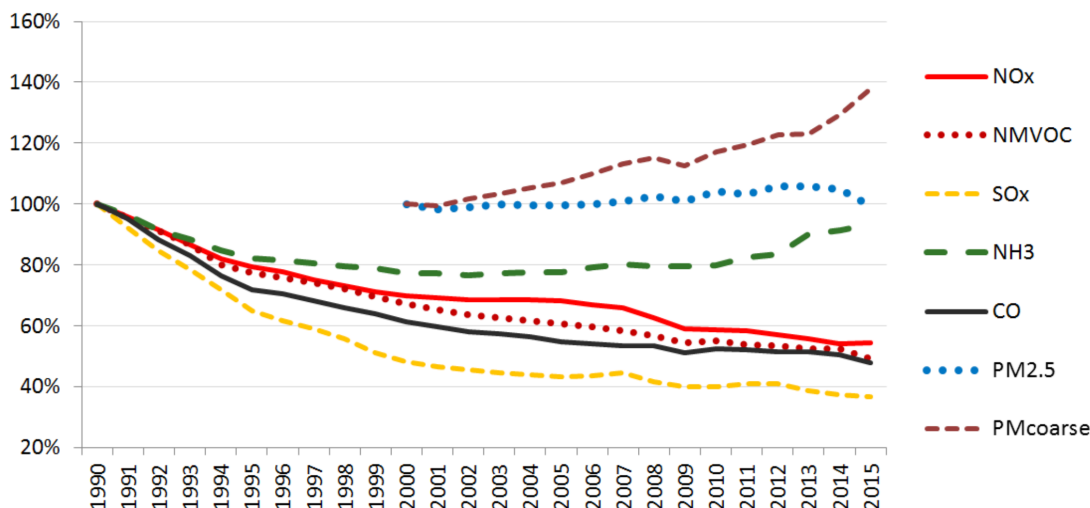


Figure 1.5 – Emissions trends in the EMEP area (including stations in most parts of Europe with scarce network in the southern and eastern countries) based on data reported by countries and gap-filled with expert estimates (shipping emission are not included, figure from EMEP (2017)).

At the same time, peak O₃ has decreased in the period 1990-2012 (EMEP, 2017). Especially during the summer season O₃ concentrations reach high values in Europe, due to high concentrations of O₃ precursors and favorable weather conditions (e.g. Querol et al., 2016). Guidelines for maximum O₃ values, as expressed e.g. by the World Health Organization (WHO, 100 $\mu\text{g}\cdot\text{m}^{-3}$ for the 8 hour running mean) or the European air quality standard (120 $\mu\text{g}\cdot\text{m}^{-3}$ for the maximum daily 8 hour running mean (MDA8)) (WHO, 2006; European Environmental Agency, 2015), are regularly exceeded.

Long-term trends estimation methodologies for ambient O₃ concentrations are often obfuscated by the effects of meteorology on O₃ formation, accumulation, and destruction (National Research Council, 1991). This is due to the strong meteorologically driven intra- and inter-annual variabilities of O₃, which lead to a high uncertainty in the calculated O₃ long-term trends. These high uncertainties obfuscate the true magnitude of the trend or possibly even affect the sign of the trend. This means that the effect of precursors emissions regulations can be masked by the effect of meteorology on O₃ concentrations. Thus, meteorological adjustment of O₃ concentrations is important in order to isolate the effect of measures taken on air quality (Camalier et al., 2007). Ordóñez et al. (2005) have highlighted the importance

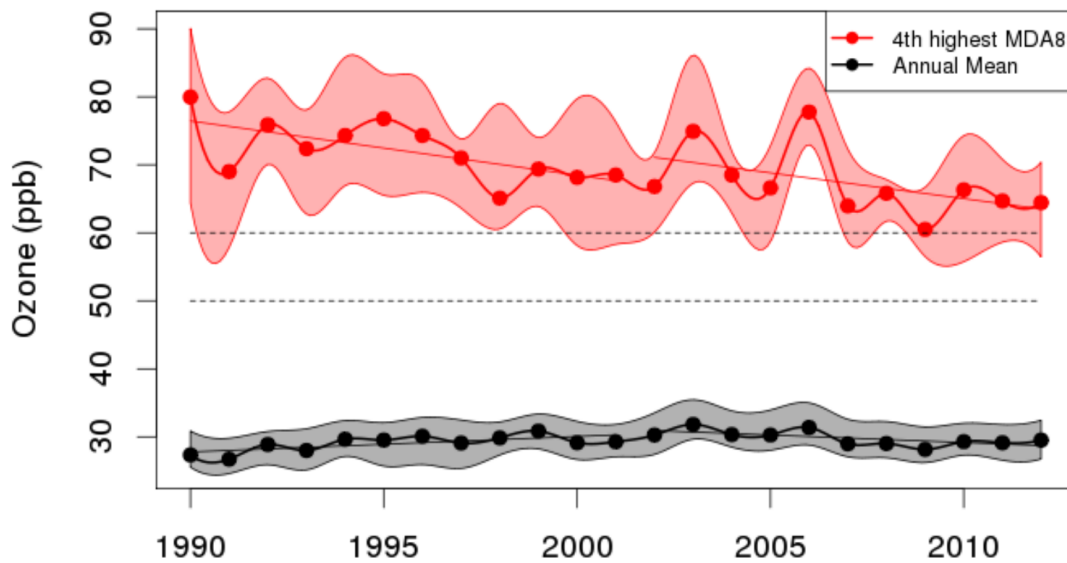


Figure 1.6 – Composite of annual mean O_3 (black) and 4th highest MDA8 (red) O_3 recorded at 55 EMEP rural monitoring sites between 1990 and 2012. The thick line is the network-wide annual median and lower/higher bounds of the shaded areas are for the 25th and 75th percentiles. Thin straight lines show the linear trend over the 1990-2001 and 2002-2012 periods and dashed lines indicate the WHO air quality guideline (50 ppb) and the EU long term objective (60 ppb). Source: EMEP, Co-operative Programme for Monitoring and Evaluation of the Long-Range Transmission of Air Pollutants in Europe (2016).

of the meteorological influence on maximum values of O_3 , which are especially relevant for public health issues.

Considering spatial variability in O_3 trend analyses is complicated due to various geographical factors that govern the temporal evolution of O_3 . Site type identification (rural, urban or suburban) alone is often not enough to interpret O_3 trends, because precursors emissions might vary greatly even among same site types. Implementation and development of air policy measures is sometimes different between countries, while meteorological and climatic influence is variable across large domains. Thus, investigation of the behavior of O_3 trends on large spatial scales requires identification of appropriate site groups in terms of O_3 concentrations features. Classification of sites based on clustering algorithms serves in identifying groups of sites with similar characteristics. So far, clustering techniques applied to measurements either have resulted in either site type or geographical classification (e.g. Lyapina et al., 2016; Carro-Calvo et al., 2017).

Chemistry-climate models are generally skillful, but they are often consistently biased when deriving O_3 long-term trends (e.g. Young et al., 2018; Gaudel et al., 2018). In general, models tend to overestimate O_3 mixing ratios, they often reproduce a small part of the observed seasonal variability, and capture approximately 25 to 45% of the observed long-term trends

(Parrish et al., 2014). Therefore, present-day O₃ might be underestimated as well as predictions of future concentrations. In addition, air-quality models have limitations in reproducing the relationship of tropospheric O₃ to some influential meteorological variables, e.g. temperature, relative humidity and solar radiation, but this varies amongst different regions (Otero et al., 2018). Im et al. (2015) reported a tendency to under-prediction of high O₃ concentrations, while in the report by Solberg (2009), trends of peak O₃ concentrations in Switzerland have been overestimated in model simulations. The above statements point out the importance of reliable trend analyses based on observations apart from modeling studies.

1.4 Scientific questions and approach

This PhD project is focused on studying the temporal trend of tropospheric O₃ concentrations in Switzerland and across Europe. The main goal is to describe and understand the response of O₃ to the reductions of its main precursors, NO_x and VOCs, after the implementation of air quality policy measures in Europe starting in the 1990s. The variable effect of meteorology on O₃ on different time scales increases the uncertainty in trend estimation methods. In addition, variability of O₃ concentrations due to climatic and meteorological conditions vary significantly between measuring stations in larger geographical domains.

The following scientific questions are addressed in this thesis:

1. How can we reduce uncertainty in O₃ trend estimation?
2. How can we reliably adjust O₃ observations for the effect of meteorology?
3. How did O₃ trends evolve at different site environments after reduction of precursors?
4. How are O₃ trends influenced by regional meteorological features?

Specifically, we study long-term trends of O₃ using high-quality surface measurement data and using sophisticated statistical methods. Long-term observational data from Swiss sites were used for the time period 1990-2014 and at European sites for the time period 2000-2015.

Adjustment of O₃ concentrations for the effect of meteorology is applied, which allows an earlier detection of significant trends and investigation of the effect of the air quality policy measures. Influence from different factors is reflected in the underlying variations in O₃ measurement data, such as local pollution sources and meteorological variations. The effect of precursors emissions changes can be seen in the long-term signal, as well as other factors such as hemispheric transport of pollutants and stratospheric-tropospheric exchange. The meteorological influence is depicted in the seasonal and short-term O₃ variations. In our approach, we decompose O₃ observations into the long-term, seasonal and short-term variations. A non-parametric time-scale decomposition algorithm is applied for this purpose to the measurements time series. Subsequently, the seasonal variability is removed from

the observations in order to adjust for inter-annual meteorological influence. Finally, the long-term trend is estimated based on the de-seasonalized O₃ time series, which results in reduced uncertainty range in the trend. Furthermore, because O₃ trend has changed after 2000s from increasing to decreasing, long-term trend estimation was done in two separate time periods to avoid under- and overestimation of the true trend in the beginning and at the end of the studied period respectively. Thus, the inflection point in the temporal evolution is detected and the trend is calculated for the two separate consecutive periods. The trend analysis for the two regimes addresses the non-monotonic temporal evolution of O₃.

Peak O₃ concentrations are driven by specific, localized meteorological conditions that favor O₃ formation. Therefore, peak O₃ concentrations are meteorologically adjusted by focusing only on conditions that lead to high O₃ events. Meteorological variables are often interconnected, such as temperature and solar radiation or humidity and cloud cover. Due to these interactions, separation of their impact on O₃ is complex. Therefore, a model for each measurement site is developed based on the meteorological variables that have the highest impact on maximum O₃ concentrations and account for interaction effects between the variables. More robust statistical models are built by this way, that explain the influence of the meteorological variables that were found to have a significant effect on O₃. The meteorological influence is removed from O₃ observations, leading to a targeted adjustment only on the specific days of the peak O₃ events.

A site type classification was performed for Switzerland based on the mean absolute NO_x concentration at the studied sites. However, on larger domains a direct classification of sites based only on site type is not sufficient, due to lack of knowledge of special local characteristics. Thus, to investigate the effect of the distance from emission sources as well as the climatic conditions on O₃ long-term trends in the European domain, a different classification approach was applied. A clustering technique was applied to the O₃ long-term and seasonal variations to classify sites based on their site type and the geographical location. We apply a multi-dimensional clustering approach based on the distinct frequency signals extracted from the observations, i.e. long-term and seasonal. The classification of stations with high similarity in O₃ temporal evolution facilitates the study of the long-term trends.

Finally, to study the effect of NO_x and VOC concentration reductions on O₃ inter-annual variability, we investigate temporal changes of the seasonal variation of O₃. The amplitude of the seasonal variability of O₃ is studied, by estimating the trend of the seasonal variation extreme (maximum and minimum) concentrations. The day of the seasonal maximum value is also identified over the studied time period, which represents the phase of O₃ inter-annual cycle.

2 Ozone time scale decomposition and trend assessment from surface observations in Switzerland.

Eirini Boleti^{1,2}, Christoph Hueglin¹ and Satoshi Takahama²

Published in Atmospheric Environment: <https://doi.org/10.1016/j.atmosenv.2018.07.039>

¹Empa, Swiss Federal Laboratories for Materials Science and Technology, Überlandstrasse 129, Dübendorf, Switzerland

²EPFL, École Polytechnique Fédérale de Lausanne, Route Cantonale, 1015 Lausanne, Switzerland

Abstract: Regulation for ozone (O₃) precursor emissions began in Europe around 1990 with control measures primarily targeting industries and traffic. To understand how these measures have affected air quality, it is important to investigate the temporal evolution of tropospheric O₃ concentrations in different types of environments. In this study, we analyze long-term trends of the concentrations of O₃ and the sum of oxidants O_x (O₃ + NO₂) in Switzerland for the last 25 years. Statistical decomposition of the observed time series is used to extract the underlying time scales, i.e. the long-term, seasonal and short-term variability. This allows subtraction of the seasonal variation of O₃ and O_x from the observations and estimation of long-term changes of de-seasonalized O₃ and O_x with reduced uncertainties. A two-regime trend calculation based on the long-term variability accounts for non-monotonic temporal evolution of O₃. In addition, adjustment of the higher frequency meteorological influence was applied, based on the time series containing the short-term variability. This led to an uncertainty reduction in the trend estimation, but only by a small factor. We observe that, despite the implementation of regulations and reduction of nitrogen oxides concentrations, for all studied sites daily mean O₃ values increased until mid-2000s. Afterwards, a decline or a leveling-off in the concentrations is observed. The start of change in the trend depends on the site type; the more polluted the site, the later is the onset of the change in trend behavior. At

Chapter 2. Ozone time scale decomposition and trend assessment from surface observations in Switzerland.

locations close to sources, the observed trend can mainly be explained by the reduced titration of O₃ by NO due to the strong reductions in nitrogen oxides emissions. At remote locations (such as the high alpine station in Jungfrauoch) that are influenced by hemispheric transport of O₃ an increase during 1990s and a decline after early 2000s is observed. The calculated temporal trends exhibit distinct differences depending on the characteristics and pollution burdens of the measurement sites; such differences have become smaller following emission reductions.

2.1 Introduction

Tropospheric ozone (O₃) is an important trace gas for air quality and is recognized as a threat for human health and agriculture (WHO, 2013; LRTAP Convention, 2015; National Research Council, 1992). It also acts as a greenhouse gas with globally averaged radiative forcing $0.4 \pm 0.2 \text{ W/m}^2$ (IPCC, 2013). O₃ either originates naturally in the stratosphere (Junge, 1962; Stohl et al., 2003) or is produced in the troposphere by photochemical reactions. These reactions involve sunlight and anthropogenic and natural O₃ precursor gases, in particular nitrogen oxides (NO_x = NO₂ + NO), volatile organic compounds (VOCs), methane (CH₄) and carbon monoxide (CO) (Maas and Grennfelt, 2016; Monks et al., 2015). Biogenic emissions are also known to have a positive effect on production of tropospheric O₃ mainly through reduction of the hydroxyl radical (OH) (Simpson, 1995). Emissions of O₃ precursors, NO_x and VOCs, have been declining in Europe and the U.S. since the 1990s due to implementation of emission control measures (Colette et al., 2011; Guerreiro et al., 2014; Henschel et al., 2015; Granier et al., 2011). For example, the Gothenburg Protocol, implemented in 1999 and revised in 2012, tackles acidification, eutrophication and ground-level O₃ in Europe, through reduction of emissions of NO_x, VOCs, sulfur dioxide (SO₂) and ammonia (NH₃). Colette et al. (2011) calculated air pollutant trends for the period 1998-2007 and observed a decrease in NO₂ concentrations across most of Europe, which is more pronounced in urban areas. In addition, VOC and NO_x emissions have decreased by 40% and 35% respectively in the European Union (Maas and Grennfelt, 2016). In Switzerland, emissions of NO_x and VOCs peaked in the mid- or late 1980s and decreased by around 30-40% in the 1990s (BAFU, 2016; Stiller et al., 2000). Since the beginning of the 2000s their decrease has been less pronounced (BAFU, 2016). Due to emission reductions of O₃ precursors, it was expected that O₃ concentrations across Europe would decline as well, as has been supported by trend estimates since 2000 (Chang et al., 2017). However, mean concentration of tropospheric O₃ in Europe was increasing in the 1990s and early 2000s (Wilson et al., 2012). Therefore, it is important to investigate and understand how tropospheric O₃ levels have changed over the last decades.

As stated in the report of the European Environmental Agency (EEA), observed O₃ trends suffer from large uncertainties associated with current trend analysis practices (Guerreiro et al., 2016). The investigation of long-term trends of O₃ due to policy decisions is obfuscated by its strong intra- and inter-annual variability. Analysis of annually-averaged concentrations eliminates the intra-annual variability on the trend estimate, but this leads to a loss of statistical

sample size and the influence of inter-annual variability occurring on shorter timescales than the desired trend signal remains. A solution to this problem is to decompose the observed O_3 concentrations into the underlying frequency modes (Chang et al., 2017); trends can be calculated from the long-term and de-seasonalized signal isolated by this approach. Additional variability that occurs on shorter time scales due to meteorological factors can be subject to statistical adjustment for refined trend analysis.

The main goal of this study is to describe and understand the response of O_3 to the reductions of NO_x and VOCs after implementation of measures since the 1990s. Thus, long-term observational data from Swiss sites were used for investigation of the temporal trends in surface O_3 and the sum of oxidants O_x ($O_x=O_3+NO_2$) for the last 25 years. In our approach, a time-scale decomposition is applied on the available time series in order to identify the underlying contributions from the long-term, seasonal and short-term variability. The seasonal variability is removed from the observations to obtain the de-seasonalized O_3 time series. Guided by the measurements, a two-regime trend analysis is used to address non-monotonic temporal evolution of O_3 . The specific for each station date of change in the trend is assessed via the long-term variability, and the trend is calculated in two separate periods. In addition, the short-term variations of O_3 and O_x are correlated with meteorological parameters of the same time scale to adjust the observations for the influence of meteorological conditions. The methodology is discussed in detail in Section 2.3, and the results are presented in Section 2.4.

2.2 Data

Measurements were provided by the regulatory air quality monitoring networks operated by the Swiss federal and cantonal authorities at 1-hour resolution between 1990 and 2014. The stations used for this study have a data availability of more than 95% (Table 3.1 and Fig. 2.4), and the metrics considered are the following: daily mean, daily maximum of 8 hour running mean of hourly O_3 concentrations (MDA8, European Parliament and Council of the European Union, 2008), and daily mean of O_x . Note that this study is focused on daily average O_3 and O_x concentrations, a complementary study focusing on the trend of daily peak O_3 is under preparation (Boleti et al., 2018b). The decomposition method used here requires complete time series and therefore gap filling is needed in order to proceed. Missing values in the data set are treated as follows: (a) an average year is calculated from the mean values of the observed concentrations for each calendar day, (b) the positions of the missing values are identified, and (c) filled with the corresponding value from the calculated average year. Percentages of missing values vary between 0.32-4.27% and number of successive missing values in the data are between 4-16 days (except for Tänikon and Grenchen 40 days, Jungfrauoch 43 days and Thônex-Foron 92 days).

For the meteorological adjustment of O_3 , information for several meteorological variables was taken from measurements at the respective site and includes: temperature ($^{\circ}C$), humidity (%), solar radiation ($W \cdot m^{-2}$), surface pressure (hPa), wind velocity ($m \cdot s^{-1}$) and precipitation

Chapter 2. Ozone time scale decomposition and trend assessment from surface observations in Switzerland.

(mm). For data sets with more than 5% and /or more than 30 successive days of missing values, meteorological data were taken from nearby sites operated by MeteoSwiss. Otherwise, missing values during less than 5% of the time and/or less than 30 continuous days were replaced by linear interpolation. For the stations in Frauenfeld and Grenchen, no complete meteorological information was available; therefore, only the de-seasonalization approach was applied without further meteo-adjustment. For a more complete description of the meteorological situation, additional meteorological variables were derived from the European reanalysis data-set (ERA-Interim) (Dee et al., 2011) in 1 degree resolution at the location (longitude-latitude-altitude) of each station, i.e. boundary layer height (m), convective available potential energy (CAPE, $\text{J} \cdot \text{kg}^{-1}$), sensible surface heat flux ($\text{W} \cdot \text{m}^{-2}$) and total cloud cover. Additionally, we considered the synoptic situation as a meteorological variable, provided as weather type classifications (WTCs, Weusthoff, 2011) from MeteoSwiss, that describe recurrent dynamical patterns. The categories include classification with 3×8 wind directions (cyclonic, anticyclonic and indifferent) and low/high pressure based on mean sea level pressure, which yields 26 different synoptic patterns. All meteorological variables, both observations and derived variables, are used in daily average resolution.

2.3 Methods

The procedure applied in the present trend analysis consists of the following steps: 1) decomposition of daily mean O_3 , MDA8 and daily mean O_x observations for each station into the underlying frequencies and calculation of long-term, seasonal, and short-term variation, 2) subtraction of the seasonal variation from the observations and calculation of the absolute trend (in ppb per year) on the de-seasonalized time series, 3) decomposition of meteorological variables into long-term, seasonal, and short-term variation and 4) adjustment of the observations for the short-term meteorological influence and calculation of trends based on the meteo-adjusted time series. The extracted long-term variability shows for most stations a change in sign after mid-2000s, and the exact time of change appears to be different for each station. For this reason, at sites where this change occurs, the slopes are calculated in two regimes, the period before and after the change, first and second period respectively. In the following, we present in detail the steps and methods performed for the current trend analysis.

2.3.1 De-seasonalized trends

The de-seasonalization of O_3 observations first requires the extraction of a representative seasonal signal. For this reason, a time scale decomposition was performed based on both a non-parametric and a parametric method. Similar to Kuebler et al. (2001), this decomposition assumes that the signal can be viewed as

$$y(t) = LT(t) + S(t) + W(t) + E(t) \quad (2.1)$$

where $y(t)$ are the observations, $LT(t)$ stands for the long-term variation, $S(t)$ the seasonal variation, $W(t)$ the short-term variation, and $E(t)$ the remainder of the decomposition. $LT(t)$ represents variations at multiannual timescales, $S(t)$ variations at monthly to yearly timescales, and $W(t)$ variations at daily to monthly timescales.

De-seasonalization with non-parametric approach

The non-parametric time scales decomposition was performed with the ensemble empirical mode decomposition (EEMD, Huang et al. (1998); Huang and Wu (2008); Wu and Huang (2009)). The method resolves the non-overlapping frequencies contained in the signal into a number of components. Each component represents a distinct frequency, from highest to lowest, that is hidden in the original signal. This procedure was performed using the *hht* library in R (R Development Core Team, 2017). The long-term, seasonal and short-term variabilities were obtained by combining the associated frequencies.

The choice of the EEMD as a decomposition method is based on the fact that EEMD, in contrast to other methods (e.g. Fourier transformation), is entirely data driven. This formulation means that the results do not rely on a priori assumptions regarding the nature of the data (e.g. stationarity, periodicity). In addition, the basis functions are not predefined but extracted directly from the data (Huang and Wu, 2008). Therefore, EEMD is considered an appropriate method for the analysis of non-linear and non-stationary time series.

The core of EEMD is the empirical mode decomposition (EMD, Huang et al., 1998; Huang and Wu, 2008). In EMD, a number of so-called intrinsic mode functions (IMFs) are calculated, with each of the IMFs representing one distinct frequency in the signal. Consequently,

$$y(t) = \sum_{j=1}^n c_j + r_n \quad (2.2)$$

where $y(t)$ is the input data, c_j the different IMFs, and r_n the remainder of the decomposition.

The IMFs are calculated through an iterative sifting process (Fig. 2.1). First, the maxima and minima of $y(t)$ for each period in the signal are identified, and cubic splines are fitted to these extrema to form an upper and a lower envelope, representing the maxima and minima respectively. Then the mean of the upper and lower envelopes is calculated (m_1) and subtracted from the input data, leading to the first protomode (h_1). The first protomode serves as the input data for the second iteration, and the procedure is repeated k times until the following stopping criteria are fulfilled: (a) the number of extrema and the number of zero crossings are equal or differ by at most one, and (b) the sum of the envelopes that define the local extrema is zero. After k iterations,

$$h_{1(k-1)} - m_{1k} = h_{1k} \quad (2.3)$$

and, eventually, the h_{1k} will be the first IMF that contains the highest frequency. Next, the first

Chapter 2. Ozone time scale decomposition and trend assessment from surface observations in Switzerland.

IMF is subtracted from the original time series. The resulting signal is used as the input for the next sifting process, which leads to extraction of the second IMF of lower frequency (h_{2k}). This procedure results in a number of IMFs and a residue. The decomposition stops when the remaining series is a monotonic function or has only one extreme.

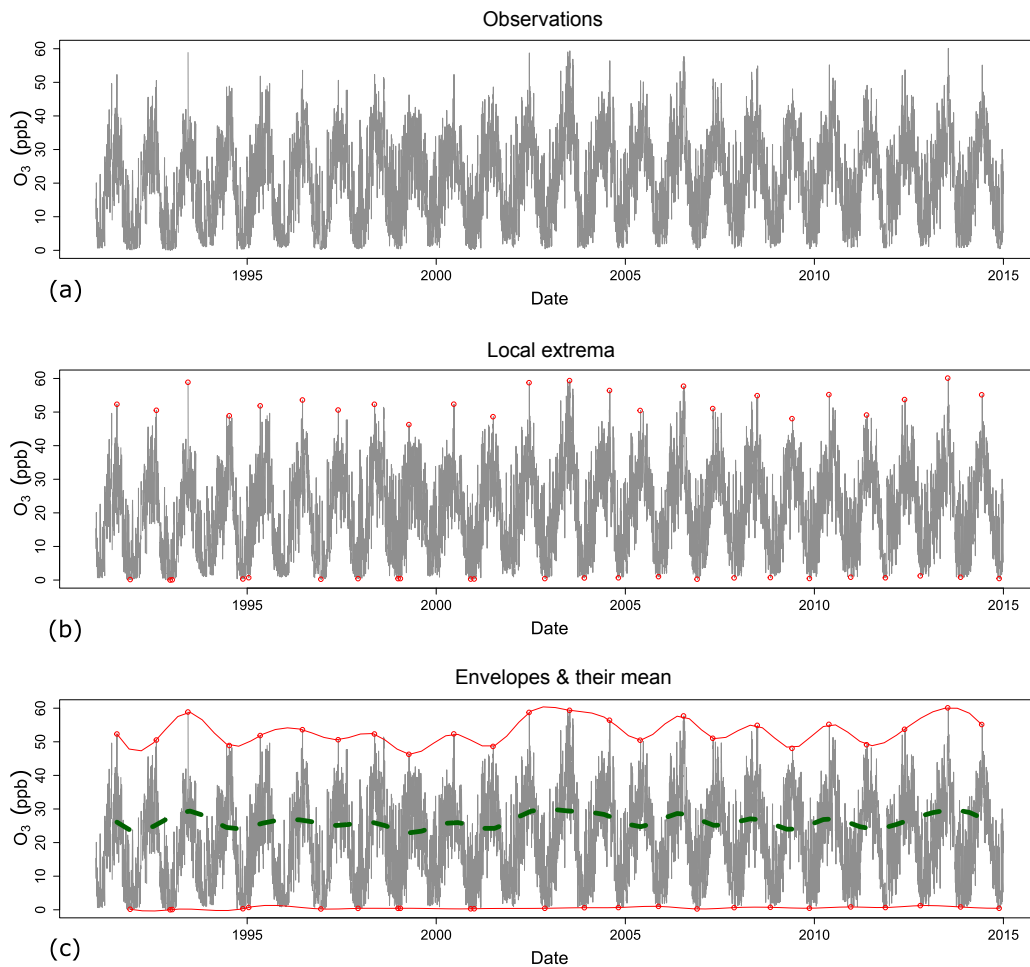


Figure 2.1 – Example of the procedure for calculating an IMF for daily mean O₃ concentrations (data set from Dübendorf). Red dots show the local extrema of the signal and red lines the fitted envelopes based on these extrema. The green dashed line is the mean of the upper and lower envelope.

EMD has some serious drawbacks in interpreting the physical meaning of the IMFs, caused by mode mixing, i.e. mixing of different frequencies in the same IMF. Therefore, the updated method EEMD is proposed by Wu and Huang (2009). In EEMD, the final IMFs are calculated as the ensemble mean of a sufficient number of EMD trials, where white noise has been added to the signal at each trial. The amplitude of the added white noise and the number of trials required were investigated and results are presented in the Appendix A. In our case 150 trials were found to lead to robust solutions, and this number was used for all EEMD analyses in this

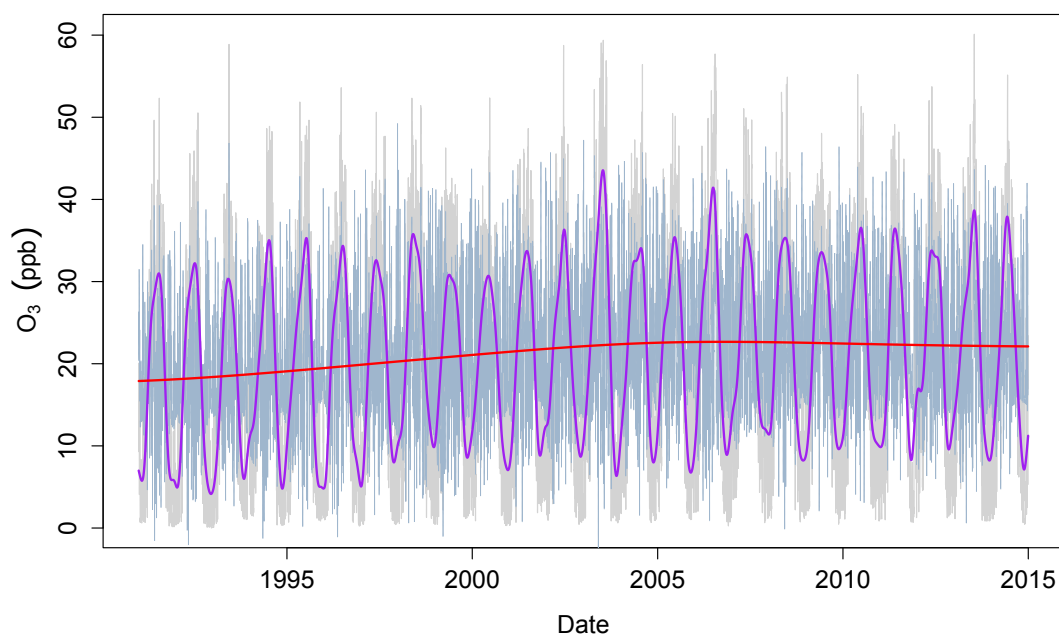


Figure 2.2 – EEMD results for daily mean O₃ concentrations in Dübendorf, a suburban background site. Shown is the daily mean observations (gray line), the long-term variation (red line) yielded from the residue of the EEMD, the seasonal variation (purple line) by adding together the IMFs 7-11 and the short term variation (light blue line) from the IMFs 1-6. For illustration reasons, the long-term signal was added to the seasonal and short-term signals.

study. The frequencies of the IMFs were obtained by means of periodograms (see Appendix A). The IMFs with periods between approximately 3 days and 3 months (IMFs 1-6) have been merged to represent the short-term variation with a resulting period of around 50 days. Periods between approximately 3 months and 3 years (IMFs 7-11) represent the seasonal variation with a period of around 11-12 months. Finally, the residue of the EEMD represents the long-term variation with a period longer than 3 years (Fig.2.2). The observed increase in O₃ long-term trend during the 1990s and the decrease after mid-2000s in the case of Dübendorf prevails in almost all studied sites. Therefore, a two-regime trend approach will be used here as the basis for identifying trends in two separate time periods with a breakpoint in between, i.e. the date where the change in the trend occurs.

De-seasonalization with parametric approach

To validate and compare the results based on the EEMD, the time scale decomposition was additionally performed using a parametric approach. This procedure was carried out by fitting the sum of harmonic functions and polynomial terms to the observations (Thoning et al.,

Chapter 2. Ozone time scale decomposition and trend assessment from surface observations in Switzerland.

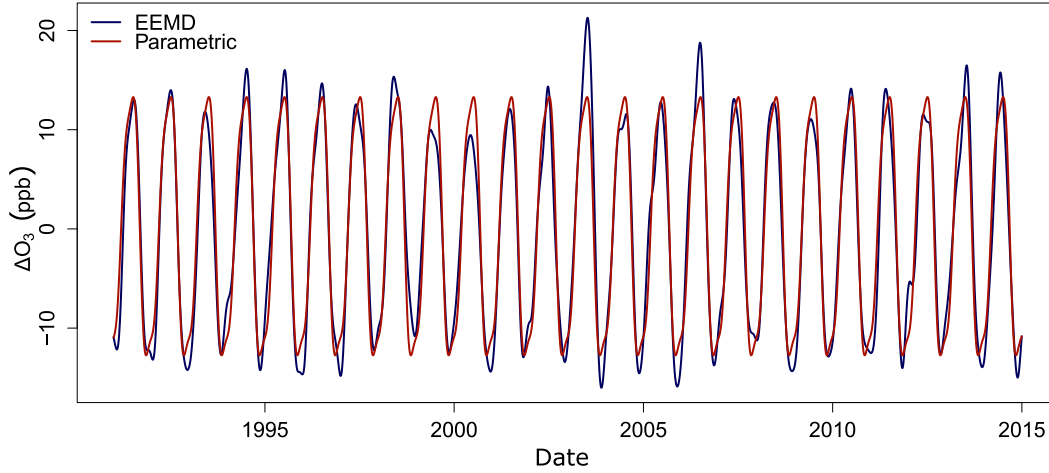


Figure 2.3 – Seasonal variation signals for daily mean O₃ concentrations in Dübendorf, obtained from the EEMD and from the parametric approach.

1989; Novelli et al., 1998). More precisely, the long-term variation is represented by

$$LT(t) = c_1 \cdot t + c_2 \cdot t^2 + c_3 \cdot t^3 \quad (2.4)$$

and the seasonal variation is estimated by

$$S(t) = \sum_{i=1}^3 [a_i \cdot \sin(2\pi t) + b_i \cdot \cos(2\pi t)], i = 1 - 3. \quad (2.5)$$

c_i are the coefficients of a third-degree linear fit on the data and a_i, b_i the coefficients of a sinusoidal fit. After subtracting $L(t)$ and $S(t)$ from the observations ($y(t)$) we obtain the short-term variation ($W(t)$) with periods ranging from days to months. Evidently, the seasonal signal has a periodicity of one year.

This comparison reveals the effect of the seasonal signal used in the de-seasonalization process on the uncertainty in the trend estimation. Fig.2.3 shows a comparison of the two seasonal variations (parametric and non-parametric) obtained at the suburban site Dübendorf. It can be seen that the parametric approach has no explicit representation of the inter-annual variability. In contrast, the EEMD (non-parametric) accounts for the year-to-year variability in the signal due to varying meteorological conditions (e.g. untypically warm summer or winter), therefore, the parametric approach is considered disadvantageous for the de-seasonalization process.

Trends estimation

The de-seasonalized time series of the studied O₃ metrics are obtained by subtracting the seasonal variation from the observations, i.e.

$$y_d(t) = y(t) - S(t) \quad (2.6)$$

where $y_d(t)$ is the de-seasonalized time series.

The trend estimate is obtained by calculation of the Theil-Sen slope (Theil, 1950; Sen, 1968), where $y_d(t)$ is aggregated to monthly mean values. The uncertainty of the calculated trend in terms of the 95% confidence interval (CI) is obtained by bootstrapping. This means that slopes are calculated multiple times blockwise with replacement of resampled data (599 times for each block; each block has length $n^{1/3}$, where n is the size of the sample). The 95% CI is determined from the variability of the Theil-Sen slopes obtained from the resampled data.

The breakpoint of the time series is identified in the long-term signal ($LT(t)$) as obtained from the EEMD analysis for each station separately. The exact time of change (if it exists) is determined as the time when the first derivative of the long-term signal changes sign.

2.3.2 Meteo-adjusted trends

Trend estimation is affected by the influence of meteorology on O₃ concentrations. Therefore, observations have been adjusted for the higher frequency meteorological effects, and trends were calculated on the meteo-adjusted data, based on both the non-parametric and the parametric approach.

This was done by estimating the relationship between O₃ and O_x concentrations and meteorological variables that are expected to have an effect on tropospheric O₃. More specifically, the effect of short-term meteorological variations on O₃ is modeled using generalized additive models (GAMs, Hastie and Tibshirani, 1990; Wood, 2006). GAMs are known to perform well in studying the relationship between meteorological phenomena and air pollutants concentrations (e.g. Barmpadimos et al. (2011)). A GAM that consists of both numerical and categorical explanatory variables can generally be written as:

$$y(t) = \alpha + \sum_{i=1}^n s_i(M_i(t)) + \sum_{j=1}^m \left(\sum_{k=1}^p b_{jk}(B_{jk}(t)) \right) + \epsilon(t) \quad (2.7)$$

where $y(t)$ is the considered time series (here the short term signal of the considered O₃ metrics), α is the intercept, s_i are smooth functions of the numeric meteorological variables M_i . B_{jk} denote the j th categorical variable in the model with j indicating the categorical variable and k the level of the categorical variable. b_{jk} are the estimated effects of the categorical variables. Finally, $\epsilon(t)$ are the model residuals.

Chapter 2. Ozone time scale decomposition and trend assessment from surface observations in Switzerland.

The advantage of GAMs is that they are very flexible and capable to account for non-linear relationships between meteorological variables and O_3 . The GAMs were estimated using the *mgcv* library in R (R Development Core Team, 2017). The meteorological parameters used in the GAMs as predictors are the following: (a) numeric: temperature, humidity, solar radiation, surface pressure, wind velocity, precipitation, height of the boundary layer, CAPE, sensible surface heat flux, total cloud cover and (b) categorical: day of the week and WTCs.

Time series of all numerical meteorological variables were decomposed into long-term, seasonal, and short-term variation using the EEMD and the parametric approach described in Section 2.3.1.

$$m(t) = LT_m(t) + S_m(t) + W_m(t) + E_m(t) \quad (2.8)$$

where subscript m indicates the meteorological variables mentioned above and $W_m(t) = 0$ for the parametric approach. Then, the relationship between the signals of the short-term variations of the O_3 metrics and the meteorological variables was estimated using GAMs.

$$W(t) = GAM(W_m(t)) + \epsilon_W \quad (2.9)$$

$$E(t) = GAM(E_m(t)) + \epsilon_E \quad (2.10)$$

where ϵ_W and ϵ_E are the model residuals. Note that only equation 2.10 applies for the parametric approach.

The variation explained by the short-term meteorological effects, as captured by the GAMs, has been removed from the de-seasonalized data as follows:

$$y_{met.adj}(t) = LT(t) + \epsilon_W + \epsilon_E \quad (2.11)$$

where $y_{met.adj}$ stands for the meteo-adjusted time series of the daily mean O_3 , MDA8 O_3 and daily mean O_x . Note that for the parametric approach $e_W = 0$ in equation 2.11. The meteo-adjusted trends were calculated using the Theil-Sen trend estimator in two regimes, as determined for the de-seasonalized trends.

2.4 Results

2.4.1 Comparison of long-term trends based on EEMD and the parametric approach

In Fig.2.5, bar-plots of the daily mean O_3 trends based on the parametric approach and the non-parametric EEMD are presented. In addition, trends directly calculated with the Theil-Sen estimator applied to the annual mean O_3 concentrations are shown as a base

Table 2.1 – Studied stations in Switzerland, ranked by increasing mean NO_x concentration from top to the bottom. The duration of the data set is also shown. Stations are categorized according to mean NO_x value during the studied period, where A: $\text{NO}_x \leq 1$ ppb, B: $1 \leq \text{NO}_x \leq 10$ ppb, C: $10 \leq \text{NO}_x \leq 20$ ppb, D: $20 \leq \text{NO}_x \leq 40$ ppb, and E: $\text{NO}_x \geq 40$ ppb. (Cat. indicates the station's category.)

Station	Code	Type	NO_x (ppb)	Time Period	Cat.
Jungfrauoch	JUN	Remote, High Alpine (3578 m a.s.l.)	0.34	1990-2014	A
Davos	DAV	Rural, Elevated (>1000 m a.s.l.)	2.87	1991-2014	B
Chaumont	CHA	Rural, Elevated (>1000 m a.s.l.)	4.16	1991-2014	B
Rigi	RIG	Rural, Elevated (>1000 m a.s.l.)	4.73	1991-2014	B
Tänikon	TAE	Rural, Background	11.38	1990-2014	C
Payerne	PAY	Rural, Background	11.57	1990-2014	C
Grenchen-Zentrum	GRE	Urban, Background	21.00	1990-2014	D
Basel-Binningen	BAS	Suburban, Background	22.28	1990-2014	D
Frauenfeld	FRA	Suburban, Background	26.13	1995-2014	D
Magadino	MAG	Rural, Background	26.17	1991-2014	D
Thônex-Foron	FOR	Suburban, Background	30.75	1990-2014	D
Dübendorf	DUE	Suburban, Background	31.45	1991-2014	D
Liestal-LHA	LIE	Suburban, Traffic	32.30	1990-2014	D
Zürich-Kaserne	ZUE	Urban, Background	33.27	1991-2014	D
Basel-St.Johann	BSJ	Urban, Background	34.60	1990-2014	D
Lugano	LUG	Urban, Background	35.45	1990-2014	D
Zürich-Stamp/str.	ZSS	Urban, Traffic	42.74	1995-2014	E
Sion	SIO	Rural, Highway	45.49	1990-2014	E
Lausanne	LAU	Urban, Traffic	53.87	1991-2014	E
Härkingen	HAE	Rural, Highway	68.00	1993-2014	E
Bern	BER	Urban, Traffic	82.00	1991-2014	E

Chapter 2. Ozone time scale decomposition and trend assessment from surface observations in Switzerland.

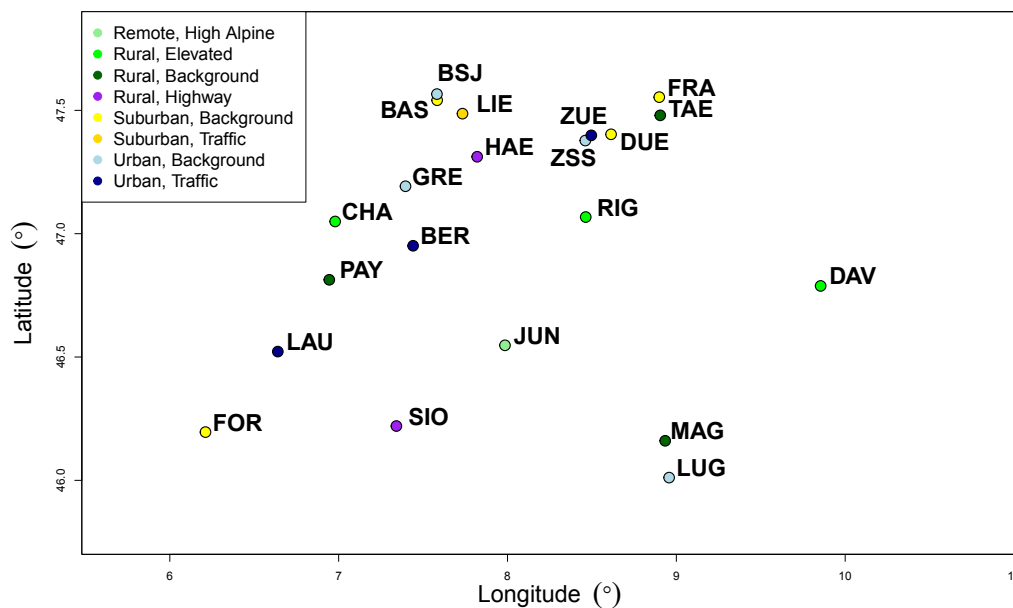


Figure 2.4 – Map of Switzerland and location of the sites that were considered for this study. The site types are distinguished by color.

case. The base case approach is a commonly used and straight forward technique for trend analysis. It is apparent from Fig.2.5 that the resulting trend estimates for all approaches are similar in magnitude. However, the uncertainties (represented by the range of the CI) for the de-seasonalized and meteo-adjusted trends are much smaller than for the base case. The trend estimation based on de-seasonalized monthly values is advantageous compared to the analysis of annual values; the higher number of observations leads to smaller uncertainties in the trend estimation. This is especially true for the meteo-adjusted data, where the short-term variability due to the influence of meteorology on O_3 has been reduced. Compared to EEMD, the parametric approach leads to higher uncertainties for the calculated trends in all stations. This is expected, because the seasonal signal derived from EEMD already captures the variation in O_3 due to the influence of meteorology on the seasonal scale. For instance, the effect of the exceptionally hot summer in 2003 and 2006 on O_3 is clearly visible in the seasonal signal obtained by the EEMD (Fig. 2.3). Ordóñez et al. (2005) have also observed high O_3 concentrations in Switzerland during summer of 2003. In addition, Schnell et al. (2014) and Carro-Calvo et al. (2017) have documented elevated O_3 in Europe during summer of 2006. This shows that de-seasonalization based on the EEMD removes a part of the meteorological influence, and can be considered as a basic type of meteo-adjustment. In contrast, the parametric approach yields a seasonal signal that has a constant amplitude and phase for the entire measurement period. We therefore conclude that de-seasonalization based on the EEMD is due to the variable amplitude and phase of the seasonal signal advantageous over the parametric approach. Consequently, further trend analysis performed within the present study is based on this method.

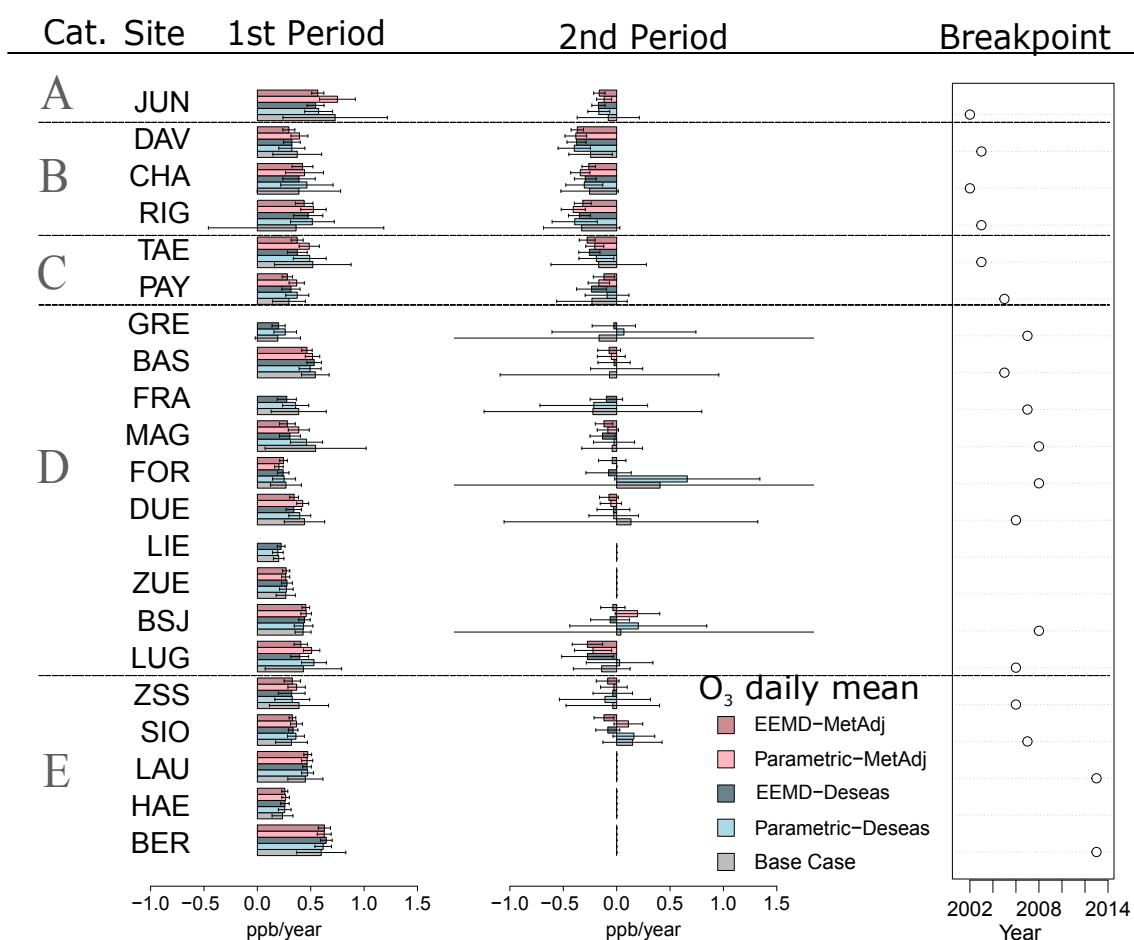


Figure 2.5 – Bar-plots for the trends of the daily mean O_3 concentrations during the identified first and second period for the five categories (indicated as Cat.). The bars show the magnitude of the Theil-Sen slopes (in ppb/year) for the studied sites (Table 2.1). The lines represent the 95% CI of the estimated trend. The blue colors show the trends estimated from de-seasonalized data, with the subtraction of the seasonal variation obtained either from the parametric approach (light blue bar) or the EEMD (dark blue bar). The pink colors show the meteo-adjusted trends based on the parametric approach (light pink bar) and EEMD (dark pink bar), respectively. The right panel indicates the time when the trend changes from positive to negative, i.e. the breakpoints as calculated from EEMD. Note that no breakpoint was found in LIE, ZUE and HAE. In LAU and BER the breakpoint occurred late, the trends in all these sites were therefore calculated for only one period. Also, the meteo-adjustment has not been applied for the sites GRE, FRA and LIE.

Chapter 2. Ozone time scale decomposition and trend assessment from surface observations in Switzerland.

2.4.2 Meteorological adjustment

The relationship between the short-term variation of O₃ and meteorological parameters has been estimated as described in Section 2.3.2. It is observed that in all sites temperature, solar radiation, humidity, CAPE and boundary layer height have a significant effect on the short-term variability of surface O₃. However, there is no clear conclusion regarding surface pressure, rain and surface sensible heat flux, which in some stations appear to affect O₃ significantly while in others the influence is not significant. The percentage of the variation of O₃ that is explained by the model is represented by the coefficient of determination R^2 . Here, the R^2 for the short-term variation ($W(t)$ estimated by EEMD) ranges between 50-64% for the daily mean concentrations (except for Jungfrauoch with 28%), 22-43% for the MDA8 (Jungfrauoch:12%) and 35-57% for O_x (Jungfrauoch: 27%). The R^2 for the even shorter time scales ($E(t)$ estimated by EEMD) for the daily mean concentration of O₃ lies between 0.5-19%, for the MDA8 0.6-8.5% and for O_x 0.7-16%. Analysis of the model residuals did not indicate violations of the model assumptions (homoscedasticity of residuals). An exception was the site in Liestal, therefore meteo-adjustment was not applied for this station. More details about the model results for each station are presented in the Appendix.

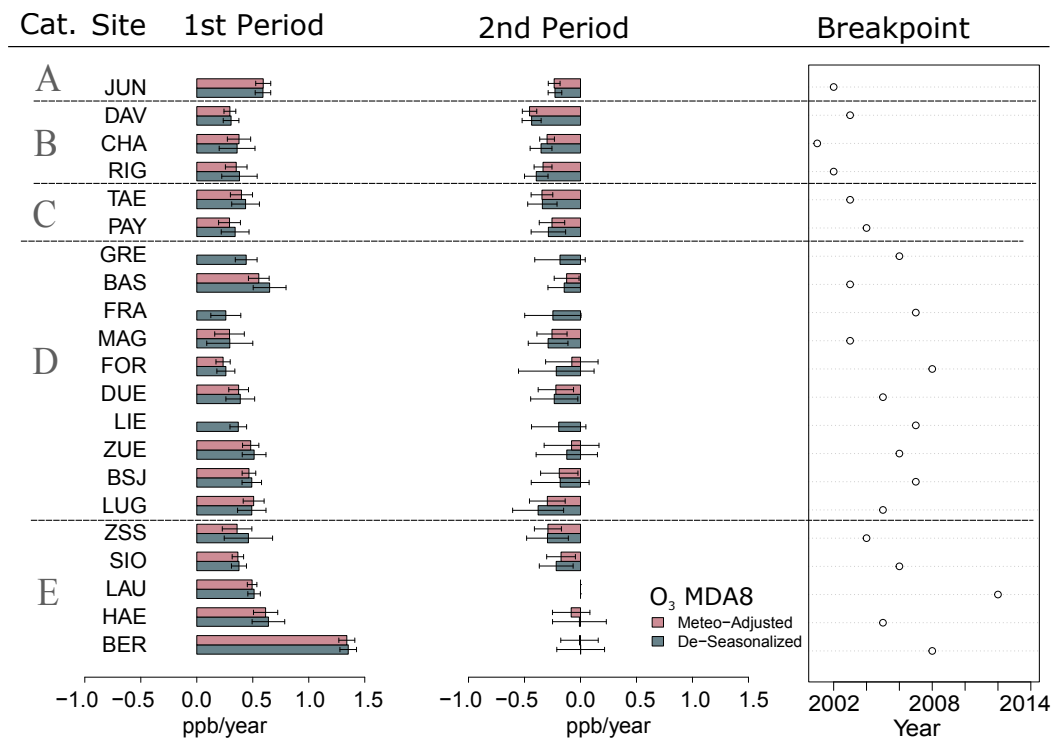
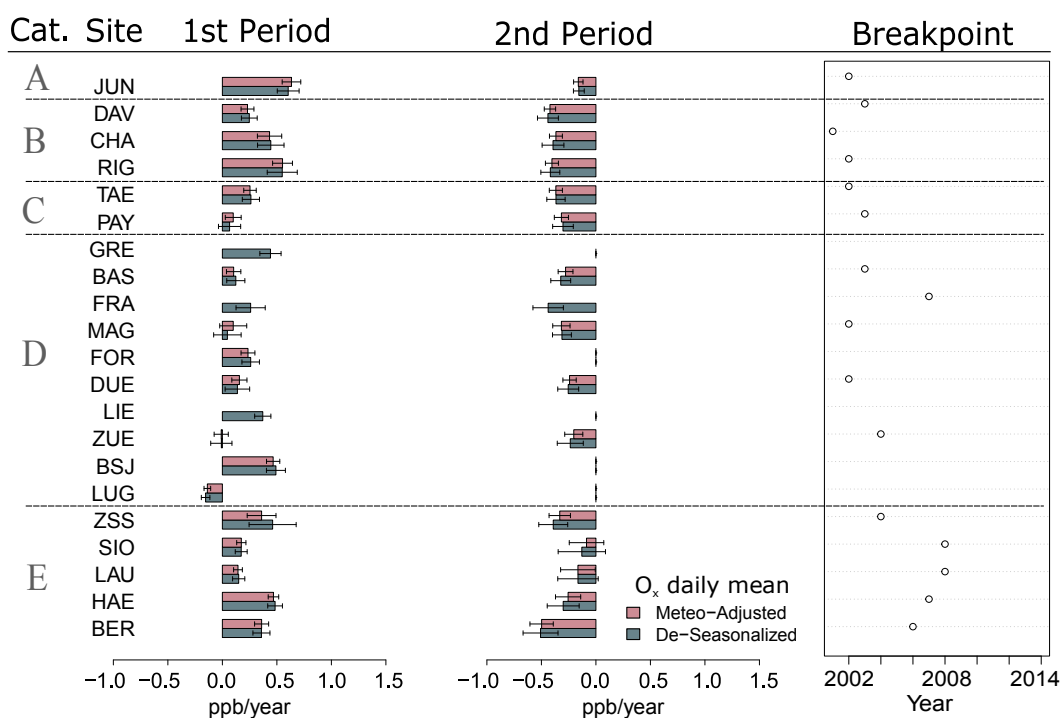


Figure 2.6 – As for Fig. 2.5 but for MDA8 O₃.

The meteo-adjustment based on EEMD reduces the variability of the O₃ concentrations and therefore leads to lower uncertainties when estimating trends. This can be seen in Figs. 2.5, 2.6 and 2.7 where trends of daily mean of O₃, MDA8 O₃ and daily mean of O_x are shown. However, the effect of the meteo-adjustment procedure as described in Section 2.3.2 has a small effect

Figure 2.7 – As for Fig. 2.5 but for daily mean O_x .

on the trends because part of the meteorological influence on O_3 has already been removed in the de-seasonalization process. Furthermore, the magnitude of the trends is negligibly affected by the meteo-adjustment. We therefore propose trend estimation of O_3 based on de-seasonalized data using EEMD as the most useful and robust approach, and this approach is considered in the following for the discussion of long-term trends of O_3 in Switzerland.

2.4.3 Trends of mean O_3 in Switzerland

For determination of the trend of mean O_3 in similar environments, the sites have been grouped into five different site categories. The categorization is based on the mean NO_x mixing ratio over the entire time period at each site, indicating the proximity of the sites to emission sources of O_3 precursors. The sites are grouped into categories A to E with: A the remote sites without influence from local sources ($NO_x \leq 1$ ppb), B the background sites with very low local pollution ($1 \leq NO_x \leq 10$ ppb), C the rural sites with low local pollution ($10 \leq NO_x \leq 20$ ppb), D the suburban and urban sites with moderate local pollution ($20 \leq NO_x \leq 40$ ppb) and E comprising all traffic sites which are highly influenced by local emissions ($NO_x \geq 40$ ppb). Note that the categories representing remote or rural environments (category A to C) consist of a smaller number of sites than the categories D and E. This is justified by the fact that remote and rural sites have a larger spatial representativeness than suburban and urban locations, where specific site characteristics typically have a larger influence on prevailing air pollution levels. The trends of daily mean O_3 , MDA8 O_3 and daily mean O_x at the sites within the

Chapter 2. Ozone time scale decomposition and trend assessment from surface observations in Switzerland.

different categories are illustrated in Figs. 2.8, 2.9 and 2.10. The average trends of all sites in the different site categories are shown in Fig. 2.11 and listed in Table 2.2.

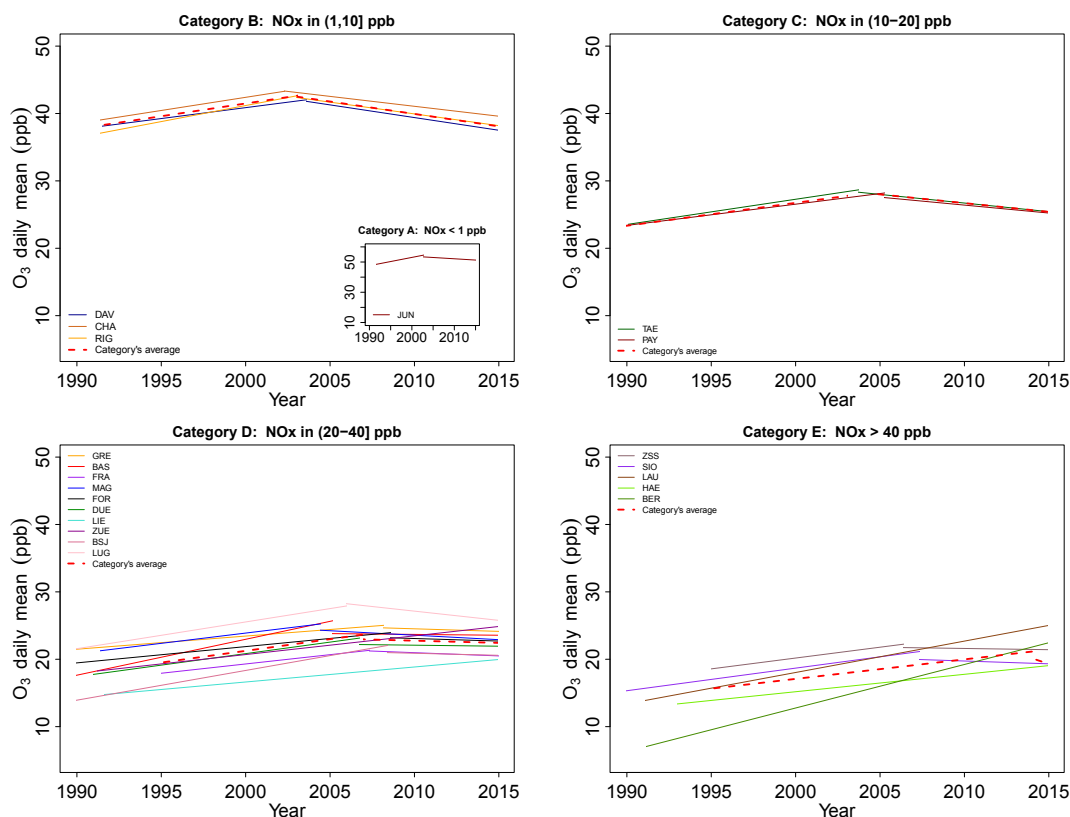


Figure 2.8 – Theil-Sen trends of daily mean O₃ concentrations estimated from monthly de-seasonalized values separated for stations in categories A-E. The categories have been defined based on the prevailing NO_x mixing ratio. The averages (red dashed lines) are based on the averaged de-seasonalized time series in each category and breakpoints on the averaged $LT(t)$.

The highest O₃ levels are observed at the high Alpine site at Jungfraujoch (3580 m a.s.l.), which is the only site in category A due to the exceptional characteristics and the high spatial representativeness of this site (Fig.2.8). At this remote location, local emissions of O₃ precursors are negligible, while long-range transport phenomena are of particular importance (Balzani-Lööv et al., 2008). At Jungfraujoch, O₃ (all metrics) was increasing by $\sim 0.54 - 0.60$ ppb/year since 1990 (Table 2.2), and started to decrease after 2002. The same temporal behavior of O₃ has been reported by Logan et al. (2012) for Alpine sites (including Jungfraujoch), as well as for regular aircraft (MOZAIC) measurements over Europe. The observed temporal trend can therefore be considered to represent the evolution of background O₃, defined as O₃ resulting from precursor emissions and transport on continental scale – including contributions from stratosphere-troposphere exchange (Cui et al., 2011). Especially after 2000s, Hess and Zbinden (2013) have documented a level off of O₃ in this region. In agreement to the O₃ trends observed at Jungfraujoch, many studies (Derwent et al., 2007; Vingarzan, 2004; Brönnimann et al., 2002) found that background concentration of O₃ has most probably been changing during the last

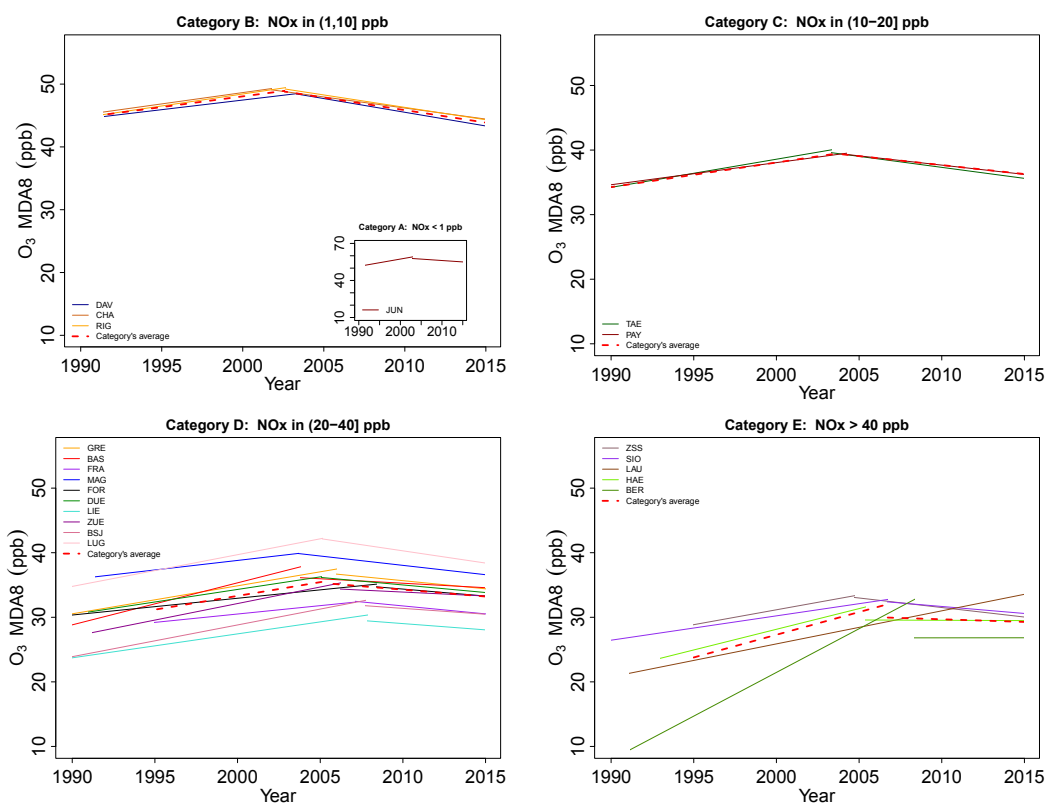


Figure 2.9 – Theil-Sen trends of MDA8 O_3 estimated from monthly de-seasonalized values separated for stations in categories A-E. The categories have been defined based on the prevailing NO_x mixing ratio. The averages (red dashed lines) are based on the averaged de-seasonalized time series in each category and breakpoints on the averaged $LT(t)$.

25 years. Derwent et al. (2007) reported increasing O_3 concentrations for filtered data from Mace Head (Ireland), a remote site that represents tropospheric background conditions when winds are prevailing from the western sector. Vingarzan (2004) reported that background O_3 in the Northern Hemisphere had been increasing since the 1970s by about 0.5-2% per year; however, the reasons for the observed trend in background O_3 over Europe are not well understood. Factors that may have contributed to these changes are changes in emissions of O_3 precursors on hemispheric scale and changes in the stratospheric input (Ordóñez et al., 2007; Logan et al., 2012; Hess and Zbinden, 2013). The emissions of the main precursors reactive hydrocarbons, NO_x and CO have been steadily decreasing in Europe and Northern America since the 1980s, whereas emissions of NO_x and CO were increasing in East Asia and India (Monks et al., 2015). Therefore, background O_3 over Europe was increasing in the 1990s when O_3 precursors from Europe and North America were decreasing and emissions in East Asia were still low compared to the other two continents (Logan et al., 2012). When background O_3 over Europe started decreasing in the 2000s, total emissions of NO_x in China were about similar to emissions in Europe and North America and continuing to rise (Logan et al., 2012). A further important O_3 precursor on the global scale is the long-lived methane

Chapter 2. Ozone time scale decomposition and trend assessment from surface observations in Switzerland.

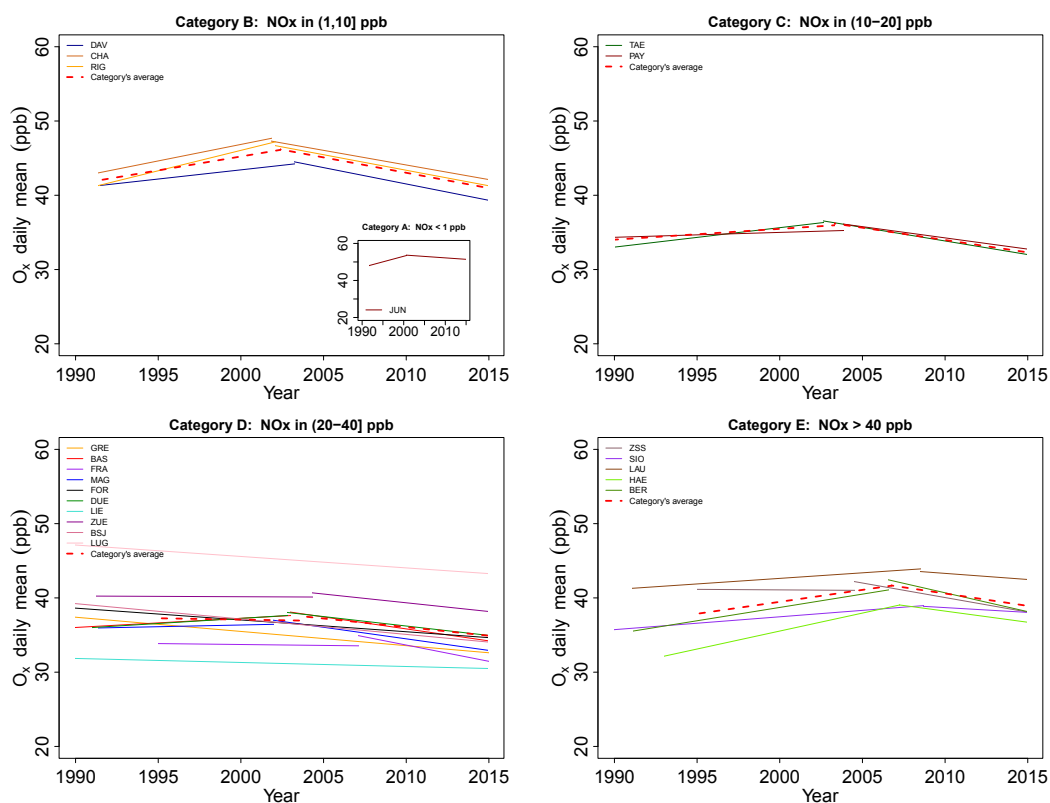


Figure 2.10 – Theil-Sen trends of daily mean O_x mixing ratios estimated from monthly de-seasonalized values separated for stations in categories A-E. The categories have been defined based on the prevailing NO_x mixing ratio. The averages (red dashed lines) are based on the averaged de-seasonalized time series in each category and breakpoints on the averaged $LT(t)$.

(CH_4). Global emissions of CH_4 have been increasing since 1950, stabilized in the 1990s and continued to rise during 2000s (Dentener et al., 2010). Therefore, the temporal changes in the global emissions of CH_4 also cannot directly be linked to the observed temporal trend in background O_3 over Europe. Finally, temporal changes of biomass burning might have contributed to the observed trends of O_3 , but the quantification of its role is beyond the scope of this study (Anderson et al., 2016; Granier et al., 2011).

The sites in category B are located in the Alps or Jura mountains at elevations above 1000 m a.s.l.. The O_3 mixing ratio is at the sites in category B lower than at Jungfrauoch but higher than at the sites of categories C to E. This is often the case in elevated sites, because O_3 production efficiency is higher at low NO_x regimes. The generally increasing O_3 mixing ratios with increasing altitude (Seinfeld and Pandis, 2016) can be explained by higher incoming solar radiation and by the larger input of stratospheric O_3 (Hess and Zbinden, 2013) at higher altitudes. In addition, sites at higher altitudes, as the ones in category B, are often sampling air in the residual layer, which is not subject to dry deposition. Compared to sites closer to the surface photochemical loss of O_3 is lower at these altitudes. The influence of local sources

of main O₃ precursors is at the sites of category B higher than at Jungfraujoch, although still small. For example, the mixing ratio of NO, a trace gas that can be regarded as an indicator for the proximity to anthropogenic sources, is at the sites of this category below 0.5 ppb (mean value between 1990 and 2014). Moreover, 50-70% of the daily maximum concentrations are associated with O₃ originating in the residual layer that is formed overnight (Neu et al., 1994). Finally, vertical mixing of air masses and transport of O₃ precursors from the polluted boundary layer to higher altitudes (Henne et al., 2003), as well as biogenic VOC emissions from nearby forests can contribute to O₃ formation at the type of locations represented by category B. O₃ mixing ratios and temporal changes at the sites of category B are therefore more strongly influenced by local and regional emissions of O₃ precursors than the remote site at Jungfraujoch (category A). The trend behavior of O₃ at all three sites in category B is similar and increasing at a slightly slower rate (all metrics, ~ 0.34 – 0.37 ppb/year) than at Jungfraujoch (Figs. 2.8 - 2.10). The time this trend changed (breakpoint), ranges at the sites of category B between 2002 and 2003; afterwards the mixing ratios of the considered metrics started to decline by ~ -0.36 to -0.41 ppb/year.

Category C represents rural locations at low altitude and consists of two sites. The mixing ratios and the trend behavior of O₃ at both sites are very similar (Figs. 2.8 - 2.10), supporting the assumption of the representativeness of the two sites for rural locations at low altitudes. Again, positive trends of all considered metrics for mean O₃ are observed until 2003-2005 and negative trends afterwards. The upward trends of daily mean O₃ and MDA8 O₃ during the first period are ~ 0.34 ppb/year and 0.38 ppb/year respectively and similar to the observed trend at the sites of category B. Note that the time of the breakpoints are later than at the sites in categories A and B. In contrast to the sites in categories A and B, where O_x is dominated by O₃, the rate of upward trend of O_x during the first period at the sites of category C is ~ 0.14 ppb/year and clearly smaller than the upward trend for daily mean O₃ and MDA8 O₃ (Fig. 2.11). It therefore appears that at the sites of category C, the observed trend of mean O₃ is driven by two different processes, the temporal change in background O₃, and the changes in O₃ formation due to declining emissions of NO_x and also non-methane VOCs (NMVOCs) in Switzerland (Lanz et al., 2008).

The influence of changing local and regional emissions of these precursors on surface O₃ is even more distinct at the sites in category D. These sites represent suburban and urban areas that are not exposed to emissions from sources in the immediate vicinity. An exception in category D is the site in Liestal, which is a suburban site next to a road with moderate traffic. At the sites in this category, the trend of daily mean O₃ mixing ratios and MDA8 O₃ are similar to the sites in category C, except that the breakpoints are further shifted to later times (2006-2008). At some of the sites in category D no breakpoint in the daily mean O₃ mixing ratio is observed, a behavior that is also apparent at some of the traffic sites in category E. Moreover, the average temporal change of O_x during the first period is for the sites in category D close to zero (-0.03 ppb/year), because some of the sites show slightly increasing O_x mixing ratios until the mid of the 2000s while at others O_x is continuously decreasing. Reasons for the diverse trends of O_x in category D could be that this category is broad in terms of NO_x

Chapter 2. Ozone time scale decomposition and trend assessment from surface observations in Switzerland.

pollution, and that O₃ concentrations at those sites are differently influenced by transport of O₃ that is formed several hours before in neighbored upwind regions. On average, the upward trend in O₃ is at the sites in category D entirely compensated by a downward trend in NO₂.

The final category E includes the sites with the highest levels of NO_x, i.e. sites that are situated next to major roads. At the three sites with the highest average NO_x mixing ratio (Lausanne, Härkingen and Bern) mean O₃ is continuously increasing since the beginning of the 1990s. As with most of the sites in category D, the upward trend in mean O₃ stopped at the two sites with the lowest NO_x levels (Zürich-Stamp/str. and Sion) in the mid of the 2000s and daily mean O₃ is declining since then. The average long-term trend of daily mean O₃ at the sites in category E leads to an upward trend of 0.29 ppb/year; this trend has stopped only recently and a breakpoint in 2014 has been found. The observed trend for MDA8 O₃ is similar to the sites in all other categories – increasing during the first period and decreasing after the breakpoint. However, the upward trend during the first period is the largest in category E (0.70 ppb/year), and it stops in 2006, i.e. later than at the other site categories. The downward trend after the breakpoint is for the sites in category E the smallest (-0.08 ppb/year). At the sites of category E, the average trend of O_x, in contrast to the suburban and urban sites in category D, clearly increases (0.32 ppb/year) until the breakpoint in 2006, when O_x started to decline at a rate of -0.33 ppb/year. For understanding the observed O₃ trends at the sites of categories D and E, two relevant reactions need to be considered Sillman (1999): (a) the NO+O₃ titration reaction, which depletes O₃ in presence of nearby NO emissions, and (b) the NO₂+OH termination reaction that leads to reduced O₃ formation with increasing NO_x to NMVOC ratios (NMVOC-limited regime). The larger reductions in ambient concentrations of NO over NO₂ at sites D and E (Fig. 2.12) and higher reaction rate of reaction (a) over that of (b) (Finlayson-Pitts and Pitts, 2000) suggests that reduced depletion from the former reaction may be partially responsible for increased O₃ concentrations near sources. However, trends in O_x, which are typically insensitive to local titration effects, are greater (relative to trends in O₃) at the traffic sites in category E compared to the sites in category D. This suggests that additional factors may play a role. For instance, directly emitted NO₂ from road traffic has been increasing from around 1995 to 2010 in many European countries including Switzerland (Grange et al., 2017); evidenced by the smaller decrease in NO₂ relative to NO_x at sites in category E compared to those in category D (Fig. 2.12). Furthermore, long-term trends of daily averaged O₃ may include effects of reaction (b) which can become more significant outside of peak traffic periods.

The analysis of the trend of the considered metrics for average mean O₃ levels shows that the implemented O₃ mitigation policies in Switzerland (reductions of NO_x and NMVOC emissions) had an effect on mean O₃. The O₃ formation processes have been changing so that except for remote and rural locations at higher altitudes, where the temporal development of hemispheric O₃ levels is the dominating factor, the differences in mean O₃ at different types of locations have during the past two decades become smaller (Fig. 2.13). The O₃ formation chemistry at urban, suburban and rural sites has become more similar (Pusede et al., 2015), and this can be expected to continue with further decreasing emissions of NO_x and NMVOCs.

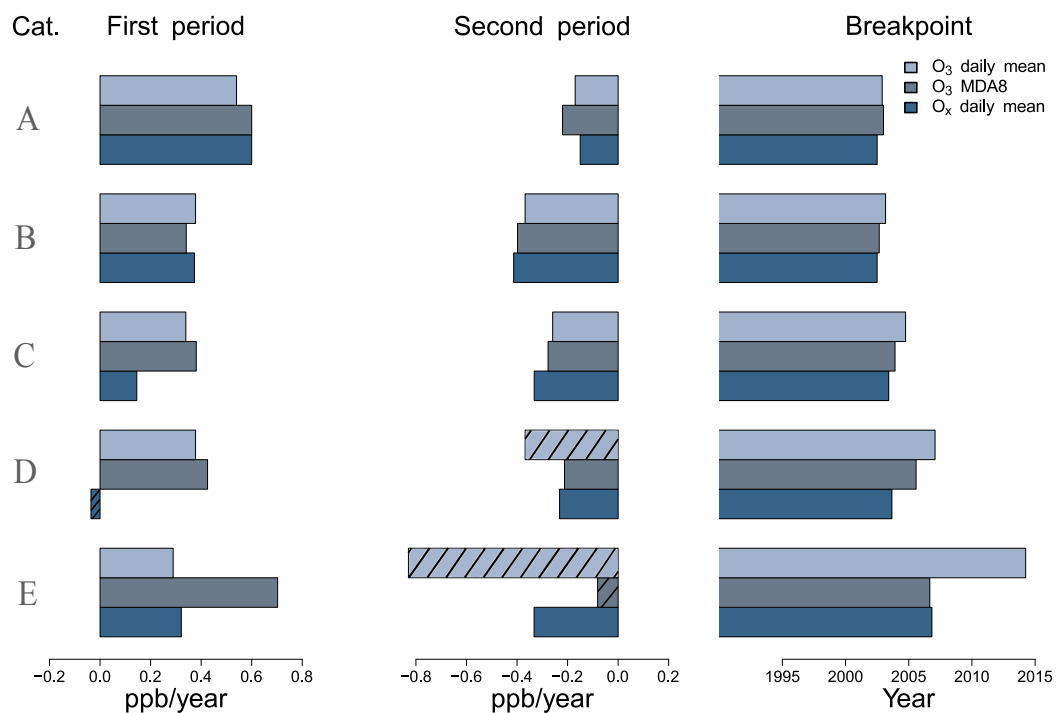


Figure 2.11 – Trends of O_3 and O_x (in ppb/year) for the site categories A to E (indicated as Cat.). Shown are the Theil-Sen trends of the averaged de-seasonalized data for each category. The two identified time periods and the breakpoint are based on the averaged $LT(t)$ at each category. The hatched bars indicate non-significant trends, i.e. with a p-value larger than 0.05.

The time of the breakpoint in the trend might be explained by the relationship between O_3 and its precursors (NO_x and NMVOCs), as conceptualized by O_3 isopleth diagrams (Finlayson-Pitts and Pitts, 2000; Thielmann et al., 2001). O_3 isopleths are typically generated via the empirical kinetic model approach (EKMA) where maximum O_3 production or concentration is described in terms of initial NO_x and NMVOC concentrations in a zero-dimensional box model. While NMVOC concentrations are not available and our analysis of O_3 trends corresponds to aggregated quantities (i.e., meteorologically-adjusted monthly concentrations of daily means), we qualitatively interpret the O_3 response to precursors across different concentration regimes through the same chemical mechanisms governing the isopleths. Limited studies (Dommen et al., 1995, 1999) suggest that urban and suburban sites in Switzerland with high NO_x emissions lie in the NMVOC-limited regime, where O_3 formation increases with decreasing NO_x and constant NMVOC concentrations. During the 2000s, NO_x concentrations at some sites might have decreased enough so that a transition to the NO_x -limited regime occurred, where O_3 concentrations decrease with decreasing NO_x . The late appearance of the breakpoint at highly polluted sites might be due to the much higher NO_x to NMVOC ratio level during the 1990s; the point of transition from the NMVOC-limited to the NO_x -limited regime has not or only recently been reached. On the other hand, at rural and remote sites O_3 is formed according to the NO_x -limited regime (Dommen et al., 1995, 1999). We therefore assume that

Chapter 2. Ozone time scale decomposition and trend assessment from surface observations in Switzerland.

Table 2.2 – Average magnitudes of the Theil-Sen trends (ppb/year) for daily mean O₃ and MDA8 O₃, and daily mean O_x for the two consecutive time periods in Swiss sites based on the EEMD de-seasonalization method and the time of breakpoint. P1 and P2 indicate the first and second period's average trend respectively and BP the average year of breakpoint in the trend. All numbers are based on the averaged de-seasonalized time series in each category and breakpoints on the averaged $LT(t)$. The numbers in italics are non-significant trends (p-value > 0.05).

Cat.	Environment	daily mean O ₃			MDA8 O ₃			daily mean O _x		
		P1	BP	P2	P1	BP	P2	P1	BP	P2
A	High alpine	0.54	2002.9	-0.17	0.60	2003	-0.22	0.60	2002.5	-0.15
B	Alpine & Pre-alpine	0.37	2003.2	-0.36	0.34	2002.6	-0.4	0.37	2002.5	-0.41
C	Rural, low altitude	0.34	2004.7	-0.26	0.38	2003.9	-0.27	0.14	2003.4	-0.33
D	Suburban & urban	0.37	2007.0	-0.36	0.42	2005.5	-0.21	-0.03	2003.6	-0.23
E	Urban, high pollution	0.29	2014.2	-0.83	0.7	2006.6	-0.08	0.32	2006.8	-0.33

at rural and remote locations, the occurrence of the breakpoint is determined by changes in background O₃. At locations closer to anthropogenic sources of precursors, the time of the breakpoint might be determined by the superposition of changes in background O₃, reduced NO titration and changes in regional O₃ production (Brönnimann et al., 2002; Ordóñez et al., 2005). In particular, we hypothesize that the latter may have been altered by a transition of O₃ production to a more NO_x-limited regime.

2.5 Conclusions

A statistical approach for estimation of O₃ trends based on time scale decomposition of multi-year observations from various surface sites in Switzerland has been applied. The non-parametric time scale decomposition (EEMD) of the time series into long-term, seasonal and short-term variations proved to be a valuable tool for a long-term O₃ trend analysis. In addition, the two-regime trend calculation revealed an interesting dependence of the O₃ response to precursors reductions on the station's pollution burden. The proposed EEMD-based de-seasonalization accounts for a large fraction of the meteorology driven year-to-year variability of O₃ and allows the estimation of temporal trends of O₃ with reduced uncertainties, without meteorological adjustment of the observations.

It was found that the daily mean O₃ and the daily maximum of the eight hour running mean of hourly O₃ mixing ratios were increasing during the 1990s; this trend changed around the mid of the decade of the 2000s when they started to decline. The year the upward trend of O₃ stopped shows a clear dependence on the type of location. The breakpoint occurs earliest at remote sites and is shifted towards later times with increasing proximity to sources of NO_x. The observed O₃ trend at the remote site Jungfrauoch is interpreted as being representative for

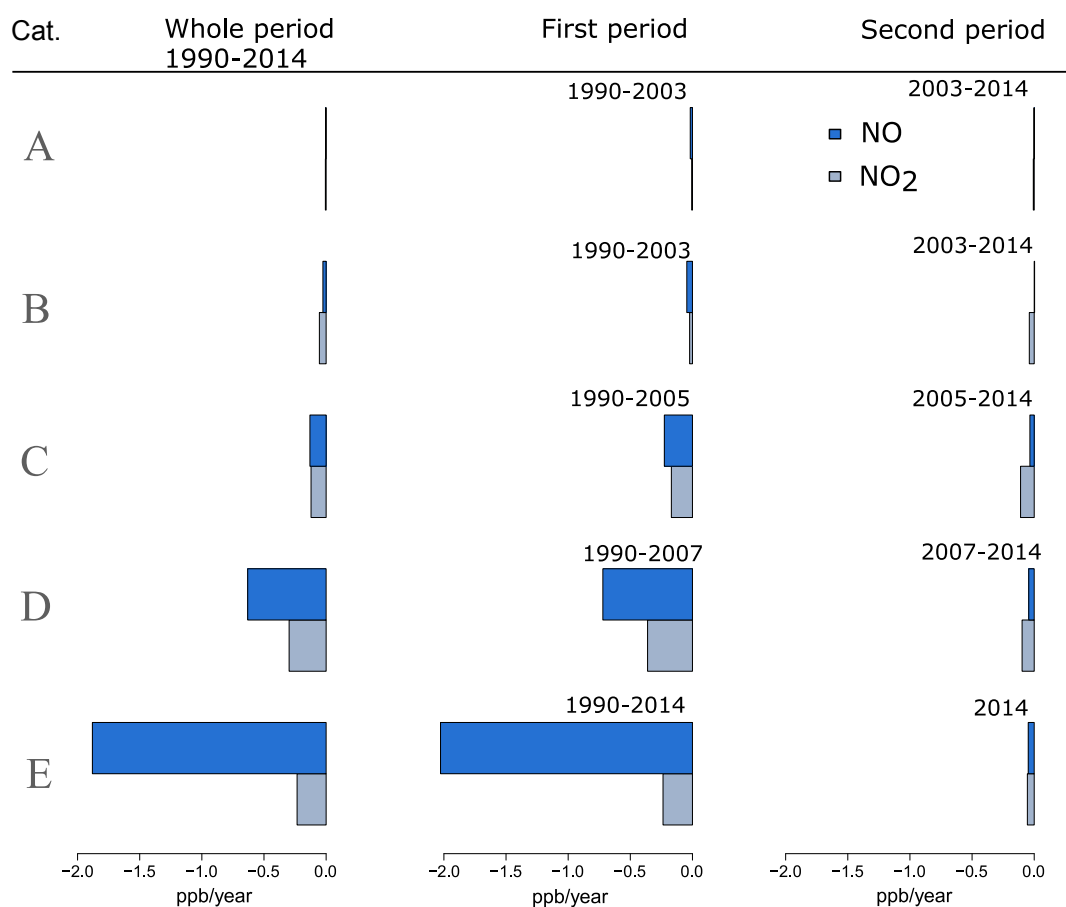


Figure 2.12 – Bar plots with the Theil-Sen trends of daily mean NO and NO₂ mixing ratios annually averaged for the whole studied period in ppb/year. Trends are also shown in two successive periods that correspond to the periods that were detected for the daily mean O₃ mixing ratios. Stations are grouped according to mean NO_x mixing ratio levels over the studied period in categories A-E (indicated as Cat.).

the temporal development of the O₃ background over Europe. Although the temporal changes of background O₃ over Europe are well described in the scientific literature, the processes leading to the observed temporal changes in background O₃ are still poorly understood. At all considered locations other than the remote site Jungfraujoch, O₃ trend can be understood as resulting from the superposition of background O₃ and the temporal changes in regional photochemical O₃ production. The importance of changes in the regional O₃ production due to changes in O₃ precursor emissions is increasing with closeness to urban environments. It is evident that the reduced titration of O₃ by NO due to the decreasing emissions of NO_x in Switzerland and large parts of Europe since around the beginning of the 1990s had a strong effect on mean O₃ mixing ratios, but, further investigation of the temporal changes of the main chemical processes for regional O₃ formation is beyond the scope of this study. It was shown that the decreasing emissions of NO_x and also NMVOCs in the urban environments resulted in an O₃ formation chemistry that is more similar to suburban and rural locations

Chapter 2. Ozone time scale decomposition and trend assessment from surface observations in Switzerland.

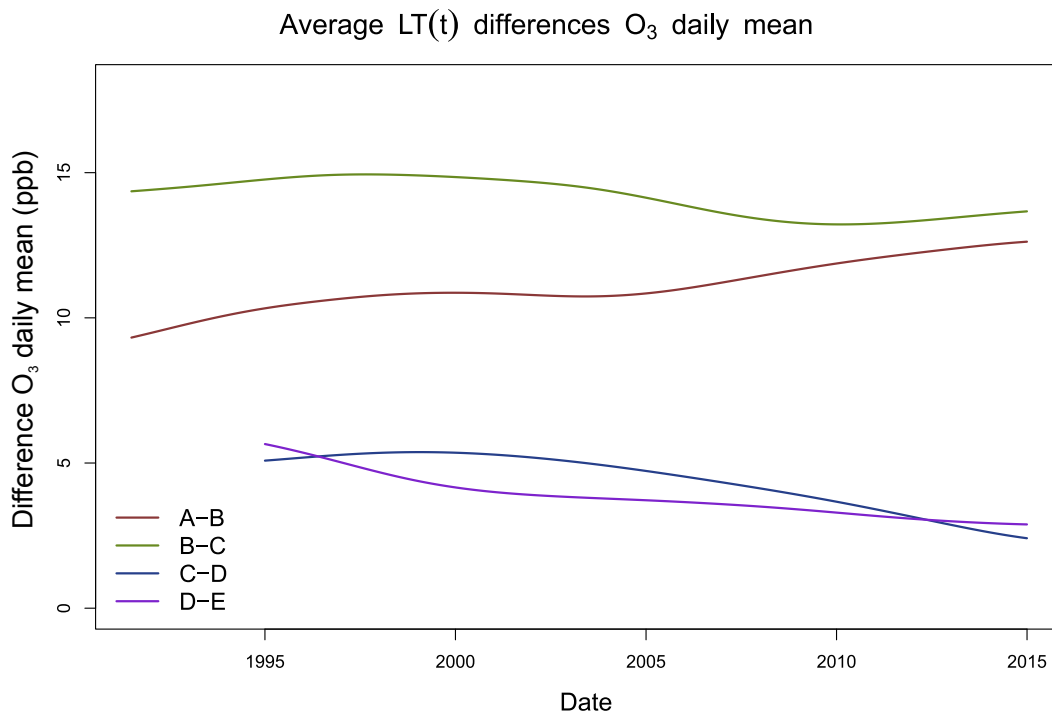


Figure 2.13 – Differences between the categories A-E of the averaged $LT(t)$. A-B is the $LT(t)$ difference between categories A and B, B-C between B and C etc.

as seen from decreasing differences in mean O_3 mixing ratios at corresponding locations. A possible transition of the urban and suburban sites from the NMVOC-limited regime to the NO_x -limited regime in a conceptual O_3 isopleth diagram could be used to interpret the change in trend behavior at these locations. The effect of emissions reductions can be seen in the temporal evolution of peak O_3 concentrations as well, where decreasing trends are observed since the 1990s (Boleti et al., 2018b). The apparent contribution of hemispheric O_3 to local surface concentrations points to the importance of global efforts towards emission reductions. Combined with changing climatic conditions, where more frequent and more intense heat events are expected, controlling O_3 concentrations becomes increasingly more relevant.

Acknowledgements We acknowledge the Swiss Federal Office of Environment (FOEN) for financing the research program. We would like to thank Dr. Stephan Henne for extracting ERA-Interim meteorological variables.

3 Trends of surface maximum ozone concentrations in Switzerland based on meteorological adjustment for the period 1990-2014.

Eirini Boleti^{1,2}, Christoph Hueglin¹ and Satoshi Takahama²

Published in Atmospheric Environment: <https://doi.org/10.1016/j.atmosenv.2019.05.018>

¹Empa, Swiss Federal Laboratories for Materials Science and Technology, Überlandstrasse 129, Dübendorf, Switzerland

²EPFL, École Polytechnique Fédérale de Lausanne, Route Cantonale, 1015 Lausanne, Switzerland

Abstract: We investigate the temporal trends of peak ozone in Switzerland for the 1990-2014 time period. The meteorological conditions have a large influence on ozone formation and drive a large part of the variability in ozone observations. Therefore, the influence of meteorology on ozone was estimated using generalized additive models and removed from the ozone observations. A variable selection method was used for model building allowing the detection of the meteorological variables that have the largest effect on the variability of daily maximum ozone at each considered station. It was found that peak concentrations of ozone have been reducing in most of the stations, indicating a positive effect of implemented air pollution control measures on locally produced ozone. In the remote, high alpine site of Jungfraujoeh a small upward trend of peak ozone was observed, most likely due to influence of hemispheric background ozone. In the most polluted traffic sites, peak ozone has for a different reason also been increasing until around 2003, when this trend started to level off. In traffic sites the increasing ozone concentrations due to reduced titration by nitrogen monoxide was the dominating process. One of the advantages of meteorological correction of ozone observations for trend estimation is that the uncertainty in the calculated trends is reduced. In addition, trend estimation based on meteorologically corrected ozone is less influenced by exceptional meteorological events during a specific time period, such as heat waves or by

temporal changes in meteorological variables.

3.1 Introduction

Ozone (O_3) is formed in the troposphere by photochemical reactions involving nitrogen oxides ($NO_x=NO_2+NO$), carbon monoxide (CO) and volatile organic compounds (VOCs). High O_3 concentrations, as expressed e.g. by the World Health Organization guideline value ($100 \mu\text{g}\cdot\text{m}^{-3}$ for the 8 hour running mean) or the European air quality standard ($120 \mu\text{g}\cdot\text{m}^{-3}$ for the maximum daily 8 hour running mean), can have severe impacts on human health and ecosystems (WHO, 2006; European Environmental Agency, 2015). In large parts of Europe, including Switzerland, exceedances occur regularly during warm months of the year, when the combination of favorable weather conditions and availability of precursors lead to increased O_3 formation (e.g. Querol et al., 2016). According to Staehelin et al. (1994), concentrations of O_3 at remote, rural regions in Europe have almost doubled between 1950s and 1990s due to increasing emissions of the O_3 precursors NO_x and VOCs. Since the beginning of 1990s emissions of NO_x and VOCs have been declining in Europe due to implementation of emission control measures (Colette et al., 2011; Guerreiro et al., 2014; Henschel et al., 2015), such as the use of catalytic converters in the petrol vehicles. The EMEP (Cooperative Programme for Monitoring and Evaluation of the Long-range Transmission of Air Pollutants in Europe) emission inventory reports that NO_x and non-methane VOC (NMVOC) emissions clearly decreased in Europe between 1990 and 2012 (?), while for Switzerland alone the reported relative reductions are 39% and 49% respectively (BAFU, 2016). As a consequence downward trends of maximum concentrations of O_3 were observed across Europe (Solberg, 2009; Yan et al., 2018; Fleming et al., 2018).

Meteorological conditions, such as high air temperature and intense solar radiation or increased wind velocity, strongly influence O_3 concentrations at the surface, as reported in the literature (Solberg, 2009; Ordóñez et al., 2005; Pearce et al., 2011). For instance, temperature appears to be a key parameter for O_3 in central Europe, especially during high O_3 events, while other important meteorological variables are humidity and solar radiation (Otero et al., 2016). Thermal decomposition of peroxyacyl nitrates (PANs) at high temperature conditions lead to higher rates of O_3 production (Sillman and Samson, 1995; Vogel et al., 1999; Bärtsch-Ritter et al., 2004). Moreover, increased humidity levels in the atmosphere enhance production of hydroxyl radicals (OH) yielding higher O_3 concentrations in the high- NO_x regime (Vogel et al., 1999).

In this study the temporal evolution of peak O_3 mixing ratios in Switzerland during 1990-2014, with and without adjustment of meteorological influence, is presented. This complements a trend analysis of mean concentrations of O_3 in Switzerland (Boleti et al., 2018a), where a method based on de-seasonalization of daily mean O_3 has been applied. For the current study, a different approach was used because peak O_3 concentrations are typically expressed by temporally localized events and, therefore, de-seasonalization is not meaningful. Our work

builds on the work by Ordóñez et al. (2005), however, in our study the effect of meteorology on peak O₃ concentrations was investigated by a different statistical approach and by application of a more refined variable selection procedure.

3.2 Data

O₃ and NO_x concentration measurements from 21 stations in Switzerland were provided by federal and cantonal authorities in hourly resolution for the time period between 1990 and 2014 (Table 3.1). Note that for 16 of the 21 sites the O₃ and NO_x data can also be sourced from AirBase, the air quality database of the European Environmental Agency. The stations included in this study cover regions north and south of the Alps and urban, suburban, rural, elevated and remote high alpine site types, they are grouped into five main categories (Boleti et al., 2018a). The five groups are based on the mean NO_x mixing ratio over the studied period, indicating the proximity of the sites to emission sources of O₃ precursors. The categories are the following: (A) the remote, high alpine site in Jungfraujoch not influenced by local sources (NO_x ≤ 1 ppb), (B) are the alpine and pre-alpine environments with very low local pollution (1 < NO_x ≤ 10 ppb), (C) the rural sites located at low altitudes (10 < NO_x ≤ 20 ppb), (D) the suburban and urban sites with moderate local pollution (20 < NO_x ≤ 40 ppb) and (E) comprising all traffic sites which are highly influenced by local emissions (NO_x ≥ 40 ppb). Due to special characteristics of the sites in Bern and Lausanne (urban sites with the strongest impact of road traffic), these sites were treated as a special category indicated as E2, while the other sites in this group are indicated as E1.

Percentages of missing values vary between 0.32-4.27% and number of successive missing values in the data are between 4-16 days (except for Tänikon and Grenchen 40 days, Jungfraujoch 43 days and Thônex-Foron 92 days).

The following metrics representing peak or excess O₃ concentrations were considered.

1. MTDM: the mean of the ten highest daily maximum O₃ concentrations between May and September based on hourly mean data. The same metric has also been calculated for the cold season of the year (October to April).
2. 4-MDA8: the mean of the four highest concentrations of the MDA8 (daily maximum of the 8-hour running mean of hourly O₃ concentrations) per year.
3. A-MDA8: the annual maximum MDA8.
4. 90-PERC: the 90th percentile of daily maximum O₃.
5. SOMO35: the cumulative excess O₃ as calculated from MDA8 exceeding 35 ppb over one year (expressed in ppb.days) (WHO, 2008). The SOMO35 metric can be used for assessment of health impacts.

Chapter 3. Trends of surface maximum ozone concentrations in Switzerland based on meteorological adjustment for the period 1990-2014.

6. AOT40: it represents the accumulation of O₃ over 40 ppb between 8 am and 8 pm from May to July (expressed in ppb.hours) (European Parliament and Council of the European Union, 2008). Based on the hourly mean concentrations the ones between 8 am and 8 pm are filtered and days with O₃ above 40 ppb are identified. The difference to 40 ppb is aggregated over the respective year.

The discussion on peak O₃ trends is focused on the MTDM and 4-MDA8. The trends of SOMO35 are also presented, although SOMO35 is not a metric for peak O₃ but representing mid-high ozone levels summed annually (Fleming et al., 2018). Trends of the remaining metrics are shown in the supplementary material.

Meteorological data were used from measurements taken at each site. The parameters considered in this study are: daily maximum air temperature (°C), daily/morning/afternoon mean relative humidity (%), daily maximum solar radiation ($W \cdot m^{-2}$), daily mean surface pressure (hPa), daily/morning/afternoon mean wind velocity ($m \cdot s^{-1}$) and daily/morning/afternoon mean precipitation (mm). Morning mean refers to average value between 6-12 hours and afternoon mean between 12-18 hours. For data sets with more than 5% and/or more than 30 successive days of missing values, meteorological data were taken from nearby sites operated by MeteoSwiss. For a more complete analysis of the meteorological influence, additional parameters were derived from the ERA-Interim data-set in a 1 degree grid at each site (longitude-latitude-altitude) for the period 1990-2014, i.e. the daily maximum height of the boundary layer (m), the daily/morning/afternoon mean convective available potential energy (CAPE, $J \cdot kg^{-1}$), daily maximum sensible surface heat flux ($W \cdot m^{-2}$), daily/morning/afternoon mean total cloud cover, daily/afternoon mean east-west/north-south surface stress ($N \cdot s \cdot m^2$). Additionally, information for the synoptic situation was used, provided as weather type classifications (WTCs, Weusthoff, 2011) from MeteoSwiss, which describe recurrent dynamical patterns. The classification includes 9 categories, namely northeast/indifferent, west-southwest/cyclonic/flat pressure, westerly flow over Northern Europe, east/indifferent, high pressure over the Alps, north/cyclonic, west-southwest/cyclonic, high pressure over Central Europe, westerly flow over Southern Europe/cyclonic.

3.3 Methodology

3.3.1 Trend estimation of peak O₃

The trend of all O₃ metrics was calculated first directly from the observations and after adjustment of the meteorological influence. This was done by calculation of the Theil-Sen slope (Theil, 1950; Sen, 1968) of the considered O₃ metrics. The Theil-Sen slope is a robust trend estimator where the trend is expressed as the median of the changes of all possible combinations of pairs in the data at distinct time. The 95% confidence interval (CI) is determined by using a resampling method (Hall, 1996; Chernick, 2008).

3.3. Methodology

Table 3.1 – Table with the studied stations in Switzerland, ranked by increasing mean NO_x concentration from top to bottom. Stations are categorized according to mean NO_x value during the studied period, where A: NO_x ≤ 1 ppb, B: 1 < NO_x ≤ 10 ppb, C: 10 < NO_x ≤ 20 ppb, D: 20 < NO_x ≤ 40 ppb, and E: NO_x ≥ 40 ppb. Category E2 indicates sites in urban environment with high traffic activity throughout the day. (Cat. indicates the station's category.)

Station	Code	Type	NO _x (ppb)	Time period	Cat.
Jungfrauojoch	JUN	Remote, High Alpine (3578 m a.s.l.)	0.3	1990-2014	A
Davos	DAV	Rural, Elevated (<1000 m a.s.l.)	2.9	1991-2014	B
Chaumont	CHA	Rural, Elevated (<1000 m a.s.l.)	4.2	1990-2014	B
Rigi	RIG	Rural, Elevated (<1000 m a.s.l.)	4.7	1991-2014	B
Tänikon	TAE	Rural	11.4	1990-2014	C
Payerne	PAY	Rural	11.6	1990-2014	C
Grenchen-Zentrum	GRE	Urban	21.0	1990-2014	D
Basel-Binningen	BAS	Suburban	22.3	1990-2014	D
Frauenfeld-Bahnhofstrasse	FRA	Suburban	26.1	1995-2014	D
Magadino	MAG	Rural	26.2	1991-2014	D
Thônex-Foron	FOR	Suburban	30.8	1990-2014	D
Dübendorf	DUE	Suburban	31.5	1991-2014	D
Liestal-LHA	LIE	Suburban, Traffic	32.3	1990-2014	D
Zürich-Alte Kaserne	ZUE	Urban	33.3	1991-2014	D
Basel-St.Johann	BSJ	Urban	34.6	1990-2014	D
Lugano	LUG	Urban	35.5	1990-2014	D
Zürich-Stampfenbachstrasse	ZSS	Urban, Traffic	42.7	1995-2014	E1
Sion	SIO	Rural, Highway	45.5	1990-2014	E1
Lausanne	LAU	Urban, Traffic	53.9	1991-2014	E2
Härkingen	HAE	Rural, Highway	68.0	1993-2014	E1
Bern	BER	Urban, Traffic	82.0	1991-2014	E2

Chapter 3. Trends of surface maximum ozone concentrations in Switzerland based on meteorological adjustment for the period 1990-2014.

3.3.2 Generalized additive models (GAMs)

The relationship between air pollutants and meteorological variables is best described by non-linear statistical models (Thompson et al., 2001), and GAMs (Hastie and Tibshirani, 1990; Wood, 2006) have been used in such applications previously (e.g. Barmpadimos et al., 2011; Carslaw et al., 2007). We use GAMs for explaining the observed daily maximum and MDA8 O₃ by the available explanatory variables, i.e.

$$O_3(t) = \alpha + \sum_{i=1}^n s_i(M_i(t)) + \sum_{j=1}^m \left(\sum_{k=1}^p b_{jk}(B_{jk}(t)) \right) + s_0(t) + \epsilon(t) \quad (3.1)$$

where $O_3(t)$ denotes the O₃ observations (daily maximum and MDA8), α is the intercept, s_i are smooth functions (thin plates splines) of the numeric meteorological variables M_i and n is the number of the continuous meteorological variables in the model. B_{jk} denote categorical variables where j is the variable, k is the category, b_{jk} are parameters for the effect of B_{jk} , m is the number of categorical variables in the model and p the number of categories. The temporal trend is modeled by the smooth function s_0 , t denotes the time variable expressed as the Julian day (number of days since January 1, 4713 BCE at noon UTC). ϵ stands for the residuals of the model. In our models the WTCs and the day of the week are included as categorical variables. The GAMs were calculated using the *mgcv* library in R (R Development Core Team, 2017).

3.3.3 Selection of meteorological variables

GAMs were constructed for two seasons (May–September and October–April) for the daily maximum and MDA8 O₃, resulting in four models per site. A selection method was applied for each of the models, to identify the most important meteorological variables for explaining O₃ variability. Amongst all available predictors, the ones that best define the model were selected based on the Akaike information criterion (AIC).

$$AIC = -2 \cdot \log(L) + k \cdot n \quad (3.2)$$

where L is the maximum value of the likelihood function for the model, k the penalty parameter for the number of explanatory variables and n the number of explanatory variables. The AIC penalizes the model when adding more variables and, hence, the model with the lowest AIC should be the simplest, yet most concise model to describe the relationship between O₃ and meteorology. In addition, we treat the effect of collinearity between explanatory variables by specifying the maximum allowed variance inflation factor (VIF). This way increased inflation is avoided, which could lead to wrong representation of correlation between the dependent variable and the explanatory variables and, thus, false interpretation of the results. The VIF of

two explanatory variables can be calculated as:

$$\text{VIF}_j = \frac{1}{1 - R_j^2} \quad (3.3)$$

where R_j^2 the corresponding coefficient of determination for a parameter j . Several test models were performed in order to select the best combination of the values used for VIF and AIC. The maximum VIF used here is 2.5, which corresponds to an accepted maximum $R^2=0.6$ between two numerical explanatory variables. A large penalty parameter k means strong penalization of models with higher number of explanatory variables. A moderate penalization of $k=15$ is usually used in the literature (e.g. Barmpadimos et al., 2011), while $k > 20$ (e.g. $k=24$) leads to models with very small number of explanatory variables and relatively low explained variability (R^2). Eventually, for the AIC penalty parameter the most appropriate value was found to be $k=20$.

The variable selection method works as follows (Barmpadimos et al., 2011; Jackson et al., 2009). (i) The first variable is selected, by constructing GAMs using each one of the available explanatory variables every time. The GAM with the variable that results in the lowest AIC is selected. (ii) The next variable is selected by adding the rest of the explanatory variables one by one in the GAM that was selected in step (i). Again, the GAM with the lowest AIC is selected. (iii) The variable that was chosen in step (i) is removed and each one of the remaining variables is added to the model. If this process results in a model with lower AIC than the model selected in step (ii), then the model from the current step is chosen. (iv) Collinearity is tested, by calculating the VIF between the newest variable in the model with all other variables that have been selected before. If it exceeds 2.5 then the new variable is removed from the model. (v) Steps (ii) to (iv) are repeated until no further reduction of the AIC can be achieved.

3.3.4 Meteorological adjustment

The meteorological adjustment was performed after identifying the best models for each station. Meteo-adjusted daily maximum and MDA8 O_3 time series were calculated as

$$\text{O}_{3_{adj}}(t) = \alpha + s_0(t) + \epsilon(t) \quad (3.4)$$

Meteorologically adjusted O_3 can be interpreted as the concentration of O_3 that would prevail on the considered day at average conditions as represented by the selected meteorological variables. For MTDM and 4-MDA8, the days of the ten highest daily maximum concentrations and of the four highest MDA8 of each year were identified from the corresponding observations. The meteo-adjusted MTDM and 4-MDA8 were calculated from $\text{O}_{3_{adj}}(t)$ for the same days that were previously identified. The meteo-adjusted 90-PERC values were calculated from the $\text{O}_{3_{adj}}(t)$. Eventually, meteo-adjusted trends were calculated using the Theil-Sen trend estimator and a linear regression model as explained in section 3.3.1. Meteo-adjustment was not applied

Chapter 3. Trends of surface maximum ozone concentrations in Switzerland based on meteorological adjustment for the period 1990-2014.

for SOMO35 and AOT40, because the cumulative sum of meteorologically adjusted O₃ above a certain threshold can hardly be interpreted and does no more represent a meaningful metric for annual or seasonal exposure to excess O₃.

3.4 Results

3.4.1 Meteorological influence on maximum O₃ concentrations

The most often selected variables in the GAMs for the daily maximum and MDA8 O₃ during warm months are the daily maximum temperature, daily mean humidity, morning mean CAPE, north-south surface stress (either daily mean or afternoon mean) and east-west surface stress (either daily mean or afternoon mean) (Table. 3.2). Similar to Ordóñez et al. (2005), daily maximum temperature was found to be the most important variable in nearly all stations. The non-linear effect of temperature on O₃ as described by the GAM models is exemplified in Fig. 3.1 for the suburban site in Dübendorf, a moderately polluted site with little emissions of ozone precursors in the immediate vicinity. Temperature can be regarded as a proxy for conditions favoring ozone formation. An important reason for this strong relationship between O₃ and temperature is that high temperature is associated with high solar radiation. Solar radiation increases photolysis rates of NO₂, which leads to increased O₃ production. In addition, emissions of precursors like biogenic VOCs increase with temperature (Coates et al., 2016). Also, reaction rates such as thermal decomposition of PAN is enhanced at high temperature, which intensifies O₃ formation (Sillman et al., 1990). The effect of temperature on O₃ is also illustrated in Fig. B.6 where daily maximum O₃ as observed at all the considered sites is grouped into five year time periods and shown for 10° C temperature bins. It seems that for temperatures above 20° C the sensitivity of daily maximum O₃ on ambient temperature is decreasing with time, an effect that has also been observed for the U.S. by Bloomer et al. (2009). A smaller rate of increase of O₃ with temperature can be expected when ambient NO_x concentrations are decreasing (Coates et al., 2016). The changing sensitivity of ozone on temperature leads to the risk that GAMs specified for the whole time period might underestimate (overestimate) the effect of temperature on O₃ in the first (last) years of the time series. Consequently, this results in too strong downward trends in meteo-adjusted peak O₃. The impact of the changing sensitivity of temperature on ozone has been tested and was found to be negligible (see supplementary material, section S7).

Daily maximum O₃ is on average decreasing with increasing mean relative humidity as shown in Fig. 3.1 for the suburban site in Dübendorf, most probably linked to increased cloudiness conditions. The opposite effect is usually observed in environments close to NO_x emissions, where high water vapor conditions enhance production of OH, and thus lead to higher O₃ production (Vogel et al., 1999; Seinfeld and Pandis, 2016). Increasing CAPE could in principle lead to higher or lower concentration of O₃, depending on the vertical gradient of O₃ as well as on the O₃ formation rate in the boundary layer. We find on average a weak positive relationship between O₃ and CAPE, meaning that O₃ concentrations are typically higher at

Table 3.2 – Table with the most often selected meteorological variables and the number of sites in which they were selected for the GAMs for the warm period May–September (in total 18 sites, where the selection was applied).

Meteorological variable	number of sites daily maximum O ₃	number of sites MDA8 O ₃
Temperature - daily maximum	16	15
Humidity - daily mean	10	14
CAPE - morning mean	5	7
East-West Surface stress - daily mean/afternoon mean	8	9
North-South Surface stress - daily mean/afternoon mean	9	9

high instability of the troposphere and strong vertical mixing as associated with high CAPE values (Davies et al., 2013). North-south/east-west surface stress are explanatory variables representing the prevailing wind conditions, i.e. increasing positive values mean increasing north-south/east-west wind velocity and increasing negative values indicate increasing wind velocities in the opposite direction. Strong wind leads to lower O₃ mixing ratios in most stations, as shown for Dübendorf in Fig. 3.1. Nevertheless, the effect of wind direction on O₃ depends on specific local conditions and can vary among the studied sites. In agreement with Ordóñez et al. (2005), the day of week has not been selected as an important explanatory variable in the GAM models for the summer months. The day of week was, however, selected in the GAM models for the cold season. Brönnimann and Neu (1997) found on the one hand that during favourable weather conditions O₃ concentrations in Switzerland were lower during weekends than on weekdays. This dependence on the day of week can for daily maximum O₃ also directly be seen in our measurements. However, including the day of week in the GAMs did not improve the models with respect to AIC (see also supplementary material). On the other hand, Brönnimann and Neu (1997) found higher O₃ concentrations on weekends compared to weekdays for weather conditions that are not favourable for O₃ formation. The effect that lower NO_x emissions during the weekend can in polluted areas lead to higher O₃ production has also been described by Marr and Harley (2002).

The meteorological variables that were selected in our GAM models agree well with the ones selected in the study by Ordóñez et al. (2005). Temperature, humidity and variables representing wind speed were selected in most stations in both studies. However, in contrast to Ordóñez et al. (2005) who found global radiation to be an important variable at many stations, radiation was hardly selected in this study. This difference is explained by the variable selection approach applied in this study that prevents co-selection of variables that are highly correlated such as radiation and temperature or multiple variables characterizing similar phenomena (e.g., WTC and wind conditions).

The meteorologically driven variability of daily maximum and MDA8 O₃ explained by the GAMs is expressed by the coefficient of determination R^2 . In the present study R^2 for the daily maximum O₃ in the warm season ranges between 52-74% (except for Jungfrauoch only 24%) and in the cold season 63-82% (in Jungfrauoch 48%), while for the MDA8 O₃ in the warm period R^2 is between 53 and 78% (in Jungfrauoch 29%) and in the cold period 50-82% (in

Chapter 3. Trends of surface maximum ozone concentrations in Switzerland based on meteorological adjustment for the period 1990-2014.

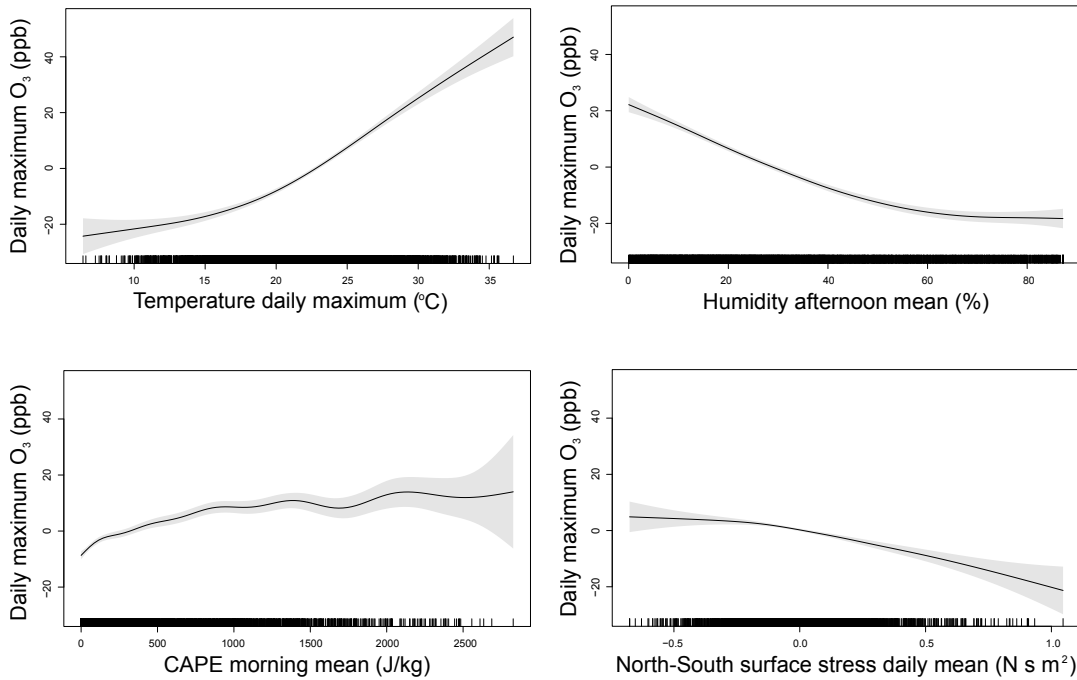


Figure 3.1 – Example of relationship between daily maximum O₃ and some of selected meteorological variables for the suburban site Dübendorf.

Jungfrauoch 50%). It should be noted that the applied meteorological adjustment allows the removal of a large fraction but certainly not all of the variability in the O₃ data that is caused by meteorology. However, partial removal of meteorology driven variability from the observations is very useful for trend estimation as detailed below. Model assumptions for normally distributed residuals are fulfilled, with models for the warm season performing better than the ones for the cold season with respect to the constant variance assumption (see supplementary material).

The meteorological adjustment leads to a reduced variability in the daily maximum and MDA8 O₃ as shown in Fig. 3.3. Note that MTDM and 4-MDA8 calculated from meteo-adjusted daily maximum and MDA8 O₃ are systematically lower than when calculated directly from the measured values (Fig. 3.4), because these metrics exclusively include observations at meteorological conditions that are favorable for O₃ formation. The meteo-adjustment leads to a normalization of the measured O₃ to concentrations that are more representative for average meteorological conditions.

3.4.2 Trends of peak O₃ concentrations

Meteo-adjustment removes meteorologically driven variability from the observations and, therefore, allows trend calculations with smaller uncertainties. Consequently, trend estima-

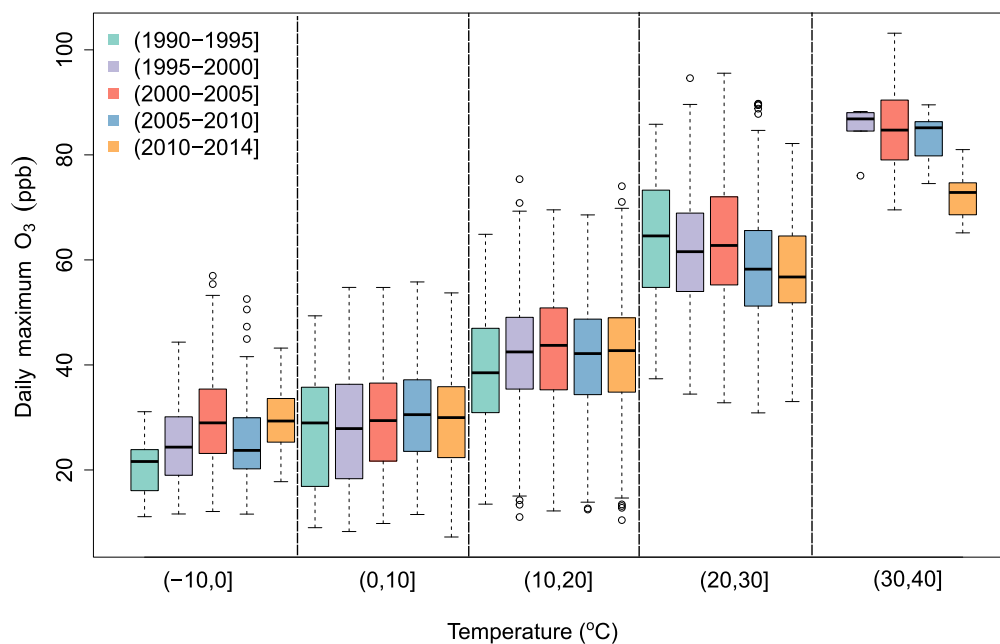


Figure 3.2 – Daily maximum O₃ for different daily maximum temperature ranges and time periods averaged for all studied sites. Box encompasses 25th to 75th percentile with a line at the median; whiskers extend to 1.5 times the interquartile range. Values for each site category are shown in the supplementary material.

tions from meteo-adjusted data were more often statistically significant compared to the trends that were directly determined from the measurements (Figs. 3.5 and 3.6). Reduced uncertainty is a main advantage of meteo-adjustment as it allows the earlier detection of significant trends in air quality measurements.

The larger negative trends estimated for most stations after meteo-adjustment can be attributed to additional removal of systematic variations in meteorological variables that occur in short-term and long-term time scales. For example, the hot summers of 2003 and 2006 (Ordóñez et al., 2005; Schnell et al., 2014; Carro-Calvo et al., 2017) were exceptionally favorable for O₃ formation, leading to less negative trends when calculated directly from the observations (supplementary material, Section S8). As can be seen in Fig. 3.7, MTDM and 4-MDA8 values corresponding to the years 2003 and 2006 stand out from the other data points. After the removal of the meteorological influence from the observations these points lie very close to the trend line, leading to the estimation of a higher negative trend. Meteo-adjustment also normalizes O₃ trends to the average meteorological condition of the study period, removing the effect of the small, long-term increase in temperature observed during the study period (supplementary material, section S8) which otherwise dampens the trend on O₃ variation that is not due to meteorological factors.

Chapter 3. Trends of surface maximum ozone concentrations in Switzerland based on meteorological adjustment for the period 1990-2014.

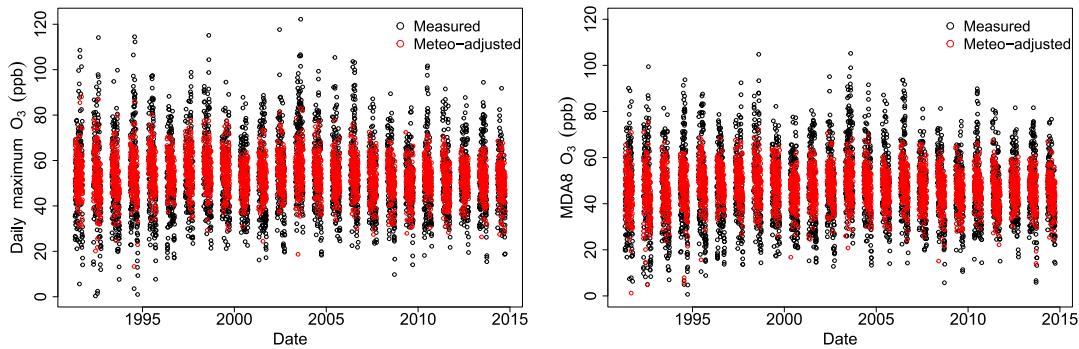


Figure 3.3 – Measured and meteo-adjusted daily maximum O₃ (left) and MDA8 O₃ (right) time series for the suburban site in Dübendorf.

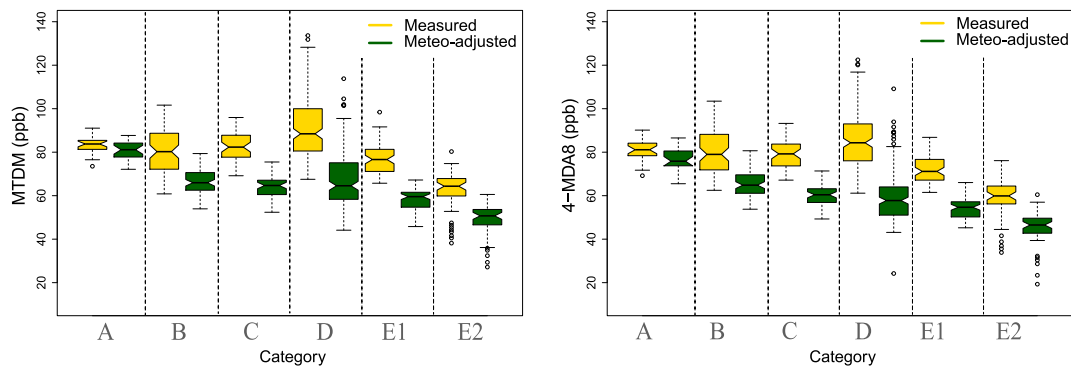


Figure 3.4 – Box-whisker plot for the MTDM and 4-MDA8 mixing ratios as calculated from measured and meteo-adjusted data separated for the different site categories.

In general, peak O₃ mixing ratios in Switzerland decreased between 1990 and 2014 (Table 3.3). MTDM and 4-MDA8 showed on average significant decreasing trends during 1990-2014 for the categories with low or moderate NO_x pollution B, C and D and for the highly polluted E1 as well (Figs. 3.5, 3.6). For the categories A and E2, i.e. remote stations and the most polluted urban traffic sites, increasing trends of MTDM and 4-MDA8 were observed. Peak O₃ trends mostly reflect changes in local photochemical production, resulting from changes in O₃ precursors concentrations. More precisely, in the studied sites NO and NO₂ mixing ratios have decreased between 1990 and 2014 (Fig. 3.8). It is clear that at the more remote sites the absolute reduction rate is much smaller than at sites closer to main NO_x sources. At sites close to traffic (categories E1 and E2) NO had a much higher rate of decrease compared to NO₂. This is partly due to the higher fraction of NO₂ in the emissions from newer generations of diesel vehicles (Grice et al., 2009; Grange et al., 2017) and partly because most of the NO_x is emitted as NO. A substantial amount of NO₂ is instantaneously formed by the reaction of NO with O₃.

The remote site of Jungfraujoch (JUN, 3580 m a.s.l.) in category A, showed an increase for MTDM and 4-MDA8 (Figs. 3.5 and 3.6). However, it was observed that the increase of the peak O₃ metrics is slowing down after beginning of 2000s, likely due to the influence of background

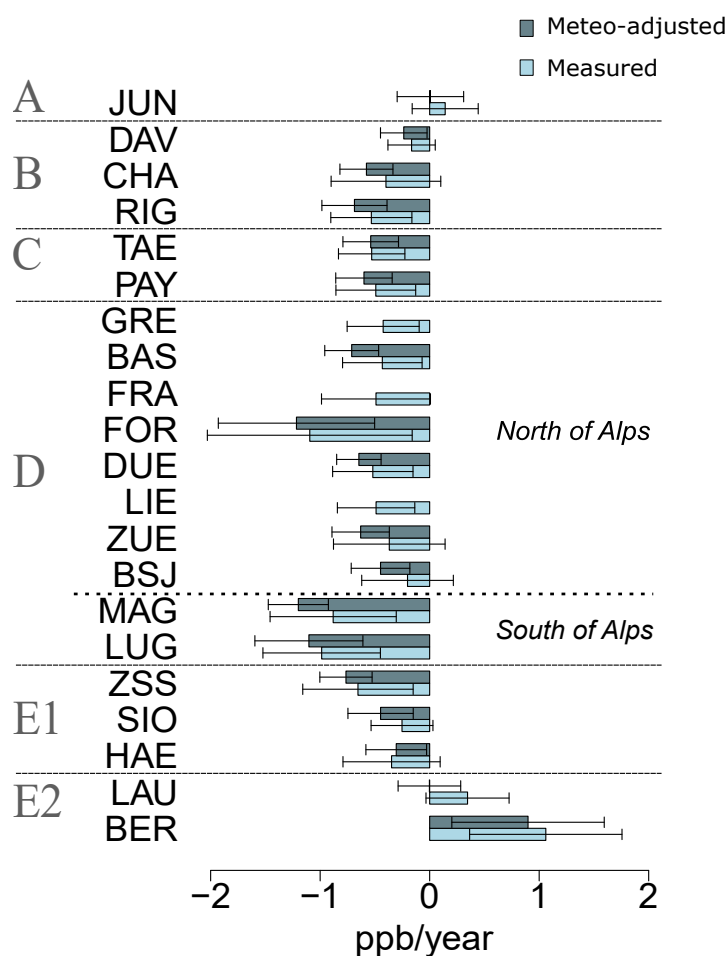


Figure 3.5 – Theil-Sen trends of MTDM for the studied sites across Switzerland. Error bars show the 95% CI. Note that, for the stations FRA, GRE and LIE, no complete meteorological information was available; therefore, meteo-adjustment was not applied.

O₃ concentrations (Derwent et al., 2007; Vingarzan, 2004). Background O₃ is attributed to hemispheric transport influenced by emissions in North America and Southeast Asia as well as transport of O₃ from the stratosphere (Derwent et al., 2004; Cooper et al., 2014; Dentener et al., 2010; Hess and Zbinden, 2013). Because locally produced O₃ at this station is very low, it is expected that mixing ratios of mean and peak O₃ have a similar temporal evolution. For daily mean O₃ at Jungfraujoch, an upward trend has been found for the time between 1990 and 2003 (+0.54 ppb/year). This trend stopped after 2003 and mean O₃ started to slightly decline by -0.17 ppb/year (Boleti et al., 2018a). At the remote site Mace Head (Ireland) a similar trend of European background O₃ as obtained for Jungfraujoch has been found. According to Derwent et al. (2018) monthly O₃ means were increasing since 1987 at a rate of +0.34 ppb/year and started to decrease after 2007 by -0.02 ppb/year².

Chapter 3. Trends of surface maximum ozone concentrations in Switzerland based on meteorological adjustment for the period 1990-2014.

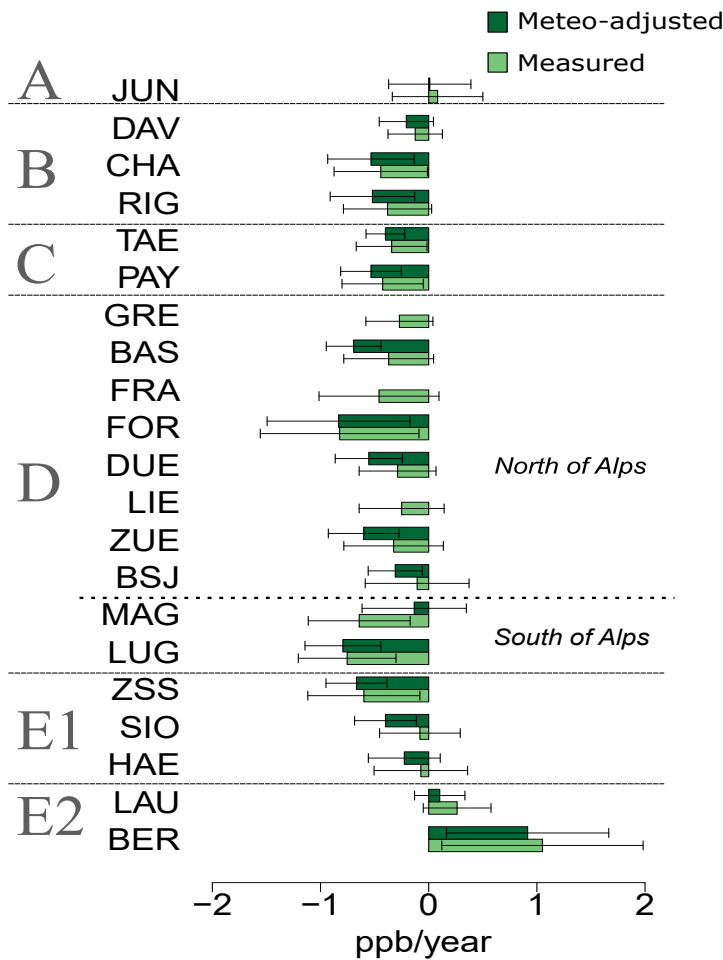


Figure 3.6 – Same as in Fig. 3.5 for 4-MDA8.

In categories B, C, D and E1 the evolution of peak O₃ trends is similar. MTDM and 4-MDA8 decreased in all cases (Figs. 3.5 and 3.6). In the environments of categories B and C, the decrease of NO_x since the 1990s has contributed to the decline of peak O₃. In the urban and suburban sites of categories D and E1 the decrease of NO₂ and NO was more pronounced than in rural and remote areas (Fig. 3.8), with the decrease rate being higher before mid-2000s compared to late-2000s (Boleti et al., 2018a). A similar trend behavior has been found for total VOCs (not shown).

A few of the urban sites in category E1 show an inflection point in the trend (Fig. 3.9). For instance in Härkingen (HAE), the trend is mostly flat until 2005 and decreases afterwards, which also leads to the calculation of a smaller negative trend for the whole period 1990-2014. This behavior can qualitatively be understood by O₃ isopleths diagrams that describe maximum O₃ production in relation to initial NO_x and VOC concentrations (Finlayson-Pitts and Pitts, 2000). At locations in the vicinity of emissions sources and high NO_x levels (VOC-

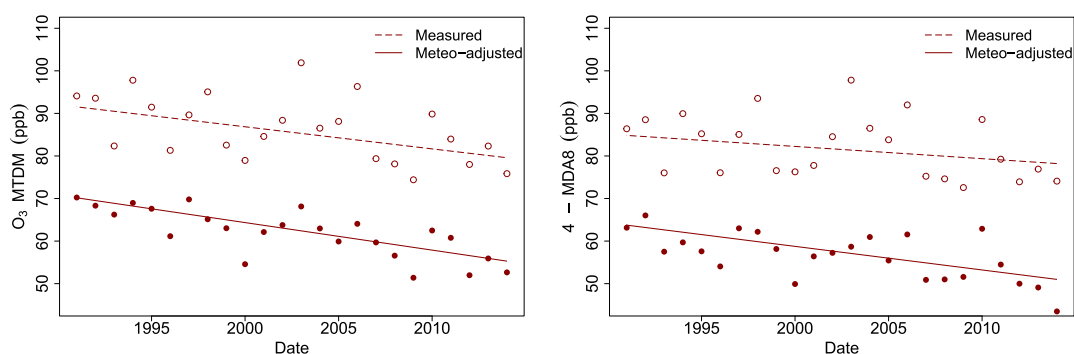


Figure 3.7 – Trends of measured and meteo-adjusted MTDM (left) and 4-MDA8 (right) for the suburban site in Dübendorf.

Table 3.3 – Theil-Sen trends (mean value per group) of MTDM, 4-MDA8 and SOMO35. First and second values indicate the measured and meteo-adjusted trend respectively. In category D the mean trends are additionally shown for the sites north and south of the Alps separately. For SOMO35 meteo-adjustment was not applied and a linear trend is not meaningful for categories A and B due an inflection point during the studied time period. Cat. indicates the station's category.

Cat.	Environment	MTDM (ppb/year)	4-MDA8 (ppb/year)	SOMO35 (ppb.days/year)
A	High alpine	0.14/0.01	0.08/0.01	-
B	Alpine & pre-alpine	-0.36/-0.5	-0.31/-0.42	-
C	Rural, low altitude	-0.51/-0.57	-0.38/-0.46	-16.76
D	Suburban & urban	-0.64/-0.85	-0.47/-0.55	2.59
<i>D</i>	<i>North of Alps</i>	<i>-0.52/-0.73</i>	<i>-0.38/-0.59</i>	<i>2.37</i>
<i>D</i>	<i>South of Alps</i>	<i>-0.93/-1.15</i>	<i>-0.69/-0.46</i>	<i>-8.21</i>
E1	Traffic sites	-0.41/-0.5	-0.25/-0.43	0.57
E2	Urban, high traffic	0.70/ 0.44	0.65/ 0.50	47.22

limited regime), reduction of NO_x without equivalent reduction of VOCs can lead to increased O_3 production, which likely has been the case for sites like HAE during the 1990s and until 2005. After mid-2000s the decrease of NO_x and VOCs levelled off at similar rates (EEA, 2017), leading to the observed downward trends until 2014.

The sites in Magadino (MAG) and Lugano (LUG), both located south of the Alps, experienced a larger decrease compared to the other sites in category D. For instance, the MTDM trend is -1.15 ppb/year averaged for MAG and LUG only, while for the other sites in category D the determined trend is -0.73 ppb/year (Table 3.3). Due to their location in the south of the Alps, these two sites have special climatic conditions and are affected by polluted air masses originating in the Milan industrial region (Brönnimann et al., 2002; Prévôt et al., 1997). As was shown with a backward trajectories analysis by Prévôt et al. (1997), O_3 precursors are transported from the Milan area towards southern Switzerland and blocked by the Alps. Therefore, higher O_3 peaks are observed in sites south of the Alps compared to the other sites

Chapter 3. Trends of surface maximum ozone concentrations in Switzerland based on meteorological adjustment for the period 1990-2014.

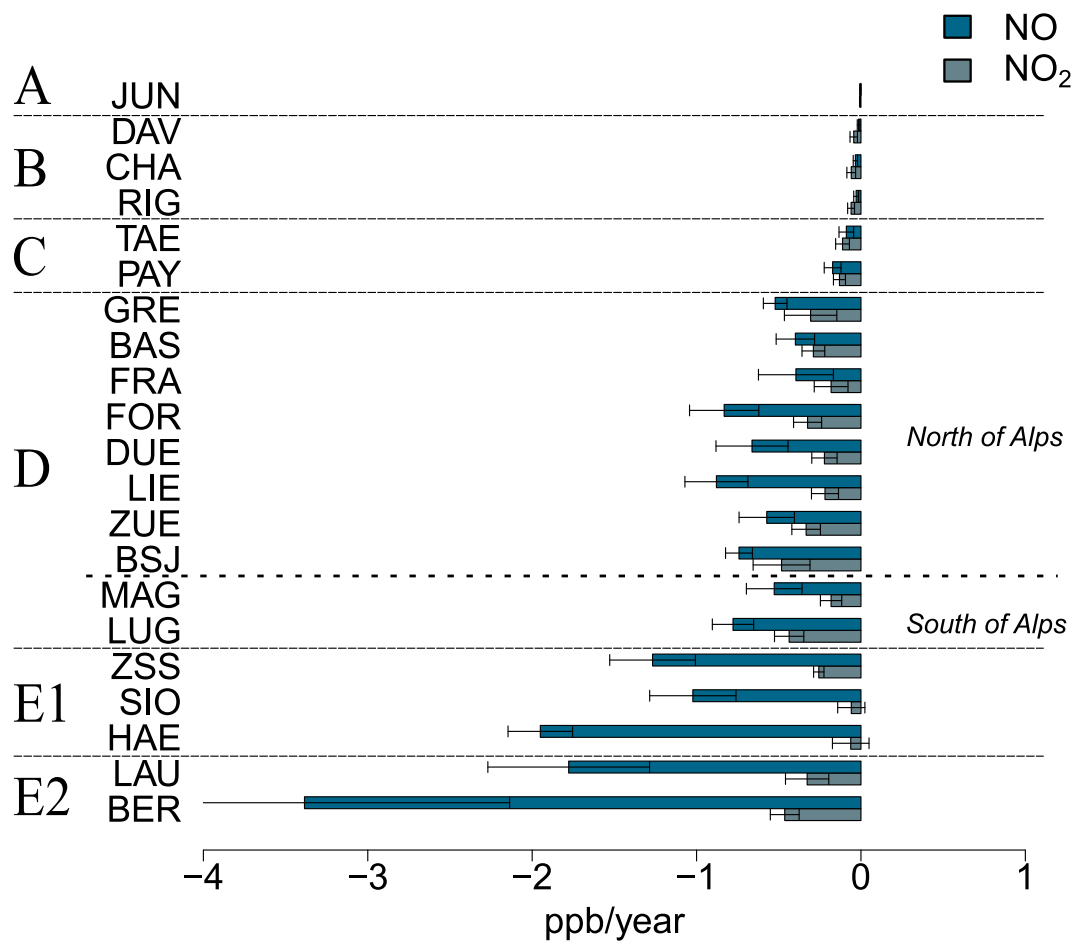


Figure 3.8 – Theil-Sen trends of daily mean NO and NO₂ during 1990-2014 (in ppb/year) for the studied sites in Switzerland based on yearly averages. Error bars show the 95% CIs obtained by the Theil-Sen trend estimator.

in category D (Fig. 3.9 in category D).

Category E2 includes the urban stations in Lausanne (LAU) and Bern (BER), that are located next to urban roads with high traffic. At these locations positive trends for the MTDM and 4-MDA8 were observed, linked to the much stronger decrease of NO compared to NO₂ (Fig. 3.8). The resulting reduced titration of O₃ by NO partly explains the positive trends at the above sites (Monks, 2000). Especially BER experienced a pronounced increase, although a level off is observed after 2004 (inset of Fig.3.9). The inflection point in BER can be explained –similar to HAE– by the changing reduction rate of NO_x in the mid-2000s. For BER, estimation of a single trend for the whole time period is not meaningful as the trend behaviour before and after 2004 would be under- and overestimated, respectively. Similar to the metrics for peak O₃, an upward trend of daily mean de-seasonalized O₃ concentrations in LAU and BER has been observed, with sign of stabilization after around 2010 (Boleti et al., 2018a). At locations close to

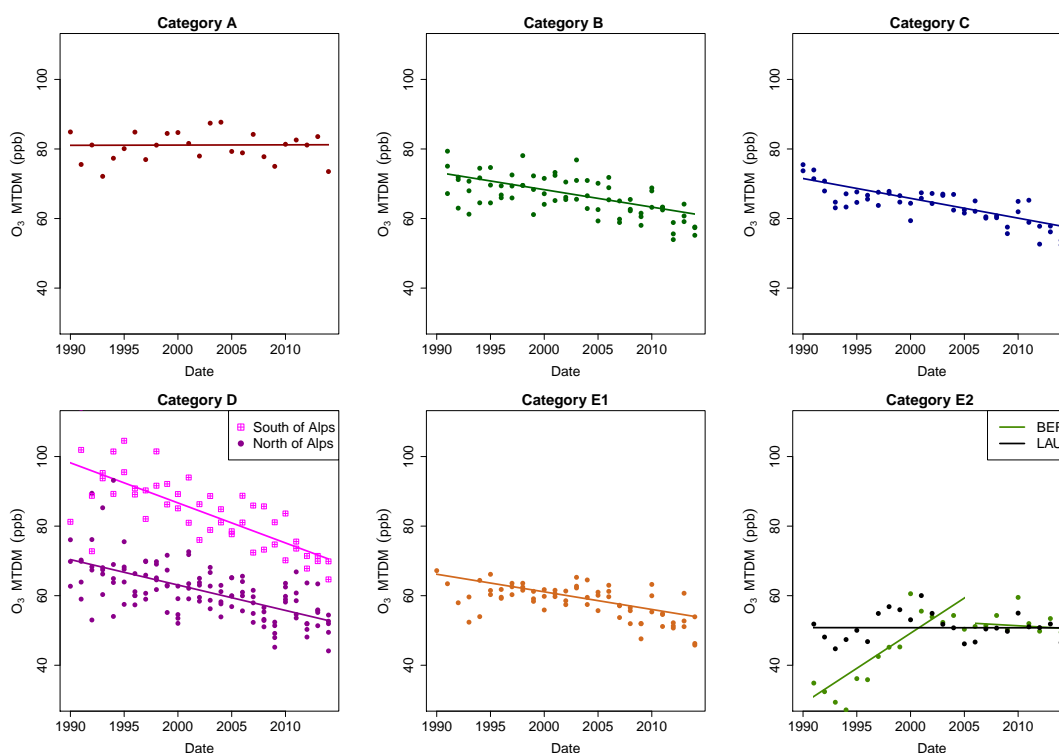


Figure 3.9 – Theil-Sen trend lines are shown as means of all sites in each category for the meteorologically adjusted MTD. Points show the yearly average value for all sites in the category. Trend in Bern (BER) is shown additionally for the MTD in two periods (1990-2004 and 2004-2014), due to exceptional behavior compared to the other studied sites. Sites in category D located south and north of the Alps are indicated with different color and shapes to point out their differences in O_3 mixing ratios trends.

sources of NO_x , it appears that the temporal trend of peak O_3 metrics is strongly influenced by the development of the morning O_3 baseline determined by the extent of NO titration. Because of the strong reductions in NO_x emissions, less titration of O_3 through reaction with NO led to generally higher O_3 levels at these locations (Boleti et al., 2018a). During meteorological conditions that are favorable for the formation of O_3 , local O_3 formation can start from a still increasing initial O_3 background. This is also exemplified by the trend in the number of days with MDA8 O_3 exceeding 35 ppb for the 1990-2014 period, which is strongest for the two urban roadside sites in category E2 (supplementary material, Fig. S4). Consequently, a positive and statistically significant trend for the SOMO35 metric has been found for the sites in category E2 (Fig. 3.10 and supplementary material Fig. S1).

At other urban, suburban and traffic related sites (categories D and E1) the number of days with MDA8 O_3 exceeding 35 ppb is also increasing and the trend of SOMO35 tends to be positive, although the trend estimates are not statistically significant. At rural sites (category C) the SOMO35 trends tend to be negative. Increase in SOMO35 at urban sites from lower values and decrease in SOMO35 in rural sites from higher values indicate that differences between

Chapter 3. Trends of surface maximum ozone concentrations in Switzerland based on meteorological adjustment for the period 1990-2014.

rural and urban have become smaller during the studied period, which reflects trends in both the mean (Boleti et al., 2018a) and peak concentrations. Exceptions are found at the sites of categories A and B, where an inflection point in SOMO35 is observed in the beginning of the 2000s. A linear trend is not suitable for characterizing this type of behavior and was therefore not estimated for these sites.

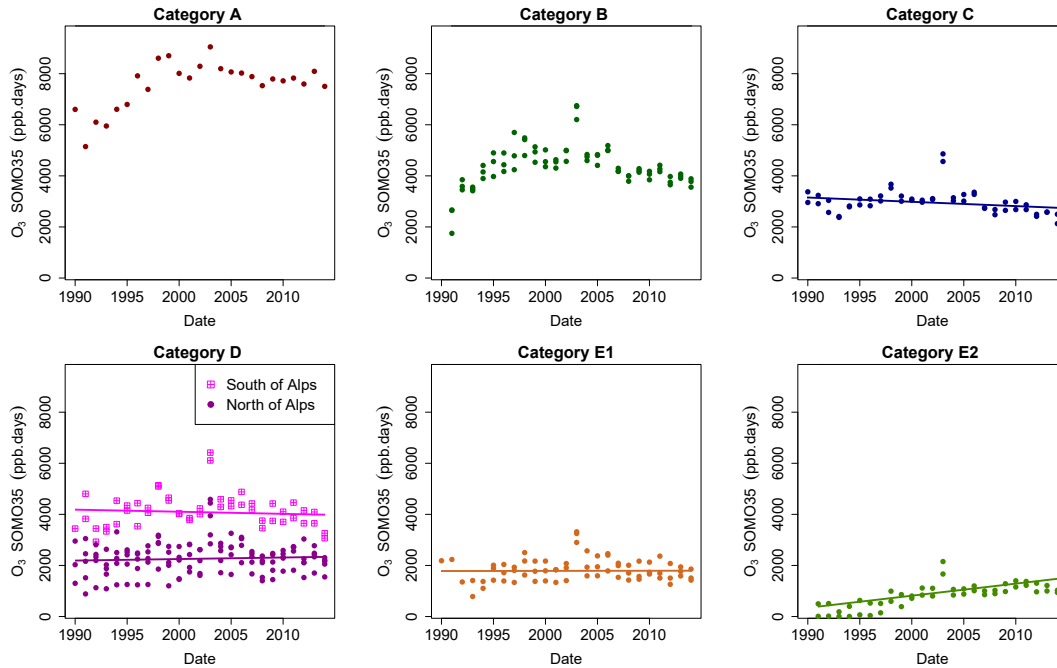


Figure 3.10 – Same as in Fig. 3.9 for SOMO35. Note that meteo-adjustment was not applied for SOMO35. A linear trend is not shown for categories A and B as there is an inflection point during the studied time period.

The calculated trends of the 90th percentile of meteo-adjusted daily maximum O_3 can be compared to the trends found earlier by Ordóñez et al. (2005). For most of the sites covered by both studies, the calculated trends agree well although different data analytical approaches have been applied to observations during different time periods. For instance, downward trends were in both studies found in Zürich (ZUE) and Dübendorf (DUE) and an upward trend in LAU. However, for the rural traffic sites HAE and Sion (SIO), an upward trend was observed by Ordóñez et al. (2005) and downward trends were found in our study. The different trends in the two time periods (1992-2002 and 1990-2014) are due to an inflection point that is observed for the sites close to traffic, with a slight increase in the 1990s and decrease after mid-2000s. When the meteo-adjustment approach used in this study is applied to the 1992-2002 time period as covered by Ordóñez et al. (2005) very similar and also not statistically significant trends have been obtained (supplementary material). Consequently, the significant trends of peak O_3 described here for the 1990-2014 period benefit from the availability of a sufficiently long time series.

The importance of long time series of observations and the effect of special meteorological

events in the trend estimation can also be seen by comparison of the results of this study with the Solberg (2009) report. In Solberg (2009), the trend of MTDM at rural Swiss sites was determined for the 1995-2005 period directly from the measurements and also from outputs of the regional EMEP Unified Chemical Transport Model. The MTDM trend as derived from the EMEP model was -1.25 ppb/year, the average trend calculated from the observations was almost zero (-0.01 ppb/year). When the methodology used in this study is applied to data from the same time period as used in Solberg (2009), significant trends of meteo-adjusted MTDM were between -0.85 and -0.5 ppb/year for most rural and suburban sites (categories B, C and D). In the latest trend assessment report by EMEP, the median trend of the SOMO35 for rural background sites across Europe during the time period 1990-2012 has been determined to be -11 ppb.days/year with a 95% confidence interval [-21, -2.4] ppb/year (EMEP, Co-operative Programme for Monitoring and Evaluation of the Long-Range Transmission of Air Pollutants in Europe, 2016). The SOMO35 trends for similar site types (category C) in Switzerland found in this study is on average -14.3 [-34, 11.8] ppb.days/year, which is not statistically significant but similar to the trends found across Europe. In the study by Fleming et al. (2018), significant negative SOMO35 trends for the period 2000-2014 were found for 20% of the non-urban sites in Europe, whereas for most of the urban sites the calculated trends were not significant. When SOMO35 trends are calculated for the same 2000-2014 period than in Fleming et al. (2018), mostly negative and significant trends were found in rural sites. For most suburban and urban sites, trends are also negative but non-significant (supplementary material, Fig. S9).

Analysis of peak O₃ trends is naturally focusing on temporal changes of O₃ selectively for conditions that are favourable for O₃ formation. In contrast, mean O₃ trends reflect changes in O₃ as a consequence of all prevailing atmospheric conditions. However, comparison of the temporal changes in peak and mean O₃ shows, that while peaks have been decreasing in rural, suburban and most urban sites in Switzerland after 1990, mean O₃ mixing ratios started decreasing or leveling off only after mid-2000s (Boleti et al., 2018a). At sites located very close to NO_x emission sources, both mean and peak O₃ have been increasing since 1990 with signs of levelling off or decrease after mid-2000s. Inflection points for the mean O₃ concentrations occurred in most cases later as for peak O₃ (Boleti et al., 2018a). Similar to our results, an inflection point for spring and summer season monthly averages has been detected in Mace Head between 2005-2008 while the annual averages peaked around 2007 (Derwent et al., 2018).

3.5 Conclusions

Peak O₃ mixing ratios have been decreasing in most stations in Switzerland between 1990 and 2014. It was shown that meteo-adjusted MTDM and 4-MDA8 decreased in rural, suburban and most urban stations by around 0.5-1.2 ppb/year and 0.4-0.6 ppb/year respectively. The behavior of the observed O₃ long-term trends depends on the site type. At urban traffic sites all studied metrics increased between 1990 and 2014, due to reduced titration of O₃. The trends of MTDM and 4-MDA8 are also positive at the remote site Jungfraujoch, here representing

Chapter 3. Trends of surface maximum ozone concentrations in Switzerland based on meteorological adjustment for the period 1990-2014.

the increasing background O₃ concentrations in Europe. The absence of significant trends of SOMO35 in suburban and urban areas indicates that health impacts from O₃ as expressed by this metric remained largely unchanged for most of the Swiss population during the past 25 years.

The selection of the most important meteorological variables led to concise statistical models describing meteorological influence on maximum O₃ concentrations at the studied sites. The most important meteorological variables for explaining the variability of O₃ are temperature and humidity, followed by the wind speed, here expressed as east-west/north-south surface stress. The day of week has been found to be an important factor variable during the cold season only. Meteo-adjustment eliminated a large part of the meteorological driven variability in O₃, allowing an earlier detection of statistically significant changes in tropospheric O₃. This technique can particularly be useful when extreme meteorological conditions (e.g. heat waves) or temporal trends in meteorological variables might influence the trend estimation. Nevertheless, the availability of sufficiently long time series is a key factor for meaningful trend analyses of tropospheric O₃.

Acknowledgements This study was supported by the Swiss Federal Office for the Environment (FOEN). We would like to thank Dr. Stephan Henne for extracting ERA-Interim meteorological variables.

4 Temporal and spatial analysis of ozone concentrations in Europe based on time scale decomposition and a multi-clustering approach.

Eirini Boleti^{1,2}, Christoph Hueglin¹, Stuart K. Grange³, André S. H. Prévôt⁴ and Satoshi Takahama²
published in *Atmos. Chem. Phys. Discuss.*, <https://doi.org/10.5194/acp-2019-909>, in review, 2019. Under review for publication in *Atmospheric Chemistry and Physics*

¹Empa, Swiss Federal Laboratories for Materials Science and Technology, Überlandstrasse 129, Dübendorf, Switzerland

²EPFL, École Polytechnique Fédérale de Lausanne, Route Cantonale, 1015 Lausanne, Switzerland

³Wolfson Atmospheric Chemistry Laboratories, University of York, York, YO10 5DD, UK

⁴PSI, Paul Scherrer Institute, 5232 Villigen, Switzerland

Abstract: Air quality measures that were implemented in Europe in the 1990s resulted in reductions of ozone precursors concentrations. In this study, the effect of these reductions on ozone is investigated by analyzing surface measurements of ozone for the time period between 2000 and 2015. Using a non-parametric time scale decomposition methodology, the long-term, seasonal and short-term variation of ozone observations were extracted. A clustering algorithm was applied to the different time scale variations, leading to a classification of sites across Europe based on the temporal characteristics of ozone. The clustering based on the long-term variation resulted in a site type classification, while a regional classification was obtained based on the seasonal and short-term variations. Long-term trends of de-seasonalized mean and meteo-adjusted peak ozone concentrations were calculated across large parts of Europe for the time period 2000-2015. A multi-dimensional scheme was used for a detailed trend analysis, based on the identified clusters, which reflect precursor emissions and meteorological influence either on the inter-annual or the short-term time scale. Decreasing mean ozone concentrations at rural sites and increasing or stabilizing at

Chapter 4. Temporal and spatial analysis of ozone concentrations in Europe based on time scale decomposition and a multi-clustering approach.

urban sites were observed. At the same time downward trends for peak ozone concentrations were detected for all site types. The effect of hemispheric transport of ozone can be seen either in regions affected by synoptic patterns in the northern Atlantic or at sites located at remote high altitude locations. In addition, a reduction of the amplitude in the seasonal cycle of ozone was observed, and a shift in the occurrence of the seasonal maximum towards earlier time of the year. Finally, a reduced sensitivity of ozone to temperature was identified. It was concluded that long-term trends of mean and peak ozone concentrations are mostly controlled by precursors emissions changes, while seasonal cycle trends and changes in the sensitivity of ozone to temperature are driven by regional climatic conditions.

4.1 Introduction

Tropospheric ozone (O₃), together with particulate matter and nitrogen dioxide (NO₂), is one of the most troublesome air pollutants in Europe (Guerreiro et al., 2016). 17,000 premature deaths every year are attributed to excess O₃ exposure, without any sign of reduction in number of fatalities (Guerreiro et al., 2016). In terms of impact on ecosystems, elevated concentrations of tropospheric O₃ are responsible for damaging agricultural production and forests mainly by reducing their growth rate. In addition, tropospheric O₃ acts as a greenhouse gas with an estimated globally averaged radiative forcing of $0.4 \pm 0.2 \text{ W/m}^2$ (IPCC, 2013). In the 1990s emission control measures on O₃ precursors, namely nitrogen oxides (NO_x=NO+NO₂) and volatile organic compounds (VOCs), were implemented in order to regulate air pollution. As a result, concentrations of NO_x and VOCs have significantly declined in Europe (EEA, 2017; Colette et al., 2011; Guerreiro et al., 2014; Henschel et al., 2015). Especially, NO_x emissions declined in Europe by 48% between 1990 and 2015 (EEA, 2017).

Surprisingly, O₃ concentrations have not decreased as was expected (Oltmans et al., 2013; Colette et al., 2018). Mean O₃ concentrations have either remained stable or even increased in rural, background areas from 1990s and until mid-2000s in many European countries (Boleti et al., 2018a; Munir et al., 2013; Paoletti et al., 2014; Querol et al., 2016; Anttila and Tuovinen, 2009, e.g.). At urban sites an increase of mean O₃ has been observed; in some cases, an increase has been found at both rural and urban sites with larger upward trends observed at urban compared to the rural sites (Paoletti et al., 2014; Querol et al., 2016; Anttila and Tuovinen, 2009). However, a change in the trend has been observed after mid-2000s, when mean O₃ concentrations have started to decline (Boleti et al., 2018a; Munir et al., 2013). On the other hand, maximum O₃ concentrations decreased continuously from the 1990s until present (Paoletti et al., 2014), except for the traffic loaded environments (Boleti et al., 2018c). Downward trends of different metrics for peak O₃ have been found at many sites across Europe (Fleming et al., 2018). However, the high year to year variability of O₃ tends to mask the long-term changes leading to a large fraction of sites with non-significant trends. Several studies based on either observations or climate models have shown that anthropogenic emissions can affect O₃ concentrations across continents (Dentener et al., 2010; Wild and Akimoto, 2001; Lin et al., 2017). The increase of background O₃ in Europe has been associated

with increasing stratospheric O₃ contribution (Ordóñez et al., 2007), as well as increased hemispheric transport of O₃ and its precursors.

A shift in the seasonal cycle of O₃ has been observed in northern mid-latitudes, i.e. the peak concentrations are now observed earlier in the year compared to previous decades with a rate of 3-6 days/decade. (Parrish et al., 2013). This shift is attributed to increasing emissions of O₃ precursors in developing countries, that led to an equatorward redistribution of precursors in the previous decades (Zhang et al., 2016). Negative trends of the 95th percentile of O₃ and positive trends for the 5th percentile have been detected across Europe (Yan et al., 2018). Simultaneous decrease of maximum concentrations in summer and increase in winter indicate a decrease of amplitude in the seasonal variation of O₃, probably as a result of the regulations in the 1990s (Simon et al., 2015).

O₃ variations are largely governed by climate and weather variability (Yan et al., 2018). Especially temperature influences O₃ concentrations in the troposphere, mainly by increasing the rates of several chemical reactions, and by increasing emissions of biogenic VOCs with increasing temperature (Sillman and Samson, 1995). Thermal decomposition of peroxyacyl nitrates (PANs) at high air temperature conditions results in elevated O₃ concentrations (Dawson et al., 2007). Indeed, extreme O₃ concentrations in central Europe are mainly associated with high temperatures (Otero et al., 2016). However, there are indications that the relationship of O₃ to temperature has changed in the last 20 years. For instance, in the U.S., O₃ climate penalty – defined as the slope of the O₃ versus temperature relationship – dropped from 3.2 ppbv/°C before 2002 to 2.2 ppbv/°C after 2002 as a result of NO_x emission reductions (Bloomer et al., 2009).

At different locations, O₃ may show a different temporal evolution due to a variety of factors, such as local pollution, topography, influence of nearby sources or even trans-boundary transport of O₃ and its precursors. In addition, meteorological conditions can vary amongst different locations within large regions such as Europe, affecting O₃ concentrations in various ways. O₃ trend studies in the past have tried to tackle this issue, mainly by using clustering techniques to categorize European measurement sites based on different O₃ metrics (e.g. Henne et al. (2010)). For instance, a site type classification representing O₃ regimes between 2007 and 2010 was obtained by Lyapina et al. (2016) using mean seasonal and diurnal variations. In addition, a geographical categorization reflecting the synoptic meteorological influence on O₃ variation between 1998 and 2012 was obtained by Carro-Calvo et al. (2017). To tackle low spatial representation of urban and rural sites across large domains, i.e. mid-latitude North America, western Europe and East Asia, Chang et al. (2017) obtained a latitude dependent site classification with lower concentrations in western and northern Europe and higher concentrations in southern Europe. These studies indicate that the selected metric used to characterize O₃ in clustering leads to site classifications that represent different aspects of O₃ variability.

In the current study, a multidimensional clustering method that captures several influencing

Chapter 4. Temporal and spatial analysis of ozone concentrations in Europe based on time scale decomposition and a multi-clustering approach.

factors for the long-term trend of O_3 is presented. The temporal and spatial evolution of O_3 concentrations between 2000 and 2015 is studied using data provided by the European Environmental Agency (EEA). Mean O_3 concentrations are decomposed into the underlying frequencies based on a non-parametric time scale decomposition method to obtain the long-term (LT), seasonal (S) and short-term (W) variations. The multidimensional clustering approach is applied to the distinct frequency signals $LT(t)$ and $S(t)$ extracted from the observations.

In addition, long-term trends of de-seasonalized daily mean O_3 and meteo-adjusted peak O_3 concentrations are calculated. Through de-seasonalization and meteo-adjustment, a significant fraction of the meteorologically driven variability of O_3 is excluded from the observations, and uncertainty in the trend estimation is reduced by a large factor. Intersections of site groups, i.e. $LT(t)$ -and $S(t)$ -clusters, are employed to guide the study of O_3 long-term trends. Furthermore, changes in the amplitude and phase of the seasonal variability of O_3 are explored based on the $S(t)$ signal obtained by the time scale decomposition methodology. Finally, long-term changes in the relationship between O_3 and temperature are estimated and discussed for the different site environments and regions in Europe.

4.2 Data

Data for O_3 surface measurements are provided by the EEA (Air Quality e-Reporting) in an hourly resolution for the period between 2000 and 2015. In this study, only time series with a maximum of 15% of missing values, and a maximum of 120 consecutive days with missing values are used, leaving the study with 291 sites across the European domain (Fig. 4.1). The daily mean and the daily maximum of the 8 hour running mean based on hourly mean concentrations (MDA8 O_3) are calculated following the definition by the European Union Directive of 2008 (European Parliament and Council of the European Union, 2008). For the representation of peak concentrations the following metrics are used: (a) MTDM, which is the mean of the ten highest daily maximum O_3 concentrations during May and September based on hourly mean data and (b) 4-MDA8, the mean of the four highest MDA8 O_3 concentrations per year.

Meteorological variables are extracted from the ERA-Interim data-set on a 1 degree grid at the location (longitude-latitude-altitude) of each station and in 3-hourly intervals. The variables considered for the meteo-adjustment of the peak O_3 metrics are temperature (K), specific humidity (kg/kg^{-1}), surface pressure (hPa), boundary layer height (m), convective available potential energy (CAPE, $J \cdot kg^{-1}$), East-West surface stress ($N \cdot s \cdot m^{-2}$) and North-South surface stress ($N \cdot s \cdot m^{-2}$).

The present trend analysis focuses on (a) the de-seasonalized daily mean and MDA8 O_3 and (b) the meteo-adjusted MTDM and 4-MDA8 concentrations. The analysis of changes in the seasonal cycle of O_3 across Europe is based on the daily mean O_3 concentrations.

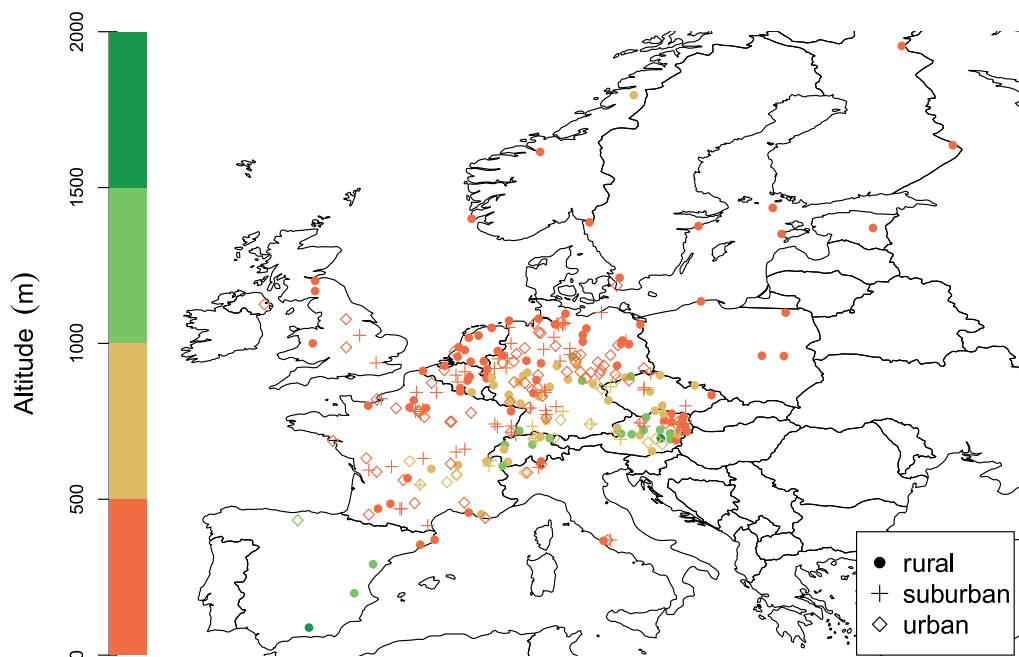


Figure 4.1 – European map showing the location of the studied sites. Type of environment (symbols) and altitude (color bar) are indicated.

4.3 Methods

4.3.1 Time scale decomposition of daily mean and MDA8 O_3

Time scale decomposition refers to decomposition of the O_3 time series into the relevant underlying frequencies:

$$O_3(t) = LT(t) + S(t) + W(t) + E(t) \quad (4.1)$$

where $O_3(t)$ is the daily mean and MDA8 O_3 time series, $LT(t)$ the long-term variation, $S(t)$ the seasonal variation, $W(t)$ the short-term variation and $E(t)$ the remainder of the decomposition. Time scale decomposition in this study is performed with a non-parametric method, called the ensemble empirical mode decomposition (EEMD, Huang et al., 1998; Huang and Wu, 2008; Wu and Huang, 2009), which is considered a powerful method for decomposing O_3 time series (Boleti et al., 2018a). The method detects the hidden frequencies in the time series based merely on the data and yields the so-called intrinsic mode functions (IMFs); each IMF

Chapter 4. Temporal and spatial analysis of ozone concentrations in Europe based on time scale decomposition and a multi-clustering approach.

represents one distinct frequency in the signal.

$$y(t) = \sum_{j=1}^n c_j(t) + LT(t) \quad (4.2)$$

where $y(t)$ is the input data, c_j the different IMFs, n the number of the IMFs and the remainder time series is the $LT(t)$ of the input data. By adding together the IMFs with frequencies between around 40 days and 3 years we obtain the seasonal variation of O_3 ($S(t) = c_7 + \dots + c_{10}$) and by adding the frequencies that are smaller than 40 days the short-term variation is acquired ($W(t) = c_1 + \dots + c_6$).

4.3.2 Cluster analysis of O_3 variations

Cluster analysis is referred to pattern recognition in high dimensional data. The main idea is to represent n objects by identifying k groups based on levels of similarity. Objects in the same group must have the highest level of similarity while objects from different groups must have low level of similarity (Jain, 2010). The partitioning around medoids (PAM) clustering algorithm is used in this study. It is based on k-means (MacQueen, 1967; Hartigan and Wong, 1979) which is a widely used clustering technique (Lyapina et al., 2016, e.g.). PAM is more robust than k-means, because it minimizes the sum of dissimilarities instead of the sum of squared euclidean distances (R Development Core Team, 2017). It works as follows: First, a set of n high dimensional objects (measurement sites) is clustered into a set of k clusters. Initially, k clusters are generated randomly and the empirical means m_k of the euclidean distance between their data points are calculated. Then, each data point is assigned to its nearest cluster center (centroid). Centroids are iteratively updated by taking the medoid of all data points assigned to their clusters. The squared error (ϵ) between the m_k and the points in the cluster (x_i) is calculated as:

$$\epsilon = \sum_{i=1}^n \|x_i - m_k\|^2 \quad (4.3)$$

Each centroid defines one of the clusters and each data point is assigned to its nearest centroid, and the iterative process is terminated when the ϵ is minimized.

For identification of the clusters the $LT(t)$, $S(t)$ and $W(t)$ of the daily mean and MDA8 O_3 were used as input time series in the PAM algorithm. A sufficient number of clusters must be defined in order to capture dominant behaviors such that redundant information is avoided but at the same time not overlooking important characteristics. To identify the optimal number of clusters the k-means algorithm is iteratively executed for a range of k values (number of clusters) and the average sum of ϵ (SSE) is calculated for each iteration, i.e. each k .

$$SSE = \sum_{i=1}^n \epsilon^2 \quad (4.4)$$

The number of clusters with the largest reduction in SSE is considered as the most representative. Eventually, the choice of the ideal number of clusters results from a combination of the SSE approach and interpretability of the obtained clusters. In addition, a Silhouette width (S_w) analysis is performed to assess the goodness of the clustering (Rousseeuw, 1987).

More details about the number of clusters, the goodness of the clustering and the S_w are provided in the Appendix C (C.1 and C.2).

4.3.3 Daily mean and MDA8 O₃ long-term trend analysis

Meteorological adjustment is essential for calculation of robust O₃ long-term trends. Thus, daily mean and MDA8 O₃ observations are de-seasonalized by subtracting the $S(t)$ obtained with the EEMD from the observations (Boleti et al., 2018a)

$$y_d(t) = y(t) - S(t) \quad (4.5)$$

where $y_d(t)$ the de-seasonalized time series and $y(t)$ the observations. Through de-seasonalization observations are adjusted for the effect of meteorology on the inter-annual time scale. Theil-Sen trends (Theil, 1950; Sen, 1968) are then calculated based on monthly mean de-seasonalized concentrations of the $y_d(t)$ for the period 2000-2015. The 95% confidence interval of the trend is obtained by bootstrapping. The Theil-Sen trends were estimated using the *openair* library in R (R Development Core Team, 2017).

4.3.4 Peak O₃ concentrations long-term trend analysis

Trend analysis of peak O₃ metrics is performed for the MTDM and the 4-MDA8 O₃, based on a meteo-adjustment approach as in Boleti et al. (2018c). A different approach for meteorological adjustment was used for the peak O₃ than for the daily mean and MDA8, because de-seasonalization is not meaningful for peak O₃ because peak ozone events are temporally localized. Thus, daily maximum and MDA8 O₃ observations were linked to the available meteorological variables through generalized additive models (GAMs, Hastie and Tibshirani, 1990; Wood, 2006) for the warm season (May-September). GAMs are instances of generalized linear models in which the model is specified as a sum of smooth functions of the covariates. A GAM can be described as:

$$O_3(t) = \alpha + \sum_{i=1}^n s_i(M_i(t)) + s_0(t) + \epsilon(t) \quad (4.6)$$

where $O_3(t)$ stands for the O₃ time series observations (daily maximum and MDA8), α is the intercept, s_i are the smooth functions (thin plates splines) of the numeric meteorological variables M_i and n denotes the number of the numeric meteorological variables in the GAM. The temporal trend is represented through the smooth function $s_0(t)$, where t is the time variable expressed by the Julian day. Finally, ϵ stands for the residuals of the model. For

Chapter 4. Temporal and spatial analysis of ozone concentrations in Europe based on time scale decomposition and a multi-clustering approach.

the GAMs, the following meteorological variables were used based on the meteorological variable selection performed by Boleti et al. (2018c): the daily maximum temperature, daily mean specific humidity, daily mean surface pressure, daily maximum boundary layer height, morning mean convective available potential energy (CAPE), daily mean East-West surface stress and daily mean North-South surface stress, as well as the Julian day. The GAMs were estimated with the *mgcv* library in R (R Development Core Team, 2017).

The meteo-adjusted daily maximum and MDA8 O₃ concentrations were calculated similar to Barmpadimos et al. (2011) as:

$$O_{3_{metadj}}(t) = \alpha + s_0(t) + \epsilon(t) \quad (4.7)$$

where α is the intercept of the model, $s_0(t)$ the time variable as Julian day, and $\epsilon(t)$ the residuals. The meteo-adjusted MTDM and 4-MDA8 concentrations were estimated based on the meteo-adjusted values ($O_{3_{adj}}(t)$) on the same days as they were identified before the meteo-adjustment. Eventually, meteo-adjusted trends were calculated with the Theil-Sen trend estimator applied on the $O_{3_{metadj}}(t)$.

4.3.5 O₃ seasonal cycle trend analysis

The S(t) signal extracted with the EEMD captures the meteorologically driven O₃ variation on yearly to multi-year time scales, and is more representative compared to parametric fitting approaches (Boleti et al., 2018a). Here, changes in the daily mean S(t) of O₃ throughout the studied period are identified as follows: the maximum and minimum O₃ value as well as the day when the maximum O₃ occurred in each year are identified in the S(t), referred here as S_{max} , S_{min} and S_{DoM} respectively (Fig. 4.2). A Theil-Sen trend estimator for each of the $S_{max}(t)$, $S_{min}(t)$ and $S_{DoM}(t)$ is applied for each site cluster, representing the long-term temporal evolution of the amplitude and phase of S(t).

4.3.6 Relationship between O₃ and temperature

The relationship between O₃ and temperature is studied for the warm season May-September. A linear regression model between daily maximum O₃ concentrations and daily maximum temperature is applied for each year throughout the studied period 2000-2015 as:

$$O_3(t)_i = \beta_{0i} + \beta_{1i} \cdot T(t)_i, i = 1, 2, ..n \quad (4.8)$$

where $O_3(t)$ is the time series of the daily maximum O₃, $T(t)$ the time series of the daily maximum temperature and n is the number of years. β_{0i} is the intercept and $\beta_{1i}(t)$ the parameter describing the linear effect of temperature on O₃. Then, a linear model is applied to $\beta_{1i}(t)$ over all years for each site cluster to identify the long-term trend of the slope between O₃ and temperature maximum values. In addition, a linear regression model is applied on the daily maximum O₃ concentrations against binned temperature ranges and in three

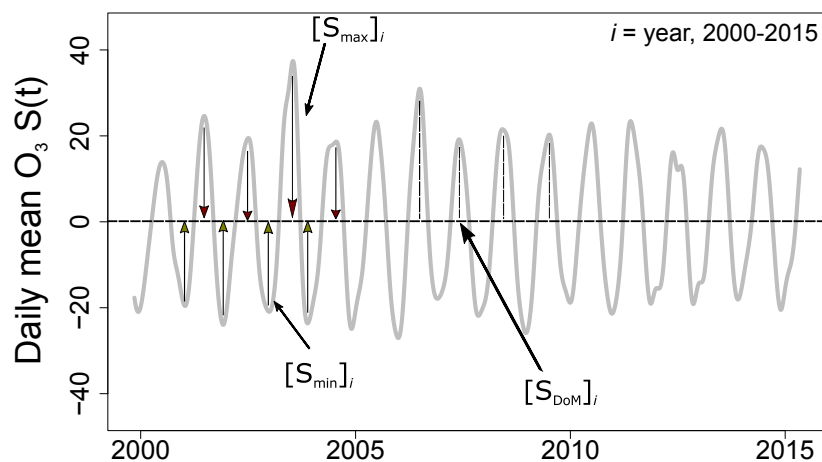


Figure 4.2 – Schematic illustration for explaining the estimation of the ($S_{max}(t)$ and $S_{min}(t)$) and the annual day of maximum of the seasonal signal ($S_{DoM}(t)$) as calculated from the daily mean O₃ time series.

consequent time periods (2000-2005, 2005-2010 and 2010-2015).

4.4 Results

4.4.1 Cluster analysis

Here, we present the results of the daily mean LT(t)- and S(t)-clustering; results for the W(t)-clustering and the cluster analysis based on the MDA8 are provided in the Appendix (C.3). Application of the clustering algorithm to the LT(t) leads to a site type classification, which largely reflects the proximity to emission sources of O₃ precursors. S(t)- and W(t)-clustering leads to a regional site classification, which reflects the importance of the climate on the annual cycle of O₃. It is observed that a few sites have a negative S_w , which means that these sites are assigned to a certain cluster although they do not really fit into any of the identified clusters (see Appendix sections C.2 and C.5). Nevertheless, the sites with negative S_w were not excluded from the data analysis as they do not have a noticeable influence on the results.

O₃ concentrations often increase with distance from emission sources of NO_x. Thus, LT(t)-clustering leads to identification of site groups with similar type of environment in terms of proximity to precursor emissions and mean O₃ concentrations, which are indicative of multiannual changes in the O₃ time series (Boleti et al., 2018a). This measurement-based classification can be more informative than reported station types, since e.g. there are rural sites with nearby pollution sources or even sites with surroundings that might have changed dramatically with time. In the following section, clusters obtained from analysis of daily mean

Chapter 4. Temporal and spatial analysis of ozone concentrations in Europe based on time scale decomposition and a multi-clustering approach.

O₃ are presented and discussed in detail; the clusters derived from MDA8 O₃ are similar and presented in the Appendix (C.3).

Cluster analysis of the long-term variation LT(t) resulted in four clusters that mainly differ in the daily mean O₃ concentration levels: Cluster 1 includes sites that are marked in the Air Quality e-Reporting data repository as being of rural site type and sites that are mostly located at higher altitudes (on average 800 to 1200 m). The sites in cluster 1 show the highest O₃ concentrations as illustrated in Fig. 4.3. The high mean O₃ concentrations indicate that the sites in cluster 1 are representing background situations with minor influence of nearby emissions of man-made O₃ precursors. This cluster is therefore denoted as background cluster ("BAC"). Cluster 2 includes mostly rural sites, that are located at lower altitudes of around 300-600 m and is therefore labelled as rural cluster ("RUR"). The sites in cluster 3 are also located at low altitudes (around 100 to 300 m) and represent rural, suburban and urban site types in similar numbers. The sites in cluster 3 seem to be influenced by nearby man-made emissions of O₃ precursors such as NO_x, leading to lower mean O₃ concentrations compared to the sites in the "RUR" cluster. Cluster 3 consists of moderately polluted sites and denoted as cluster MOD. Finally, cluster 4 consists mostly of urban and suburban sites showing the lowest daily mean O₃ concentrations likely due to the proximity to sources of NO_x emissions and the resulting enhanced depletion of O₃ through reaction with NO. Consequently, cluster 4 is denoted as the highly polluted cluster ("HIG").

The LT(t) signal as derived from the daily mean and MDA8 O₃ observations increases for "BAC" and "RUR" until around beginning of 2000s and decreases afterwards. For the "MOD" and "HIG" clusters the same pattern was observed, but the decrease starts much later than in the rural sites, i.e. around end of 2000s. Especially in the "HIG" sites mostly a level-off is observed after 2010 rather than a decrease. Similar temporal evolution with inflection points in the LT(t) has been observed in the study by Boletti et al. (2018a) which was focused on trends of average O₃ concentrations in Switzerland.

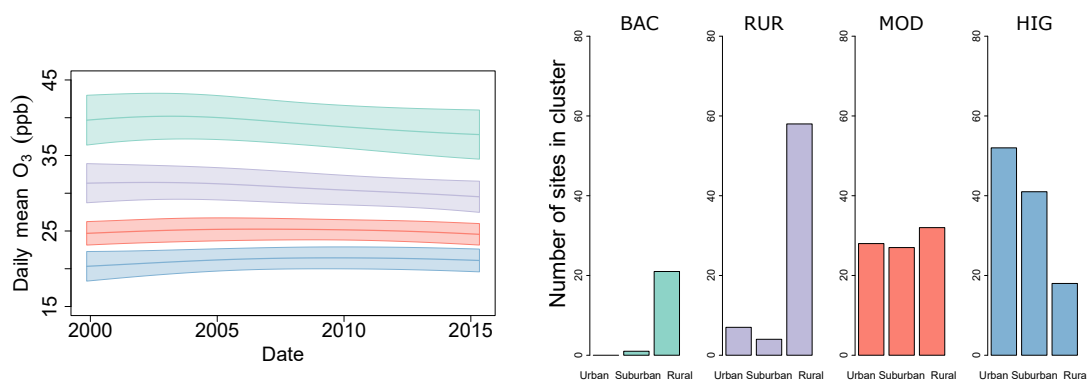


Figure 4.3 – Clusters based on daily mean O₃ LT(t). Average LT(t) in each cluster with \pm the standard deviation (left) and histograms for the site type included in each cluster.

Clusters derived from the daily mean S(t) show a regional representation most likely due to

the influence of the climatic conditions on the annual cycle of O_3 . The following five clusters were obtained from the daily mean $S(t)$ (Fig. 4.4): (1) "CentralNorth" comprises northern and eastern part of Germany, Netherlands and some eastern sites in Czech Republic, Poland and Austria, (2) "CentralSouth" covers most part of Austria, Switzerland and some sites in the Southwest of Germany, (3) "West" incorporates the biggest part of France, Belgium and Spain, (4) "PoValley" includes the sites located in the Po Valley, an industrial region in Northern Italy. (5) "North" covers most of the UK and Scandinavia. The sites in "PoValley" display the most pronounced $S(t)$, mainly due to the Mediterranean weather conditions, e.g. high temperatures. At the same time high NO_x and VOC emissions in this region leads to higher O_3 concentrations. The "North" cluster has the smallest seasonal variability, due to generally low O_3 concentrations, and lower temperature conditions in this region. Especially in the Scandinavian sites meteorological conditions are rather unfavorable for O_3 formation. Also, the regions included in the "North" cluster are influenced by cyclonic systems arriving in Europe through the North Atlantic ocean, that carry air pollutants into Europe (Stohl, 2002; Dentener et al., 2010). Thus, the influence of background O_3 , i.e. O_3 inflow from northern America and eastern Asia, is high in these sites (Derwent et al., 2004, 2013). In all clusters (except in the "North") the hot summers of 2003 and 2006 are visible in the $S(t)$ signal, which shows that the $S(t)$ signal can capture important events in O_3 variability that are driven by seasonal meteorological phenomena.

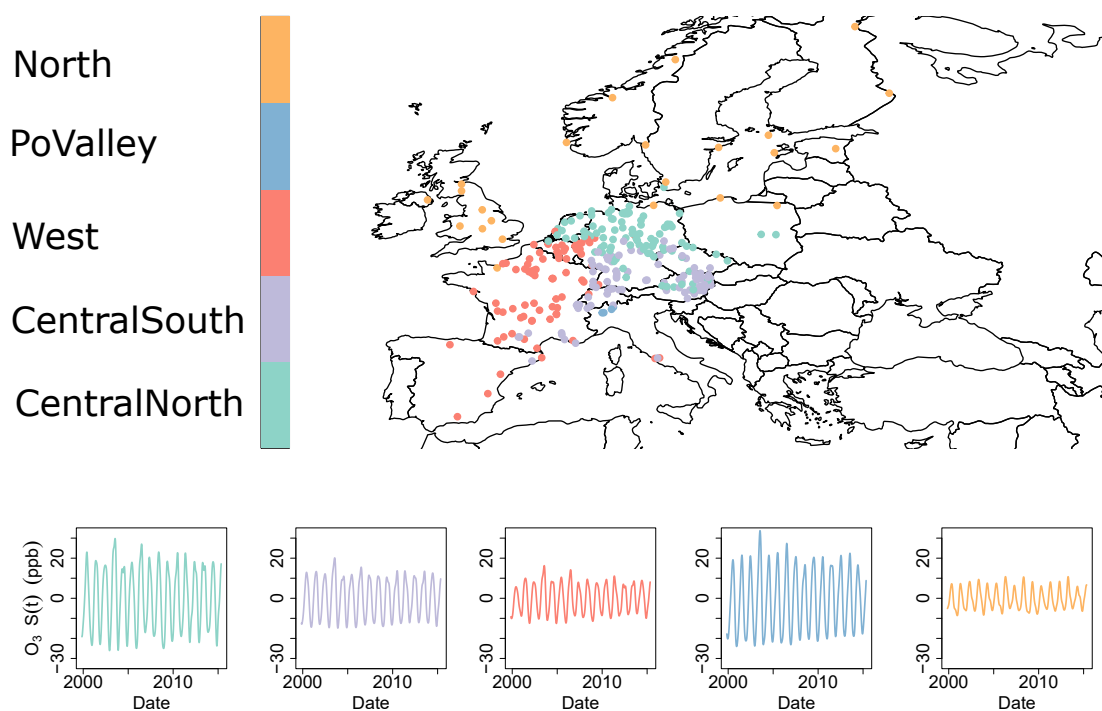


Figure 4.4 – Map with the site clusters derived from daily O_3 $S(t)$, and average $S(t)$ in each site cluster.

A two-dimensional classification scheme is achieved by employing the $LT(t)$ - and $S(t)$ -clusters.

Chapter 4. Temporal and spatial analysis of ozone concentrations in Europe based on time scale decomposition and a multi-clustering approach.

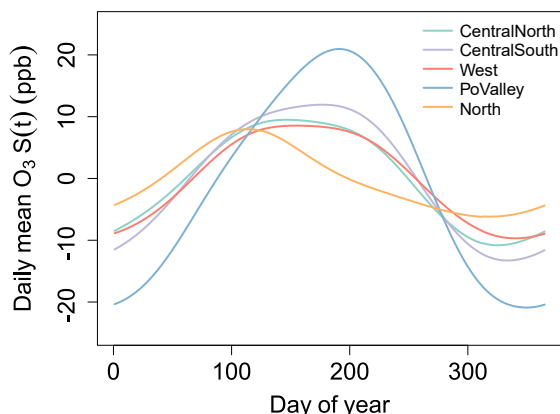


Figure 4.5 – Annual cycle of daily mean O₃ S(t) for the daily mean S(t) clusters.

Our results are in good agreement with previous classification studies, where by using different O₃ metrics similar classifications have been obtained. For instance, the spatial analysis based on gridded O₃ data (MDA8) across Europe by Carro-Calvo et al. (2017) resulted in a regional site classification. The gridded data used by Carro-Calvo et al. (2017) were obtained by spatial interpolation leading to a larger and regular geographical coverage compared to the available observations. Compared to Carro-Calvo et al. (2017), similar geographical clusters were identified here, except for the Iberian Peninsula, eastern Europe, northern Scandinavia and the Balkan states that do not appear as separate clusters in our analysis. This is most probably due to the small number of observational sites in the above regions. More specifically, the sites in the "West" cluster correspond to the Western European and the Iberian Peninsula clusters as extracted by Carro-Calvo et al. (2017), the "North" cluster covers the British Isles, northern Scandinavia, the Baltic region and parts of the north-central Europe clusters of Carro-Calvo et al. (2017). Moreover, the "CentralNorth" cluster includes the north-central, and eastern Europe and parts of the south-central clusters, while the "CentralSouth" cluster corresponds to the south-central cluster of Carro-Calvo et al. (2017). Finally, the "PoValley" cluster is embedded in the south central cluster of Carro-Calvo et al. (2017). In contrast to our study, O₃ concentration during summer have exclusively been used for the cluster analysis by Carro-Calvo et al. (2017), therefore conditions when the correlation of O₃ and meteorological variables such as temperature is typically strongest. Four site type clusters were found based on the LT(t) in this study, which are similar to the five site type clusters identified by Lyapina et al. (2016). Similar site classifications are obtained because the L(t) signal of this study and the mean seasonal and diurnal profiles of Lyapina et al. (2016) both capture the O₃ concentration levels distinguishing specific pollution regimes.

4.4.2 Trends of daily mean O₃ concentrations

The daily mean LT(t)- and S(t)-clusters identified in section 4.4.1 are used for assessment of the temporal trends for the different site types and geographical locations. Overall, decreasing O₃ trends are found for rural sites, while there is a tendency for increasing O₃ in more polluted urban environments (Fig. 4.6). The number of sites that belong in each of the identified groups is shown in Table 4.1. In 64% of all sites significant trends (p-value<0.05) were identified for the daily mean O₃; 61% among the significant trends were negative and 39% positive.

Most rural sites – "BAC" and "RUR" – experienced decreasing daily mean O₃ concentrations in all regions, as expected following the NO_x and VOC reductions in Europe (Fig. 4.6). At the "MOD" and "HIG" sites a levelling-off or increase is observed respectively, especially in "CentralNorth", "West" and "North" regions. At the "HIG" sites the positive trends can be partly explained by the increase of NO₂ to NO_x ratio, originating from the diesel vehicles, that have increased in the European car fleet (Solberg, 2009). In addition, the strong reduction of NO_x concentrations that led to less titration of O₃ by NO, could also explain the positive trends at urban and suburban sites. The late inflection point at urban sites (LT(t) of "HIG" cluster in Fig. 4.3) can be an additional effect of the reduced titration of O₃, which leads to positive trends at the "HIG" sites. Flat trends at central European sites, might partially be explained by the increasing influence of North American and Asian emissions, that have counterbalanced the decrease of European NO_x and VOC concentrations (Derwent et al., 2018; Yan et al., 2018).

In agreement with our results, significant decreases of daytime average and summertime mean of MDA8 O₃ at European rural sites and small and non-significant downward trends of MDA8 at urban sites have been found previously for the time period 2000-2014 (Chang et al., 2017). Similarly, in a report by Guerreiro et al. (2016) it was found that between 2000 and 2014 annual mean O₃ and annual mean MDA8 O₃ have been decreasing in rural background sites, while at more polluted sites influenced by nearby man-made precursor emissions, upward trends have been detected.

Table 4.1 – Number of sites in each site group based on the LT(t) and S(t) clusters.

Cluster	BAC	RUR	MOD	HIG	Sum
CentralNorth	5	8	33	48	94
CentralSouth	8	29	27	28	92
West	9	16	21	31	77
PoValley	0	2	2	0	4
North	0	16	4	4	24
Sum	22	71	87	111	Total: 291

O₃ trends at sites in the cluster "North" indicate changes in background O₃, especially in the "RUR" ones that are mostly free from local emissions. Here, decreasing trends of daily mean O₃ were found in "RUR" sites, while in the "MOD" and "HIG" the trends are slightly increasing. It is interesting to compare the trends in the "North" cluster with the temporal evolution of O₃ in Mace Head (remote station in northwestern Ireland), which is representative for inflow

Chapter 4. Temporal and spatial analysis of ozone concentrations in Europe based on time scale decomposition and a multi-clustering approach.

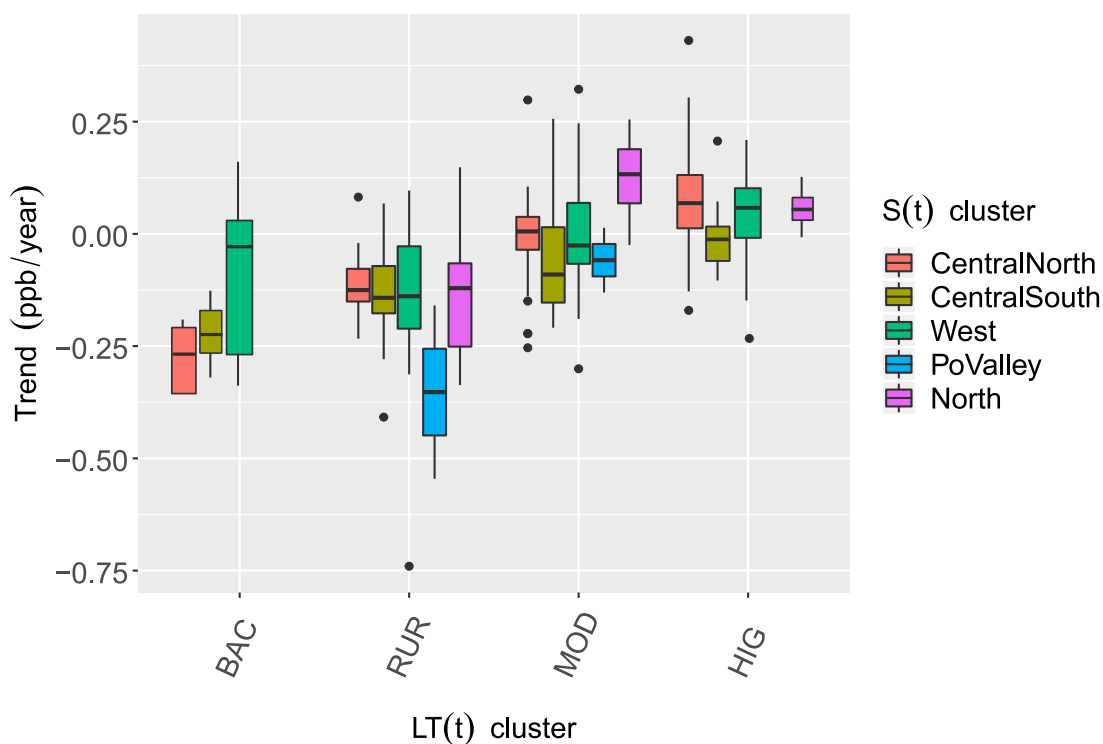


Figure 4.6 – Box-plots of de-seasonalized daily mean O₃ trends for the LT(t)- and S(t)-clusters. LT(t)-clusters represent a site type classification while the S(t)-clusters a geographical one that is influenced by climatic conditions.

of background O₃ into Europe. For this reason, we estimated the LT(t) variation of MDA8 O₃ and the Theil-Sen trend for the site in Mace Head (Fig. 4.7). An inflection point was identified in the LT(t) in 2006, i.e. MDA8 O₃ has been increasing between 1988 and 2006 and started to slightly decline after 2006. De-seasonalized Theil-Sen trends were estimated 0.08 ppb/year [0.06,0.1] for the first period and -0.04 ppb/year [-0.09,0.02] for the second period.

Similarly, Derwent et al. (2018) have found an increase of 0.34 ± 0.07 ppb/year with a deceleration rate after 2007 of -0.0225 ± 0.008 ppb/year² at the same station, based on a combination of filtered measurement data and modeling output (Lagrangian dispersion). The inflection point in mid-2000s might be the reason for the flat trend of the annual average O₃ during 2000s as estimated by Derwent et al. (2013).

4.4.3 Trends of peak O₃ concentrations

Peak O₃ concentrations in summertime are attributed to increased photochemical production during this time of the year, and the spring maximum in remote locations is linked to increased stratospheric influx as well as hemisphere-wide photochemical production during that season

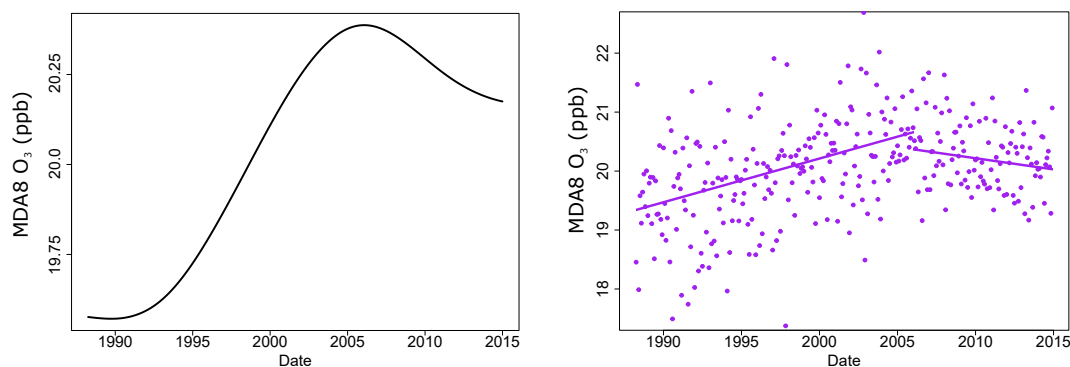


Figure 4.7 – MDA8 LT(t) in Mace Head extracted with the EEMD (left) and the corresponding de-seasonalized Theil-Sen trend (right).

(Holton et al., 1995; Monks, 2000). In this study, significant negative meteo-adjusted MTDM trends were observed at 62% of the sites, while without meteo-adjustment significant negative trends were identified at only 19% of the sites. The higher number of sites with significant trends after the meteo-adjustment indicates the advantage of using meteo-adjusted observations in the trend estimation. This argument is supported in the study by Fleming et al. (2018), where significant negative trends of the 4th highest MDA8 O₃ between 2000 and 2014 have been detected at only 18% of the studied sites across Europe, while at a large proportion of sites either weak negative to weak positive or no trends at all were found. The non-significant trends have been attributed by Fleming et al. (2018) to the influence of meteorology which is not considered in their trend estimation.

Trends of meteo-adjusted MTDM are discussed here for the daily mean O₃ LT(t)- and S(t)-clusters. MTDM decreased for all site types and regions during the studied period 2000-2015. However, in the "RUR" cluster MTDM showed the strongest decrease among all LT(t)-clusters (Fig. 4.8). Interestingly, in the "BAC" cluster (especially the "West" cluster) the decrease of MTDM was not so pronounced, likely due to the increase of hemispheric transport of O₃ in Europe (Derwent et al., 2007; Vingarzan, 2004). The same pattern was observed at the high alpine site of Jungfraujoch, which is representative for European continental background O₃ concentrations (Balzani-Lööv et al., 2008; Boleti et al., 2018c). Also, "HIG" sites in "CentralSouth" showed slightly smaller decrease of MTDM compared to the other regions, possibly due to industrialization in the neighboring eastern Europe (Vestreng et al., 2009).

Our results are in line with a modeling sensitivity study, where negative trends of the 95th percentile of O₃ concentrations were found in European rural background sites for the period 1995-2014 (Yan et al., 2018). For the shorter time period between 1995 and 2005, downward trends of measured MTDM have been observed for most parts of Europe as well (in the range [-0.12, -0.55] ppb/year), with the highest decrease in the Czech Republic, UK and the Netherlands (on average -1 ppb/year) and very small (nearly flat) in Switzerland (Solberg, 2009). In our study, measured MTDM trends (2000-2015) for these regions are in the same

Chapter 4. Temporal and spatial analysis of ozone concentrations in Europe based on time scale decomposition and a multi-clustering approach.

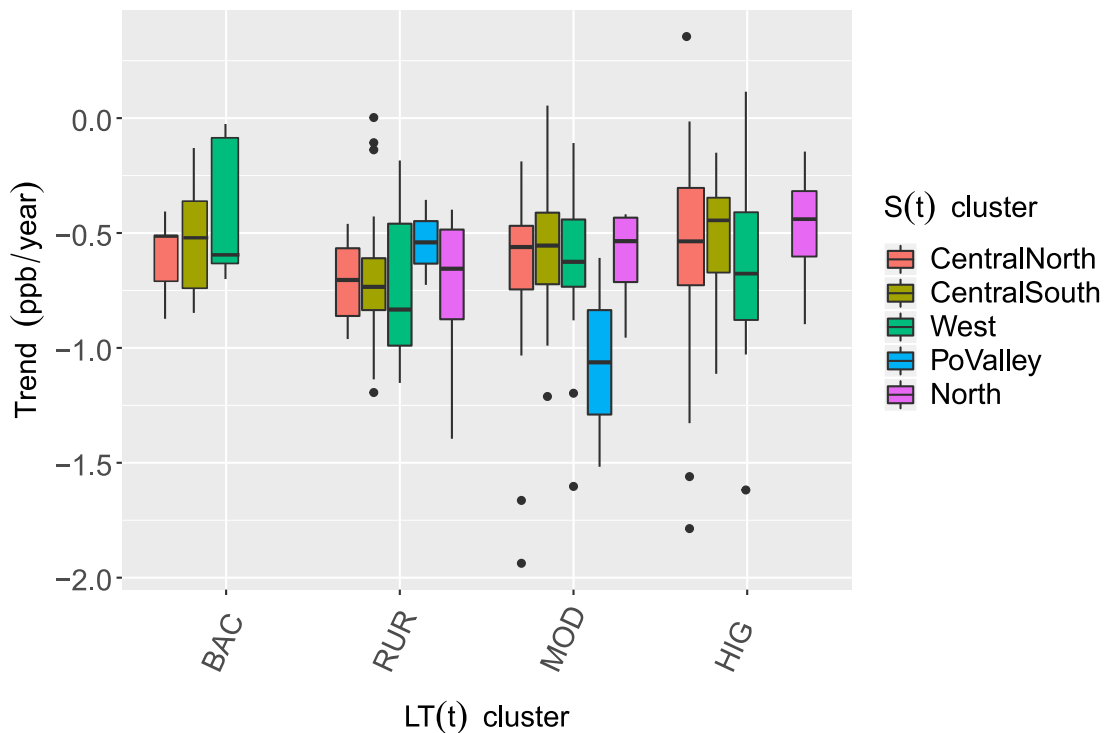


Figure 4.8 – Box-plots of meteo-adjusted MTDM trends for the daily mean O₃ LT(t)- and S(t)-clusters. LT(t)-clusters represent a site type classification while the S(t)-clusters a geographical one that is influenced by climatic conditions.

range, i.e. the average decrease was estimated between -0.28 and -0.55 ppb/year. Smaller trends in Switzerland and central Northeast Germany have been observed by Solberg (2009), which agrees with our result for the "CentralSouth" sites that showed the smallest average trend among all clusters. The flat trend in Switzerland during 1995-2005 is probably linked to the disproportional decrease of NO_x and VOCs until beginning of 2000s, when an inflection point has been observed at most polluted sites (Boleti et al., 2018a). In Germany, a mixed behavior was observed by Solberg (2009), with the northeastern part showing a stronger decrease and the central Northeast region a smaller decrease. Similar to our differentiation between the clusters, average MTDM trends within the "CentralNorth" cluster (with northern and northeastern Germany included) were higher and within the "CentralSouth" (covering central parts of Germany) lower.

4.4.4 O₃ seasonal cycle trends

Analysis of S(t) allows studying the characteristics of the annual cycle of O₃ without influence of short-term meteorological phenomena and long-term variations. Here, the trends of $S_{max}(t)$,

$S_{min}(t)$ and $S_{DoM}(t)$ are presented for the five regions identified based on $S(t)$ as calculated from daily mean O_3 . A declining amplitude of $S(t)$ and simultaneously a phase shift towards an earlier time in the year can be observed for the 2000 to 2015 period (Table 4.2).

More specifically, an overall decrease in O_3 $S_{max}(t)$ by around 0.05-0.18 ppb/year and a simultaneous increase of $S_{min}(t)$ with a rate of around 0.25 ppb/year was observed for all $S(t)$ -clusters (Fig. 4.9). However, in the "North" cluster the decrease of the $S_{max}(t)$ was very small and non-significant, probably due to the pronounced influence of background O_3 at these sites. The most pronounced shortening of $S(t)$ amplitude can be seen at the "PoValley" sites, where the downward trend of peak O_3 is largest (Fig. 4.8). The increase in the $S_{min}(t)$ may be partially due to the decreased titration of O_3 after reductions of NO_x emissions and probably due to the increased influx of O_3 towards north and northwest Europe and more cyclonic activity in the north Atlantic during winter as well (Pausata et al., 2012). A decrease of the 95th percentile and an increase of 5th percentile of O_3 for the period 1995-2014 has been also identified in the EMEP network (rural background sites) (Yan et al., 2018). Lower summertime peaks as a result of decreased photochemical production and higher O_3 concentrations during the winter months due to decreased O_3 titration have been found in European air masses between 1987 and 2012 (Derwent et al., 2013) as well.

The trend of O_3 $S_{DoM}(t)$ is for all regions negative, i.e. the occurrence of the day of maximum O_3 has shifted to earlier days within the year with a rate of -0.47 to -1.35 days/year (Table 4.2, Fig. 4.10). The observed shift of the day of seasonal maximum might be linked to the increase of emissions in East Asia that have contributed to increased transport of air pollution to middle- and northern latitudes (Zhang et al., 2016) where the effect on O_3 is probably greater due to greater convection, reaction rates and NO_x sensitivity (Derwent et al., 2008; West et al., 2009; Fry et al., 2012; Gupta and Cicerone, 1998). In addition, changes in meteorological factors have affected the seasonal variation of O_3 . For instance, a similar behavior with an earlier onset of the summer date (the calendar day on which the daily circulation/temperature relationship switches sign) has been observed by Cassou and Cattiaux (2016) using observational data, while Peña-Ortiz et al. (2015) have found that summer period is extending with a rate of around 2.4 days/decade based on gridded temperature data in Europe. The positive phase of the NAO leads to increased O_3 concentrations in Europe through higher westerly winds across the North Atlantic, and enhanced transport of air pollutants from North America to Europe (Creilson et al., 2003). Changes in the NAO have led to increased westerly flow over the North Atlantic during the 1980s and 1990s, which in turn resulted to elevated O_3 in northwestern Europe especially in winter and spring time (Pausata et al., 2012). The enhanced hemispheric transport of air pollutants from North America to Europe is related to more increased transport through frontal systems (Creilson et al., 2003; Eckhardt et al., 2003). Increased O_3 in winter and spring, but not in summer, might lead to a shifting from a pronounced maximum in late summer to a broader spring-summer peak (Cooper et al., 2014). At the "West" sites a slightly stronger shift of the S_{DoMax} was observed compared to other clusters, while at the "North" sites the decrease was the smallest. The early spring maximum in the "North" sites in April can be explained by higher NO_x that is released from PAN and alkyl nitrates that are produced

Chapter 4. Temporal and spatial analysis of ozone concentrations in Europe based on time scale decomposition and a multi-clustering approach.

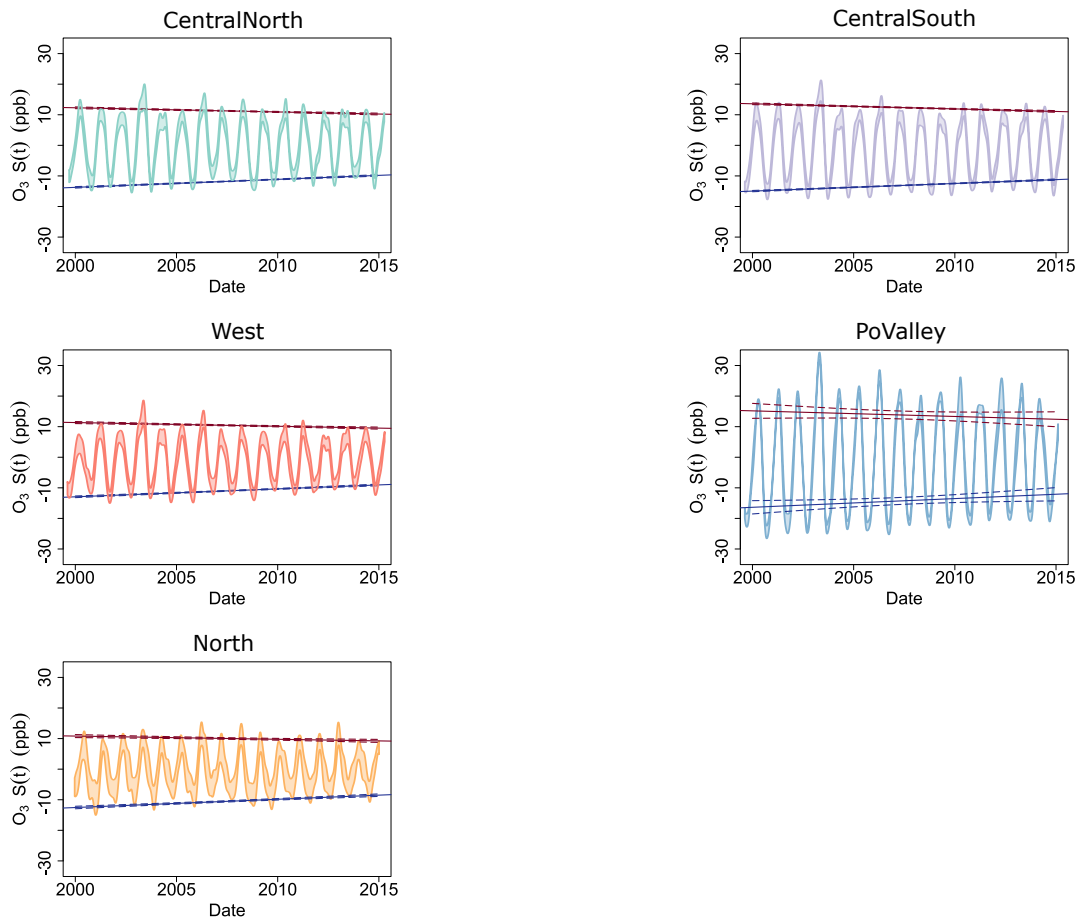


Figure 4.9 – Temporal evolution of S_{max} and S_{min} for the daily mean $O_3 S(t)$ clusters together with the average $S(t)$ (bands indicate the average pm the standard deviation). Lines show the linear trends of S_{max} and S_{min} and dashed lines the 90% confidence interval.

during winter at northern latitudes (Brice et al., 1984; Bloomer et al., 2010).

4.4.5 O_3 and temperature relationship

The O_3 sensitivity to temperature is a useful metric for validation of precursor reduction scenarios and emission inventories in chemistry-transport models (Oikonomakis et al., 2018). Here, we present the long-term trends of the relationship between the daily maximum O_3 concentrations and daily maximum temperature during the warm season from May to September between 2000 and 2015. Daily maximum O_3 and temperature are chosen in order to represent peak O_3 concentrations formed during the considered days.

Decreasing sensitivity of O_3 with respect to temperature was observed during the considered time period in all regions (Fig. 4.11). Fig. 4.11 shows the decreasing slopes of linear regression lines of maximum O_3 against temperature for successive year groups. The decrease is

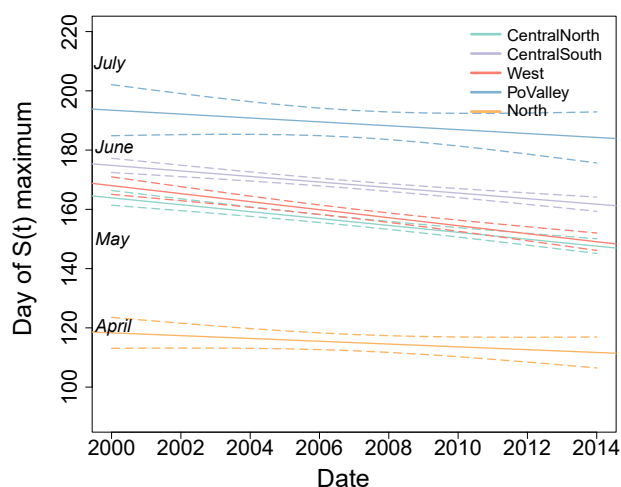


Figure 4.10 – Linear trends of the S_{DoMax} for the daily mean $S(t)$ clusters (dashed lines show the 90% confidence interval).

Table 4.2 – Linear trends of S_{max} , S_{min} and S_{DoMax} for the daily mean O_3 $S(t)$ clusters during 2000-2015. ** indicate highly significant trend (p-value < 0.01), * significant (p-value < 0.05) and – indicate non-significant trend (p-value > 0.05).

Daily mean O_3 $S(t)$ -Cluster	Trend S_{max} (ppb/year)	Trend S_{min} (ppb/year)	Trend S_{DoMax} (days/year)
CentralNorth	-0.14 ± 0.04 (**)	0.26 ± 0.03 (**)	-1.16 ± 0.18 (**)
CentralSouth	-0.17 ± 0.03 (**)	0.25 ± 0.02 (**)	-0.93 ± 0.17 (**)
West	-0.12 ± 0.04 (**)	0.26 ± 0.03 (**)	-1.35 ± 0.21 (**)
PoValley	-0.18 ± 0.6 (-)	0.30 ± 0.56 (-)	-0.65 ± 0.61 (-)
North	-0.05 ± 0.1 (-)	0.24 ± 0.07 (**)	-0.47 ± 0.38 (-)

consistent for all calculated regional clusters except for "North". For most regions in Europe a significant downward trend of the slope of around 0.04-0.05 ppb/K/year was found (Table 4.3). At "PoValley" sites the decrease was more pronounced (-0.083 ppb/K/year). At the same time the average correlation between O_3 and temperature is the highest compared to the other regions, because of large reductions of precursors concentrations in this region which is characterized by high industrial emissions. At the "North" sites the weakest correlation of O_3 to temperature was observed and the trend is non-significant. This is expected because at these high latitudes mean temperature is lower compared to other regions in Europe, thus, photochemical production of O_3 is weak during the time when O_3 typically reaches its maximum concentration.

In relation to the $LT(t)$ -clusters, it was observed that the higher the pollution burden of the site the stronger the trend of O_3 to temperature slope (Table 4.4). As shown here, the "HIG" and "MOD" sites have higher trends compared to the clusters "BAC" and "RUR". Our results are in line with a box-model study that tested the O_3 -temperature relationship under different

Chapter 4. Temporal and spatial analysis of ozone concentrations in Europe based on time scale decomposition and a multi-clustering approach.

NO_x level scenarios (Coates et al., 2016). Coates et al. (2016) have shown that at high NO_x conditions O₃ increases more strongly with temperature, while the increase is less pronounced when moving to lower NO_x conditions.

Table 4.3 – Linear trends of the O₃-temperature slope (based on daily maximum values) for the daily mean O₃ S(t)-clusters for the time period 2000-2015. ** indicate highly significant trend (p-value < 0.01), * significant (p-value < 0.05) and – indicate non-significant trend (p-value > 0.05).

Daily mean O ₃ S(t)-Cluster	Trend (ppb/K/year)	Standard deviation	p-value
CentralNorth	-0.042	0.003	**
CentralSouth	-0.04	0.003	**
West	-0.05	0.004	**
PoValley	-0.083	0.016	**
North	-0.016	0.013	-

Table 4.4 – Linear trends of the O₃-temperature slope (based on daily maximum values) for the daily mean O₃ LT(t)-clusters for the time period 2000-2015. ** indicate highly significant trend (p-value < 0.01), * significant (p-value < 0.05) and – indicate non-significant trend (p-value > 0.05).

Daily mean O ₃ LT(t)-Cluster	Trend (ppb/K/year)	Standard deviation	p-value
BAC	-0.038	0.006	**
RUR	-0.034	0.006	**
MOD	-0.043	0.003	**
HIG	-0.046	0.003	**

4.5 Conclusions

In this study, a classification of 291 sites across Europe was performed for the time period 2000-2015. The clustering algorithm applied on the long-term changes LT(t) and the seasonal cycle S(t) of daily mean O₃ resulted in a site type and geographical site classification respectively. Such a classification scheme can be of significant use for O₃ trends studies in large spatial domains and in model evaluation studies (e.g. Otero et al., 2018). Our approach captures several features of O₃ variations, i.e. pollution level from the L(t)-clustering and influence of the climatic conditions from the S(t)-clustering, and presents a unifying perspective on past studies that report different site type labels based on cluster analysis using different metrics of O₃ concentrations. The regional differentiation is hampered by sparse or missing measurement sites in some regions, e.g. eastern Europe or the Balkan peninsula. However, in the last years the number and spatial distribution of sites with longer and more dense measurements has improved.

A trend analysis of de-seasonalized mean O₃ concentrations and meteo-adjusted peak O₃ concentrations was implemented for the considered sites. By using LT(t)- and S(t)-clusters, patterns of O₃ long-term trends across Europe were investigated, based on the multi-dimensional

site classification scheme. Long-term trends of de-seasonalized daily mean O₃ are decreasing at the rural sites, while in suburban and urban sites they are either stable or slightly increasing. Positive or flat trends indicate that reduction of precursors has been less effective in reducing O₃ concentrations in heavily polluted environments. On the other hand, downward trends in peak O₃ concentrations were observed in all regions, as a result of precursors emissions reductions. However, peak O₃ has been decreasing with the smallest rate at higher altitude sites especially in the western part of Europe due to the influence of background O₃ imported from North America and East Asia.

The analysis of S(t) extrema revealed a decrease in summertime maxima and an increase in wintertime minima, pointing to a decreasing amplitude of the seasonal cycle of O₃. At the same time the occurrence of the day of maximum has shifted from summer to spring months with a rate of around -0.5 to -1.3 days/year. Changes in the S(t) might be attributed on one hand to the precursors reductions in Europe, and, on the other hand, to changing weather patterns in the northern Atlantic and increase of emissions in southern East Asia.

Finally, the sensitivity of O₃ to temperature has weakened since 2000 with a rate of around 0.084 ppb/K/year, i.e. formation of O₃ became weaker at high temperature conditions due to decreasing NO_x concentrations. It was shown that differences in changes to this sensitivity across sites are mainly driven by regional meteorological conditions.

Acknowledgements We kindly thank the Swiss Federal Office of Environment for funding this project and Dr. Stephan Henne for extracting the ERA-Interim meteorological variables.

Chapter 4. Temporal and spatial analysis of ozone concentrations in Europe based on time scale decomposition and a multi-clustering approach.

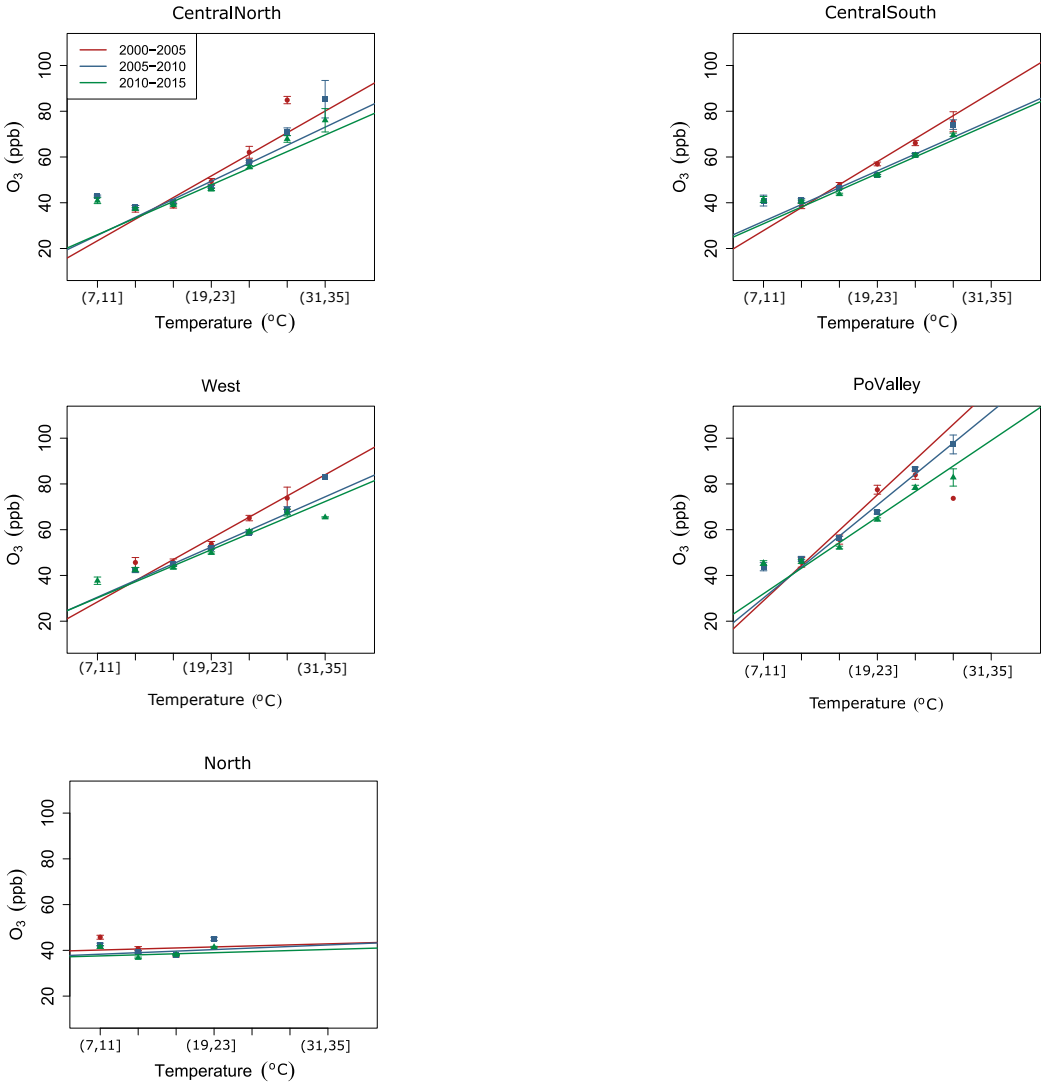


Figure 4.11 – Linear trend of the slope between O₃-temperature daily maximum values for the warm season between May and September. The trends are calculated on the average values for each daily mean S(t) cluster and for the year groups 2000-2005, 2005-2010 and 2010-2015. Points show the mean value for the indicated temperature bin together with the corresponding standard deviation.

5 Conclusions

O₃ concentrations were analyzed for their temporal evolution over the last 25 years in Switzerland and the last 15 years in Europe. Long-term evolution of O₃ reflects mostly changes of its precursors as well as hemispheric transport of air pollutants and stratospheric-tropospheric exchange, and allows to investigate the effect of air quality policy measures on O₃. However, the seasonal and short-term O₃ variability, originating from meteorology, obfuscates the long-term trend estimation. The estimation of the distinct time scale O₃ variations can differentiate features that control O₃ concentrations. By removing the inter-annual meteorologically induced variability, de-seasonalized O₃ observations were estimated. For the mean O₃ concentrations a novel long-term trend estimation approach, based on the de-seasonalized observations, led to a significant reduction of uncertainty, without additional use of meteorological observations. Inflection points were identified in O₃ temporal evolution and are an important feature that influence its long-term trend estimation. The two-regime trend analysis of mean O₃ concentrations proved especially useful to understand the temporal trends, and it revealed an interesting dependence on the site type. For the analysis of the peak O₃, trends were estimated on meteorologically corrected concentrations, as predicted through generalized additive models and after a detailed meteorological variables selection. Identifying the most influential meteorological variables led to more concise statistical models that describe the relationship of O₃ to meteorology. Finally, in order to study O₃ in the European domain and to identify the factors that mostly influence O₃ trends, a two-dimensional site classification was applied on O₃ distinct time scales variations. Important features that govern O₃ long-term trends were depicted in the acquired site groups, i.e. precursors emissions and geographical location influence.

5.1 Time scale decomposition

Time scale decomposition proved to be a powerful tool when studying O₃ long-term trends, because O₃ is influenced by various features on different time scales. Application of the non-parametric EEMD on the daily mean O₃ concentrations yielded an accurate estimation of the underlying time scale variabilities, i.e. the long-term, seasonal and short-term variation. More

specifically, the long-term signal, depicts mostly the effect of precursors emissions reductions on O_3 in the decadal time scale, together with other factors such as influence of hemispheric transport of pollutants and stratospheric O_3 contribution. The seasonal variation represents the influence of monthly to inter-annual meteorological conditions, such as temperature seasonal cycle or heat waves and accounts for the largest part of meteorologically influenced variation of O_3 . The short-term variation showed the meteorological influence in the daily to weekly time scale, e.g. synoptic weather patterns.

In contrast to parametric methodologies, EEMD is based merely on the input data and is not driven by predefined parameters. Thus, EEMD is appropriate for studying non-linear and non-stationary time series, as is the case for O_3 concentrations. EEMD is able to capture specific or exceptional events in the observational data that cannot be captured when using parametric methods. For instance seasonal meteorological events, such as the hot summers in 2003 and 2006, were observed in the seasonal variation signal when using the EEMD on O_3 daily mean concentrations. By extracting the variation of O_3 that is generated by such events, the trend estimation is highly improved in terms of statistical significance level. In addition, non-monotonic temporal evolution (inflection points) was identified in the long-term variation and the estimation of long-term trends was performed in two separate time periods (two-regime trend approach). The two-regime trend approach was very useful, because overestimation or underestimation of the trends was avoided, especially when the inflection point occurred around the middle of the studied time series.

However, EEMD has some aspects that require careful handling. For instance, the number of ensemble members need to be predefined, so that it does not affect the results. In addition, post-processing of the obtained frequency variations requires a very good understanding of the underlying processes in order to decide the frequency components that can be combined. Finally, EEMD is a computationally costly algorithm.

5.2 Meteorological adjustment practices

5.2.1 Mean O_3 meteorological adjustment

Mean O_3 concentrations are largely influenced by meteorological effects on the seasonal time scale. The de-seasonalization of daily mean O_3 observations is effective in adjusting the observations for a large proportion of the meteorologically driven inter-annual variability. The extraction of the EEMD seasonal variation from the observations leads to removal of a high proportion of meteorologically influenced variability. Thus, by using the de-seasonalized O_3 observations, a significant reduction in the uncertainty range of the estimated long-term trends is achieved. Further meteo-adjustment on the short-term variation of daily mean O_3 observations does not significantly reduce uncertainty range of the trend, which means that the largest part of meteorological influence is already removed through the de-seasonalization. Essentially, the de-seasonalization based on the EEMD is a form of meteorological adjustment

process that overcomes the necessity of meteorological observational data sets. This is especially useful for trend analyses in larger spatial domains, where observational data sets of meteorological variables are usually not easy to acquire.

5.2.2 Peak O₃ meteorological adjustment

For the meteorological adjustment of the peak O₃ concentrations, application of statistical models (GAMs) is an appropriate approach for describing the relationship between O₃ and meteorological variables. GAMs explain O₃ relation to meteorology in such a way that non-linear influences are well captured. The variable selection algorithm used in our study allows identification of the meteorological variables that are most important for O₃ variability at each studied station in Switzerland, while interaction effects among meteorological variables are eliminated. Through the variable selection procedure, more concise statistical models were eventually employed that realistically represent meteorological influence on O₃. It was observed that temperature and humidity are the most influential variables for O₃ variation. Also, surface stress accounts for a large part of O₃ variability, which represents the relationship of O₃ to wind velocity and direction.

Removing the meteorological influenced variation as estimated by the GAMs, meteo-adjusted O₃ peak concentrations were obtained. The adjustment was performed by using the specific days when the peak values were identified before application of the meteorological adjustment. By targeting these days we could study the effect of the meteorological adjustment on the specific high O₃ events. Trend calculation based on the meteo-adjusted concentrations led to a significant reduction of uncertainty in the resulting trends estimates. An important reason is that high O₃ events driven by anomalous weather conditions are effectively adjusted to more average weather conditions. Our approach can particularly be useful in case of extreme meteorological conditions (e.g. heat waves) or temporal trends in meteorological variables that might influence the trend estimation. However, the uncertainty reduction is partly achieved through the use of long enough observations as well, basically by increasing the sample size in the trend estimation.

When studying relationship of O₃ with meteorology over longer time periods it is possible that some interactions do not stay the same due to changes in emissions and climate. By using an average relationship between O₃ and a meteorological parameter in the GAM throughout the studied period, it could possibly lead to under- and overestimation of the trend over different periods. The magnitude and relevance of such a possible bias for the O₃ trend analysis can be estimated, by applying GAMs limited to different time periods and replacing the functions describing the relationship of O₃ to a meteorological variable in the GAM for the whole time period. The resulting trends can be considered as an upper and lower bound of the effect of changing temperature sensitivity of O₃ on the trend estimation.

5.3 Clustering based on different time scale variations

To investigate the factors that govern O₃ long-term trends in Europe, a clustering approach for the European measurement sites was performed. On the one hand, a site type clustering based on NO_x emission levels is sufficient at small spatial scales (e.g. within a country or a small region) combined with knowledge of the sites special features. Such a categorization proved to be useful for the study in Switzerland, but in the larger domain of Europe a more sophisticated approach was applied. On the other hand, meteorological features vary amongst Europe, thus, it is important to identify regions with similar meteorological influence on O₃ trends. The distinct time scale variations of the mean O₃ concentrations obtained through the EEMD, i.e. the long-term and seasonal, were employed to classify sites across most parts of Europe. Applying a clustering algorithm on the long-term and seasonal variation resulted in a two-dimensional site classification scheme, where different spatio-temporal characteristics of O₃ were described. More specifically, the clustering based on the long-term variation resulted in a site type classification, mainly driven by O₃ concentrations levels. Proximity to O₃ precursors emission sources is represented by the clustering on the long-term variation; high altitude rural sites, moderate polluted environments and sites close to emission sources were identified. Interestingly, at Swiss sites the NO_x concentrations groups have resulted in a similar site type classification as in Europe based on the long-term variation clustering. Seasonal clustering resulted in a geographical site classification, due to influence from inter-annual meteorological phenomena. Especially in the site groups based on the seasonal clustering important features were identified, e.g. influence of background O₃ in northern parts of UK and Scandinavia. Such a clustering methodology is advantageous over larger spatial scales rather than within smaller regions, because climatic differences amongst locations located close to each other are not well distinguished. Eventually, a two-dimensional site classification is achieved here for most parts of Europe, which captures both emissions and climatic conditions and allows a more detailed study O₃ long-term trends at the distinct site categories.

5.4 Long-term O₃ trends

5.4.1 Mean O₃ trends

In Switzerland, upward trends of the de-seasonalized daily mean O₃ and the de-seasonalized MDA8 O₃ mixing ratios were observed during the 1990s and early 2000s; after around the mid-2000s they started to decline. The year that the downward trend of O₃ began clearly depends on the type of the site environment; the closer to precursors emissions sources the later the inflection point (breakpoint). At rural sites with low precursors emissions the inflection point is observed in early 2000s, with a clear decrease afterwards. At urban sites, especially close to traffic emissions sources, upward trends are observed until late 2000s with signs of stabilization afterwards. The increase in the 1990s is attributed to the rapid decrease of NO_x and disproportional decrease of VOCs, which led to decreased efficiency of the O₃

titration reaction. At the same time the increase of background concentrations in Europe has contributed to the observed trends, which can usually be seen at remote, high altitude sites. Thus, the increase of O₃ at the alpine, remote site of Jungfrauoch and the subsequent decrease after 2003 is a good proxy for the temporal evolution of background O₃ over Europe.

In most parts of Europe a similar behavior to Switzerland was observed, where de-seasonalized O₃ concentrations decreased at rural sites during the time period 2000-2015, probably due to the reduction of NO_x and VOCs emissions. At urban sites an increase or a levelling off is observed, which is again linked to reduced titration of O₃ by NO. At the stations mostly affected by hemispheric transport in Europe a decrease was observed at rural areas and a levelling off at urban and suburban sites. In agreement with the results based on the Swiss sites, an inflection point was observed in the long-term trend; probably an effect of the changing background O₃. At rural sites the change occurred in the early 2000s and around mid- to late 2000s at the suburban and urban sites, which leads to an underestimation of the rate of increase or decrease. Additionally, the decrease of O₃ at rural sites and increase at urban ones, indicates that these environments become more similar with time in terms of O₃ concentration levels.

Furthermore, the inter-annual cycle of mean O₃ concentrations has experienced significant changes between 2000 and 2015 in most parts of Europe. More specifically, maximum seasonal concentrations have been reducing since 2000, while the minimum seasonal concentrations have been increasing. As a result, an amplitude reduction of the seasonal variation has occurred. In addition, a phase shift of the seasonal variation has been observed, i.e. maximum seasonal concentrations occur earlier in the year.

5.4.2 Peak O₃ trends

Meteo-adjusted peak O₃ steadily decreased since 1990 in Switzerland, showing the effect of legislation control measures. However, peak O₃ increased at remote high altitude sites, due to rising background O₃ during the same time period. At urban sites close to traffic emission increasing trends were found as well; an effect of the reduced titration by NO after NO_x strong reductions.

Similarly, in most parts of Europe meteo-adjusted peak O₃ decreased between 2000 and 2015, with the highest decrease observed at rural sites and the lowest at urban environments. Locations close to eastern European countries experienced smaller decrease compared to other parts of Europe, likely due to increased emissions from industrialization in the 1990s in eastern Europe. The influence of hemispheric transport is seen at high altitude sites mostly in western Europe, where the decrease of O₃ was counteracted by an increase of background O₃. Regions in southern Europe are more complex, because meteorological conditions that are favorable for O₃ formation are more frequent and intense. An inflection point is visible in the peak O₃ trends at sites located close to traffic, due to (a) disproportional parallel decrease of NO_x and VOCs during 1990s and (b) change in reduction rate of NO_x and VOCs in mid-2000s.

Finally, a decrease in the sensitivity of maximum O_3 to temperature was observed. It was shown that formation of O_3 became weaker at high temperatures due to decreasing NO_x concentrations, an effect that is more pronounced in regions with climatic conditions that favor O_3 production.

5.5 Outlook

The following issues have arisen through this PhD thesis that require further investigation.

The inflection point was observed in the temporal trend of mean O_3 concentrations at all kinds of environment and at polluted environments for the peak O_3 concentrations. At the same time the date of change is highly dependant on the type of environment, i.e. proximity to emission sources. The reasons behind the occurrence of this inflection point in the estimated trends of O_3 is not fully understood and is an important point for further investigation. A possible explanation for this observed change in the trend is a transition from VOC-limited to a NO_x -limited conditions in the studied regions, due to the pronounced decrease of NO_x concentrations especially at urban sites. However, the role of VOCs in this context could not be quantified during this study, because long-term VOC measurements are not available. Alternative to measurements, modeling studies are a useful approach to shed light to the complex interaction of NO_x and VOCs to O_3 concentrations and enrich our understanding in O_3 response to precursors reductions. A study of the VOC to NO_x ratio change based on box-models (similar to the EKMA approach) over the last 25 years could acquire interesting conclusions.

In our study there are strong indications that hemispheric transport of O_3 contributes significantly to the observed concentration trends. Background O_3 can be estimated through measurements at remote locations that are not influenced by local emissions, but, this approach does not provide detailed information on the exact origin of the pollutants. Thus, complementary studies based on chemistry-transport models, that provide estimations of the origin of air pollutants at a certain location are needed. Source attribution studies focused on sector and regions of origin utilize either so-called "labeling" techniques (Kranenburg et al., 2013) or sensitivity simulations (Galmarini et al., 2017) to estimate the amount of imported pollution. Such an analysis can focus on a more accurate estimation of the contribution of background O_3 to the total concentrations measured at the surface of a specific region. The temporal evolution of background O_3 over the last 25 years at different site groups (similar to the present study) can be estimated with long-term model simulations, that can potentially provide a better understanding of the observed trends.

A Appendix A

A.1 Convergence tests for ensemble empirical mode decomposition

To test the influence of the number of trials, we applied the ensemble empirical mode decomposition (EEMD) method on the daily mean O₃ concentrations in Basel (Fig.A.1). In this application, we ran the EEMD algorithm for different number of trials, spanning the interval from 10 to 200. From the decomposed time series, we removed the seasonal variation and from the remaining part we calculated the trend using Theil-Sen trend estimation. Then we repeated the above procedure 10 times for each tested value of number of trials and we calculated the mean and standard deviation of the observed trend. These values were plotted against the respective number of trials, as shown in Fig. A.1. In addition, the amplitude of the added white noise has been tested (Fig.A.2). We see that the estimated trend is affected by the choice of noise amplitude, which if it is too small does not allow the EEMD to function optimally while if it is too big it will cover the signal. More precisely, Fig.A.2 shows that there is a small plateau for noise amplitude values in the $[0.05, 0.2] \times \text{RMS}$ interval (RMS: root mean square error), for which the trend is around the value 0.53. However, when the noise amplitude is $0.1 \times \text{RMS}$, we observe a local minimum in the standard deviation among all the sets of 10 individual realizations. We note here that a global minimum is observed for amplitudes close to $0.9 \times \text{RMS}$, but in this region the signal is heavily influenced by the noise. In short, hereafter a noise amplitude $0.1 \times \text{RMS}$ will be used for the rest of our analysis, which is also in pair with the value used by Wu and Huang (2009) when discussing applications of EEMD to signal decomposition.

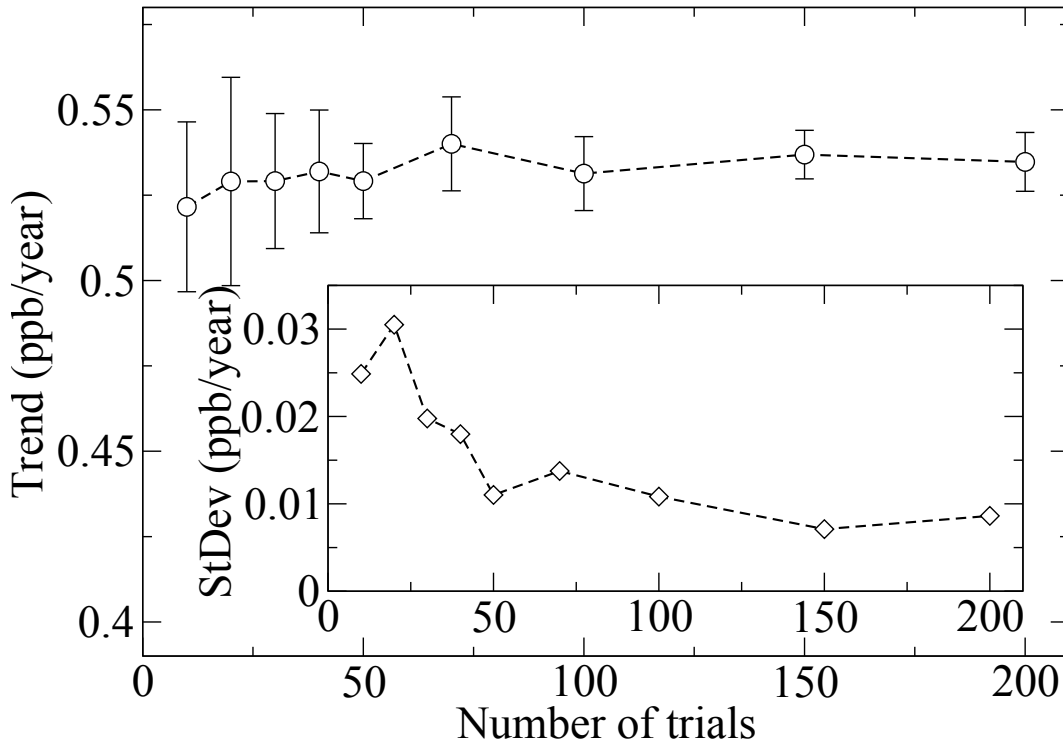


Figure A.1 – The convergence test results for the sufficient number of trials in the EEMD. Here we show the number of trials performed for each case study (10 tests for each case) against the corresponding magnitude of the Theil-Sen trend (data from Basel). In the inset we show the standard deviation for each of the cases.

A.2 Frequency analysis

The signals obtained by the EEMD and the parametric approach were analyzed with a periodogram (Fig. A.3) to estimate the associated represented frequencies. The periodogram for the EEMD was calculated using the Hilbert spectrum (Huang et al., 1998). After merging the intrinsic moded functions (IMFs) 1-6 the short-term variation signal was obtained with a period of around 50 days and from the IMFs 7-11 the seasonal variation with a period of around 330 days. The short-term signal obtained by the parametric approach has a period of around 7 days and the associated seasonal signal has a period of around 330 days.

A.3 Generalized additive models

Here, we show details of the generalized additive models (GAMs) applied in our study to find the correlation between the short-term variation of O_3 and the corresponding variations of

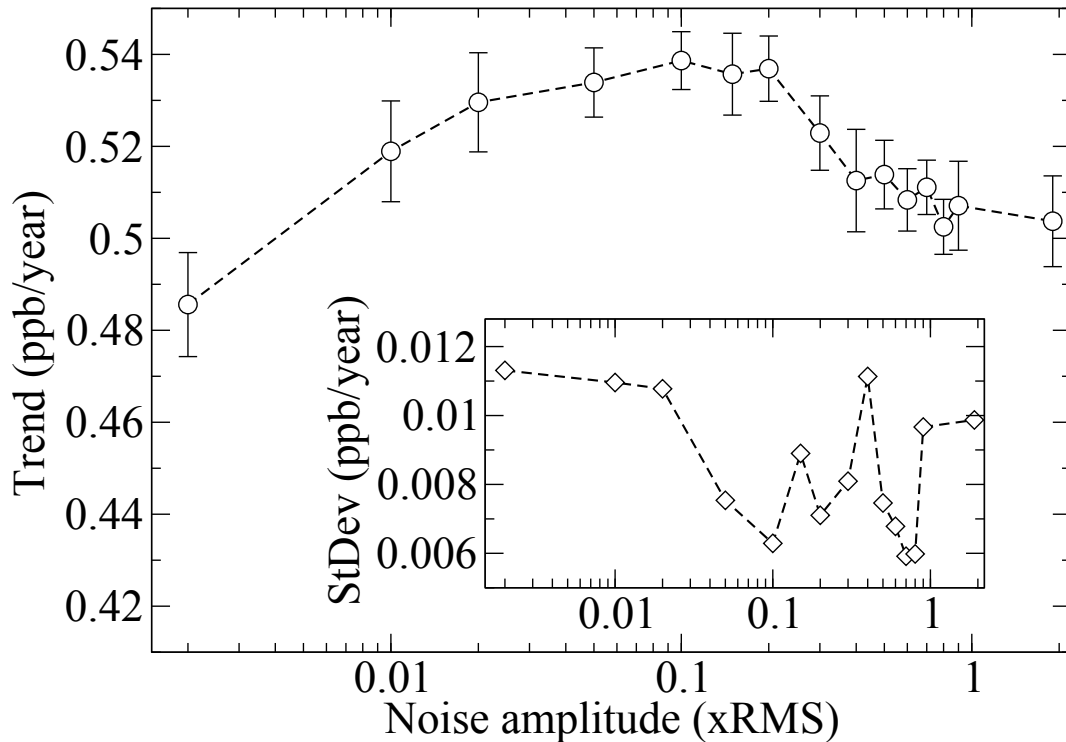


Figure A.2 – The convergence test for the amplitude of the added white noise series. We show the noise amplitude against the calculated Theil-Sen trend for each noise amplitude and in the inset the corresponding standard deviation (data from Basel).

the meteorological variables. In Fig. A.4 we show the R^2 for each station and for the different metrics analyzed, i.e. daily mean O_3 , MDA8 O_3 and daily mean O_x . In Fig. A.5 we can observe an example of the relationship between short-term variation of daily mean O_3 and short-term variation of meteorological predictors in Dübendorf, a suburban site at the northeast of Zürich city. We can see the expected positive relationship between O_3 and temperature as well as with solar radiation. Relative humidity has a negative relationship with O_3 , because water vapour leads to O_3 depletion through the reactions: $O_3 + h\nu \rightarrow O(^1D) + O_2$ followed by $O(^1D) + H_2O \rightarrow 2OH$. Also, high relative humidity is linked to increased fog/cloudiness, i.e. conditions that do not favor O_3 formation. However, OH radicals might lead to increased O_3 mixing ratios, but mostly in high NO_x conditions. We can also see that increasing precipitation leads to decreasing O_3 , probably due to the associated weather conditions (increased cloudiness) that are not favorable for O_3 production. Increasing wind leads to higher O_3 concentrations probably due to enhanced transportation of precursors from the nearby, more polluted city of Zürich. Probably, dilution of air masses at high wind speed enhances O_3 production, but the impact of wind is in general very diverse (Jacob and Winner, 2009). Surface pressure and total

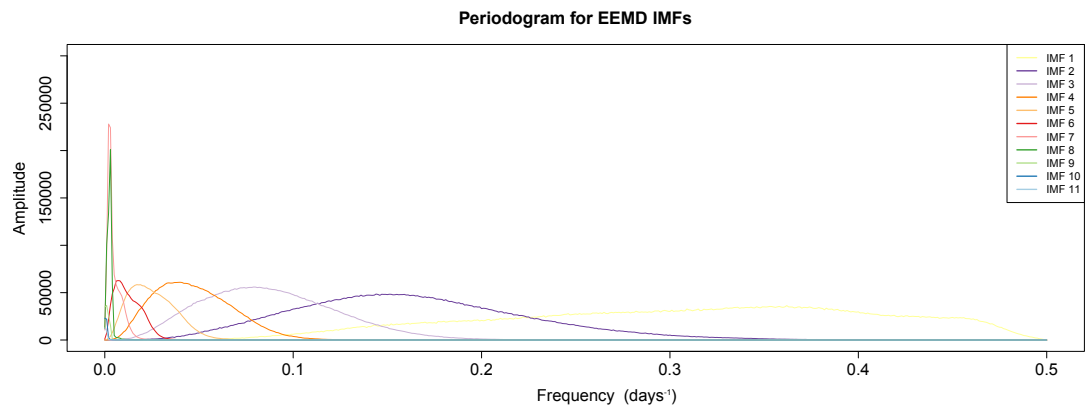


Figure A.3 – Periodogram based on Hilbert spectrum for the suburban site of Dübendorf.

cloud cover do not have a significant influence in this station.

A.3. Generalized additive models

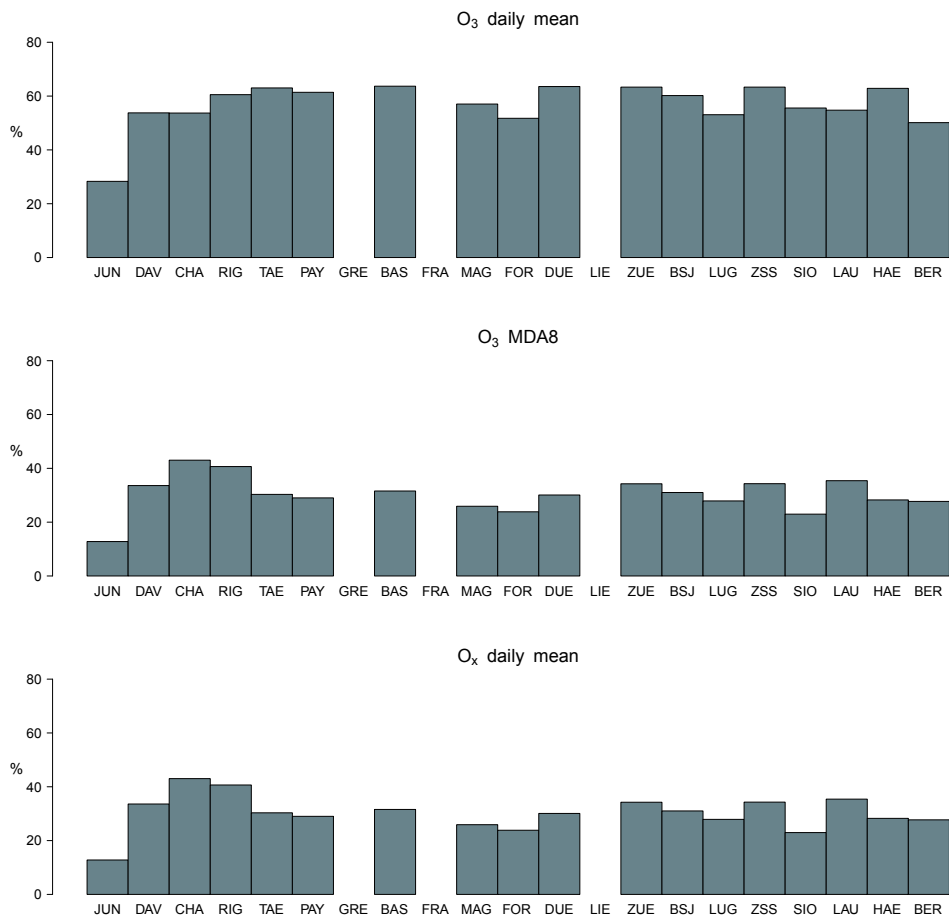


Figure A.4 – Percentage of meteorologically driven variability of daily mean O₃, MDA8 O₃ and daily mean O_x concentrations for the studied stations explained by the GAMs. Meteorological adjustment is not applied for the sites GRE, FRA and LIE.

Appendix A. Appendix A

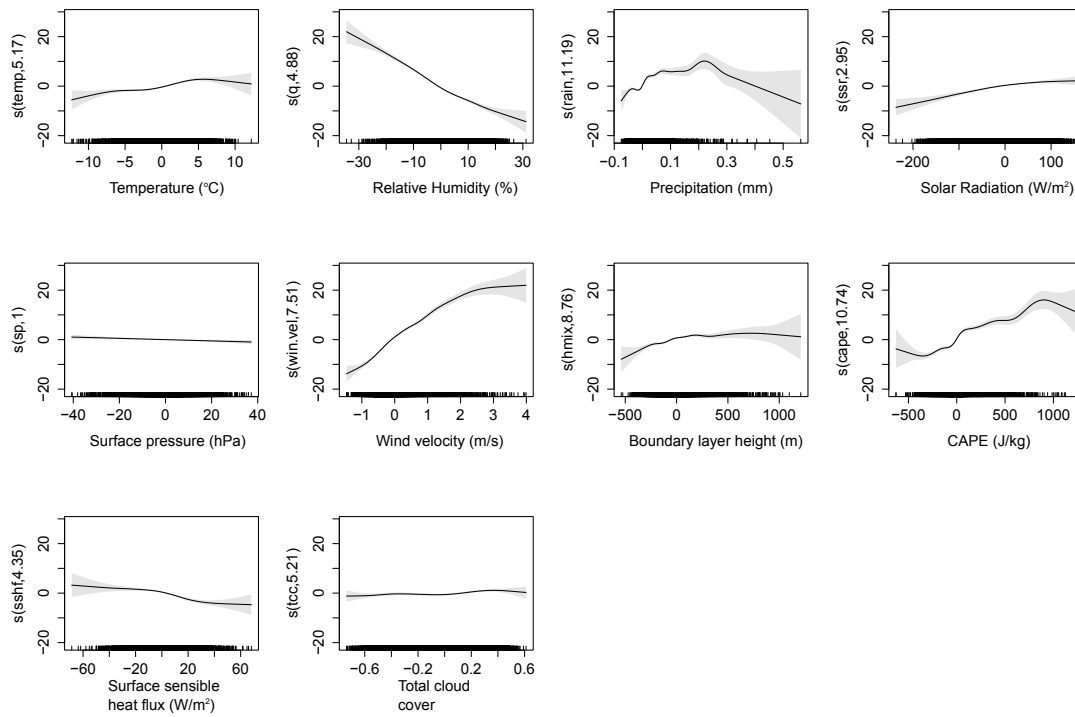


Figure A.5 – Example of relationship between short-term variability of daily mean O_3 concentration and daily means of meteorological variables for Dübendorf. Note that x- and y-axis refer to short-term variation of the parameters and not the actual daily mean values.

A.4 Trends based on NO categorization

The site categories were estimated by mean NO mixing ratio, in addition to the mean NO_x mixing ratio, because the reaction of NO with RO₂ and HO₂ is very important for photochemical formation of O₃. Trends are presented here based on the NO categorization (Figs. A.6-A.8). Categories stay the same as with the NO_x categorization, except that some sites in category D are rearranged. This does not change the main conclusions for the trends as presented and discussed in the main paper.

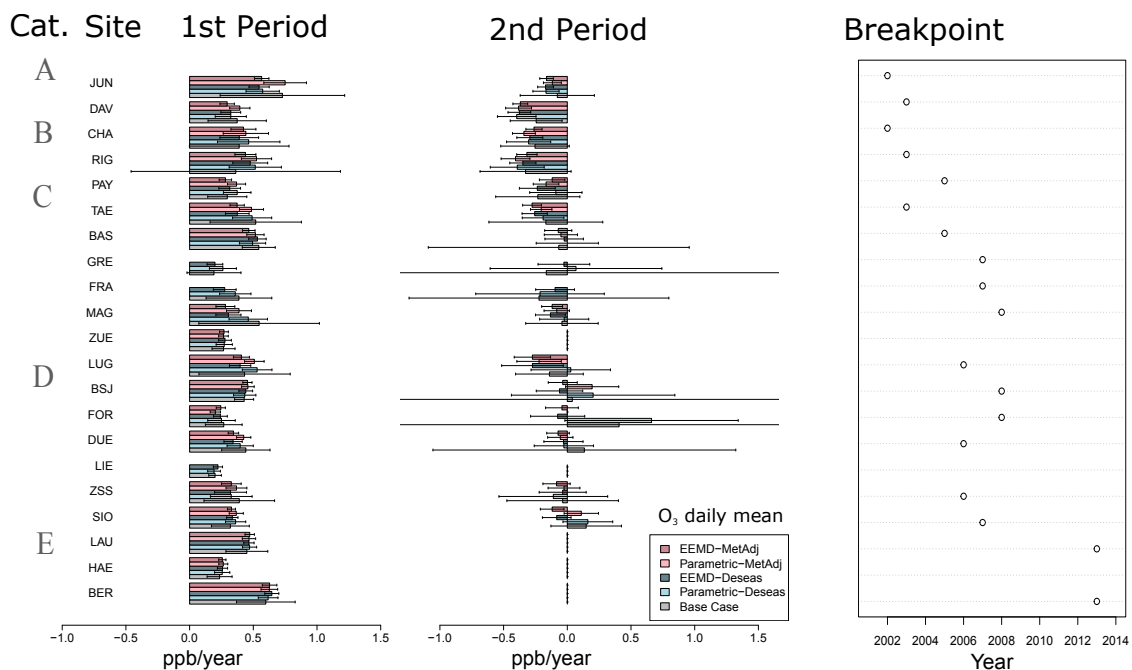


Figure A.6 – Bar-plots for the trends of the daily mean O₃ concentrations during the identified first and second period for the five categories based on mean NO mixing ratio (indicated as Cat.). The bars show the magnitude of the Theil-Sen slopes (in ppb/year) for the studied sites. The lines represent the 95% CI of the estimated trend. The blue colors show the trends estimated from de-seasonalized data, with the subtraction of the seasonal variation obtained either from the parametric approach (light blue bar) or the EEMD (dark blue bar). The pink colors show the meteo-adjusted trends based on the parametric approach (light pink bar) and EEMD (dark pink bar), respectively. The right panel indicates the time when the trend changes from positive to negative, i.e. the breakpoints as calculated from EEMD. Note that due to late breakpoints in Lausanne (LAU) and Bern (BER) the trend in these sites was calculated in one period. Also, the meteo-adjustment has not been applied for the sites GRE, FRA and LIE.

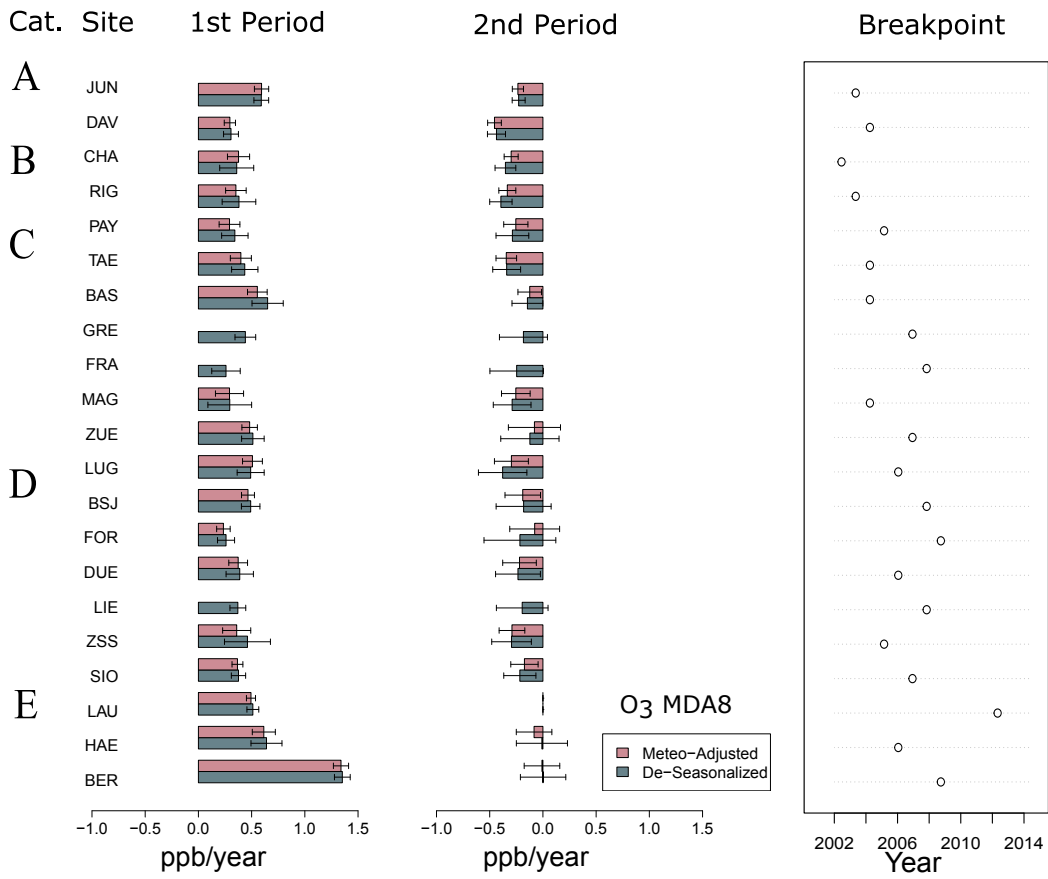


Figure A.7 – As for Fig. A.6 but for MDA8 O₃.

A.4. Trends based on NO categorization

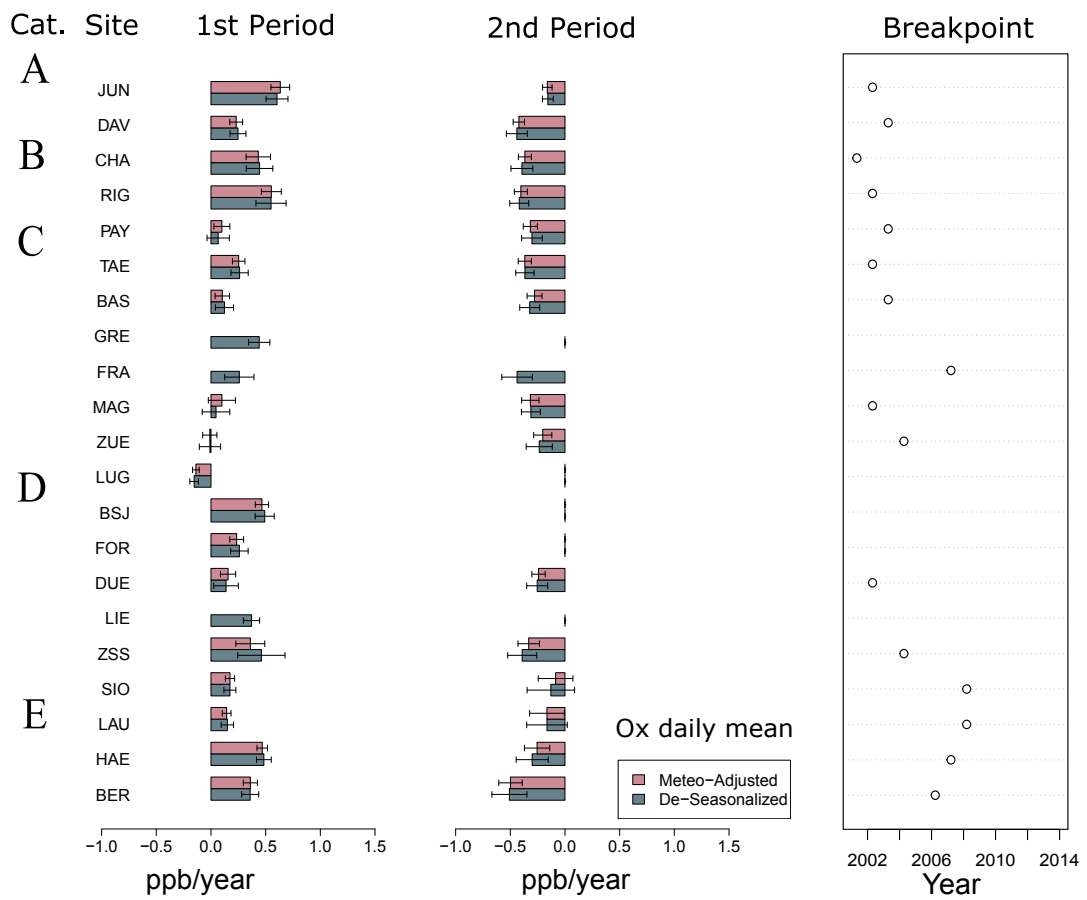


Figure A.8 – As for Fig. A.6 but for daily mean O_x .

B Appendix B

B.1 Trends of 90th percentile, A-MDA8, AOT40 and MTDM-cold season

In this section trends of the A-MDA8, the 90th percentile of daily maximum O₃, the AOT40 and the MTDM between October and April are shown (Figs. B.1-B.5). The 90-PERC and the A-MDA8 decrease for categories B, C, D and E1 and increase for A and E2. AOT40 measures the accumulation of hourly mean mixing ratios above a threshold of 40 ppb and represents the risks of O₃ damage to vegetation (EMEP, 2017). It increases for categories A and E2, while for most rural and suburban sites it decreases. MTDM in the cold season (January-April and October-December) is increasing for categories A and E, while for B, C and D no general conclusion can be made and depends on the specific site.

Additionally, the Theil-Sen trend in Härkingen (HAE) is shown alone in Fig. B.4. It can be observed that the trend is mostly flat until around 2005 and the decrease starts afterwards.

Appendix B. Appendix B

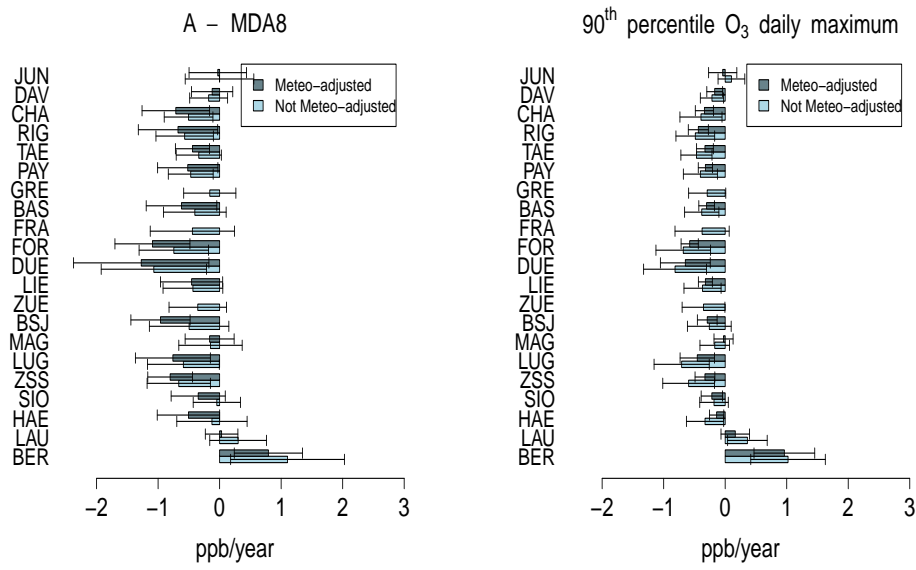


Figure B.1 – Bar-plots with the Theil-Sen slopes for the annual maximum O₃ (A-MDA8) and the 90th percentile of daily maximum O₃ before and after meteo-adjustment.

B.1. Trends of 90th percentile, A-MDA8, AOT40 and MTDM-cold season

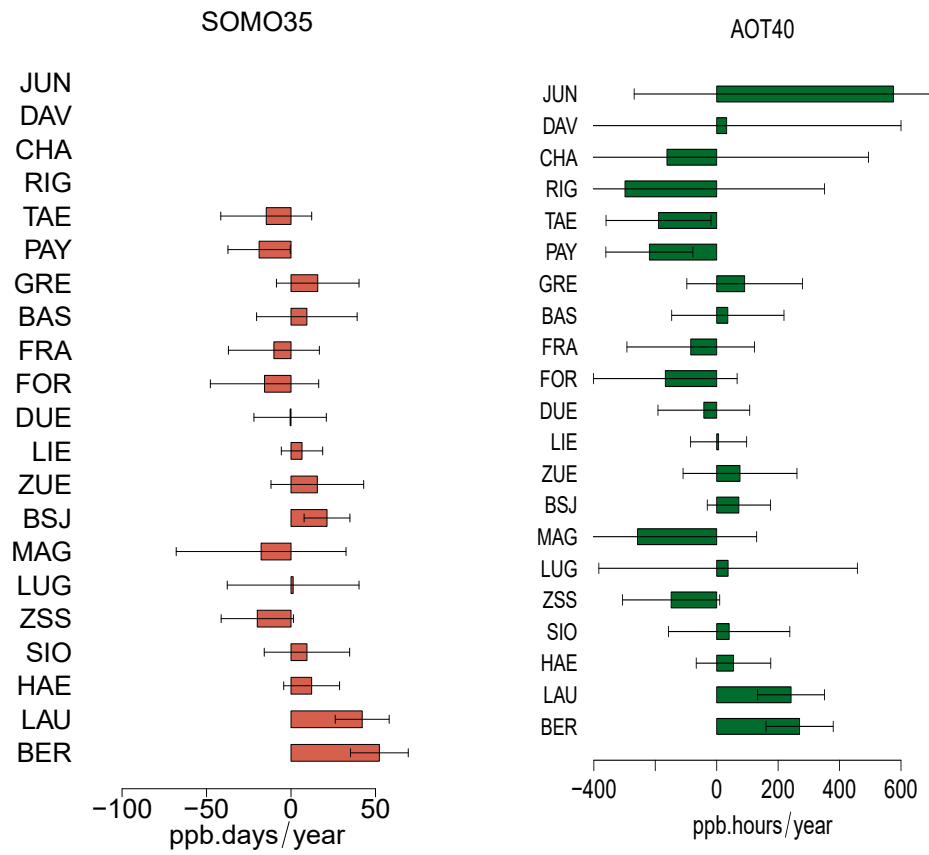


Figure B.2 – Same as Fig. B.1 for the SOMO35 and AOT40 without meteo-adjustment. Note that SOMO35 trends are not shown due to an inflection point during the studied period (see discussion of results in the main text).

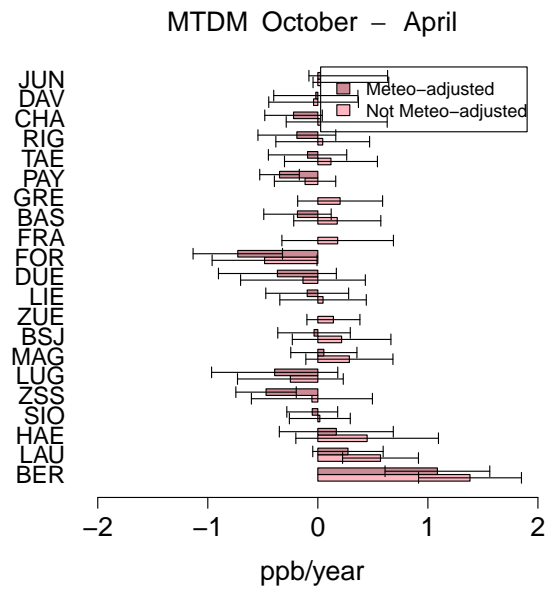


Figure B.3 – Same as Fig. B.1 for the MTDM between October and April.

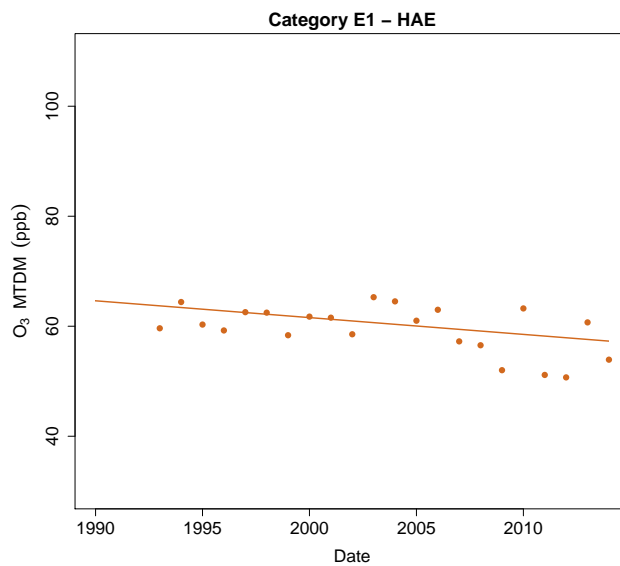


Figure B.4 – Theil-Sen trend of MTDM for the season May to September for the site in Härkingen (HAE).

B.1. Trends of 90th percentile, A-MDA8, AOT40 and MTDM-cold season

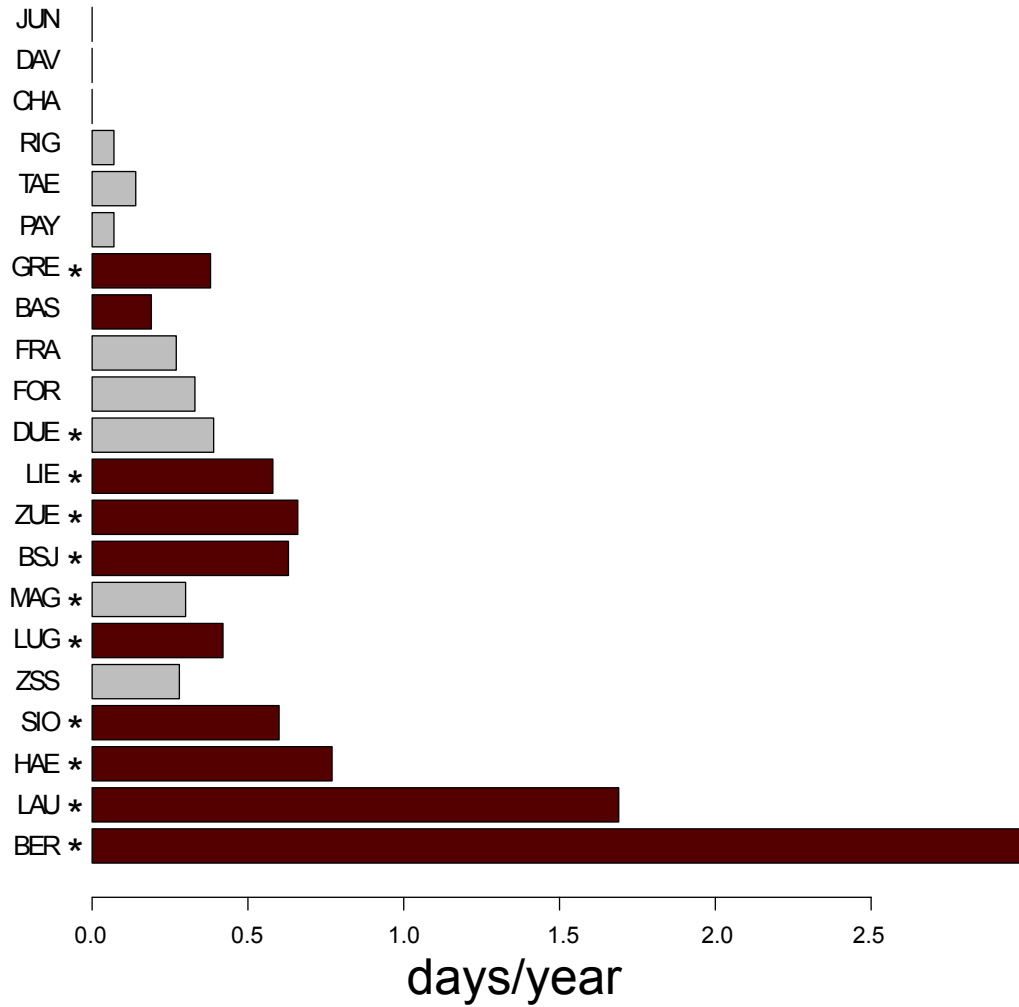


Figure B.5 – Theil-Sen trends of the number of days with MDA8 O₃ >35 ppb during summer months (June, July and August). Red bars indicate the sites where positive SOMO35 trends were found, and * the significant trends (p-value<0.1).

B.2 Daily maximum O₃ and temperature

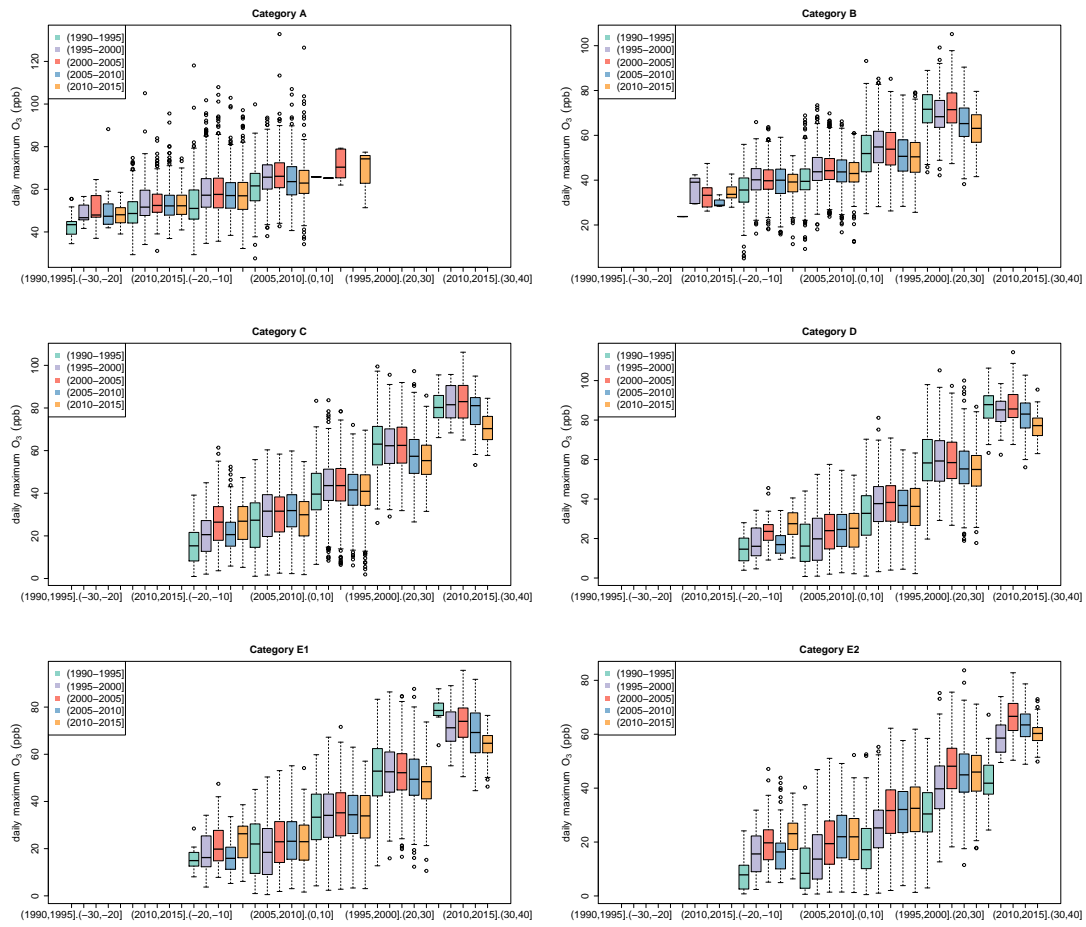


Figure B.6 – Box-and-whisker plots for daily maximum O₃ in different temperature ranges and time periods averaged for the sites categories.

B.3 Daily maximum O₃ and day of week

The day of week was observed in relation to daily maximum O₃ concentrations (Fig. B.7). It was observed that in rural sites daily maximum O₃ is lower during weekends for the warm season May to September (e.g. in Chaumont (CHA)). In the urban sites daily maximum O₃ is higher during weekends for the cold season October to April (e.g. in Zürich (ZUE)).

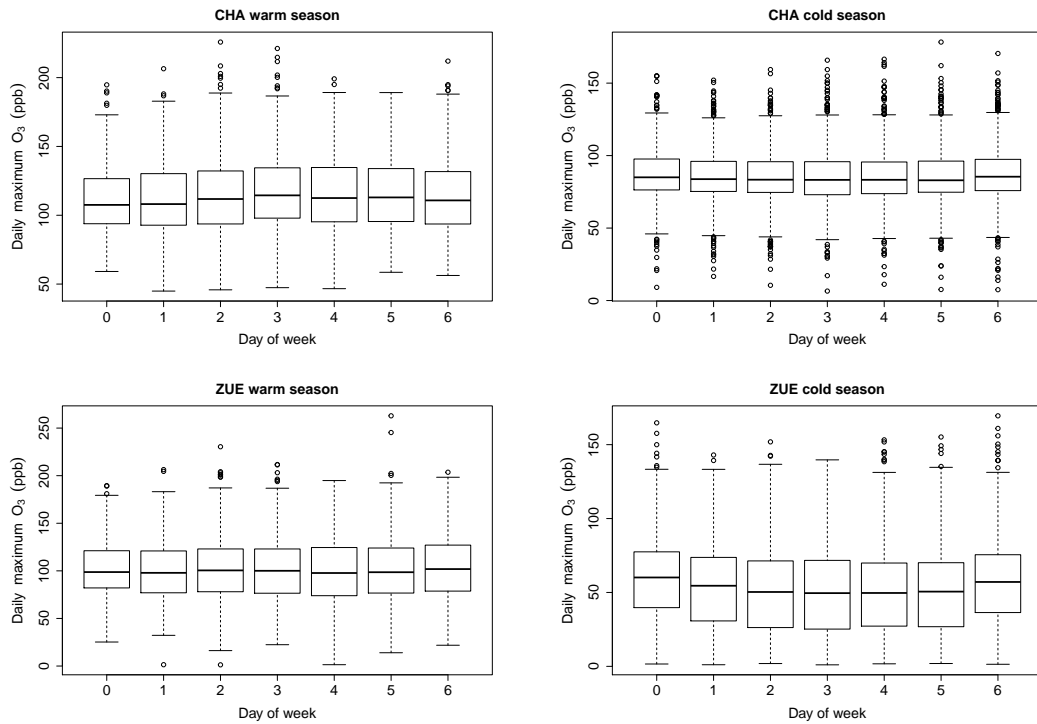


Figure B.7 – Whisker-plot for the daily maximum O₃ and the day of week for the sites in Chaumont (CHA) and Zürich (ZUE). Warm season refers to the months May to September and cold season to the months October to April.

B.4 Comparison to different time periods

The current meteo-adjustment methodology was compared to the findings by Ordóñez et al. (2005) for the trend of the 90th percentile of the daily maximum O₃ during the time period 1992-2002. In addition, MTDM trends (meteo-adjusted and not meteo-adjusted) were compared to trends based on raw observations and modeled values as were estimated by Solberg (2009) for the period between 1995 and 2005.

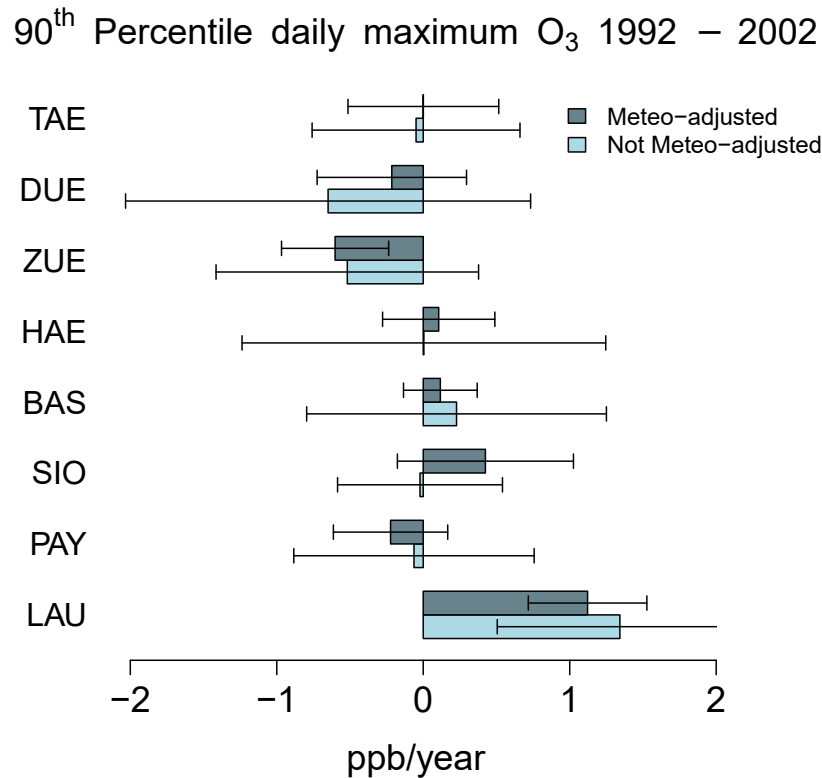


Figure B.8 – Theil-Sen trends of the 90th percentile of daily maximum O₃ during the warm season for the time period 1992-2002.

B.4. Comparison to different time periods

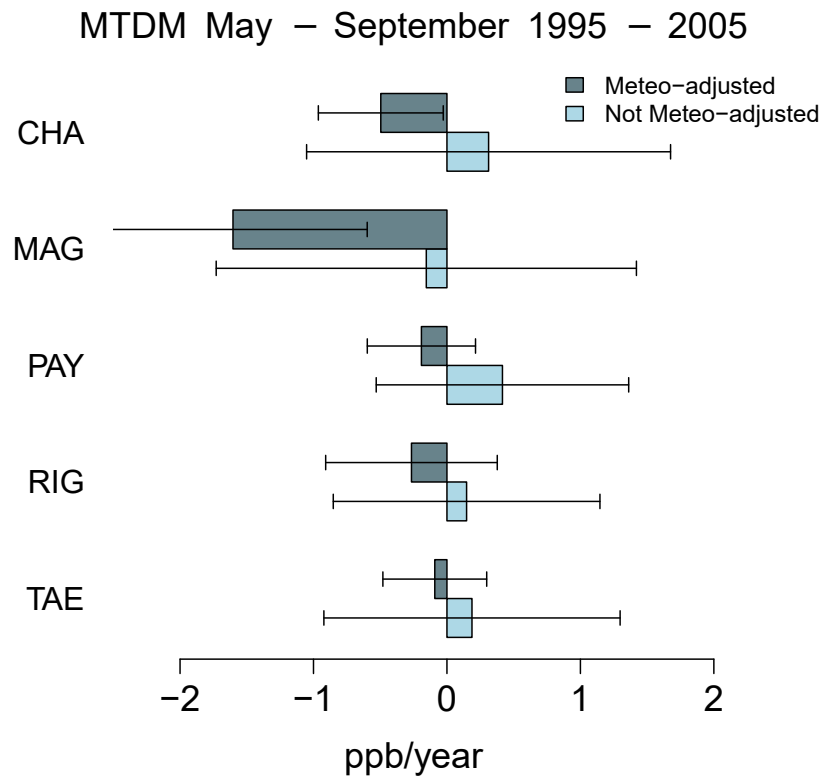


Figure B.9 – MTDM Theil-Sen trends during the warm season for the time period between 1995 and 2005.

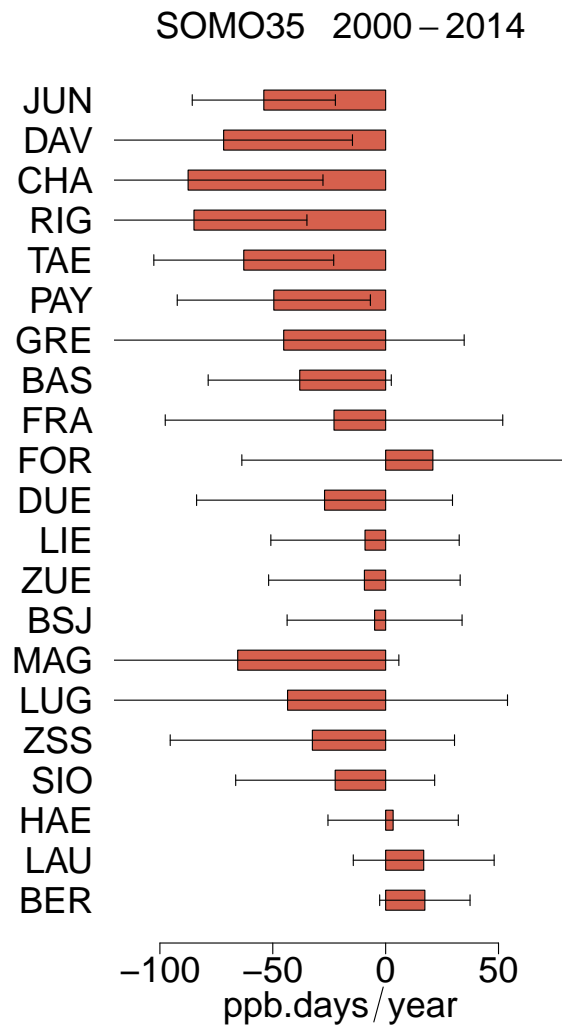


Figure B.10 – SOMO35 Theil-Sen trends during the warm season for the time period between 2000 and 2014.

B.5 Variables selected in the GAMs

In Figs. B.11 to B.14 the parameters selected for summer and winter models respectively are shown. The rank essentially designates the importance of the meteorological variable for O₃ variability for the individual sites.

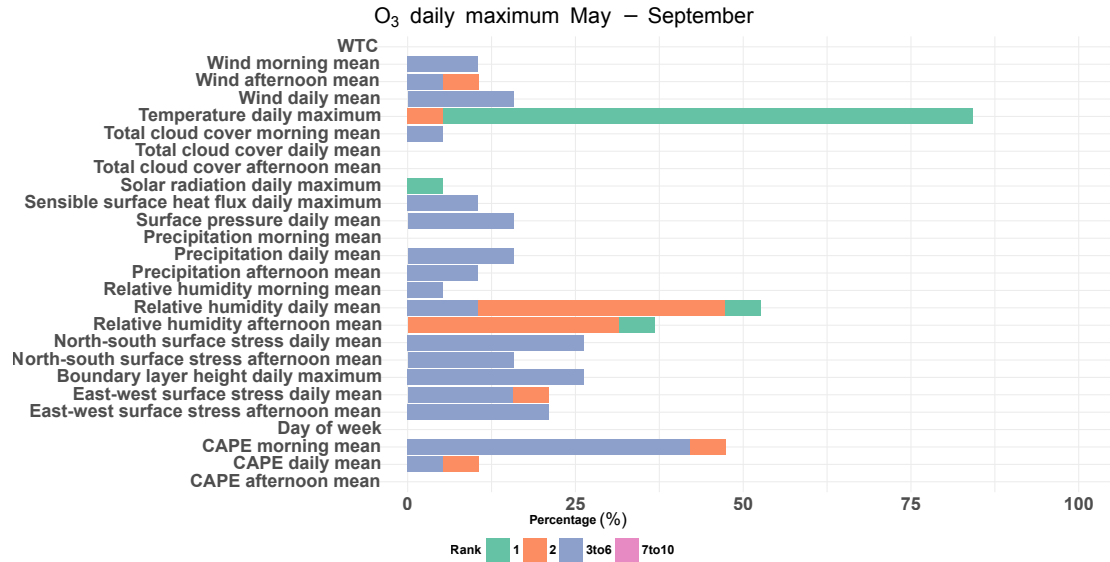


Figure B.11 – Bar charts for frequency of occurrence (%) and ranking (1st, 2nd, 3rd-6th, and 7th-10th position) of the meteorological variables in the GAMs for O₃ daily maximum in the warm period (May-September) after the model selection. The percentage shows the frequency of occurrence of the parameter in the models and colors show the ranking of the parameter in the model, i.e. as a 1st parameter, as a 2nd, between 3rd and 6th position and 7th to 10th position.

In addition, a test for the choice of AIC has been performed (Fig. B.15), i.e. the variable selection algorithm was used for different AIC values and the resulted number of explanatory variables and R² was plotted against AIC. One can observe that the small AIC (e.g. between 2-10) leads to high number of selected variables and for AIC higher than 14 there is a plateau for number of variables and after 28 the number explanatory variables reduces again.

Appendix B. Appendix B

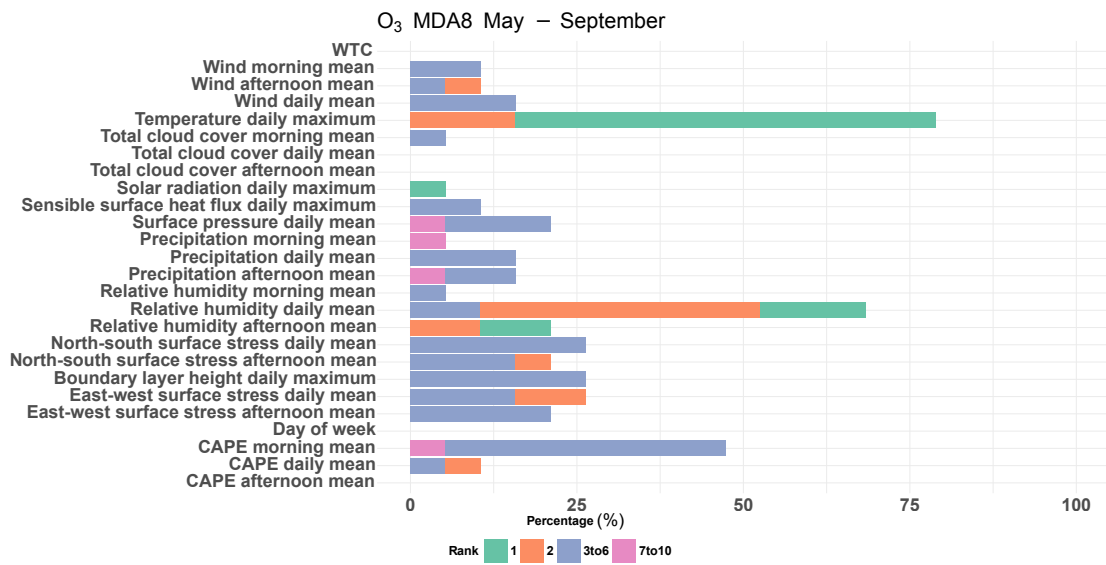


Figure B.12 – Same as Fig. B.11 but for MDA8 O₃.

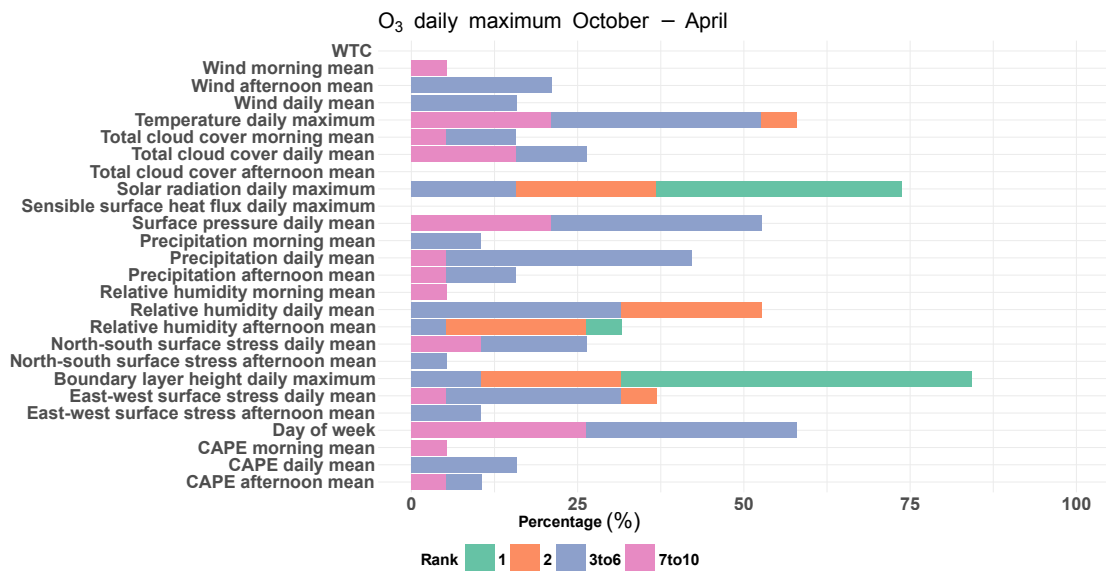


Figure B.13 – Same as Fig. B.11 but for the cold period.

B.5. Variables selected in the GAMs

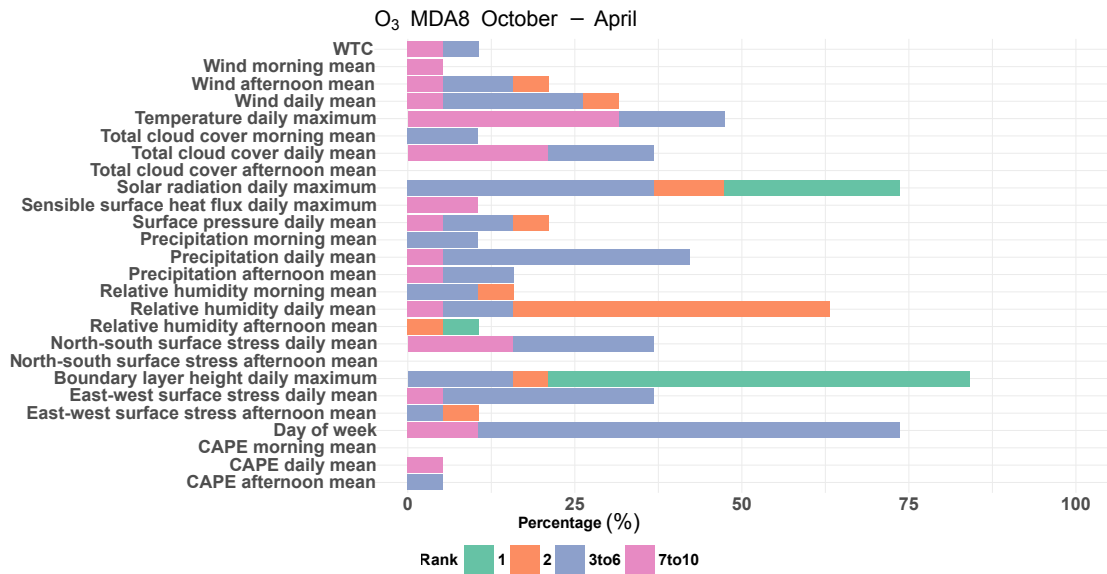


Figure B.14 – Same as Fig. B.11 but for MDA8 O₃ in cold period.

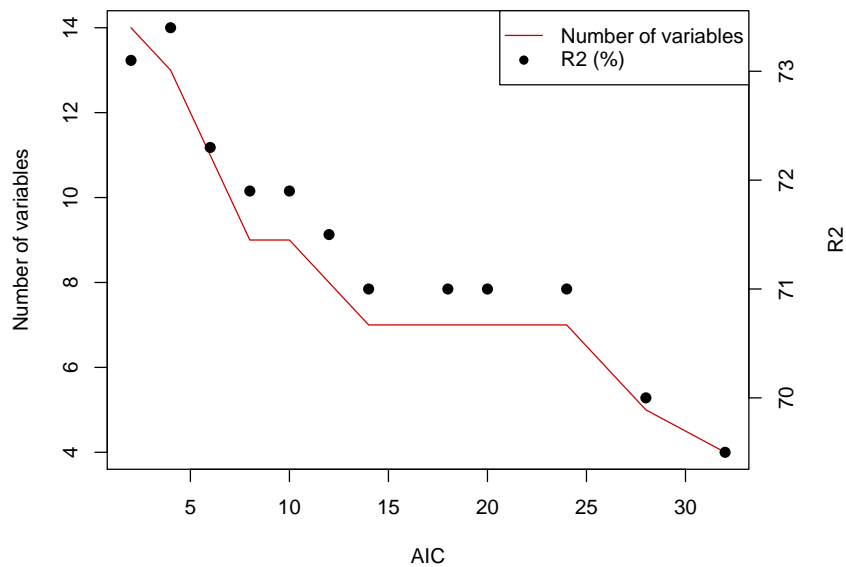


Figure B.15 – A test regarding the choice of AIC in the variable selection approach.

B.6 Generalized additive models

In this study GAMs have been implemented for each site by using the selected meteorological variables for the daily maximum O_3 and MDA8. For each metric, the warm (May to September) and cold (October to April) season was filtered. In Fig. B.16 we show the variance of O_3 (in %) explained by the GAMs.

An example of the relationship between daily maximum O_3 and MDA8 and the selected meteorological variables in the cold season is shown in Fig. B.17. In addition, a representative analysis of the model assumptions for the same models can be seen in Fig. B.19.

The relation between O_3 and the Julian day is shown in Fig. B.18. The reduction O_3 with time is clearly captured, which is also calculated by the Theil-Sen trend estimator.

A comparison between the observations and the fitted values in the GAM is shown in Fig. B.20. We can see that the model generally predicts intermediate values with little overall bias, the highest peak values are often underestimated. However, negative residuals of the high ozone peaks are small in magnitude (with fewer number of points) in comparison to the remaining residuals. Therefore, this systematic underestimation is not expected to exert influence or leverage in the model that would substantially affect the long-term trends.

B.6. Generalized additive models

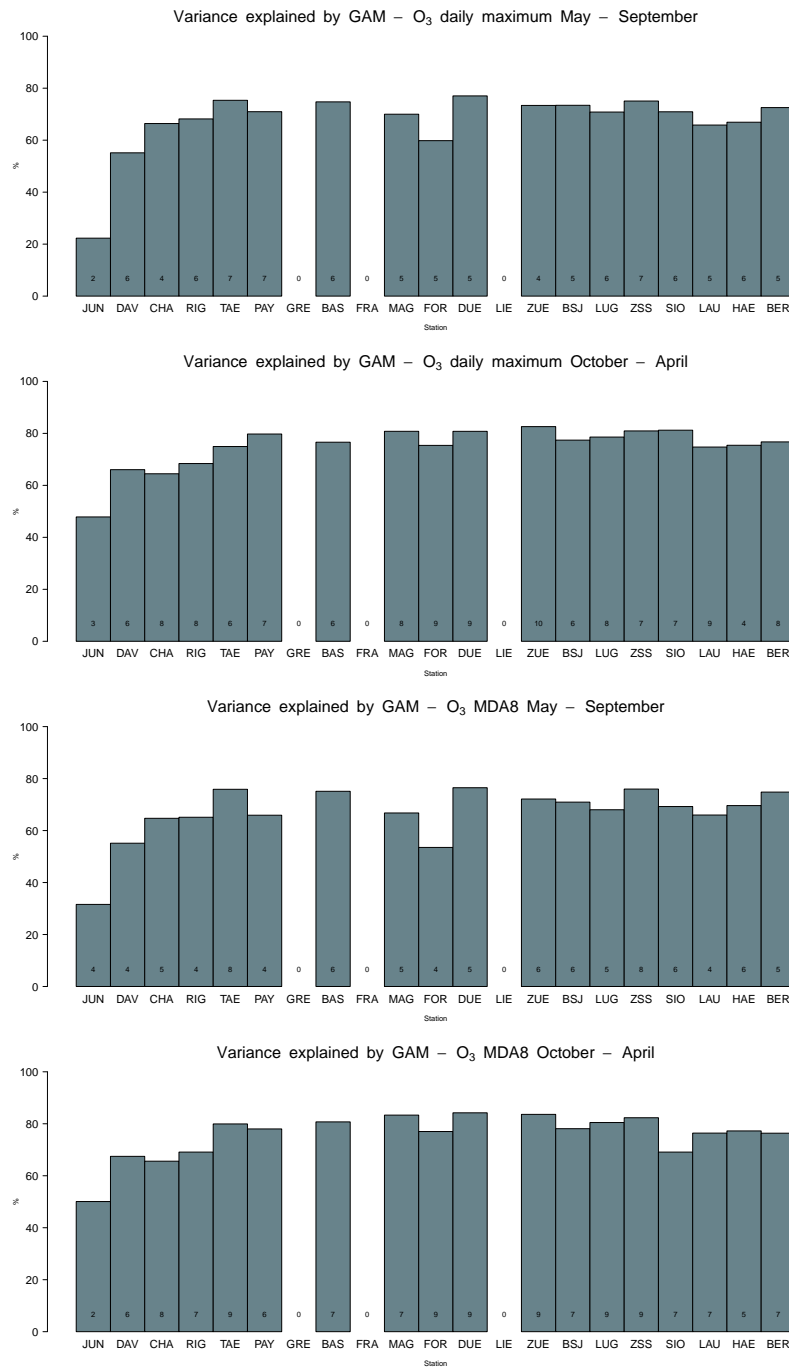


Figure B.16 – Bar-plots for the variation of O₃ (R^2) explained by the most important meteorological variables and time. The value in the bars indicates the number of meteorological variables that were selected in the model selection procedure.

Appendix B. Appendix B

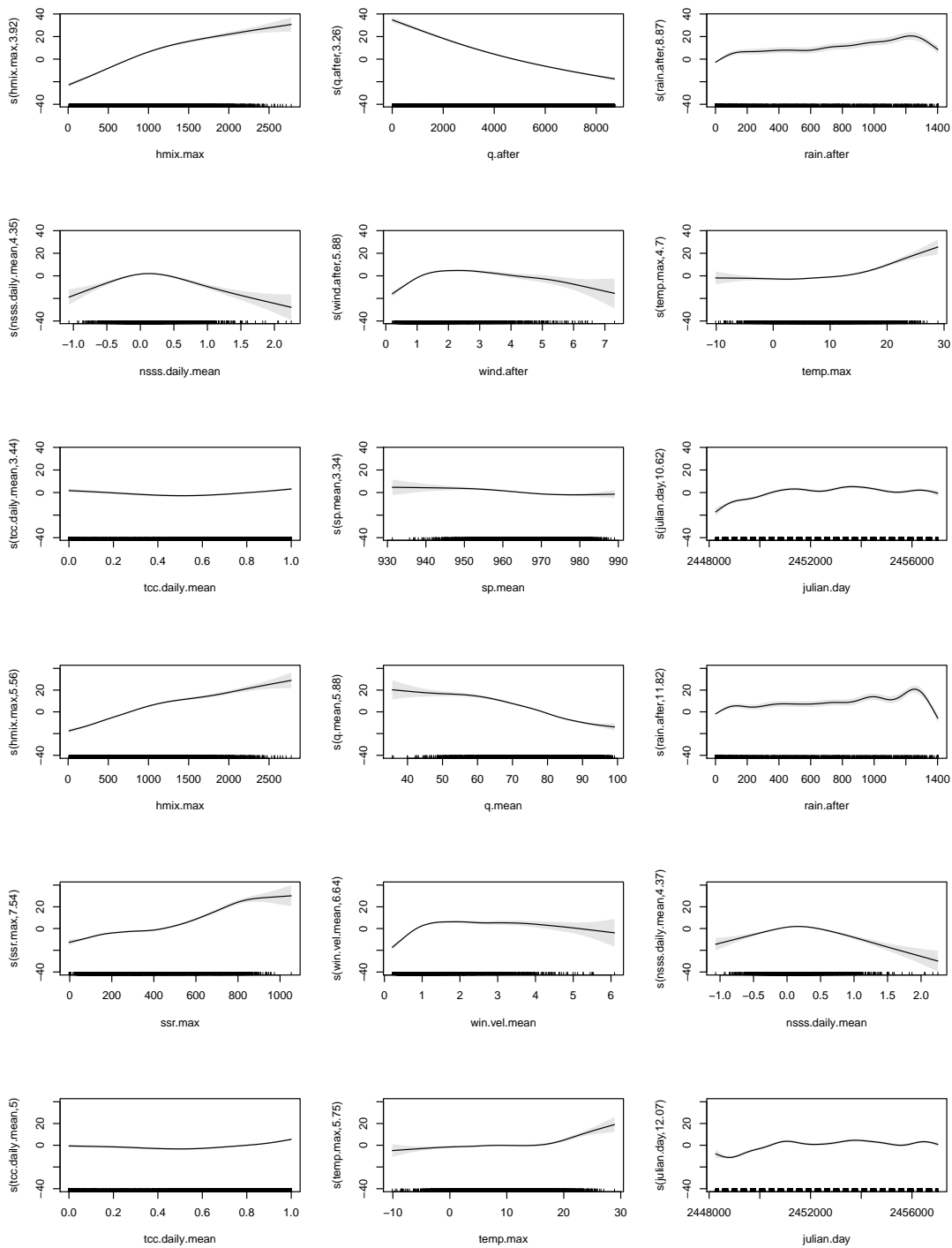


Figure B.17 – Example of relationship of O₃ daily maximum and the selected meteorological variables for the suburban site Dübendorf. Above we show the results for the daily maximum values and below for the MDA8 values during the cold season October-April.

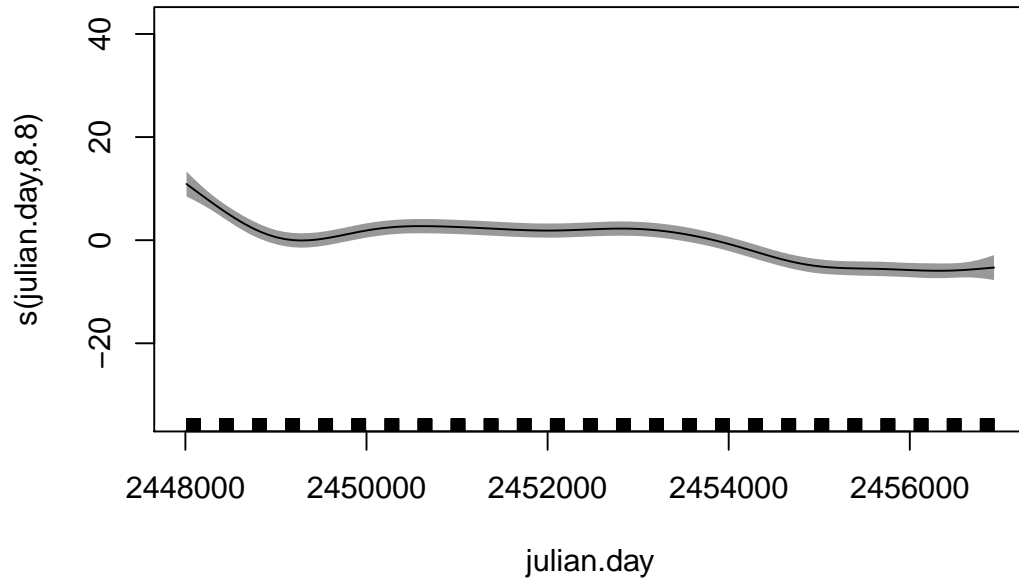


Figure B.18 – Example of relationship of O₃ daily maximum and the Julian day parameter ($s_0(t)$).

Appendix B. Appendix B

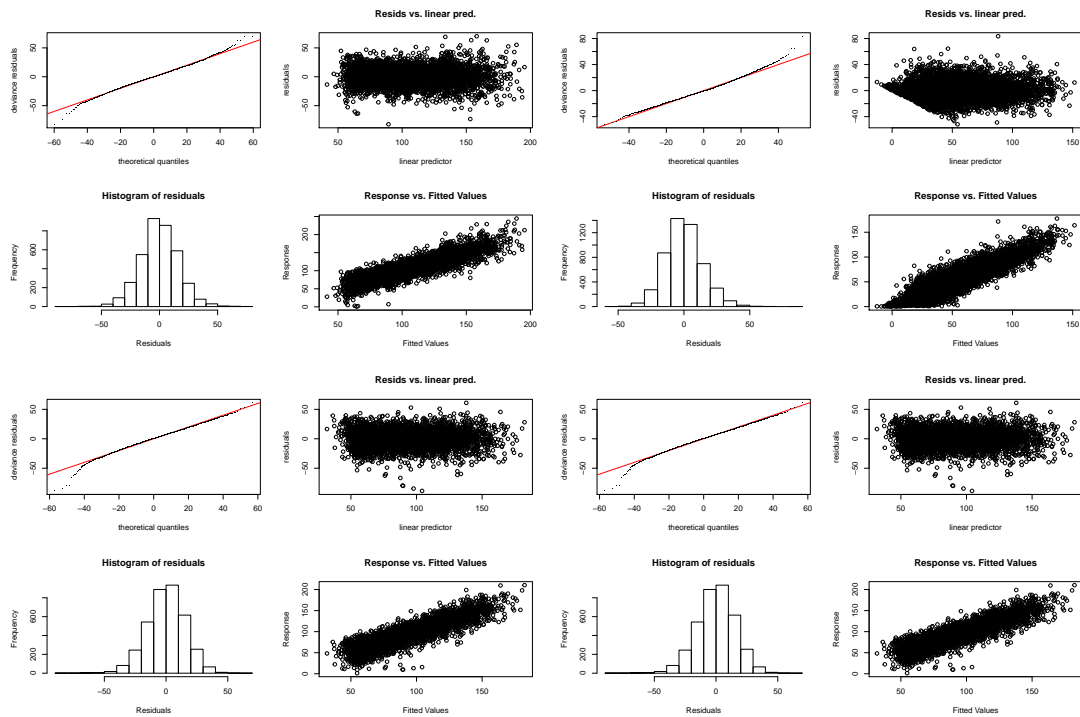


Figure B.19 – Model assumptions check for GAMs O_3 daily maximum (left) and MDA8 (right) in warm (up) and cold (down) season for the suburban site Dübendorf.

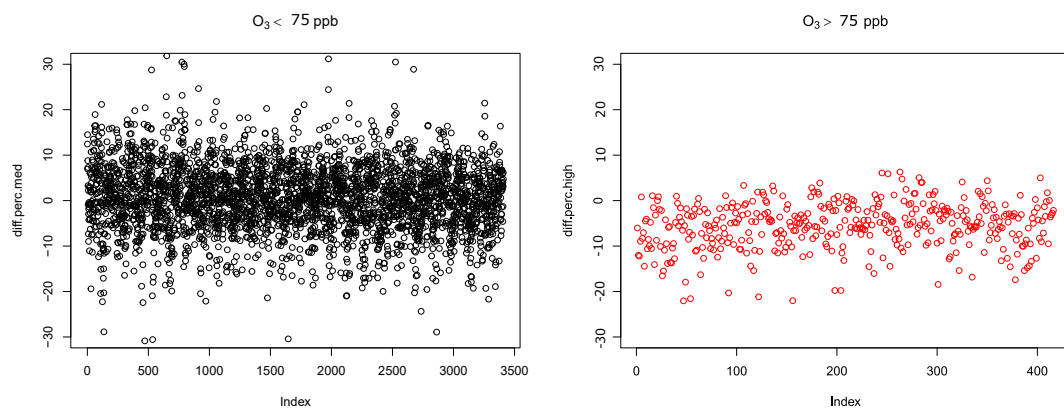


Figure B.20 – A comparison of the observations with the fitted values in the GAM. The percentage of the difference $(O_3^{fitted} - O_3^{observed}) / O_3^{fitted} \%$ is shown in the y-axis for the intermediate values (< 150 ppb, left) and the extreme values (> 150 ppb, right).

B.7 O₃ and temperature sensitivity in the GAMs

Sensitivity of O₃ to temperature has changed throughout the studied period. To address this issue here, a GAM during different periods is performed. Additionally a GAM with only O₃ and temperature for the same time periods is performed to compare the resulted R². We observed that the relationship between O₃ and temperature stays mostly stable throughout the studied period. Small deviations are observed for the period 2002-2007 due to probably high O₃ events due to the 2003 heat wave and also for the last time period 2008-2014 which is probably related to the reduced sensitivity of O₃ to temperature. However, these deviations are small as one can see in the partial plots and in the R₂ values, and they do not influence the overall trend estimations and conclusions of the study.

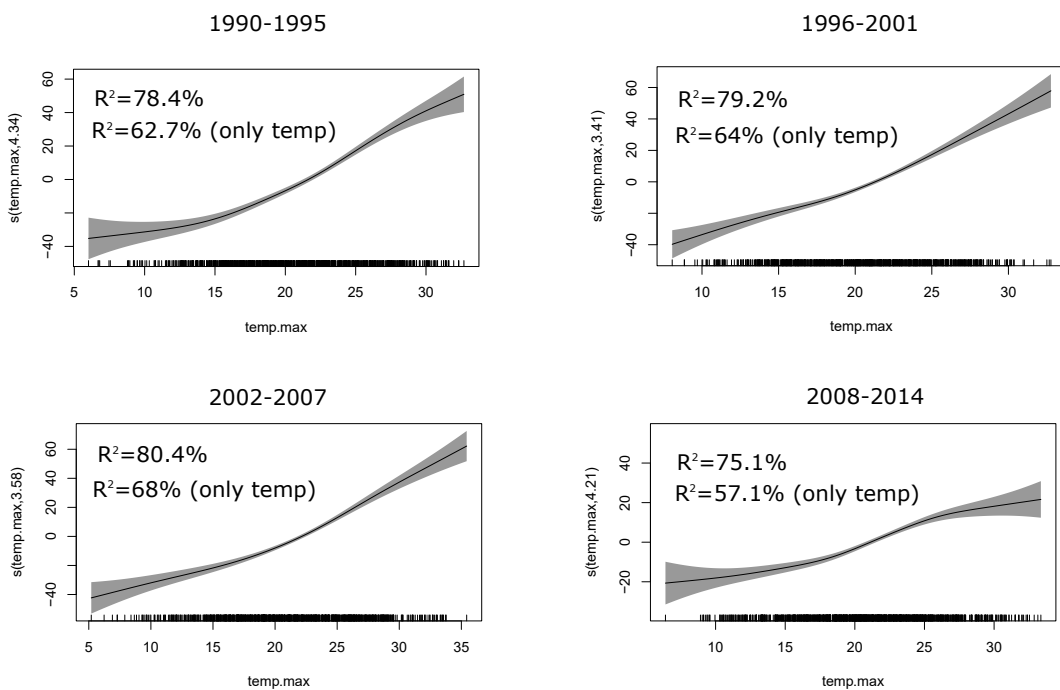


Figure B.21 – Partial plots between O₃ and temperature daily maximum values for the indicated time periods.

B.8 Comparison of Theil-Sen trends and Linear Regression

By comparing the Theil-Sen trend estimator with the linear regression for MTDM May-September, 4-MDA8, it can be observed that the two approaches agree mostly well with each other in calculation of the slope and the confidence intervals (CIs) of the trends (Fig. B.22). For the metric 4-MDA8 there are some discrepancies, due to the few data points (4 per year compared to 10 per year for the MTDM) that are used for the calculation.

In this section we tested the effect of the hot summers in 2003 and 2006 on the Theil-Sen trend

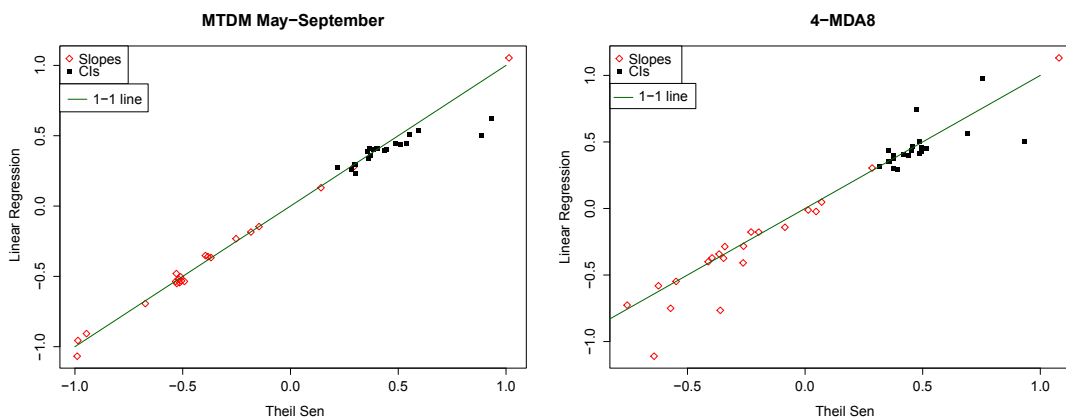


Figure B.22 – Scatter plot comparing the Theil-Sen and Linear Regression slopes for the MTDM between May and September and 4-MDA8. Straight line shows the 1-1 line.

estimation. The values for 2003 and 2006 were replaced by average concentrations based on the previous and the next year’s mean value. Theil-Sen trends from the raw measurements and the ones with the average values for 2003 and 2006 are shown in Fig. B.23. It is observed that by using average values for the years 2003 and 2006 the trend is systematically lower than the trend based on the raw observations, i.e. either more negative for negative trends or less positive for the positive trends. In addition, small upward trends of temperature were observed during the studied time period (Fig. B.24), which contributed to calculation of lower trends based on the meteo-adjusted O₃ compared to the trends based on the measured O₃.

B.8. Comparison of Theil-Sen trends and Linear Regression

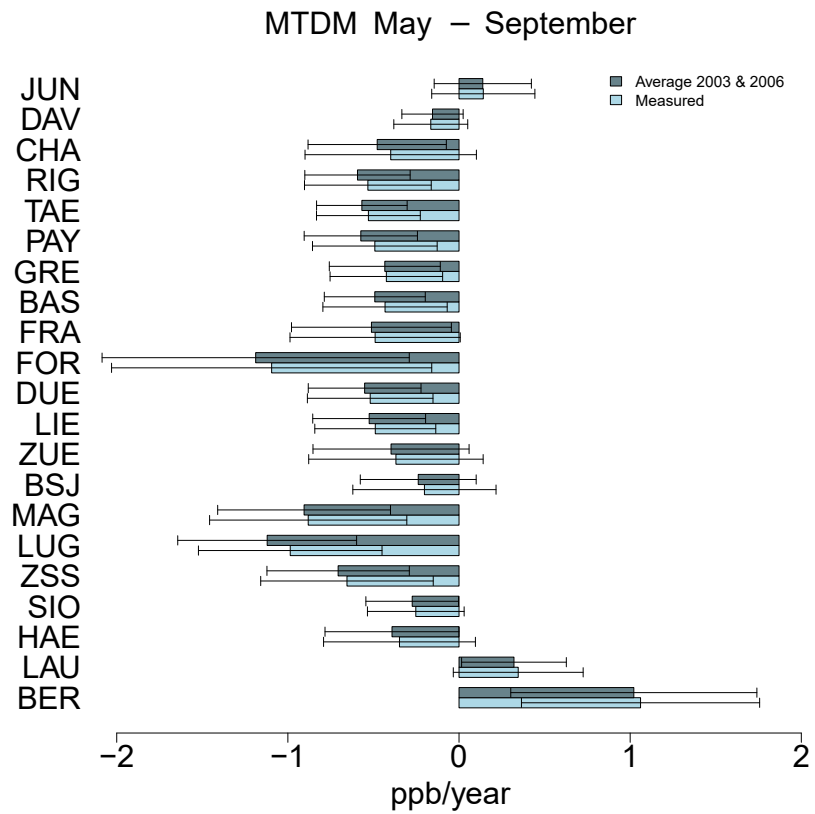


Figure B.23 – Comparison of the Theil-Sen trends with and without the effect of the hot summers 2003 and 2006.

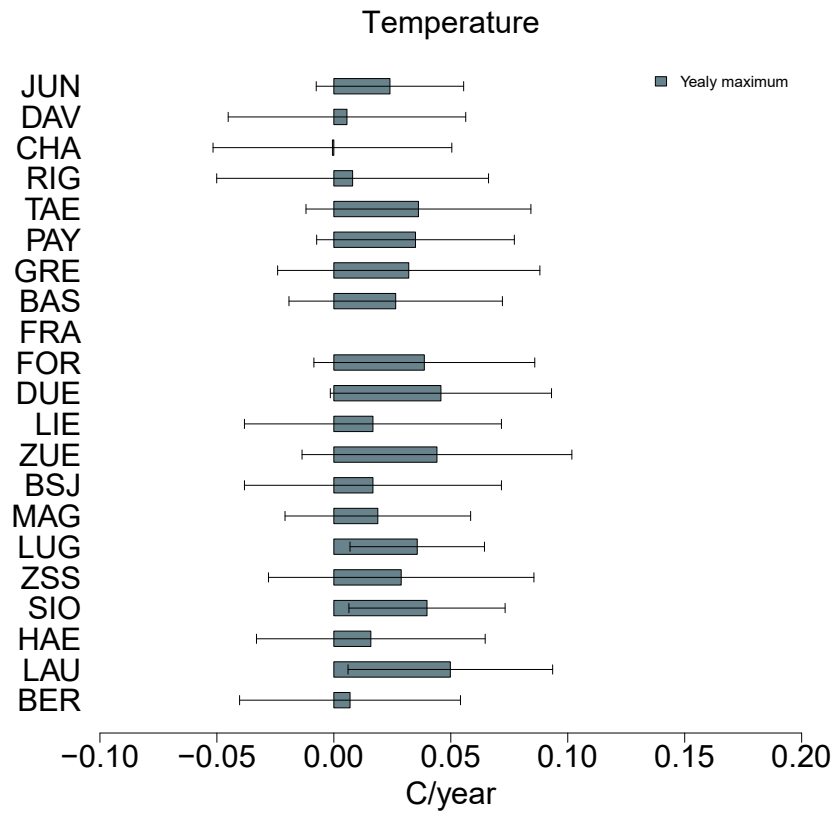


Figure B.24 – Theil-Sen trends of daily maximum temperature (yearly average).

C Appendix C

C.1 Choice of number of clusters

The analysis of the appropriate number of clusters is shown in Figs. C.1 and C.2. The sum of squared distance error within a cluster is plotted against the number of clusters. The number of clusters where the sum of squared distance error is mostly minimized is considered to be the most appropriate choice.

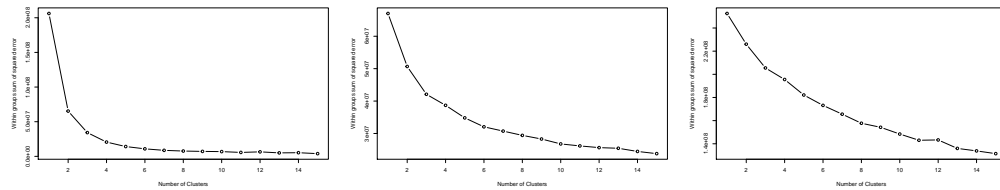


Figure C.1 – Sum of squared distance error within a cluster against number of clusters for daily mean O_3 $LT(t)$, $S(t)$ and $W(t)$.

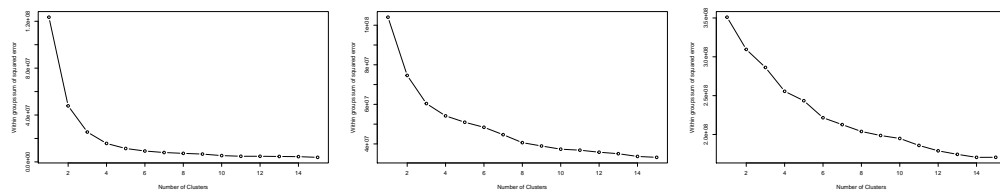


Figure C.2 – Same as Fig. C.1 but for MDA8 O_3 .

C.2 Assessment of clusters

Silhouette width (S_w) is considered a good metric to assess the goodness of a clustering. Positive Silhouette width values mean that objects within the cluster have high similarity while negative ones mean that the objects have a low similarity with the rest objects in the cluster. Here, a S_w is assigned to each member of the cluster (here each measurement site) to assess the level of similarity in the cluster. It is defined as:

$$S_w = \frac{b(i) - a(i)}{\max[a(i) - b(i)]} \quad (\text{C.1})$$

where $a(i)$ the average distance (dissimilarity) of i with all other data points within the same cluster and $b(i)$ the lowest average distance of i to all points in any other cluster, of which i is not a member. Positive S_w value for a specific site means that similarity to other sites in the cluster is high. A negative S_w indicates that a site is more similar to a site from another cluster than to its own cluster centroid, and is an indication of lower similarity to other sites in its own cluster.

S_w plots for daily mean O_3 are shown in Figs. C.3-C.5 and for the MDA8 O_3 in Figs. C.6-C.8.

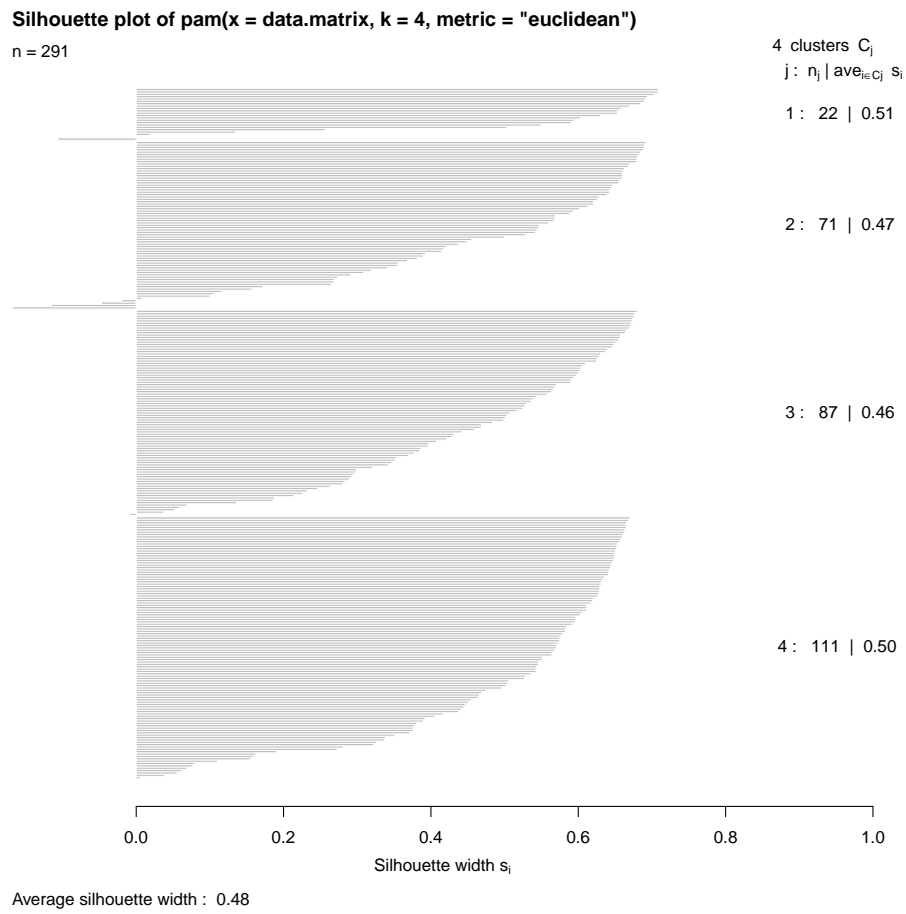


Figure C.3 – Silhouette width plots for daily mean O_3 $LT(t)$.

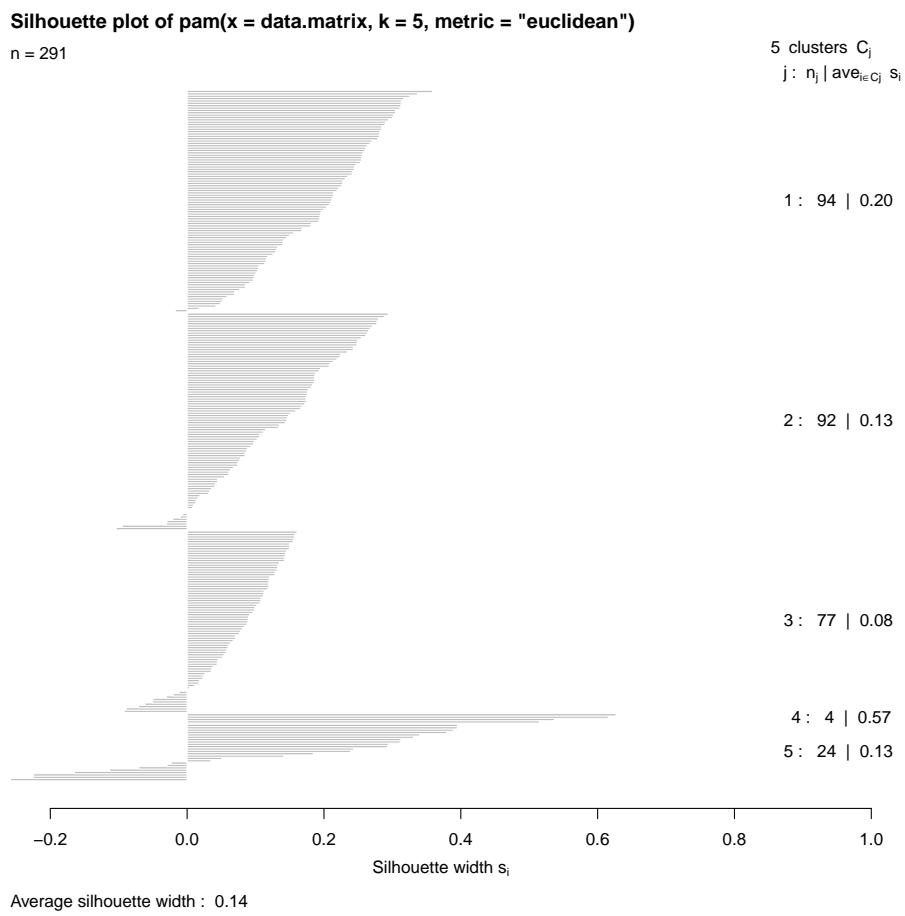


Figure C.4 – Same as in Fig. C.3 but for $S(t)$.

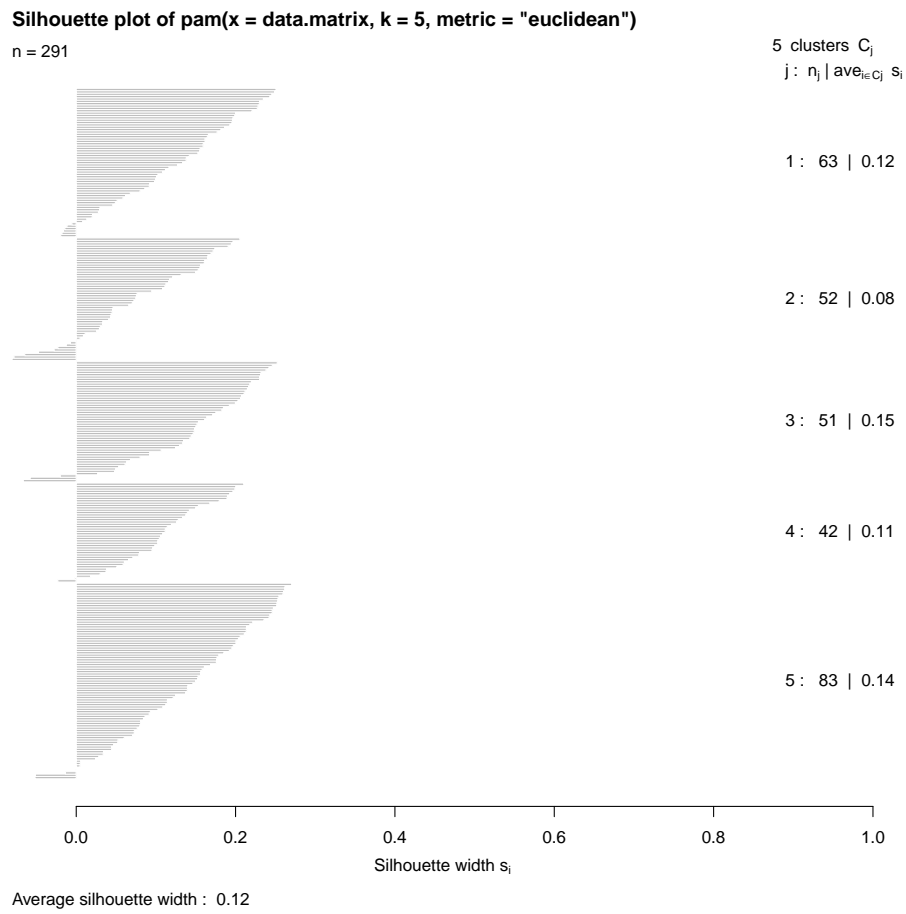


Figure C.5 – Same as in Fig. C.3 but for $S(t)$.

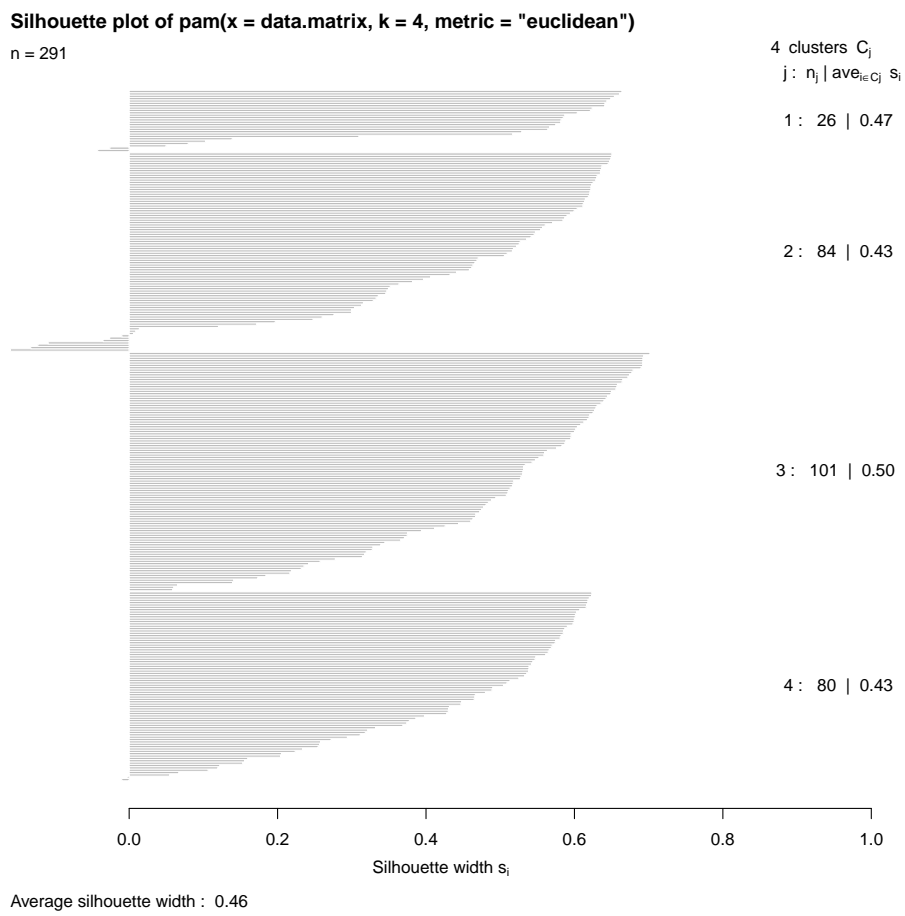


Figure C.6 – Same as in Fig. C.3 but for MDA8 LT(t).

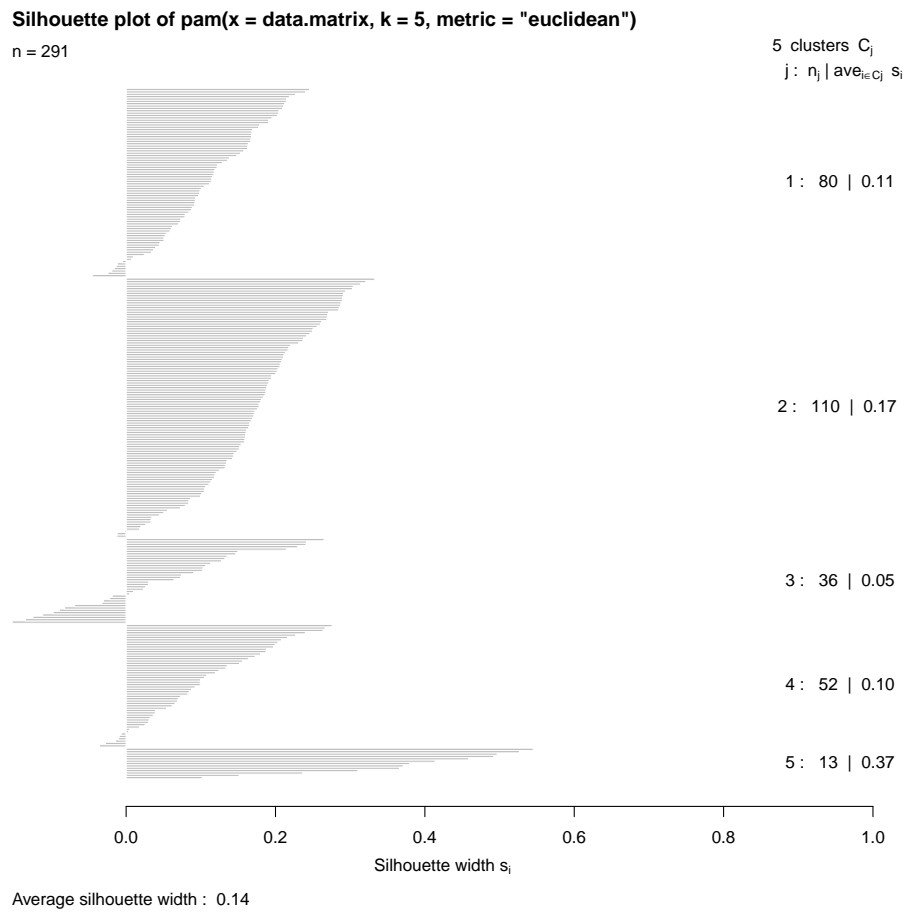


Figure C.7 – Same as in Fig. C.6 but for $S(t)$.

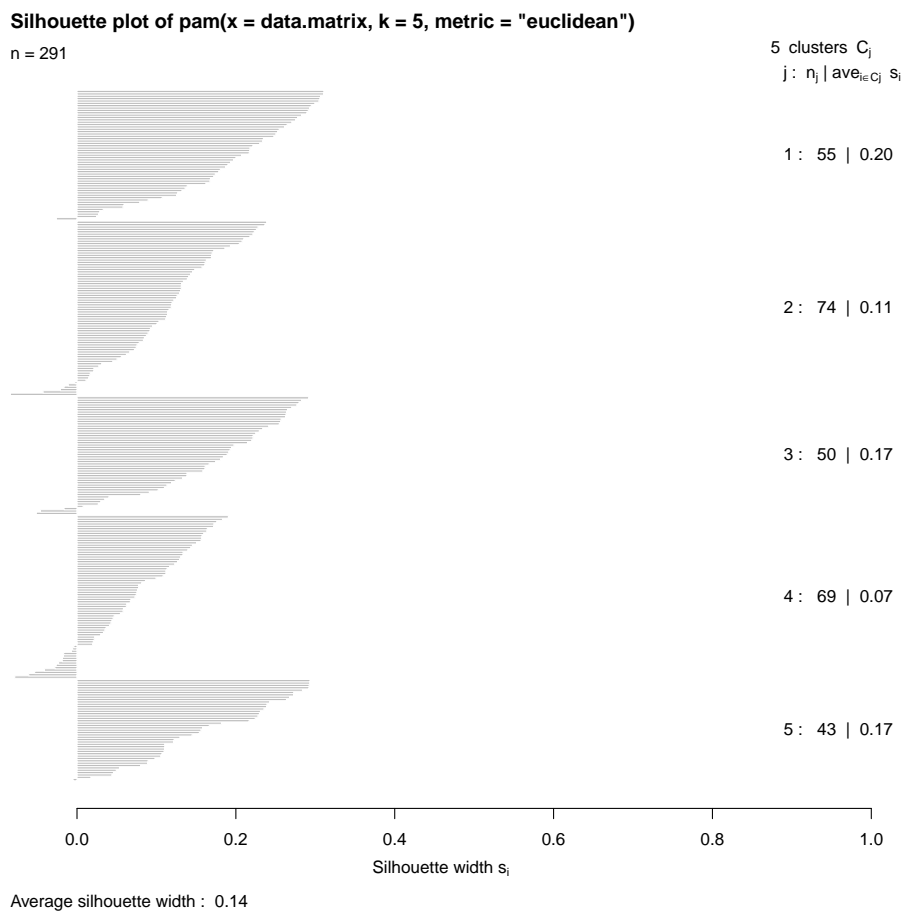


Figure C.8 – Same as in Fig. C.6 but for $W(t)$.

C.3 Additional information on clusters

In this section we present more detailed information about the clusters extracted from the daily mean and MDA8 O₃ LT(t), S(t) and W(t). From the MDA8 O₃ S(t) the following five clusters were identified: (1) “West” contains biggest part of France, Belgium and Spain, (2) “East” includes eastern and central Germany, eastern Austria and Czech Republic, (3) “Central” covers most part of Switzerland, some sites in central Germany and eastern Austria, (4) “North” is the cluster covering sites in northern Germany (North Sea region) and Netherlands, (5) “Atlant-Infl” covers most of the UK, some sites in the West coast and Scandinavia influenced by background O₃.

The five clusters obtained from the MDA8 O₃ W(t) are the following: (1) “CentralEast” covers the region of eastern Austria, Czech Republic and Poland, (2) “Central” for central and southern Germany and northern Switzerland, (3) “NorthWest” is the cluster in northern France, Belgium and south UK (4) “SouthWest” in central and southern France, Spain and Italy, and (5) “NorthEast” includes the region of northern Germany, Netherlands and southern Scandinavia.

The following five clusters for daily mean O₃ W(t) were obtained (Fig. C.12): (1) “CentralEast” that includes eastern Austria, Czech Republic, Poland and stations in Baltic and northern Scandinavia, (2) “Central” with stations in south-western Germany and Switzerland, (3) “NorthWest” covering the UK, northern France and Belgium, (4) “SouthWest” with southern France and Spain, i.e. mostly the Mediterranean region, and (5) “NorthEast” for northern Germany, Netherlands and southern Scandinavia.

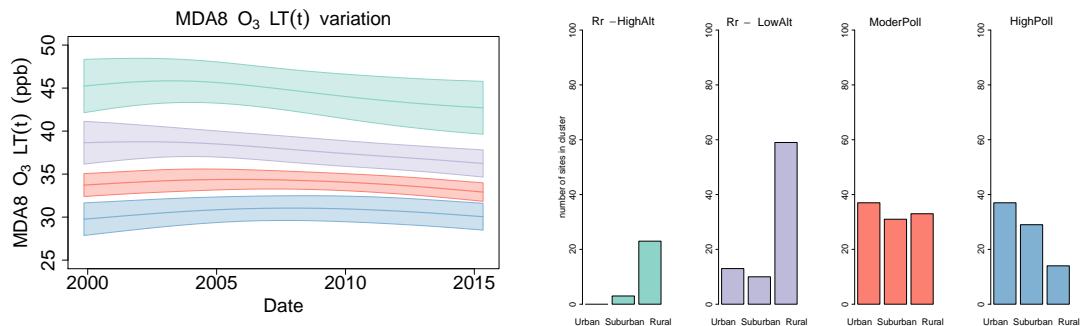


Figure C.9 – Clusters based on MDA8 O₃ LT(t). Map indicating the sites that belong in each cluster and average LT(t) in each cluster with \pm the standard deviation of the sites that have SW>0.

The daily mean and MDA8 O₃ W(t)-clustering resulted in clusters with a regional dependence, because it is mainly driven by short-term local meteorological conditions. Comparing the clustering based on S(t) and W(t), we conclude that both lead to a similar regional site classification. However, there are some differences: (a) the “Central” obtained by the daily mean S(t)-clustering is divided in the W(t)-clustering in two clusters the “Central” (south-western Germany and Switzerland without the Austrian sites of the S(t) cluster “Central”) and the “CentralEast” (eastern Austria, Czech Republic, Poland and Baltic region, in S(t) those sites fall

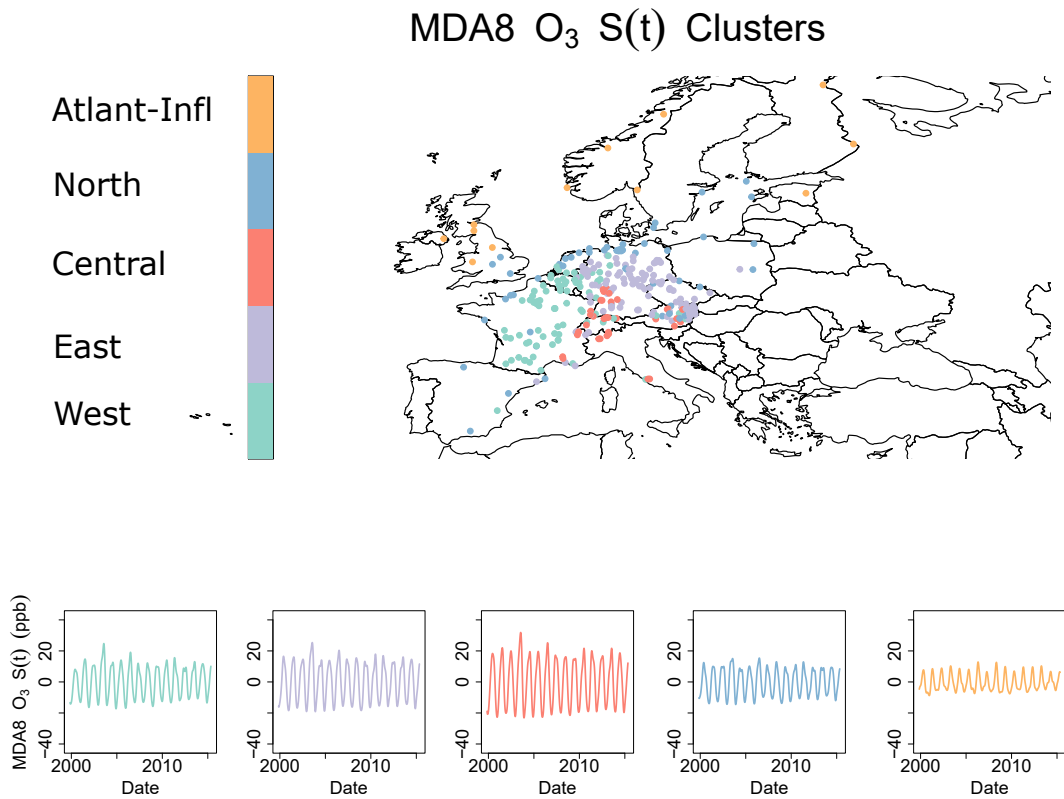


Figure C.10 – Clusters derived from MDA8 O₃ S(t). Map indicating the sites that belong in each cluster and average S(t) (standard deviation) in each cluster of the sites that have SW>0.

into the cluster "NorthEast"), (b) the "West" in the S(t)-clusters appears in the W(t)-clusters as two separate clusters the "NorthWest" (UK, northern France and Belgium) and "SouthWest" (southern France and Spain), which in the S(t)-clusters belong together in the "West" cluster.

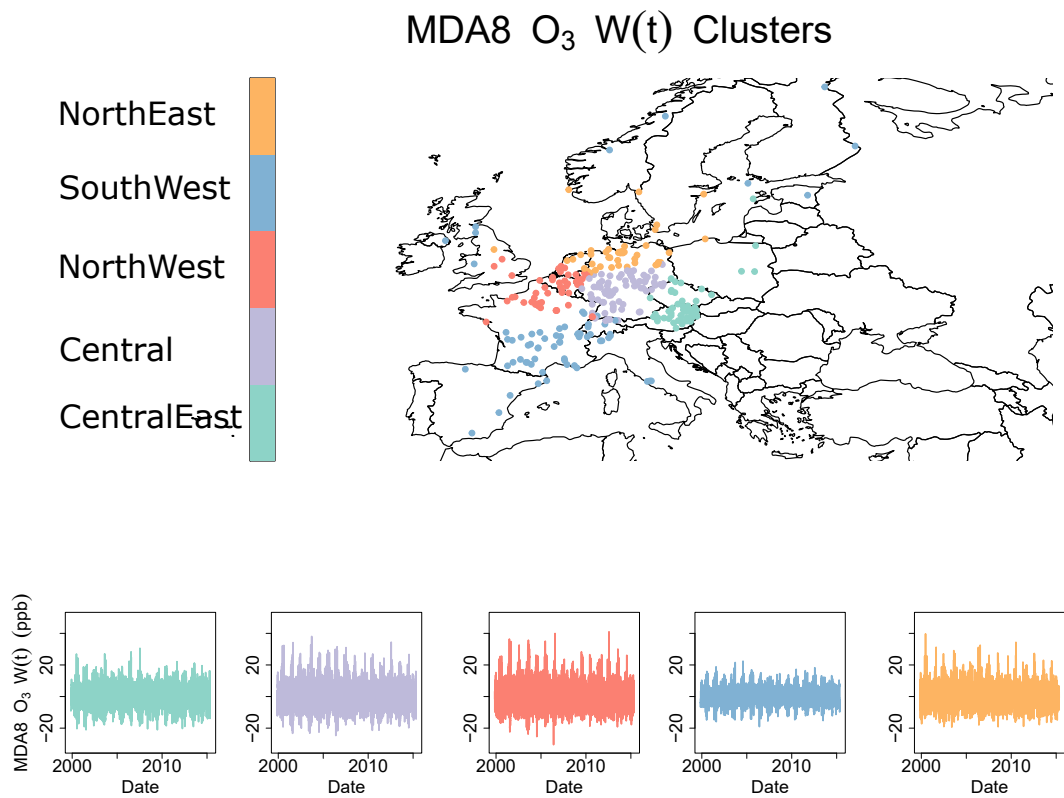


Figure C.11 – Clusters derived from MDA8 O₃ W(t). Map indicating the sites that belong in each cluster and average W(t) in each cluster of the sites that have SW>0.

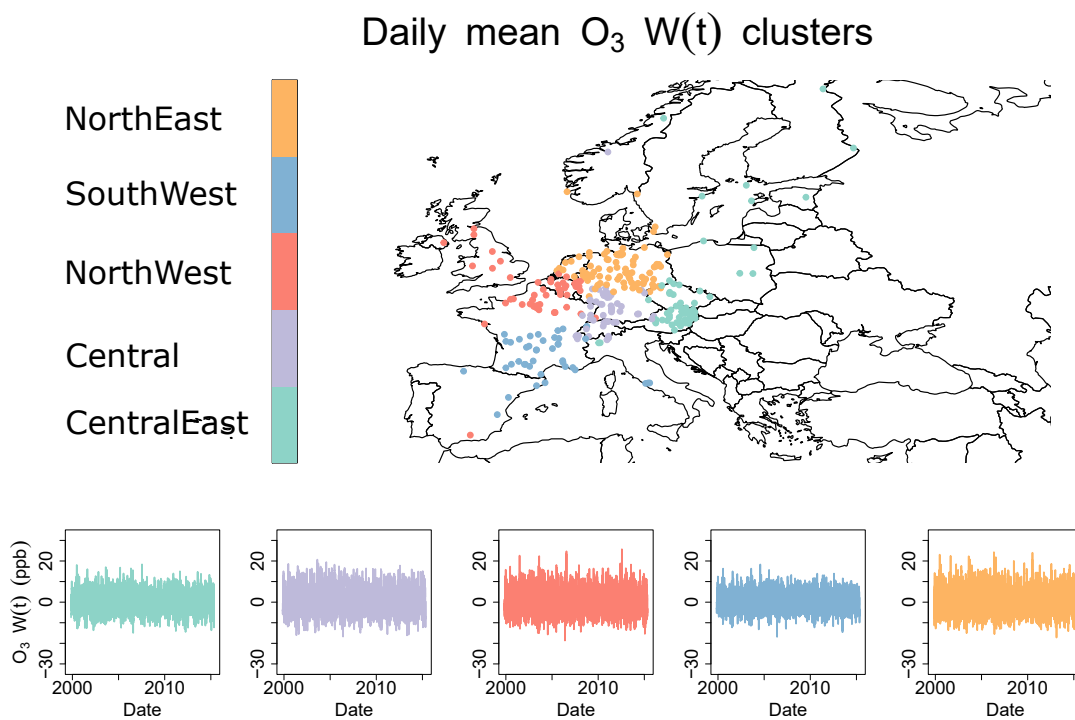


Figure C.12 – Clusters derived from daily mean O₃ W(t). (a) Map indicating the sites that belong in each cluster and average W(t) in each cluster of the sites that have SW>0.

C.4 MDA8 and 4-MDA8 trends

Trends of MDA8 O₃ concentrations are negative in most sites. (Fig. C.13). For the MDA8 O₃ in 69% of all sites significant trends were found (80% among the significant trends were negative and 19% positive). The most pronounced decrease is observed in rural sites ("Rural-HighAlt" and "Rural-LowAlt"). The level off or small increase in the "HighPoll" stations can be attributed to the smaller rate of reduction of VOCs, which resulted to reduced titration of O₃ by NO.

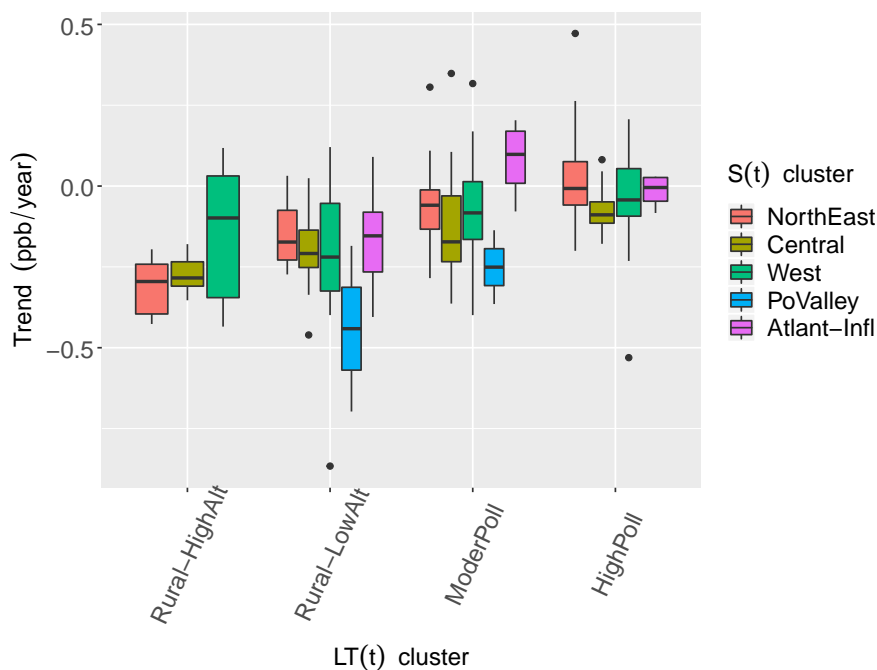


Figure C.13 – De-seasonalized MDA8 O₃ trends for the daily mean O₃ LT(t)- and S(t)-clusters.

Significant negative meteo-adjusted 4-MDA8 trends (Fig. C.14) were observed in 47% of the sites respectively, while without meteo-adjustment significant negative trends were identified in only 18% of the sites. Overall, in 96% of all sites negative 4-MDA8 trends respectively were calculated.

C.5 Sites with negative Silhouette width

Here, the sites with negative SW that were not considered in the discussion of the trends are presented. In the LT(t)-clustering four sites with negative SW were identified (Fig. C.15), in the S(t) 26 sites (Fig. C.16) and in the W(t) 24 sites. This is probably due to some distinct differences in the LT(t), S(t) and W(t) compared to the rest sites in the cluster. By excluding these sites from the discussion of the long-term trends, we avoid strong deflections from the average behavior in the cluster.

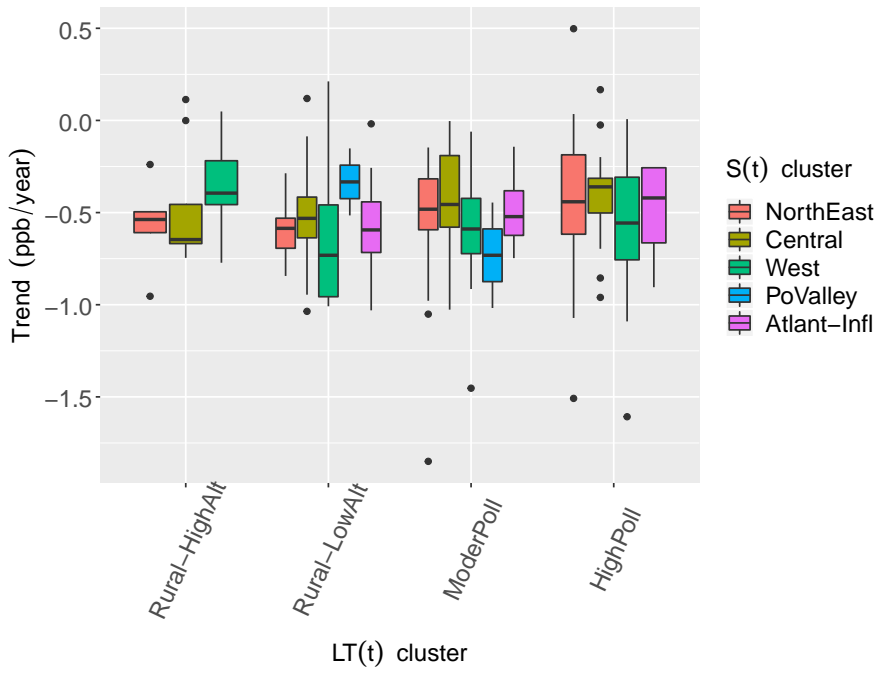


Figure C.14 – Trends of meteo-adjusted 4-MDA8 for the daily mean O₃ LT(t)- and S(t)-clusters.

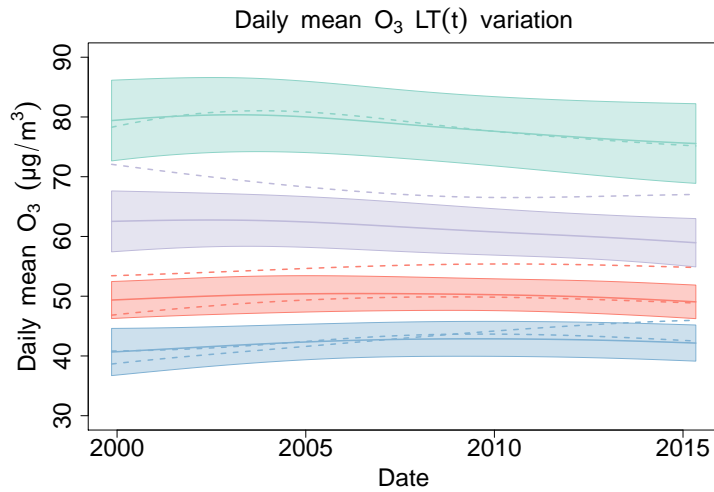


Figure C.15 – Sites with negative SW in the LT(t)-clustering, in comparison with the clusters average LT(t).

C.5. Sites with negative Silhouette width

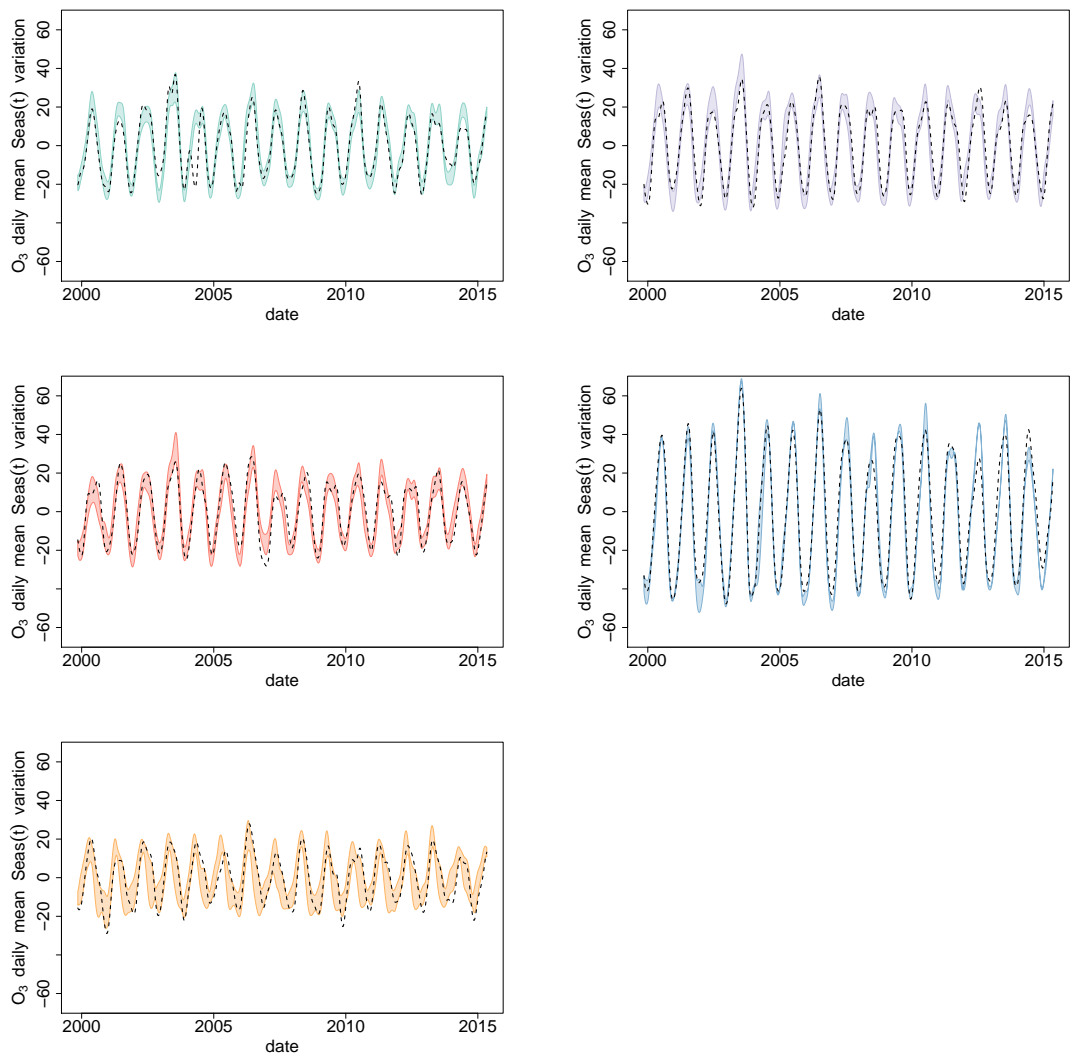


Figure C.16 – Example cases of sites with negative SW in the S(t)-clustering (black dashed line) in comparison with the clusters average S(t).

Bibliography

Akimoto, H.

2003. Global Air quality and Climate. *Science*, 302:1716–1719.

Anderson, D. C., J. M. Nicely, R. J. Salawitch, T. P. Canty, R. R. Dickerson, T. F. Hanisco, G. M. Wolfe, E. C. Apel, E. Atlas, T. Bannan, S. Bauguitte, N. J. Blake, J. F. Bresch, T. L. Campos, L. J. Carpenter, M. D. Cohen, M. Evans, R. P. Fernandez, B. H. Kahn, D. E. Kinnison, S. R. Hall, N. R. P. Harris, R. S. Hornbrook, J.-f. Lamarque, M. L. Breton, J. D. Lee, C. Percival, L. Pfister, R. B. Pierce, D. D. Riemer, A. Saiz-lopez, B. J. B. Stunder, A. M. Thompson, K. Ullmann, A. Vaughan, and A. J. Weinheimer

2016. A pervasive role for biomass burning in tropical high ozone/low water structures. *Nature Communications*, 7(May 2015):1–13.

Anttila, P. and J. P. Tuovinen

2009. Trends of primary and secondary pollutant concentrations in Finland in 1994-2007. *Atmospheric Environment*, 44(1):30–41.

BAFU

2016. NABEL Luftbelastung 2015. Technical Report UZ-1624-D, BAFU, Swiss Federal Office of Environment, Empa, Swiss Federal Laboratories for Materials Science and Technology.

Balzani-Lööv, J. M., S. Henne, G. Legreid, J. Staehelin, S. Reimann, A. S. H. Prévôt, M. Steinbacher, and M. K. Vollmer

2008. Estimation of background concentrations of trace gases at the Swiss Alpine site Jungfraujoch (3580 m asl). *Journal of Geophysical Research Atmospheres*, 113(22):1–17.

Barnpadimos, I., C. Hueglin, J. Keller, S. Henne, and A. S. H. Prévôt

2011. Influence of meteorology on PM10 trends and variability in Switzerland from 1991 to 2008. *Atmospheric Chemistry and Physics*, 11(4):1813–1835.

Bärtsch-Ritter, N., J. Keller, J. Dommen, and A. S. H. Prévôt

2004. Effects of various meteorological conditions and spatial emission resolutions on the ozone concentration & ROG/NO_x limitation in the Milan area (I). *Atmospheric Chemistry and Physics Discussions*, 3(1):733–768.

Bibliography

- Bell, M. L., R. D. Peng, and F. Dominici
2006. The Exposure – Response Curve for Ozone and Risk of Mortality and the Adequacy of Current Ozone Regulations. *Environmental Health Perspectives*, 114(4):532–536.
- Bloomer, B. J., J. W. Stehr, C. a. Piety, R. J. Salawitch, and R. R. Dickerson
2009. Observed relationships of ozone air pollution with temperature and emissions. *Geophysical Research Letters*, 36(9):1–5.
- Bloomer, B. J., K. Y. Vinnikov, and R. R. Dickerson
2010. Changes in seasonal and diurnal cycles of ozone and temperature in the eastern U.S. *Atmospheric Environment*, 44(21-22):2543–2551.
- Bloomfield, P., J. Royle, L. J. Steinberg, and Q. Yang
1996. Accounting for meteorological effects in measuring urban ozone levels and trends. *Atmospheric Environment*, 30(17):3067–3077.
- Boleti, E., C. Hueglin, and S. Takahama
2018a. Ozone time scale decomposition and trend assessment from surface observations in switzerland. *Atmospheric Environment*.
- Boleti, E., C. Hüglin, and S. Takahama
2018b. Trends of ozone maximum concentrations in switzerland based on meteorological adjustment for the period 1990-2014. *under preparation*.
- Boleti, E., C. Hüglin, and S. Takahama
2018c. Trends of surface maximum ozone concentrations in switzerland based on meteorological adjustment for the period 1990-2014. *under revision in Atmospheric Environment*.
- Brice, K. A., S. A. Penkett, D. H. F. Atkins, F. Sandalls, D. Bamber, A. Tuck, and G. Vaughan
1984. Atmospheric measurements of peroxyacetylnitrate (PAN) in rural, south-east England: seasonal variations, winter photochemistry and long-range transport. *Atmospheric Environment*, 18(12):2691–2702.
- Brönnimann, S., B. Buchmann, and H. Wanner
2002. Trends in near-surface ozone concentrations in Switzerland: The 1990s. *Atmospheric Environment*, 36(17):2841–2852.
- Brönnimann, S. and U. Neu
1997. Weekend-weekday differences of near-surface ozone concentrations in Switzerland for different meteorological conditions. *Atmospheric Environment*, 31(8):1127–1135.
- Camalier, L., W. Cox, and P. Dolwick
2007. The effects of meteorology on ozone in urban areas and their use in assessing ozone trends. *Atmospheric Environment*, 41(33):7127–7137.
- Carro-Calvo, L., C. Ordóñez, R. García-Herrera, and J. L. Schnell
2017. Spatial clustering and meteorological drivers of summer ozone in Europe. *Atmospheric Environment*, 167:496–510.

- Carslaw, D. C., S. D. Beevers, and J. E. Tate
2007. Modelling and assessing trends in traffic-related emissions using a generalised additive modelling approach. *Atmospheric Environment*, 41:5289–5299.
- Cassou, C. and J. Cattiaux
2016. Disruption of the European climate seasonal clock in a warming world. *Nature Climate Change*, Pp. 589–594.
- Chang, K.-L., I. Petropavlovskikh, O. R. Cooper, M. G. Schultz, and T. Wang
2017. Regional trend analysis of surface ozone observations from monitoring networks in eastern North America, Europe and East Asia. *Elementa*, 5(50):1–22.
- Chernick, M. R.
2008. *Bootstrap Methods, A guide for practitioners and researchers*.
- Coates, J., K. A. Mar, N. Ojha, and T. M. Butler
2016. The influence of temperature on ozone production under varying NO_x conditions – a modelling study. *Atmospheric Chemistry and Physics*, 16:11601–11615.
- Colette, A., C. Granier, O. Hodnebrog, H. Jakobs, A. Maurizi, A. Nyiri, B. Bessagnet, A. D’Angiola, M. D’Isidoro, M. Gauss, F. Meleux, M. Memmesheimer, A. Mieville, L. Rotüil, F. Russo, S. Solberg, F. Stordal, and F. Tampieri
2011. Air quality trends in Europe over the past decade: A first multi-model assessment. *Atmospheric Chemistry and Physics*, 11(22):11657–11678.
- Colette, A., F. Tognet, L. Létinois, V. Lemaire, F. Couvidat, R. M. A. D. Amo, I. A. G. Fernandez, I. R. Juan-aracil, H. Harmens, C. Andersson, S. Tsyro, A. Manders, and M. Mircea
2018. Long-term evolution of the impacts of ozone air pollution on agricultural yields in Europe A modelling analysis for the 1990-2010 period. Technical Report November, European Environmental Agency.
- Cooper, O. R., D. D. Parrish, a. Stohl, M. Trainer, P. Nédélec, V. Thouret, J. P. Cammas, S. J. Oltmans, B. J. Johnson, D. Tarasick, T. Leblanc, I. S. McDermid, D. Jaffe, R. Gao, J. Stith, T. Ryerson, K. Aikin, T. Campos, A. Weinheimer, and M. A. Avery
2010. Increasing springtime ozone mixing ratios in the free troposphere over western North America. *Nature*, 463(7279):344–348.
- Cooper, O. R., D. D. Parrish, J. Ziemke, N. V. Balashov, M. Cupeiro, I. E. Galbally, S. Gilge, L. Horowitz, N. R. Jensen, J.-F. Lamarque, V. Naik, S. J. Oltmans, J. Schwab, D. T. Shindell, a. M. Thompson, V. Thouret, Y. Wang, and R. M. Zbinden
2014. Global distribution and trends of tropospheric ozone: An observation-based review. *Elementa: Science of the Anthropocene*, 2:000029.
- Creilson, J. K., J. Fishman, and a. E. Wozniak
2003. Intercontinental transport of tropospheric ozone: A study of its seasonal variability across the North Atlantic utilizing tropospheric ozone residuals and its relationship to the North Atlantic Oscillation. *Atmospheric Chemistry and Physics Discussions*, 3(4):4431–4460.

Bibliography

- Cui, J., S. Pandey Deolal, M. Sprenger, S. Henne, J. Staehelin, M. Steinbacher, and P. Nédélec
2011. Free tropospheric ozone changes over Europe as observed at Jungfraujoch (1990–2008): An analysis based on backward trajectories. *Journal of Geophysical Research*, 116(D10):D10304.
- Davies, L., C. Jakob, P. May, V. V. Kumar, and S. Xie
2013. Relationships between the large-scale atmosphere and the small-scale convective state for Darwin, Australia. *Journal of Geophysical Research Atmospheres*, 118:11534–11545.
- Davis, J. M., B. K. Eder, D. Nychka, and Q. Yang
1998. Modeling the effects of Meteorology on Ozone in Houston using Cluster Analysis and Generalized Additive Models. *Atmospheric Environment*, 32(14):2505–2520.
- Dawson, J. P., P. J. Adams, and S. N. Pandis
2007. Sensitivity of ozone to summertime climate in the eastern USA : A modeling case study. *Atmospheric Environment*, 41:1494–1511.
- Dee, D. P., S. M. Uppala, a. J. Simmons, P. Berrisford, P. Poli, S. Kobayashi, U. Andrae, M. a. Balmaseda, G. Balsamo, P. Bauer, P. Bechtold, a. C. M. Beljaars, L. van de Berg, J. Bidlot, N. Bormann, C. Delsol, R. Dragani, M. Fuentes, a. J. Geer, L. Haimberger, S. B. Healy, H. Hersbach, E. V. Hólm, L. Isaksen, P. Kållberg, M. Köhler, M. Matricardi, a. P. McNally, B. M. Monge-Sanz, J. J. Morcrette, B. K. Park, C. Peubey, P. de Rosnay, C. Tavolato, J. N. Thépaut, and F. Vitart
2011. The ERA-Interim reanalysis: Configuration and performance of the data assimilation system. *Quarterly Journal of the Royal Meteorological Society*, 137:553–597.
- Denman, K. L., G. Brasseur, A. Chidthaisong, P. Ciaia, P. M. Cox, R. E. Dickinson, D. Hauglustaine, C. Heinze, E. Holland, J. D., L. U., R. S., da Silva Dias P.L., W. S.C., and Z. X.
2007. Couplings between changes in the climate system and biogeochemistry. in: Climate change 2007: The physical science basis. contribution of working group i to the fourth assessment report of the intergovernmental panel on climate change [solomon, s., d. Qin, m. Manning, z. chen, m. marquis, k.b. averyt, m. tignor and h.l. miller (eds.)]. Technical report, Cambridge University Press, Cambridge, United Kingdom and New York, NY, USA.
- Dentener, F., T. Keating, and H. Akimoto
2010. Hemispheric transport of air pollution, part a: Ozone and particulate matter. Technical Report 11.II.E.7, UNECE.
- Derwent, R., P. Simmonds, A. Manning, and T. Spain
2007. Trends over a 20-year period from 1987 to 2007 in surface ozone at the atmospheric research station, Mace Head, Ireland. *Atmospheric Environment*, 41(39):9091–9098.
- Derwent, R., D. S. Stevenson, W. J. Collins, and C. E. Johnson
2004. Intercontinental transport and the origins of the ozone observed at surface sites in Europe. *Atmospheric Environment*, 38(13):1891–1901.

- Derwent, R. G.
2008. New Directions : Prospects for regional ozone in north-west Europe. *Atmospheric Environment*, 42:1958–1960.
- Derwent, R. G., A. J. Manning, P. G. Simmonds, and S. O. Doherty
2013. Analysis and interpretation of 25 years of ozone observations at the Mace Head Atmospheric Research Station on the Atlantic Ocean coast of Ireland from 1987 to 2012. *Atmospheric Environment*, 80:361–368.
- Derwent, R. G., A. J. Manning, P. G. Simmonds, and S. O. Doherty
2018. Long-term trends in ozone in baseline and European regionally-polluted air at Mace Head , Ireland over a 30-year period. *Atmospheric Environment*, 179:279–287.
- Derwent, R. G., D. S. Stevenson, R. M. Doherty, W. J. Collins, M. G. Sanderson, and C. E. Johnson
2008. Radiative forcing from surface noxemissions: spatial and seasonal variations. *Climatic Change*, 88(3):385–401.
- Doherty, R. M., O. Wild, D. T. Shindell, G. Zeng, I. A. Mackenzie, W. J. Collins, A. M. Fiore, D. S. Stevenson, F. J. Dentener, M. G. Schultz, P. Hess, R. G. Derwent, and T. J. Keating
2013. Impacts of climate change on surface ozone and intercontinental ozone pollution : A multi-model study. *Journal of Geophysical Research:Atmospheres*, 118:3744–3763.
- Dommen, J., A. Neftel, A. Sigg, and D. J. Jacob
1995. Ozone and hydrogen peroxide during summer smog episodes over the Swiss Plateau: measurements and model simulations. *Journal of Geophysical Research*, 100(D5):8953–8966.
- Dommen, J., A. Prévôt, A. Hering, T. Staffelbach, G. Kok, and R. Schillawski
1999. Photochemical production and aging of an urban air mass. *Journal of Geophysical Research: Atmospheres*, 104(D5):5493–5506.
- Eckhardt, S., A. Stohl, S. Beirle, N. Spichtinger, P. James, C. Forster, C. Junker, T. Wagner, U. Platt, and S. G. Jennings
2003. The North Atlantic Oscillation controls air pollution transport to the Arctic. *Atmospheric Chemistry and Physics*, 3:1769–1778.
- EEA
2017. Air quality in Europe — 2017 report. Technical Report 13.
- EMEP
2017. Transboundary particulate matter, photo-oxidants, acidifying and eutrophying components. Technical Report 1.
- EMEP, Co-operative Programme for Monitoring and Evaluation of the Long-Range Transmission of Air Pollutants in Europe
2016. Air pollution trends in the EMEP region between 1990 and 2012. Technical Report 1,

Bibliography

- EMEP Task Force on Measurements and Modelling (TFMM), Chemical Co-ordinating Centre (CCC), Meteorological Synthesizing Centre-East (MSC-E), Meteorological Synthesizing Centre-West (MSC-W).
- European Environmental Agency
2015. Air quality in Europe-2015 report. Technical Report 5, European Environmental Agency.
- European Parliament and Council of the European Union
2008. Directive 2008/50/EC of the European Parliament and of the Council of 21 May 2008 on ambient air quality and cleaner air for Europe. Technical report, European Parliament and Council of the European Union.
- Finlayson-Pitts, B. and J. Pitts
2000. *Chemistry of the Upper and Lower Atmosphere: Theory, Experiments, and Applications*. Academic Press.
- Finlayson-Pitts, B. J. and J. N. Pitts
1986. *Atmospheric chemistry : fundamentals and experimental techniques*. New York : Wiley. "A Wiley-Interscience publication."
- Fiore, A. M., J. T. Oberman, M. Y. Lin, L. Zhang, O. E. Clifton, D. J. Jacob, V. Naik, L. W. Horowitz, J. P. Pinto, and G. P. Milly
2014. Estimating North American background ozone in U . S . surface air with two independent global models : Variability , uncertainties , and recommendations. *Atmospheric Environment*, 96:284–300.
- Flaum, J. B., S. T. Rao, and I. Zurbenko
1996. Moderating the Influence of Meteorological Conditions on Ambient Ozone Concentrations. *Journal of the Air & Waste Management Association*, 46(February 2015):35–46.
- Fleming, Z. L., R. M. Doherty, E. V. Schneidemesser, C. S. Malley, O. R. Cooper, J. P. Pinto, A. Colette, X. Xu, D. Simpson, M. G. Schultz, A. S. Lefohn, S. Hamad, R. Moolla, and S. Solberg
2018. Tropospheric Ozone Assessment Report : Present-day ozone distribution and trends relevant to human health. *Elementa: Science of the Anthropocene*, 6(12).
- Fowler, D., K. Pilegaard, M. Sutton, P. Ambus, M. Raivonen, J. Duyzer, D. Simpson, H. Fagerli, S. Fuzzi, J. K. Schjørring, et al.
2009. Atmospheric composition change: ecosystems–atmosphere interactions. *Atmospheric Environment*, 43(33):5193–5267.
- Fry, M. M., V. Naik, J. J. West, M. D. Schwarzkopf, A. M. Fiore, W. J. Collins, F. J. Dentener, D. T. Shindell, C. Atherton, D. Bergmann, B. N. Duncan, P. Hess, I. A. MacKenzie, E. Marmer, M. G. Schultz, S. Szopa, O. Wild, and G. Zeng
2012. The influence of ozone precursor emissions from four world regions on tropospheric composition and radiative climate forcing. *J. Geophys. Res.*, 117(D7):D07306.

- Galmarini, S., B. Koffi, E. Solazzo, T. Keating, C. Hogrefe, M. Schulz, A. Benedictow, J. J. Griesfeller, G. Janssens-Maenhout, G. Carmichael, J. Fu, and F. Dentener
2017. Technical note: Coordination and harmonization of the multi-scale, multi-model activities htap2, aqmeii3, and mics-asia3: simulations, emission inventories, boundary conditions, and model output formats. *Atmospheric Chemistry and Physics*, 17(2):1543–1555.
- Gaudel, A., O. R. Cooper, G. Ancellet, B. Barret, A. Boynard, J. P. Burrows, C. Clerbaux, P. Coheur, J. Cuesta, E. Cuevas, S. Doniki, G. Dufour, and F. Ebojje
2018. Tropospheric Ozone Assessment Report : Present-day distribution and trends of tropospheric ozone relevant to climate and global atmospheric chemistry model evaluation. *Elementa: Science of the Anthropocene*, 6(39).
- Grange, S. K., A. C. Lewis, S. J. Moller, and D. C. Carslaw
2017. Lower vehicular primary emissions of NO₂ in Europe than assumed in policy projections. *Nature Geoscience*, (2).
- Granier, C., B. Bessagnet, T. Bond, A. D. Angiola, H. D. V. D. Gon, G. J. Frost, A. Heil, J. W. Kaiser, S. Kinne, Z. Klimont, S. Kloster, and J.-f. Lamarque
2011. Evolution of anthropogenic and biomass burning emissions of air pollutants at global and regional scales during the 1980-2010 period. *Climatic Change*, 109:163–190.
- Grice, S., J. Stedman, A. Kent, M. Hobson, J. Norris, J. Abbott, and S. Cooke
2009. Recent trends and projections of primary NO₂ emissions in Europe. *Atmospheric Environment*, 43(13):2154–2167.
- Gryparis, A., B. Forsberg, K. Katsouyanni, A. Analitis, G. Touloumi, J. Schwartz, E. Samoli, S. Medina, H. R. Anderson, E. M. Niciu, H. Wichmann, B. Kriz, M. Kosnik, J. Skorkovsky, J. M. Vonk, and Z. Do
2004. Acute Effects of Ozone on Mortality from the “ Air Pollution and Health : A European Approach ” Project. *American Thoracic Society*, 170(10):1080–1087.
- Guerreiro, C. B., V. Foltescu, and F. de Leeuw
2014. Air quality status and trends in Europe. *Atmospheric Environment*, 98:376–384.
- Guerreiro, C. B., A. Gonzalez Ortiz, F. de Leeuw, M. Viana, and J. Horalek
2016. Air quality in Europe — 2016 report. Technical Report 28, EEA (European Environmental Agency).
- Gupta, M. L. and R. J. Cicerone
1998. Perturbation to global tropospheric oxidizing capacity due to latitudinal redistribution of surface sources of NO_x, CH₄ and CO. *Geophysical Research Abstracts*, 25(21):3931–3934.
- Hall, P.
1996. *The Bootstrap and Edgeworth Expansion.*, volume 45.

Bibliography

- Hartigan, J. A. and M. A. Wong
1979. Algorithm as 136: A k-means clustering algorithm. *Journal of the Royal Statistical Society. Series C (Applied Statistics)*, 28(1):100–108.
- Hastie, T. and R. Tibshirani
1990. Generalized Additive Models. *Statistical Science*, 1(3):297–310.
- Henne, S., D. Brunner, D. Folini, S. Solberg, J. Klausen, and B. Buchmann
2010. Assessment of parameters describing representativeness of air quality in-situ measurement sites. *Atmospheric Chemistry and Physics*, 10(8):3561–3581.
- Henne, S., M. Furger, S. Nyeki, M. Steinbacher, B. Neininger, S. F. J. de Wekker, J. Dommen, N. Spichtinger, A. Stohl, and A. S. H. Prévôt
2003. Quantification of topographic venting of boundary layer air to the free troposphere. *Atmospheric Chemistry and Physics*, 3(5):5205–5236.
- Henschel, S., A. Le Tertre, R. W. Atkinson, X. Querol, M. Pandol, A. Zeka, D. Haluza, A. Analitis, K. Katsouyanni, C. Bouland, M. Pascal, S. Medina, and P. G. Goodman
2015. Trends of nitrogen oxides in ambient air in nine European cities between 1999 and 2010. *Atmospheric Environment*, 117:234–241.
- Hess, P. G. and R. Zbinden
2013. Stratospheric impact on tropospheric ozone variability and trends: 1990-2009. *Atmospheric Chemistry and Physics*, 13(2):649–674.
- Holton, J. R., P. H. Haynes, M. E. McIntyre, A. R. Douglass, R. B. Rood, and L. Pfister
1995. Stratosphere-Troposphere exchange. *Reviews of Geophysics*, 33:403–439.
- Hsu, J. and M. J. Prather
2009. Stratospheric variability and tropospheric ozone. *Journal of Geophysical Research*, 114(March):1–15.
- Huang, N. E., Z. Shen, S. R. Long, M. C. Wu, H. H. Shih, Q. Zheng, N. C. Yen, C. C. Tung, and H. H. Liu
1998. The empirical mode decomposition and the Hilbert spectrum for nonlinear and non-stationary time series analysis. *Proceedings of the Royal Society of London. Series A: Mathematical, Physical and Engineering Sciences*, 454(1971):903–995.
- Huang, N. E. and Z. Wu
2008. A Review on Hilbert-Huang Transform : Method and Its Applications to Geophysical Studies. *Reviews of Geophysics*, 46(2008):1–23.
- Im, U., R. Bianconi, E. Solazzo, I. Kioutsioukis, A. Badia, A. Balzarini, R. Baró, R. Bellasio, D. Brunner, C. Chemel, G. Curci, J. Flemming, R. Forkel, L. Giordano, P. Jiménez-Guerrero, M. Hirtl, A. Hodzic, L. Honzak, O. Jorba, C. Knote, J. J. Kuenen, P. A. Makar, A. Manders-Groot, L. Neal, J. L. Pérez, G. Pirovano, G. Pouliot, R. S. Jose, N. Savage, W. Schroder, R. S.

- Sokhi, D. Syrakov, A. Torian, P. Tuccella, J. Werhahn, R. Wolke, K. Yahya, R. Zabkar, Y. Zhang, J. Zhang, C. Hogrefe, and S. Galmarini
2015. Evaluation of operational on-line-coupled regional air quality models over Europe and North America in the context of AQMEII phase 2. Part I: Ozone. *Atmospheric Environment*, 115:404–420.
- IPCC
2013. Climate change 2013: The physical science basis. Contribution of Working Group I to the Fifth Assessment Report of the Intergovernmental Panel on Climate Change, 1535 pp.
- Jackson, L. S., N. Carslaw, D. C. Carslaw, and K. M. Emmerson
2009. Modelling trends in OH radical concentrations using generalized additive models. *Atmospheric Chemistry and Physics*, 9(6):2021–2033.
- Jacob, D. J., J. A. Logan, and P. P. Murti
1999. Effect of rising Asian emissions on surface ozone in the United States. *Geophysical Research Letters*, 26(14):2175–2178.
- Jacob, D. J. and D. A. Winner
2009. Effect of Climate Change on Air Quality. *Atmospheric Environment*, 43:51–63.
- Jaffe, D., T. Anderson, D. Covert, R. Kotchenruther, B. Trost, J. Danielson, W. Simpson, J. Harris, and G. Carmichael
1999. Transport of Asian Air Pollution to North America. *Geophysical Research Abstracts*, 26(6):711–714.
- Jain, A. K.
2010. Data clustering: 50 years beyond K-means. *Pattern Recognition Letters*, 31(8):651–666.
- Johnson, C., W. Collins, D. Stevenson, and R. Derwent
1999. Relative roles of climate and emissions changes on future tropospheric oxidant concentrations. *Journal of Geophysical Research*, 104:18631–18645.
- Junge, C. E.
1962. Global ozone budget and exchange between stratosphere and troposphere. *Tellus*, 14(4).
- Kranenburg, R., A. J. Segers, C. Hendriks, and M. Schaap
2013. Source apportionment using LOTOS-EUROS: module description and evaluation. *Geoscientific Model Development*, 6(3):721–733.
- Kuebler, J., H. V. D. Bergh, and A. G. Russell
2001. Long-term trends of primary and secondary pollutant concentrations in Switzerland and their response to emission controls and economic changes. *Atmospheric Environment*, 35:1351–1363.

Bibliography

- Lanz, V. A., C. Hueglin, B. Buchmann, M. Hill, R. Locher, J. Staehelin, and S. Reimann
2008. Receptor modeling of C2-C7 hydrocarbon sources at an urban background site in Zurich, Switzerland : changes between 1993-1994 and 2005-2006. *Atmospheric Chemistry and Physics*, 8:2313–2332.
- Lewis, A. C., M. J. Evans, J. Methven, N. Watson, J. D. Lee, J. R. Hopkins, R. M. Purvis, S. R. Arnold, J. B. McQuaid, L. K. Whalley, M. J. Pilling, D. E. Heard, P. S. Monks, A. E. Parker, C. E. Reeves, D. E. Oram, G. Mills, B. J. Bandy, D. Stewart, H. Coe, P. Williams, and J. Crosier
2007. Chemical composition observed over the mid-Atlantic and the detection of pollution signatures far from source regions. *Journal of Geophysical Research*, 112:1–17.
- Lin, M., L. W. Horowitz, R. Payton, A. M. Fiore, and G. Tonnesen
2017. Us surface ozone trends and extremes from 1980 to 2014: quantifying the roles of rising asian emissions, domestic controls, wildfires, and climate. *Atmospheric Chemistry & Physics*, 17(4).
- Logan, J. A., J. Staehelin, I. A. Megretskaia, J. Cammas, V. Thouret, H. Claude, H. D. Backer, M. Steinbacher, H. Scheel, R. Stübi, M. Fröhlich, and R. Derwent
2012. Changes in ozone over Europe : Analysis of ozone measurements from sondes , regular aircraft (MOZAIC) and alpine surface sites. *Journal of Geophysical Research*, 117(D09301):1–23.
- LRTAP Convention
2015. Draft chapter iii: Mapping critical levels for vegetation, of the manual on methodologies and criteria for modelling and mapping critical loads and levels and air pollution effects, risks and trends.
- Lyapina, O., M. G. Schultz, and A. Hense
2016. Cluster analysis of European surface ozone observations for evaluation of MACC reanalysis data. *Atmospheric Chemistry and Physics*, 16:6863–6881.
- Maas, R. and P. Grennfelt
2016. Towards Cleaner Air. Scientific Assessment Report. Technical report, EMEP Steering Body and Working Group on Effects of the Convention on Long-Range Transboundary Air Pollution, Oslo.
- MacQueen, J. B.
1967. Kmeans Some Methods for classification and Analysis of Multivariate Observations. *5th Berkeley Symposium on Mathematical Statistics and Probability 1967*, 1(233):281–297.
- Marr, L. C. and R. A. Harley
2002. Spectral analysis of weekday–weekend differences in ambient ozone, nitrogen oxide, and non-methane hydrocarbon time series in california. *Atmospheric Environment*, 36(14):2327–2335.

- Matyssek, R., D. F. Karnosky, G. Wieser, K. Percy, E. Oksanen, T. E. E. Grams, M. Kubiske, D. Hanke, and H. Pretzsch
2010. Advances in understanding ozone impact on forest trees: Messages from novel phytotron and free-air fumigation studies. *Environmental Pollution*, 158(6):1990–2006.
- Matyssek, R., H. Sandermann, G. Wieser, F. Booker, and S. Cieslik
2008. The challenge of making ozone risk assessment for forest trees more mechanistic. *Environmental Pollution*, 156(3):567–582.
- Mills, G., G. Ball, F. Hayes, J. Fuhrer, L. Ska, B. Gimeno, L. D. Temmerman, and A. Heagle
2000. Development of a multi-factor model for predicting the effects of ambient ozone on the biomass of white clover. *Environmental Pollution*, 109:533–542.
- Mills, G., H. Pleijel, C. S. Malley, B. Sinha, O. R. Cooper, M. G. Schultz, H. S. Neufeld, D. Simpson, K. Sharps, G. Gerosa, H. Harmens, K. Kobayashi, and P. Saxena
2018. Tropospheric Ozone Assessment Report : Present-day tropospheric ozone distribution and trends relevant to vegetation. *Elementa: Science of the Anthropocene*, 6(47).
- Monks, P. S.
2000. A review of the observations and origins of the spring ozone maximum. *Atmospheric Environment*, 34:3545–3561.
- Monks, P. S., A. T. Archibald, A. Colette, O. Cooper, M. Coyle, R. Derwent, D. Fowler, C. Granier, K. S. Law, G. E. Mills, D. S. Stevenson, O. Tarasova, V. Thouret, E. von Schneidmesser, R. Sommariva, O. Wild, and M. L. Williams
2015. Tropospheric ozone and its precursors from the urban to the global scale from air quality to short-lived climate forcer. *Atmospheric Chemistry and Physics*, 15(15):8889–8973.
- Munir, S., H. Chen, and K. Ropkins
2013. Science of the Total Environment Quantifying temporal trends in ground level ozone concentration in the UK. *Science of the Total Environment*, 458-460:217–227.
- National Research Council
1991. *Rethinking the ozone problem in urban and regional air pollution*. National Academies Press.
- National Research Council
1992. *Rethinking the ozone problem in urban and regional air pollution*. National Academies Press.
- Neu, U., T. Künzle, and H. Wanner
1994. On the relation between ozone storage in the residual layer and daily variation in near-surface ozone concentration-A case study. *Boundary-Layer Meteorology*, 69(3):221–247.
- Novelli, P. C., K. A. Masarie, and P. M. Lang
1998. Distributions and recent changes of carbon monoxide in the lower troposphere. *Journal of Geophysical Research D: Atmospheres*, 103(D15):19015–19033.

Bibliography

- Oikonomakis, E., S. Aksoyoglu, G. Ciarelli, U. Baltensperger, H. Prévôt, and A. Stephan
2018. Low modeled ozone production suggests underestimation of precursor emissions (especially no x) in europe. *Atmospheric Chemistry & Physics*, 18(3).
- Oltmans, S. J., a. S. Lefohn, D. Shadwick, J. M. Harris, H. E. Scheel, I. Galbally, D. W. Tarasick, B. J. Johnson, E. G. Brunke, H. Claude, G. Zeng, S. Nichol, F. Schmidlin, J. Davies, E. Cuevas, a. Redondas, H. Naoe, T. Nakano, and T. Kawasato
2013. Recent tropospheric ozone changes - A pattern dominated by slow or no growth. *Atmospheric Environment*, 67:331–351.
- Ordóñez, C., D. Brunner, J. Staehelin, P. Hadjinicolaou, J. A. Pyle, M. Jonas, H. Wernli, and A. S. H. Prévot
2007. Strong influence of lowermost stratospheric ozone on lower tropospheric background ozone changes over Europe. *Geophysical Research Letters*, 34(7):1–5.
- Ordóñez, C., H. Mathis, M. Furger, S. Henne, C. Hüglin, J. Staehelin, and A. S. H. Prévôt
2005. Changes of daily surface ozone maxima in Switzerland in all seasons from 1992 to 2002 and discussion of summer 2003. *Atmospheric Chemistry and Physics*, 5(5):1187–1203.
- Otero, N., J. Sillmann, K. A. Mar, H. W. Rust, S. Solberg, C. Andersson, M. Engardt, R. Bergström, B. Bessagnet, A. Colette, F. Couvidat, C. Cuvelier, S. Tsyro, H. Fagerli, M. Schaap, A. Manders, M. Mircea, G. Briganti, A. Cappelletti, M. Adani, M. D'Isidoro, M.-T. Pay, M. Theobald, M. G. Vivanco, P. Wind, N. Ojha, V. Raffort, and T. Butler
2018. A multi-model comparison of meteorological drivers of surface ozone over europe. *Atmospheric Chemistry and Physics*, 18(16):12269–12288.
- Otero, N., J. Sillmann, J. L. Schnell, H. W. Rust, and T. Butler
2016. Synoptic and meteorological drivers of extreme ozone concentrations over Europe. *Environmental Research Letters*, 11(2):24005.
- Paoletti, E., A. De Marco, D. C. S. Beddows, R. M. Harrison, and W. J. Manning
2014. Ozone levels in European and USA cities are increasing more than at rural sites, while peak values are decreasing. *Environmental Pollution*, 192(June):295–299.
- Parrish, D. D., J. Lamarque, V. Naik, L. Horowitz, D. T. Shindell, J. Staehelin, R. Derwent, O. R. Cooper, H. Tanimoto, A. Volz-Thomas, S. Gilge, H.-E. Scheel, M. Steinbacher, and M. Fröhlich
2014. Long-term changes in lower tropospheric baseline ozone concentrations: Comparing chemistry-climate models and observations at northern midlatitudes. *Journal of Geophysical Research*, 119:5719–5736.
- Parrish, D. D., K. S. Law, J. Staehelin, R. Derwent, O. R. Cooper, H. Tanimoto, a. Volz-Thomas, S. Gilge, H.-E. Scheel, M. Steinbacher, and E. Chan
2012. Long-term changes in lower tropospheric baseline ozone concentrations at northern mid-latitudes. *Atmospheric Chemistry and Physics*, 12(23):11485–11504.

- Parrish, D. D., K. S. Law, J. Staehelin, R. Derwent, O. R. Cooper, H. Tanimoto, a. Volz-Thomas, S. Gilge, H. E. Scheel, M. Steinbacher, and E. Chan
2013. Lower tropospheric ozone at northern midlatitudes: Changing seasonal cycle. *Geophysical Research Letters*, 40(8):1631–1636.
- Pausata, F. S. R., L. Pozzoli, E. Vignati, and F. J. Dentener
2012. North Atlantic Oscillation and tropospheric ozone variability in Europe: model analysis and measurements intercomparison. *Atmospheric Chemistry and Physics*, 12:6357–6376.
- Pearce, J. L., J. Beringer, N. Nicholls, R. J. Hyndman, and N. J. Tapper
2011. Quantifying the influence of local meteorology on air quality using generalized additive models. *Atmospheric Environment*, 45(6):1328–1336.
- Peña-Ortiz, C., D. Barriopedro, and R. García-Herrera
2015. Multidecadal variability of the summer length in Europe. *Journal of Climate*, 28(13):5375–5388.
- Prévôt, A. S. H., J. Staehelin, L. Kok, D. Schillawski, B. Neininger, T. Staffelbach, A. Neftel, H. Wernli, and J. Dommen
1997. The Milan photooxidant plume. *Journal of Geophysical Research*, 102(D19):23375–23388.
- Pusede, S. E., A. L. Steiner, and R. C. Cohen
2015. Temperature and Recent Trends in the Chemistry of Continental Surface Ozone. *Chemical Reviews*, 115:3898–3918.
- Querol, X., A. Alastuey, C. Reche, A. Orío, M. Pallares, F. Reina, J. J. Dieguez, E. Mantilla, M. Escudero, L. Alonso, G. Gangoiti, and M. Millán
2016. On the origin of the highest ozone episodes in Spain. *Science of the Total Environment*, 572(X):379–389.
- R Development Core Team
2017. *R: A Language and Environment for Statistical Computing*. R Foundation for Statistical Computing, Vienna, Austria. ISBN 3-900051-07-0.
- Rousseeuw, P. J.
1987. Silhouettes : a graphical aid to the interpretation and validation of cluster analysis. *Journal of Computational and Applied Mathematics*, 20:53–65.
- Schnell, J. L., C. D. Holmes, A. Jangam, and M. J. Prather
2014. Skill in forecasting extreme ozone pollution episodes with a global atmospheric chemistry model. *Atmospheric Chemistry and Physics*, Pp. 7721–7739.
- Schultz, M., R. Schmitt, K. Thomas, and A. Volz-Thomas
1998. Photochemical box modeling of long-range transport from North America to Tener-

Bibliography

- ife during the North Atlantic Regional Experiment (NARE) 1993. *Journal of Geophysical Research*, 103:13477–13488.
- Seinfeld, J. and S. Pandis
2016. *Atmospheric Chemistry and Physics: From Air Pollution to Climate Change*. John Wiley, Hoboken, NJ.
- Sen, P.
1968. Estimates of the regression coefficient based on Kendall's tau. *Journal of American Statistical Association*, 63(324):1379–1389.
- Sillman, S.
1999. The relation between ozone, NO_x and hydrocarbons in urban and polluted rural environments. *Atmospheric Environment*, 33(C):1821–1845.
- Sillman, S., J. A. Logan, and S. C. Wofsy
1990. The sensitivity of ozone to nitrogen oxides and hydrocarbons in regional ozone episodes. *Journal of Geophysical Research: Atmospheres*, 95(D2):1837–1851.
- Sillman, S. and P. J. Samson
1995. Impact of temperature on oxidant photochemistry in urban, polluted rural and remote environments. *Journal of Geophysical Research-Atmospheres*, 100(D6):11497–11508.
- Silva, R. A., J. J. West, Y. Zhang, S. C. Anenberg, D. T. Shindell, W. J. Collins, S. Dalsoren, G. Faluvegi, G. Folberth, L. W. Horowitz, T. Nagashima, V. Naik, S. Rumbold, and R. Skeie
2013. Global premature mortality due to anthropogenic outdoor air pollution and the contribution of past climate change. *Environmental Research Letters*, 8.
- Simon, H., A. Reff, B. Wells, J. Xing, and N. Frank
2015. Ozone trends across the United States over a period of decreasing NO_x and VOC emissions. *Environmental Science and Technology*, 49(1):186–195.
- Simpson, D.
1995. Biogenic emissions in Europe 2 . Implications for ozone control strategies. *Journal of Geophysical Research*, 100(D11):22891–22906.
- Solberg, S.
2009. Assessment of ground-level ozone in EEA member countries, with a focus on long-term trends. Technical Report 7, EEA, European Environmental Agency.
- Staehelin, J., J. Thudium, R. Buehler, A. Volz-Thomas, and W. Graber
1994. Trends in surface ozone concentrations at Arosa (Switzerland). *Atmospheric Environment*, 28(1):75–87.
- Stevenson, D. S., F. J. Dentener, M. G. Schultz, K. Ellingsen, T. P. C. V. Noije, O. Wild, G. Zeng, M. Amann, C. S. Atherton, N. Bell, D. J. Bergmann, and I. Bey
2006. Multimodel ensemble simulations of present-day and near-future tropospheric ozone. *Journal of Geophysical Research*, 111.

- Stevenson, D. S., P. J. Young, V. Naik, J. Lamarque, D. T. Shindell, A. Voulgarakis, and R. B. Skeie
2013. Tropospheric ozone changes , radiative forcing and attribution to emissions in the Atmospheric Chemistry and Climate Model Intercomparison Project (ACCMIP). *Atmospheric Chemistry and Physics*, (October 2012):3063–3085.
- Stiller, B., T. Bocek, F. Hecht, G. Machado, P. Racz, and M. Waldburger
2000. NABEL-Luftbelastung 1999. Technical Report 196pp, BUWAL (Swiss Agency for Environment, Forests, and Landscape).
- Stohl, A.
2002. On the pathways and timescales of intercontinental air pollution transport. *Journal of Geophysical Research*, 107(D23):1–17.
- Stohl, A., P. Bonasoni, P. Cristofanelli, W. Collins, J. Feichter, A. Frank, C. Foster, E. Gerasopoulos, H. Gäggeler, P. James, T. Kentarchos, H. Kromp-Kolb, B. Krüger, C. Land, J. Meloen, A. Papayannis, A. Priller, P. Seibert, M. Sprenger, G. Roelofs, H. Scheel, C. Schnabel, P. Siegmund, L. Tobler, T. Trickl, H. Wernli, V. Wirth, P. Zanis, and C. Zerefos
2003. Stratosphere-troposphere exchange: A review, and what we have learned from STAC-CATO. *Journal of Geophysical Research*, 108(D12):8516.
- Taraborrelli, D., M. G. Lawrence, J. N. Crowley, T. J. Dillon, S. Gromov, C. B. M. Gross, L. Vereecken, and J. Lelieveld
2012. Hydroxyl radical buffered by isoprene oxidation over tropical forests. *Nature Geoscience*, 5:190–193.
- The Royal Society
2008. Ground-level ozone in the 21st century: future trends, impacts and policy implications. Technical Report October, The Royal Society.
- Theil, H.
1950. A rank-invariant method of linear and polynomial regression analysis, part 3. In *Proceedings of Koninklijke Nederlandse Akademie van Wetenschappen A*, volume 53, Pp. 1397–1412.
- Thielmann, A., A. Prévôt, G. F.C., and J. Staehelin
2001. Empirical ozone isopleths as a tool to identify ozone production regimes. *Geophysical Research Letters*, 28(12):2369–2372.
- Thompson, M., J. Reynolds, L. H. Cox, P. Guttorp, and P. D. Sampson
2001. A review of statistical methods for the meteorological adjustment of tropospheric ozone. *Atmospheric Environment*, 35(3):617–630.
- Thoning, K. W., P. P. Tans, and W. D. Komhyr
1989. Atmospheric carbon dioxide at Mauna Loa Observatory: 2. Analysis of the NOAA GMCC data, 1974–1985. *Journal of Geophysical Research*, 94(D6):8549.

Bibliography

- Vestreng, V., L. Ntziachristos, A. Semb, S. Reis, I. S. A. Isaksen, and L. Tarras
2009. Evolution of NO_x emissions in Europe with focus on road transport control measures. *Atmospheric Chemistry and Physics*, 9:1503–1520.
- Vingarzan, R.
2004. A review of surface ozone background levels and trends. *Atmospheric Environment*, 38(21):3431–3442.
- Vogel, B., N. Riemer, H. Vogel, and F. Fiedler
1999. Findings on NO_y as an indicator for ozone sensitivity based on different numerical simulations. *Journal of Geophysical Research*, 104(D3):3605–3620.
- West, J. J., A. M. Fiore, L. W. Horowitz, and D. L. Mauzerall
2006. Global health benefits of mitigating ozone pollution with methane emission controls. *Proceedings of the National Academy of Sciences*, 103(11):3988–3993.
- West, J. J., V. Naik, L. W. Horowitz, and A. M. Fiore
2009. Effect of regional precursor emission controls on long-range ozone transport – part 1: Short-term changes in ozone air quality. *Atmospheric Chemistry and Physics*, 9(16):6077–6093.
- Weusthoff, T.
2011. Weather Type Classification at MeteoSwiss - Introduction of new automatic classification schemes. Technical Report 235, MeteoSwiss.
- WHO
2006. Air quality guidelines for particulate matter, ozone, nitrogen dioxide and sulfur dioxide: global update 2005: summary of risk assessment. Technical report, World Health Organization.
- WHO
2008. Health risks of ozone from long-range transboundary air pollution. Technical report, World Health Organization.
- WHO
2013. Review of evidence on health aspects of air pollution: Revihaap project: final technical report. Technical report, World Health Organization.
- Wild, O.
2007. Modelling the global tropospheric ozone budget: exploring the variability in current models. *Atmospheric Chemistry and Physics*, 7:2643–2660.
- Wild, O. and H. Akimoto
2001. Intercontinental transport of ozone and its precursors in a three-dimensional global ctm. *Journal of Geophysical Research: Atmospheres*, 106(D21):27729–27744.

- Wilson, R. C., Z. L. Fleming, P. S. Monks, G. Clain, S. Henne, I. B. Konovalov, S. Szopa, and L. Menut
2012. Have primary emission reduction measures reduced ozone across Europe? An analysis of European rural background ozone trends 1996–2005. *Atmospheric Chemistry and Physics*, 12(1):437–454.
- Wood, S.
2006. *Generalized Additive Models: An Introduction with R*. Chapman & Hall/CRC press.
- Wu, Z. and N. E. Huang
2009. Ensemble Empirical Mode Decomposition: A noise-assisted data analysis method. *Advances in Adaptive Data Analysis*, 1(1):1–41.
- Yan, Y., A. Pozzer, N. Ojha, J. Lin, and J. Lelieveld
2017. Analysis of European ozone trends in the period 1995–2014. *Atmospheric Chemistry and Physics Discussions*, (December).
- Yan, Y., A. Pozzer, N. Ojha, J. Lin, and J. Lelieveld
2018. Analysis of European ozone trends in the period 1995–2014. *Atmospheric Chemistry and Physics*, (December).
- Young, P. J., A. T. Archibald, K. W. Bowman, J. Lamarque, V. Naik, D. S. Stevenson, and S. Tilmes
2013. Pre-industrial to end 21st century projections of tropospheric ozone from the Atmospheric Chemistry and Climate Model Intercomparison Project (ACCMIP). *Atmospheric Chemistry and Physics*, 13:2063–2090.
- Young, P. J., V. Naik, A. M. Fiore, A. Gaudel, J. Guo, M. Y. Lin, J. L. Neu, D. D. Parish, H. E. Rieder, J. L. Schnell, S. Tilmes, O. Wild, L. Zhang, J. Ziemke, J. Brandt, A. Delcloo, R. M. Doherty, C. Geels, M. I. Hegglin, L. Hu, U. Im, R. Kumar, A. Luhar, L. Murray, D. Plummer, J. Rodriguez, A. Siaz-Lopez, M. G. Schutz, M. T. Woodhouse, and G. Zeng
2018. Tropospheric Ozone Assessment Report : Assessment of global-scale model performance for global and regional ozone distributions , variability , and trends. *Elementa: Science of the Anthropocene*, 6(10).
- Zhang, Y., O. R. Cooper, A. Gaudel, A. M. Thompson, P. Nédélec, S.-Y. Ogino, and J. J. West
2016. Tropospheric ozone change from 1980 to 2010 dominated by equatorward redistribution of emissions. *Nature Geoscience*, 1(November).



Eirini Boleti

Curriculum Vitae

PERSONAL DETAILS

Address Langstrasse 239, 8005, Zurich, Switzerland
Phone +41 76 26 44010
E-mail eirini.boleti@gmail.com
Permit C, valid until July 2020
Birth date 21 June, 1982

WORK EXPERIENCE

Consultant for Air Quality

November 2018-October 2019

TNO, the Netherlands Organisation for applied scientific research
Department of Climate, Air & Sustainability, Utrecht, the Netherlands

- Modeling studies for air quality assessments, forecasts, deposition and source apportionment
- Data analysis and visualization of model output and model validation
- Acquisition of new projects
- Compile and deliver project reports
- Represent the team in international conferences, forums and plenary meetings
- Provide stakeholders with research output as a guideline to derive strategies for improving air quality

Research Associate

May 2015-October 2018

Empa, Air Pollution/Environmental Technology Laboratory, Dübendorf, Switzerland

- Application of machine learning techniques for air quality
- Analysis of long-term air pollutants data sets
- Development of statistical methods for long-term and seasonal patterns recognition
- Application of clustering techniques to identify similar measuring stations in Europe
- Investigating the effect of policy making decisions on air quality

Physics tutor

Sept. 2010 - June 2013

Private, Switzerland

- Teaching physics and mathematics to Gymnasium students
- Teaching mathematics to university students

Physics teacher

Sept. 2006 - June 2010

Private school "Methodos", Greece

- Teaching physics, mathematics and chemistry to Highschool students
- Preparatory courses for the University entrance exams for senior Highschool students
- Responsible for the preparation of teaching material
- Spokesperson on behalf of the school, responsible for communicating with the parents

EDUCATION

PhD in Statistical Analysis of Air Pollutants Concentrations

May 2015 - November 2019

Empa, Air Pollution/Environmental Technology Laboratory
EPFL, Air Particle Research Laboratory

- Long-term trends and seasonality of air pollutants concentrations
- Time scale decomposition of ozone concentrations time series
- Spatial and temporal analysis of large data sets
- Clustering techniques for identification of stations with similar behavior

MSc. Atmospheric and Climate Science

Sept. 2013 - March 2015

ETH Zürich, Institute of Atmosphere and Climate

Quantitative understanding of climate processes and their interactions

In depth understanding of the climate system, aspects of the atmosphere and weather phenomena

MSc. Computational Physics

Sept. 2006 - Febr. 2009

Aristoteles University of Thessaloniki (Greece), Department of Physics

Training in various programming languages

Computer simulations of physical phenomena

Degree (Diploma) in Physics

Sept. 2000 - Sept. 2006

Aristoteles University of Thessaloniki (Greece), Department of Physics

Specialization field: "Atmosphere and Environment Physics"

PROJECTS

- *Brightskies*, collaboration with Airbus Defense & Space for assimilation of satellite data in air quality model
- Source apportionment for quantifying contribution of sectors and countries on local concentrations of air pollutants (TOPAS, <https://topas.tno.nl/>)
- Nitrogen deposition in Germany (PINETI), study for the German government on deposition of nitrogen components over the last 10 years.

SKILLS

Data analysis: R(advanced), PYTHON(intermediate)

Chemistry-transport modeling, air quality models

Geospatial data analysis: QGIS, ArcGIS

OS: WINDOWS and LINUX

Typesetting: L^AT_EX, WORD

Office suits: Open/Libre Office, Microsoft Office

LANGUAGES

Greek (mother tongue)

English (Professional level,C1)

German (Professional level,C1)

HOBBIES

Canoeing

Baking (bread, international specialties) <https://moefel.net>

Inline skating